



Prepared for the U.S. Department of Energy
under Contract DE-AC05-76RL01830

PNNL-29592

Open-Source High-Fidelity Aggregate Composite Load Models of Emerging Load Behaviors for Large-Sale Analysis

PNNL Team:

Yuan Liu Pavel Etingov Soumya Kundu Zhangshuan Hou Qiuhua Huang
Huifen Zhou Malini Ghosal Daniel James Jian Zhang Yulong Xie

LBNL Team:

Peter Cappers, Annika Todd Blick

Other Contributors:

Yu Zhang Yingying Tang Zhigang Chu David Chassin Indrasis Chakraborty

January 2020



Proudly Operated by Battelle Since 1965

DISCLAIMER

This report was prepared as an account of work sponsored by an agency of the United States Government. Neither the United States Government nor any agency thereof, nor Battelle Memorial Institute, nor any of their employees, makes **any warranty, express or implied, or assumes any legal liability or responsibility for the accuracy, completeness, or usefulness of any information, apparatus, product, or process disclosed, or represents that its use would not infringe privately owned rights.** Reference herein to any specific commercial product, process, or service by trade name, trademark, manufacturer, or otherwise does not necessarily constitute or imply its endorsement, recommendation, or favoring by the United States Government or any agency thereof, or Battelle Memorial Institute. The views and opinions of authors expressed herein do not necessarily state or reflect those of the United States Government or any agency thereof.

PACIFIC NORTHWEST NATIONAL LABORATORY
operated by
BATTELLE
for the
UNITED STATES DEPARTMENT OF ENERGY
under Contract DE-AC05-76RL01830

Printed in the United States of America

**Available to DOE and DOE contractors from the
Office of Scientific and Technical Information,
P.O. Box 62, Oak Ridge, TN 37831-0062;
ph: (865) 576-8401
fax: (865) 576-5728
email: reports@adonis.osti.gov**

**Available to the public from the National Technical Information Service
5301 Shawnee Rd., Alexandria, VA 22312
ph: (800) 553-NTIS (6847)
email: [<https://www.ntis.gov/about>](mailto:orders@ntis.gov)
Online ordering: <http://www.ntis.gov>**

Open-Source High-Fidelity Aggregate Composite Load Models of Emerging Load Behaviors for Large-Sale Analysis

January 2020

Yuan Liu (Principal Investigator, PNNL)
Soumya Kundu (PNNL)
Qiuhua Huang (PNNL)
Malini Ghosal (PNNL)
Jian Zhang (PNNL)
Peter Cappers (LBNL)
Yu Zhang (PG&E)
Zhigang Chu (ASU)
Indrasis Chakraborty (LLNL)

Pavel Etingov (Project Manager, PNNL)
Zhangshuan Hou (PNNL)
Huifen Zhou (PNNL)
Daniel James (PNNL)
Yulong Xie (PNNL)
Annika Todd Blick (LBNL)
Yingying Tang (Microsoft)
David Chassin (SLAC)

Prepared for
the U.S. Department of Energy
under Contract DE-AC05-76RL01830

Pacific Northwest National Laboratory
Richland, Washington 99354

Abstract

The goal of this project is to accurately model the dynamic loads for power system planning and operation and to address the challenges inherent in such modeling. Existing load models are inadequate to handle the increasing proliferation of residential air conditioner loads and distributed energy resources, the emerging trends of price-responsive demand, and the growing importance of protective devices in equipment and buildings. A need has emerged to develop a fundamentally new class of load models and next-generation data tools.

This work proposes to develop a set of regional-level, scalable open source load models and tools, including large-scale aggregate load protection, concept of price responsive demand, advanced load composition data, next-generation load model data tools, and advanced composite load model calibration and validation frameworks to address new challenges in the representation of next-generation load models.

Acknowledgement

This Grid Modernization Laboratory Consortium (GMLC) project was supported by the U.S. Department of Energy (DOE) Office of Electricity Delivery and Energy Reliability as part of Advanced Grid Modeling Program. The authors gratefully thank Dr. Ali Ghassemian from DOE for his continuing support, help and guidance. Pacific Northwest National Laboratory is operated for the U.S. Department of Energy by Battelle Memorial Institute under Contract DE-AC05-76RL0 1830.

Contents

Abstract	v
Acknowledgement	vi
Contents	1
Figures	5
Tables.....	10
1.0 Background and Task Definition.....	12
1.1 Background	12
1.2 Tasks and Deliverables.....	13
2.0 Description of Data Source for Estimating Next-Generation Regional Level Load Composition	15
2.1 Introduction	15
2.2 Data Sources.....	15
2.2.1 Summary of Residential End-Use Load Consumer Assessment Program	15
2.2.2 Summary of Load Shape Library (LSL)	16
2.2.3 Summary of Northwest Energy Efficiency Alliance (NEEA) Residential Building Stock Assessment (RBSA) Data	18
2.2.4 Summary of Market Analysis and Information System (MAISY) Utility Customer Energy Use and Hourly Load Databases	19
2.2.5 Summary of Energy Consumption Surveys by U.S. Energy Information Administration (EIA)	19
3.0 Estimation of Residential Load Composition Using Weighted Difference Approach	21
3.1 Introduction	21
3.2 Climate Zone	22
3.3 Re-Categorization of LSL's RBSA End-Uses	25
3.4 Generation of ELCAP-format Load Shape Data Using LSL's RBSA Database	26
3.5 Popularization of the RBSA Load Shapes	29
3.6 Summary	30
4.0 Estimation of Residential Load Composition Using Cross-Correlation Method	32
4.1 NEEA RBSA Data	32
4.2 Model Development.....	32
4.2.1 End-Use Re-Categorization and Season Conditions	33
4.2.2 Cross-Correlation-Based Methodology.....	35
4.3 Results	36
4.4 Summary	38
5.0 Estimation of Residential and Commercial Load Composition Using Machine Learning Techniques.....	40
5.1 Introduction	40

5.2	Data	41
5.3	Methodology	41
5.4	Results	42
5.4.1	Development and Validation of Machine-Learning (ML) Models for Residential Load.....	42
5.4.2	ML Models for Residential and Commercial Cooling	49
5.4.3	Summary	52
5.5	Load Shape Estimation for Eastern Interconnection (EI) and Electric Reliability Council of Texas (ERCOT).....	52
5.5.1	Background	52
5.5.2	Target Zones: Eastern Interconnection and ERCOT.....	52
5.5.3	Weather Data of Eastern Climate Zones	53
5.5.4	Results	54
6.0	Aggregate Motor Protection Modeling.....	56
6.1	Background	56
6.2	Protection Methods	57
6.3	Typical Commercial Building Prototypes and Controls	59
6.4	EnergyPlus Simulation.....	61
6.5	Optimization-Based Protection Aggregation Algorithm.....	62
6.5.1	Protections: Mathematical Modeling	63
6.5.2	Aggregate Protection Modeling	65
6.5.3	Numerical Results	67
6.5.4	Summary	69
6.6	Cross-Categorical Transfer Learning Algorithm	69
6.6.1	Transfer Learning Problem Definition	69
6.6.2	Transferable Layers.....	69
6.6.3	Non-Transferable Layers.....	72
6.6.4	Numerical Results	73
7.0	Simulation Platform Development for Performance Data Extraction	76
7.1	Transmission and Distribution (T&D) Simulations	76
7.1.1	Introduction	76
7.1.2	Integrated T&D Dynamic Co-Simulation	77
7.1.3	Test System	78
7.1.4	Simulation Results.....	82
7.2	Commercial Feeder Modeled in GridLAB-D	87
7.2.1	Input Parameters.....	88
7.2.2	Matlab Codes.....	89
7.2.3	Output Files.....	89

7.2.4	Simulation Results.....	90
7.3	Commercial Feeder Model Modeled in PSCAD.....	93
7.3.1	Categorization of Motor Loads	93
7.3.2	Five Types of Protection	93
7.3.3	Voltage-Dependent Protection Schemes	95
7.3.4	Current Overload Protection	96
7.3.5	Thermal Protection.....	96
7.3.6	Capacitor Bank Over-Voltage Tripping	96
7.3.7	Study Cases	96
7.3.8	Summary	99
7.4	Residential Feeder Modeled in GridLAB-D	99
7.4.1	Identification of End-Use Loads in Residential Houses.....	100
7.4.2	Protection Models for Residential End-Use Motors	101
7.4.3	Motor Model and Mechanical Torque.....	102
7.4.4	Simulation Cases	103
7.4.5	Summary	107
8.0	Next Generation Load Model Data Tool	108
8.1	LMDT 2.0	108
8.1.1	Load Model Database.....	109
8.1.2	Rules of Association.....	110
8.1.3	Feeder Configuration.....	111
8.1.4	Motor Parameters Screen	111
8.1.5	Bus Data	112
8.1.6	Area/Zone/Owner Data	112
8.2	Load Model Creation Process Using Second-Generation LMMDT.....	113
8.2.1	Generate Load Records by Bus Level.....	114
8.2.2	Generate Load Records by Group	116
8.3	LMDT Version History	117
8.3.1	LMDT 2.1.....	117
8.3.2	LMDT 2.2.....	120
9.0	Investigation on Motor Progressive Tripping.....	123
9.1	Motor Progressive Tripping	123
9.2	Individual Unit Test	124
9.3	System-Level Test.....	129
10.0	Price Responsive Aggregate Load Model Development Plan.....	135
10.1	Berkeley Lab Residential Hourly Impact Analysis.....	142
10.2	Residential Demand Model Specification.....	143
10.3	LBNL Recommended Values for Price Elasticities	145

11.0 Load Model Calibration and Validation	148
11.1 Trial and Error Approach	148
11.1.1 Description of Micro-PMUs.....	148
11.1.2 Load Model Validation Process	149
11.1.3 Simulation Results.....	154
11.1.4 Summary	157
11.2 Machine Learning Approach.....	157
11.2.1 PSCAD Model.....	157
11.2.2 Validation Framework.....	159
11.2.3 Performance Results.....	163
12.0 Conclusions and Future Works.....	166
13.0 References	168

Figures

Figure 1.1 A Typical FIDVR Event [3]	13
Figure 1.2 Aggregate Composite Load Modeling	14
Figure 2.1 Typical Residential End-Uses Load Shape.....	18
Figure 3.1 Composite Load Model Data Requirements.....	21
Figure 3.2 Structure of LCM	22
Figure 3.3 Map Depicting Geographic Region for Each Climate Zone [16]	23
Figure 3.4 Geographical Segregation of Surveyed Cities	24
Figure 3.5 Original RBSA 15-min Interval Load Shape Extracted for NWC Climate Zone (in June).....	27
Figure 3.6 End-use Mapping Information and Representative Month for Each Type of Season	28
Figure 3.7 Generated Data Sheet Using RBSA Load Shape Database.....	28
Figure 3.8 Change of Component Fraction in the Load Composition Model for a Residential Feeder in NWC Climate Zone, Hot Summer Day, Hour = 16 (4:00pm)	29
Figure 3.9 Load Shapes of Appliance and Electronics End Uses for the Pacific Northwest 4 Climate Zones on a Hot Summer Day (Study Type = 2).....	29
Figure 3.10 Cooling Load Shapes for All 12 Climate Zones under New RBSA Dataset.....	30
Figure 3.11 Flow Chart of the Process to Update Residential Load Shapes.....	31
Figure 4.1 Flowchart of the Process for Updating LCM Residential Load Shape Data	33
Figure 4.2 Hot Summer , Cooling Load Shapes for Four Reference Climate Zones	36
Figure 4.3 Normal Summer (Left Two Subplots) and Hot Summer (Right Two Subplots), Cooling Load Shapes for Eight Target Climate Zones	37
Figure 4.4 Normal Summer , Vent Load for Eight Target Climate Zones	37
Figure 4.5 Normal Summer , Total Load for Eight Target Climate Zones.....	38
Figure 5.1 Marginal Distribution, Scatter Plots, and Cross-Correlation Coefficients between the NEEA RBSA Load Components and Weather Condition Variables. Pairs with Absolute Correlation Values <0.5 are Not Shown.	43
Figure 5.2 Time Series of Heating and Dew Point Temperature on Different Seasonal Conditions (Study Days, Day 1 = normal summer, Day 2 = hot summer, Day 3 = cool summer, Day 4 = shoulder (fall or spring), Day 5 = winter).	44
Figure 5.3 Heat Map of Absolute Pearson Correlation Coefficients among Load Components and Weather Attributes.....	45
Figure 5.4 PCA Biplot of All Load Components and Climate Condition Variables. Top: Observations Colored per Climate Zone; Bottom: Observation Points Colored by Seasons. ..	46
Figure 5.5 The RT Model for Heating	48
Figure 5.6 Test Accuracy of Heating by RF and RT Models	49
Figure 5.7 RT Model for Commercial Cooling	50
Figure 5.8 RT Model for Residential Cooling	51
Figure 5.9 Testing Accuracy of RT and RF Models of Cooling.....	51

Figure 5.10 Map Depicting Geographic Region for Each Climate Zone [50]	53
Figure 5.11 Western Temperature Time Series Plot.....	54
Figure 5.12 Eastern Temperature Time Series Plot	54
Figure 5.13 Cooling Estimation of Eastern United States for Day 2 (Hot Summer)	55
Figure 6.1 Typical Load Tripping Profile.....	56
Figure 6.2 Protection Parameters for Electronic Relays	57
Figure 6.3 Snapshot of Building Motor Loads and Protection Schemes.	58
Figure 6.4 Load Protection Profile for a Building Proto-type	60
Figure 6.5 Aggregation of Protection Profiles across All Building Types, Based on Floor-Space Ratios.....	60
Figure 6.6 Aggregated Protection Profile for Phoenix, AZ, for a Typical Day in January.....	61
Figure 6.7 Examples of Protection Diagrams for Various Protection Schemes. Black Region Denotes the Trip Zone.	64
Figure 6.8 Aggregate Protection Diagram and Load Tripping	65
Figure 6.9 Simplified Model of the Aggregate Protection Scheme	66
Figure 6.10 Simplified Aggregate Protection for Example 1.	68
Figure 6.11 True and Simplified Aggregate Protection Schemes for the Test Case in [63].	68
Figure 6.12 Architecture of the Transferable Layers	70
Figure 6.13 Change in Reconstruction Error and True Positive Rate (TPR) with Change in Encoding Dimension.....	71
Figure 6.14 Confusion Matrix of Feature Space of Dimension 30	71
Figure 6.15 Architecture of the Whole Proposed Framework (Combination of Transferable and Non-Transferable Layers).....	73
Figure 6.16 Comparison of Reconstruction Error and Training Epoch, with and without Transfer Learning	74
Figure 6.17 Error Histogram of Voltage Level at Faults and Motor Load Fraction	74
Figure 6.18 Simplified Protection Diagrams for Case1 with 20% Uncertainty.....	75
Figure 6.19 Simplified Protection Diagrams for Case2 with 10% Uncertainty	75
Figure 6.20 Simplified Protection Diagrams for Case3 with 20% Uncertainty.....	75
Figure 7.1 A Flowchart of Developing Enhanced Motor Protection Models Based on Integrated T&D Dynamic Simulation.....	76
Figure 7.2 The Interactions between the T&D Solvers: (Left) at Each Iteration Step of Power Flow Calculation; (Right) at Each Step of Network Solution during Dynamic Simulation.....	77
Figure 7.3 Iterative Information Exchange at Each Time Step.....	78
Figure 7.4 One-Line Diagram of the IEEE 39-Bus Test System.....	78
Figure 7.5 Case Summary of the IEEE 39-Bus Test System.....	79
Figure 7.6 One-Line Diagram of the Feeder GC-12.47-1.....	80
Figure 7.7 Illustration of Protection Parameter Setting of the Five Protection Types: (Top) Tripping Voltage and Time Delay; (Bottom) Reconnection Voltage and Time Delay	82
Figure 7.8 Phase A Voltages at Nodes meter_1, meter_2 and meter_3 in the Feeder	83

Figure 7.9 Trip Time and Reconnection Time for All Three Phase Motors	84
Figure 7.10 Aggregate Real Power of Three-Phase Induction Motors: (a) MA;(b) MB; (c) MC	85
Figure 7.11 Aggregate MVA of Non-Tripped Three-Phase Induction Motors: (a) MA;(b) MB; (c) MC	86
Figure 7.12 Normalized Fraction of Non-Tripped Three-Phase Induction Motors: (a) MA; (b) MB; (c) MC	87
Figure 7.13 Commercial Building Protection Parameters	88
Figure 7.14 Types of Commercial Buildings.....	88
Figure 7.15 Motor Parameters	89
Figure 7.16 Sample Output File.....	90
Figure 7.17 Zoomed-in Diagram of GC-12.47-1 Feeder	91
Figure 7.18 Rotor Speed of Motors in Large Office Building.....	92
Figure 7.19 Rotor Speed of Motors in Hotel Building.....	92
Figure 7.20 Schematic of Protection Logics	96
Figure 7.21 Distribution Feeder Schematic	97
Figure 7.22 IEEE 39 Bus Transmission System.....	97
Figure 7.23 Voltages at Bus 18 (Feeder Head) and Measurement Point	98
Figure 7.24 (a) Performance of thermal protection (P3) and contactor (P4) for Scenario A. (b) Performance of thermal protection (P3) for Scenario B, in a roof top unit fractional condenser motor in a medium size retail building	99
Figure 7.25 Implementation of Contactor Protection	102
Figure 7.26 Implementation of Thermal Protection.....	102
Figure 7.27 Triangular-Wave Mechanical Torque for A/C Compressor	103
Figure 7.28 Case 1: Mechanical Torque (T_{mech}), Terminal Current Magnitude ($ I_s $), Terminal Voltage Magnitude ($ V_s $), Electrical Torque (T_e) and Rotor Speed (w_r)	103
Figure 7.29 Case 2: Mechanical Torque (T_{mech}), Terminal Current Magnitude ($ I_s $), Terminal Voltage Magnitude ($ V_s $), Electrical Torque (T_e) and Rotor Speed (w_r)	104
Figure 7.30 Residential Feeder Model (SFH Stands for Single-Family Home; MFH Indicates Multi-Family Home).....	105
Figure 7.31 Phase-A Voltage at Node 45	106
Figure 7.32 A/C Compressor in Multi-Family Home 1: Motor Mechanical Torque (T_{mech}), Terminal Current Magnitude ($ I_s $), Terminal Voltage Magnitude ($ V_s $), Electrical Torque (T_e), Rotor Speed (w_r) and Stator Winding Temperature	107
Figure 8.1 LMDT 1.0 Main Graphical User Interface (GUI).	108
Figure 8.2 LMDT 2.0 Main Graphical User Interface (GUI).	109
Figure 8.3 Example of Commercial and Residential End Use Data.	110
Figure 8.4 Rules of Association Screen.	110
Figure 8.5 Feeder Configuration Setup.....	111
Figure 8.6 Motor Parameters.	112
Figure 8.7 Bus Data.	112

Figure 8.8 Area Data.....	113
Figure 8.9 Composite Load Model Records Creation (Steps 1-4).....	114
Figure 8.10 Composite Load Model Records Creation by Bus (Steps 5-8).....	115
Figure 8.11. Composite Load Model Records Creation by Bus (Step 9).....	115
Figure 8.12 Composite Load Model Records Creation by Group (Steps 5-8).....	116
Figure 8.13 Composite Load Model Records Creation by Group (Step 9).....	117
Figure 8.14 Configuration xml File Structure.....	118
Figure 8.15 Feeders xml Schema.....	118
Figure 8.16 Commercial Load xml Schema.	119
Figure 8.17 Residential Load xml Schema.	119
Figure 8.18 Motor Torque-Slip Characteristic Screen.....	120
Figure 8.19 Load Composition Pie Chart.	120
Figure 8.20 Climate Zone Definition Map.....	121
Figure 8.21 Presets for West, East and North America.	121
Figure 8.22 DG Screen.	122
Figure 9.1 Contactor Protection [92]	123
Figure 9.2 Controller Protection	124
Figure 9.3 Two-Bus System for Testing Individual MOTORLD Model	125
Figure 9.4 Motor Parameters	125
Figure 9.5 Contactor Test Results.....	126
Figure 9.6 Test Results of Controller Protection with Single Motor Trip Curve.....	127
Figure 9.7 Test Results of Controller Protection with Dual (Fastest and Slowest) Trip Curves	128
Figure 9.8 Test Results of Controller Protection with Dual Trip Curves under Two Successive Voltage Dips	129
Figure 9.9 One-Line Diagram of Minni-WECC. All Generators and High-Voltage Buses Shown [93].....	130
Figure 9.10 Two Forms of WECC Composite Load Model Formation	131
Figure 9.11 Fraction of Motor A Not Tripped in the Formulated Composite Load Model (idv) and PSLF Built-In Composite Load Model (cmpldw) at Bus 8	133
Figure 9.12 Fraction of Motor A Not Tripped in the Formulated Composite Load Model (idv) and PSLF Built-In Composite Load Model (cmpldw) at Bus 11	133
Figure 9.13 Voltages at Buses 82, 8, and 11 for Simulation Scenarios with the Two Forms of Composite Load Model Formation	134
Figure 10.1. Relationship between Major DR Opportunity and Change in End-Use Electricity Consumption by Customer Class.....	139
Figure 10.2 Hourly Average Load Impact Estimates for Voluntary TOU Treatments over all Weekday Non-holidays.....	143
Figure 11.1 Composite Load Model Validation Concept	148
Figure 11.2 Distribution PMU System Configuration [125]	149

Figure 11.3 Composite Load Model Creation	150
Figure 11.4 Implementation of Load Model Validation Tool	151
Figure 11.5 Distribution of Paired Deviations	153
Figure 11.6 Flowchart Implementation of Load Model Calibration Process.....	154
Figure 11.7 Schematic for Load Model Calibration	154
Figure 11.8 An Example of the Load Model Calibration (Event 1).....	155
Figure 11.9 An Example of the Load Model Calibration (Event 2).....	155
Figure 11.10 An Example of the Load Model Calibration (Event 3).....	156
Figure 11.11 Overall System Model and Feeder Configuration	158
Figure 11.12 Parameters Defining a Fault Scenario	159
Figure 11.13 Feeder Response for Various Simulation Cases.....	159
Figure 11.14 Single TT-GRU Architecture	161
Figure 11.15 Schematic of the Whole Proposed Framework	163
Figure 11.16 Performance Profile (V_{feeder} vs. P_{feeder}) of Predicted Composite Load Model (Dashed Line) and Detailed Feeder Model (Solid Line).....	164
Figure 11.17 Time Series Comparison of Feeder Head Active Power Produced by Detailed Feeder Model and Predicted Composite Load Model	165

Tables

Table 2.1 Key Features of Light Load Model Sourced to ELCAP	16
Table 2.2 Key Features of End-Use Load Shapes in Load Shape Library.....	17
Table 2.3 Features of End-Use Properties of the Energy Consumption Surveys	19
Table 3.1 WECC 12 Climate Zones.....	23
Table 3.2 Division of Surveyed Cities Based on Climate Zones	24
Table 3.3 Number of Sites (Houses) that Contain Each Specific End-Use	25
Table 3.4 Mapping from RBSA End-Uses to ELCAP End-Uses	26
Table 4.1 Mapping RBSA End Uses into LCM Categories.....	34
Table 4.2 Relation Between Months and Season Conditions	34
Table 4.3 Load Compositions in Per Unit for NWC Climate Zone Residential Composite Load Model.....	38
Table 5.1 Mutual Information among Load Components and Weather Attributes	47
Table 5.2 The Highest Accuracy Scores of RT Models and the Corresponding RT Model Complexity (i.e., Depths) for Each Load Component.	47
Table 5.3 Feature Importance in RT and RF Models for Cooling	50
Table 5.4 Eastern Climate Zones with Represent Cities.....	53
Table 6.1 Building Prototypes	62
Table 6.2 Test Case Protection Parameters.....	68
Table 6.3 Variation of Reconstruction Error with Different Tried Transferable Layer Architectures.....	72
Table 7.1 Basic Information of the Feeder GC-12.47-1	79
Table 7.2 Main Motor-Driven Appliances in the Large Office, Small Offices and Hotel.....	81
Table 7.3 Connection of the Three Types of Commercial Buildings	91
Table 7.4 Static Loads, Motor Loads and Associated Protections.....	94
Table 7.5 Algorithm of Voltage Dependent Protection	95
Table 7.6 End Uses in Single-Family and Multi-Family Homes.....	100
Table 7.7 Connection of 21 Residential Homes.....	105
Table 7.8 Protection Parameters	106
Table 9.1 Protection Parameters for Contactor Test	125
Table 9.2 Controller Protection Parameters for Single Motor Trip Curve.....	126
Table 9.3 Controller Protection Parameters for Dual (Fastest and Slowest) Motor Trip Curves ...	127
Table 9.4 Load Composition for Minni-WECC Load Models	132
Table 10.1 Count of Participants by Customer Class, DR Opportunity and State in WECC [100].....	136
Table 10.2 Potential Peak Demand Reduction (MW) by Customer Class, DR Opportunity, and State in WECC [100]	136
Table 10.3 Major WECC Regional DR Opportunities for Price Responsive Load Model [100] [101].....	137

Table 10.4 Major End-Uses Affected by DR Opportunities by Customer Class [101] [102]	137
Table 10.5. Elasticity Estimates by Customer Class, Retail Rate, Season and End-Use	142
Table 10.6 Own-Price Elasticity Estimation Groupings	144
Table 10.7 LBNL Recommended Values	145
Table 11.1 Priority List of Parameters	152
Table 11.2 Calibrated Parameters of the Composite Load Model	156
Table 11.3 Numerical Comparison of Results.....	157
Table 11.4 Time and Memory Comparison between Fully Connected and TT-Layer	162
Table 11.5 NIPALS Algorithm.....	162
Table 11.6 Names of Predicted Parameters	163

1.0 Background and Task Definition

1.1 Background

Modern power systems are facing a rapidly growing level of variability and uncertainty due to the increasing level of variable resources and random market forces. The performance of bulk power systems is analyzed using computer models that represent the systems' behavior under normal or abnormal conditions. Both technical and commercial segments of the industry must be confident that the simulation models and database are accurate and up to date. First, having realistic models is critical to ensuring reliable and economic power system operation. If transfer limits are set using overly optimistic models, a grid operator may operate the system beyond its capability, increasing the risk of widespread outages such as occurred during summer of 1996. If the models are too pessimistic, the operator may be overly conservative and impose unnecessary restrictions on system operating limits, increasing the risk of power shortages and higher costs in energy-deficient regions. Second, accurate representation of electrical loads is crucial to evaluating the vulnerability of the bulk system to instability in the seconds after a major system event. Third, correct models are essential to design and implement appropriate control responses and to make sure system operation satisfies the required contingency constraints.

Bulk power transmission system planning requires accurate models of all the major generation, transmission, and load components. Loads play an increasingly important role in power system dynamic stability and load representation has historically been the least accurate of the three components modeled to help control a system.

As the load changes during the day, the generators follow, and the power flows can be calculated. However, for historical reasons, most load models are based on time-invariant, voltage-dependent polynomial load representations. The loads may be represented as constant impedance (Z), constant current (I), or constant power (P). Recently it has been understood that these models no longer provide a true representation of the dynamic response of the load, particularly in view of the increased penetration of residential air conditioners in recent years. The problem stems from load models not capturing the electromechanical behavior of modern motors and load-protection devices in the moments after a fault occurs on the power system.

A fault-induced delayed voltage recovery (FIDVR) event is the phenomenon in which system voltage remains at significantly reduced (inadequate) levels for several seconds after a transmission, sub-transmission, or distribution fault has been cleared. Such faults have increased significantly in Southern California and Florida over the past several years.

A typical FIDVR event is depicted in Figure 1.1. The effect is thought to be caused by the stalling of highly concentrated single-phase induction-motor loads with constant or reciprocating mechanical torque in response to low voltage [1] [2]. The stalled motors draw more reactive power from the grid, holding the local voltage down, which results in a vicious cycle: After several seconds of being stalled, motors' protection devices trip the motors to prevent them from overheating. As a result, there is a large decrease in the load on the power system, with a potential secondary effect of high system voltage ("power bump"). That bump is particularly likely if the protection response is slower than the voltage regulation response of the system. Once the system finally catches up to events and reduces power to the grid, the protection devices of motors just coming back online trip again, and the cycle starts once more. The fact that FIDVR events are not well represented in power system studies has increased interest in load modeling, particularly of loads with a high penetration of motors, because dynamic load behavior profoundly influences the system dynamic response.



Figure 1.1 A Typical FIDVR Event [3]

IEEE provided initial guidance on load modeling in the early 1990s. The Western Electricity Coordinating Council (WECC) has long recognized the need for better load modeling and has undertaken significant efforts to improve load representation in dynamic simulations. An “interim” load model [4] was approved in early 2000’s and the model had 20% of load represented as induction motors across the entire system and for all study conditions. The motor load was still connected at a high-voltage transmission bus. The “interim” model was developed to address operational issues on the California-Oregon Intertie made apparent by the 1996 outages. During the approval process, WECC emphasized the “interim” nature of the model and argued the need for more comprehensive load modeling. It was recognized that the advance of computing capability would permit significant improvements beyond the interim model. The experience gained since the development of this new model has confirmed that the improvements were both possible and greatly needed.

WECC’s Modeling and Validation Work Group (MVWG)/ Load Modeling Task Force (LMTF) led the development of the composite load model for dynamic simulations. The composite load model is implemented in GE PSLF [5] and Siemens PTI PSS/E [6]. Comparable models are being developed in PowerWorld Simulator [7] and PowerTech’s TSAT programs [8]. Eastern Interconnection and Electric Reliability Council of Texas (ERCOT) have been monitoring and participating in load modeling activities in recent years as well.

1.2 Tasks and Deliverables

This report is prepared to answer the need for a fundamentally different, new class of load models and next generation of data tools. Such tools can provide improved outcomes compared with existing ones. PNNL aims to address the new load trends to handle the increasing proliferation of electronics loads and residential air conditioner loads, the emerging trends of price-responsive demand, and the growing importance of protective devices in equipment and buildings. Moreover, the PNNL research team has developed an aggregate motor protection model to augment and enhance the composite load model. Further, we intend to address the data challenges embodied in these phenomena. The planned next-

generation regional load composition data model and Load Model Data Tool will incorporate these many changes to the current model, enhancing the supply of power to consumers throughout the U.S.

The accomplished deliverables include:

- An updated load shape database with respect to residential sector power consumption for Western Electricity Coordinating Council (WECC), Eastern Interconnection (EI) and Electric Reliability Council of Texas (ERCOT)
- Electro-magnetic transient (EMT) distribution feeder models implemented in PSCAD and GridLAB-D for data extraction and model validation.
- Aggregate motor protection model implemented by Matlab code to generate two-dimensional protection profile for motor components in WECC composite load models
- Trial-and-error and machine-learning based approaches for building initial prototype of load model validation tool
- Development plan report of price responsive aggregate load model
- The second-generation load model data tool (LMDT) for open-source distribution

Four tasks are defined in this project. The major deliverables of these four tasks are correlated and represented in Figure 1.2, which shows the essential elements of the aggregate composite load model and the key approaches to achieve these elements.

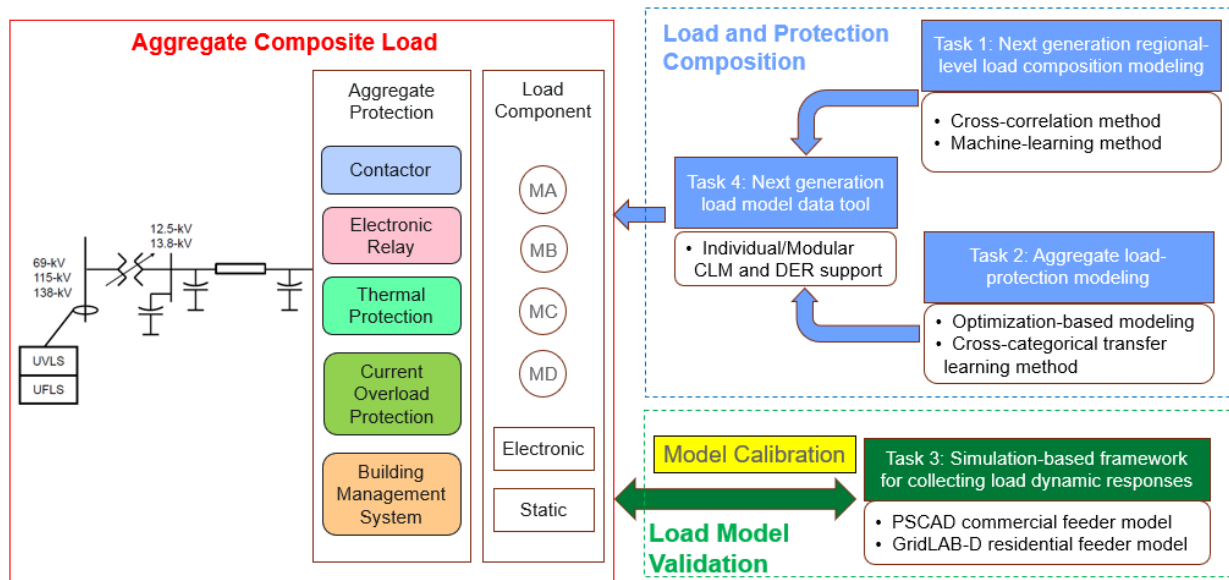


Figure 1.2 Aggregate Composite Load Modeling

2.0 Description of Data Source for Estimating Next-Generation Regional Level Load Composition

2.1 Introduction

Because power planning and operation tasks heavily depend on static and dynamic simulation studies, adequate and accurate power system models play an essential role. Inaccurate, incomplete or insufficient load models can significantly skew study results, leading to conclusions that deviate from reality and faulty system designs and decision making. Poor modeling can also have severe consequences such as power outage or cascading faults and system failures. The number of FIDVR events has been increasing in Southern California, Tennessee, Kansas and Florida since the late 1980s and early 1990s. On July 2, 1996, voltage instability resulted from the loss of steady state equilibrium conditions caused by reactive power deficiency in the Idaho area. The power failure affected parts of Alberta and British Columbia, western Mexico, Idaho, Montana, Utah, New Mexico, California, and Arizona, impacting more than two million people. Moreover, with recent rapid development of smart grid technologies, over 50 million smart meters had been deployed in the US, reaching 43% of US families according to Edison Foundation's Institute for Electric Innovation 2014 report [9]. This number is consistently increasing from 7 million since 2007, and will continue to increase in the near future, which will increase price responsive demand coverage tremendously every year. It brings new challenges and requirements to the load modeling.

Load composition modeling will include:

1. Aggregating distribution loads according to standard load classes
2. Specifying the types of devices comprised by those load classes
3. Assigning the appropriate composition of the aggregated load to the various components of a suitable load model structure

This approach uses a common load model structure and associated set of parameter values throughout the system model. What is changed throughout the system model is the percentage composition (e.g., percentage motor load versus static load) from bus to bus. In most cases, even this percentage composition may be kept constant throughout the system model because of the lack of better knowledge.

The bottom-up method for load composition estimation uses results from building population surveys, building simulations, and end-use metering programs to develop estimates for the fractions of loads that are operating at any given time. Typically, the data collected is separated hierarchically by customer class, building type, and end-use type, which includes residential, commercial, industrial, and agricultural loads broken down in facility types.

2.2 Data Sources

2.2.1 Summary of Residential End-Use Load Consumer Assessment Program

The Bonneville Power Administration (BPA) conducted the End-use Load and Consumer Assessment Program (ELCAP) from 1986 through 1989 and obtained hourly and sub-hourly electricity demand information from a variety of residential and commercial end uses. The original residential-sector load consumption data from ELCAP were processed and utilized in the development of light load composition model in our previous research effort [3]. The currently adopted light load composition model sourced to

ELCAP contains hourly load shapes of 12 end uses in 12 WECC climate zones and 5 typical seasons. A brief summary of the features of light load model sourced to ELCAP is tabulated in Table 2.1.

Table 2.1 Key Features of Light Load Model Sourced to ELCAP

<i>Residential End Uses</i>	<i>Climate Zones in WECC Region</i>	<i>Study Day Type</i>
<ul style="list-style-type: none"> ▪ Heating ▪ Cooling ▪ Vent ▪ Water Heat ▪ Cooking ▪ Refrigeration ▪ External Lighting ▪ Internal Lighting ▪ Electronics ▪ Appliances ▪ Miscellaneous ▪ Vehicle 	<ul style="list-style-type: none"> ▪ Northwest Coast (NWC) ▪ Northwest Valley (NWV) ▪ Northwest Inland (NWI) ▪ Rocky Mountain North (RMN) ▪ Northern California Coast (NCC) ▪ Northern California Valley (NCV) ▪ Northern California Inland (NCI) ▪ Southern California Coast (SCC) ▪ Southern California Valley (SCV) ▪ Southern California Inland (SCI) ▪ Desert Southwest (DSW) ▪ High Desert (HID) 	<ul style="list-style-type: none"> ▪ Normal Summer (index=1) ▪ Hot Summer (index=2) ▪ Cool Summer (index=3) ▪ Shoulder (index=4) ▪ Winter (index=5)

The ELCAP residential load shape data generally become obsolete because of increasing penetration of electronics loads, enlarged capacity of residential air conditioner loads, and increase in equipment efficiency in recent years. Newer data sources need to be discovered to derive residential load composition for next-generation regional level WECC composite load models. Several up-to-date power and energy consumption data sources are introduced in the next sub-chapters. Some of them are used in this project.

2.2.2 Summary of Load Shape Library (LSL)

Load Shape Library has been developed and maintained by Electric Power Research Institute (EPRI) since 2010. The end-use load shape data contained in the tool was obtained from simulations using the EPRI NESSIE (National Electric System Simulation Integrated Evaluator) model platform. The inputs to NESSIE were derived from data estimation conducted by the U.S. Energy Information Agency's (EIA's) National Energy Modeling System (NEMS) and derived from data collected by EPRI through laboratory testing and research [10].

The tool stores hourly end-use load data of three sectors for thirteen North American Electric Reliability Corporation (NERC) regions and six season and day types. The three sectors include commercial, residential and industrial end-uses. Several end-use load types are characterized for each sector. Table 2.2 is generated to generalize all considered features of end-use load shapes in EPRI's LSL.

Table 2.2 Key Features of End-Use Load Shapes in Load Shape Library

<i>Sectors</i>	<i>Regions</i>	<i>Season and Day Type</i>
Residential	<ul style="list-style-type: none"> • Central Air Conditioning (CAC) • Clothes Dryer • Clothes Washer • Dishwasher • Heating • Lighting • Refrigerator • Television & Personal Computing (TV & PC) • Water Heating 	<ul style="list-style-type: none"> • East Central Reliability Coordination Agreement (ECAR) • Electric Reliability Council of Texas (ERCOT) • Mid-Atlantic Area Council (MAAC) • Mid-America Interconnected Network (MAIN) • Mid-Continent Area Power Pool (MAPP) • Northeast Power Coordinating Council – New York (NPCC/NY)
Commercial	<ul style="list-style-type: none"> • Cooling • Heating • Lighting, External • Lighting, Internal • Office Equipment • Refrigeration • Ventilation • Water Heating 	<ul style="list-style-type: none"> • Northeast Power Coordinating Council – New England (NPCC/NE) • Southeast Reliability Council (non-Florida) (SERC/STV) • Southeast Reliability Council (Florida) (SERC/FL) • Southwest Power Pool (SPP) • Western States Coordinating Council – Northwest (WSCC/NWP)
Industrial	<ul style="list-style-type: none"> • HVAC • Lighting • Machine Drives • Other • Process Heating 	<ul style="list-style-type: none"> • Western States Coordinating Council – Rocky Mountain Area (WSCC/RA) • Western States Coordinating Council – California/Nevada (WSCC/CNV)

A typical load shape curve can be shown in Figure 2.1 below. The peak power consumption of the selected end-use loads is scaled to 1 kW. The actual power consumed by end-uses are obtained by multiplying the scaled load shape time series with a pre-determined scaling factor to match real load profile.

Load Shape of Residential End-Uses in WSCC/NWP Region during Peak Summer Day

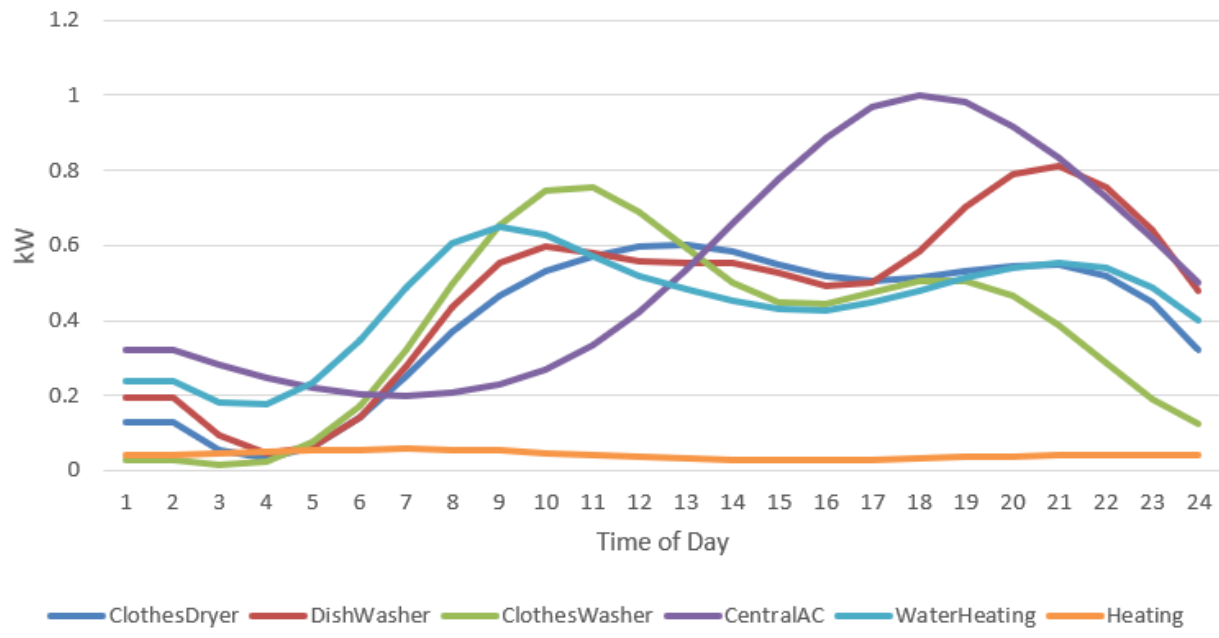


Figure 2.1 Typical Residential End-Uses Load Shape

Several pros and cons of Load Shape Library are highlighted:

- End-use load shapes can be used by utilities to develop applications in load forecasting, integrated resource planning (IRP), and demand-side management (DSM) evaluations.
- Load Shape Library provides best-available data. The confidence and accuracy of the data are unknown.
- End-use data does not capture behavioral and other unobservable effects, in which case metered data would be the preferred choice of the industry.

2.2.3 Summary of Northwest Energy Efficiency Alliance (NEEA) Residential Building Stock Assessment (RBSA) Data

Northwest Energy Efficiency Alliance sponsored this residential building stock assessment study [11] to develop an inventory and profile of existing residential building stock in the Pacific Northwest based on field data from a representative, random sample of existing homes. The RBSA study was conducted across four states (WA, OR, ID, MT) for three categories of residences: single-family homes, manufactured homes, and multifamily homes. EPRI collaborated with NEEA to incorporate the RBSA load shape study results into EPRI's Load Shape Library (LSL). The dataset used in Load Shape Library 4.0 comprises of 103 single-family residential premises with 15-min interval end-use metered data. The data ranges from April 2012- March 2013. The raw RBSA load shape data from NEEA website and the processed RBSA data stored in EPRI's LSL 4.0 are both downloaded and used in this project.

2.2.4 Summary of Market Analysis and Information System (MAISY) Utility Customer Energy Use and Hourly Load Databases

The MAISY database [12] incorporates large utility customer load consumption data for each state and utility service area. It contains individual customer record energy use and end-use data including 8760 hourly and 15-minute interval loads. The database records commercial and residential customer data covering different business categories (medical office, fast food restaurant, etc.) and various house types (single-family, multi-family, mobile homes, etc.). Detailed segmentation and deep drill-down capabilities are highlighted in development of the database. The data are stored and rendered in either Excel workbooks or EnergyApps software. The MAISY database has been applied by over 100 organizations for technology and energy-related market analysis, product development and assessment, cost-of-service studies, energy efficiency, smart grid analysis.

2.2.5 Summary of Energy Consumption Surveys by U.S. Energy Information Administration (EIA)

U.S. Energy Information Administration [13] publicized energy consumption survey data of residential, commercial and manufacturing sectors. The residential energy consumption survey (RECS) collects total annual energy consumption data of housing units, based on end-uses, for the entire U.S. and for different census regions and divisions. The number of housing units, and average consumption per housing unit are also available. The commercial building energy consumption survey (CBECS) documents statistics of commercial end-use electricity consumption for different commercial building types, census regions and divisions. The manufacturing energy consumption survey (MECS) provides statistic electricity (and other fuel) consumption information for a variety of end-uses in different manufacturing industries and in different regions. Table 2.3 summarizes the properties of these series of energy consumption surveys regarding the end-use statistics.

Table 2.3 Features of End-Use Properties of the Energy Consumption Surveys

	RECS	CBECS	MECS
Year	2009	2012	2010
End-uses	<ul style="list-style-type: none">• Space heating• Water heating• Air-conditioning• Refrigerators• Other appliances (not shown separately, including: cooking appliances, clothes washers, dryers, dishwashers, televisions, computers, small electronic devices, pools, hot tubs, and lighting)	<ul style="list-style-type: none">• Space heating• Cooling• Ventilation• Water heating• Lighting• Cooking• Refrigeration• Office Equipment (e.g. computers, servers, copiers, FAX machines, cash registers, printers, mainframe computer systems, typewriters)• Computing• Other	<ul style="list-style-type: none">• Conventional boiler use• Process heating• Process cooling and refrigeration• Machine drive• Electro-chemical processes• Other process use• Facility HVAC• Facility lighting• Other facility support• Onsite transportation• Other non-process use

Housing or building or industry types	<p>Housing:</p> <ul style="list-style-type: none"> • Single-family • Multi-family • Mobile homes 	<p>Commercial Buildings:</p> <ul style="list-style-type: none"> • Education • Food sales • Food service • Health care • Lodging • Mercantile • Office • Public assembly • Public order and safety • Religious worship • Service • Warehouse and storage • Other • Vacant 	<p>Industries:</p> <ul style="list-style-type: none"> • Food • Beverage and tobacco products • Textile and product mills • Apparel • Leather and allied products • Wood products • Paper • Printing and related support • Petroleum and coal products • Chemicals • Plastics and rubber products • Nonmetallic mineral products • Primary metals • Fabricated metal products • Machinery • Computer and electronic products • Elec. equip., appliances, components • Transportation equipment • Furniture and related products • Miscellaneous <p>(Note: detailed industry sub-categories are not listed)</p>
Regions and divisions	<ul style="list-style-type: none"> • West (Mountain north / south, Pacific) • Northeast (New England, Middle Atlantic) • Midwest (East / West North Central) • South (South Atlantic, East / West South Central) 	The same as RECS	<ul style="list-style-type: none"> • West • Northeast • Midwest South • South
Relevant contents	<ul style="list-style-type: none"> • Total energy consumption (Btu) • Average energy consumption (Btu/house) • Number of houses 	<ul style="list-style-type: none"> • Total electricity consumption (kWh) • Electricity energy intensity (kWh/sqft) 	<ul style="list-style-type: none"> • Net demand for electricity (kWh) • Other fuel consumption (Not relevant to our research goal)

3.0 Estimation of Residential Load Composition Using Weighted Difference Approach

3.1 Introduction

The WECC LMTF led development and implementation of a composite load model (CMPLDW in PSLF; CMLDBLU1 in PSS/E) [14] to replace simpler load models previously used in most popular transmission-level power system simulation programs. The composite load model includes distribution feeder equivalent data (e.g., substation transformer characteristics, feeder equivalent impedances), load component parameters (e.g., motor impedances, time constants and inertias), load model composition data (e.g., fractions of motor, static and electronic loads) and protection parameters [3]. An illustration is shown in Figure 3.1.

Traditionally, measurement-based approaches to characterize composite load models introduced a top-down method in which a load model structure is defined, and the component compositions are estimated directly from field measurement data [15]. The major limitations of this top-down approach include (a) insufficient disturbance data suitable for estimating load model composition, and (b) multiple solutions to the optimization problem, resulting in more than one estimated composition sets.

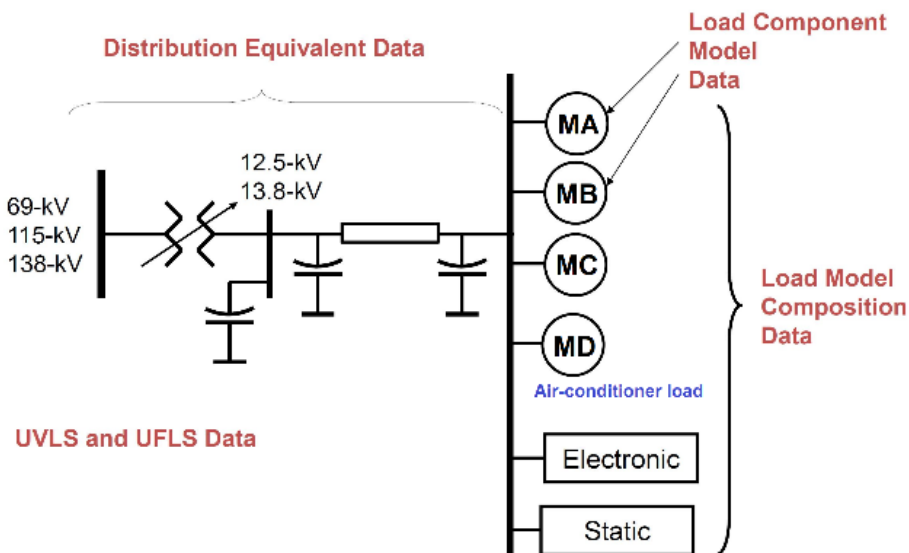


Figure 3.1 Composite Load Model Data Requirements

A bottom-up approach, based on building population surveys, building simulations, and end-use metering programs, was previously proposed by WECC LMTF to estimate the fractions of different load components, such as motors, constant impedance/current/power loads, and electronic loads at any given time [3] [16]. PNNL in collaboration with the BPA developed an Excel version of the load composition model (LCM) using the bottom-up approach. For commercial buildings in the LCM, the California Commercial End-Use Survey (CEUS) was used as the primary source for commercial load composition [17]. For residential loads, the End-use Load and Consumer Assessment Program (ELCAP) data were used to estimate load composition [18] [19]. Figure 3.2 shows the implementation of the Excel LCM. The final outputs of LCM are the load fractions of different components in the composite load model illustrated by Figure 3.1.

The ELCAP was a major data collection program undertaken by the BPA from 1983 through 1990 to obtain metered end-use power consumption data in residential and commercial sectors. The 1983-1990 ELCAP data provides an overview of power consumption patterns in residential homes in the Pacific Northwest. The residential load shape data in the initial prototype of LCM were derived from ELCAP data. The ELCAP was conducted in the late 1980's and the data are now outdated. In addition, growing penetration of electronic loads in residential homes spurs the update of load shape data in the new version of LCM.

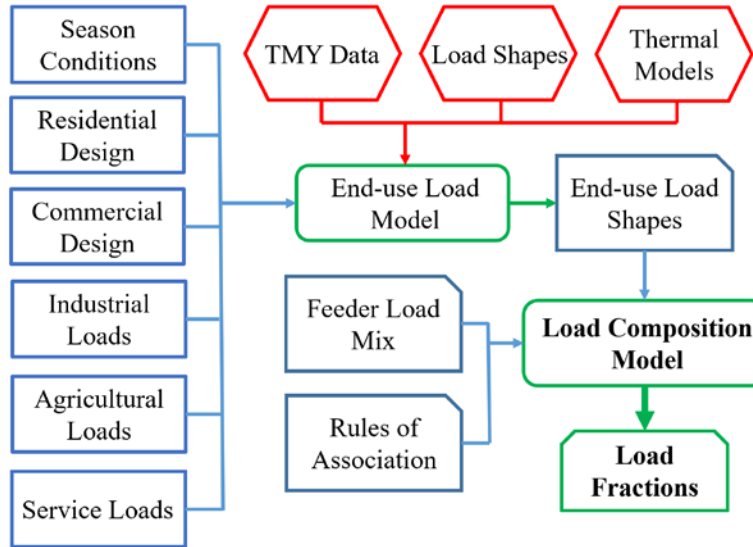


Figure 3.2 Structure of LCM

Chapters 3 – 5 present PNNL’s current efforts to update the residential load composition data in the LCM using recent data sources and various mathematic algorithms. The studies utilize the recent load shape results from the residential building stock assessment (RBSA) study sponsored by the Northwest Energy Efficiency Alliance (NEEA). The WECC interconnection system includes a total of 12 climate zones. The NEEA RBSA study was only conducted in the Pacific Northwest regions, consisting of four typical climate zones. For the other eight WECC climate zones, up-to-date residential load shape data are currently unavailable and need to be derived using existing data sources.

3.2 Climate Zone

This section discusses the divisions of WECC climate zones and definitions of five season conditions. The LCM datasets include load composition for 12 climate zones in WECC, shown in Table 3.1, and 5 types of season conditions, including normal summer, hot summer, cool summer, shoulder (spring or fall), and winter [3].

The first four climate zones in Table 3.1 are labeled as reference climate zones, which include the cities in the region of NEEA RBSA study and have the RBSA load shape data available. The other eight climate zones are defined as target climate zones, which do not have direct measurement data. Table 3.1 also shows the number of cities participating in the NEEA RBSA study and their distribution in the four reference climate zones [20]. Figure 3.3 shows approximate boundaries for WECC climate zones.

Table 3.1 WECC 12 Climate Zones

	ID	Climate Zone	Number of Surveyed Cities
Reference Climate Zones	NWC	Northwest Coast	21
	NWV	Northwest Valley	13
	NWI	Northwest Inland	25
	RMN	Rocky Mountain North	7
Target Climate Zones	NCC	Northern California Coast	N/A
	NCV	Northern California Valley	N/A
	NCI	Northern California Inland	N/A
	SCC	Southern California Coast	N/A
	SCV	Southern California Valley	N/A
	SCI	Southern California Inland	N/A
	DSW	Desert Southwest	N/A
	HID	High Desert	N/A

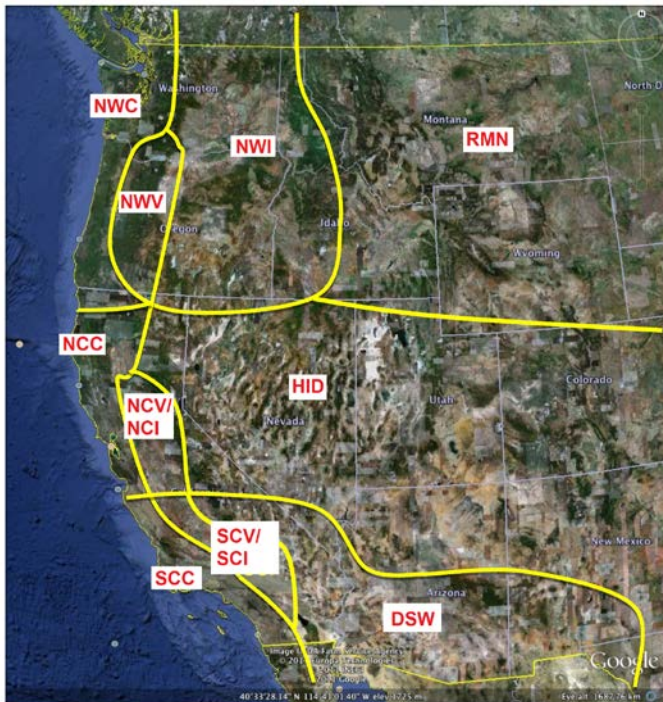


Figure 3.3 Map Depicting Geographic Region for Each Climate Zone [16]

The ELCAP load shape data reflect power consumption pattern of Pacific Northwest residential homes back in 1980's and gradually become outdated. The RBSA load shape data implemented in EPRI's LSL 4.0 provides an overview of residential load profiles in Pacific Northwest for the year 2012-2013. The LSL-version RBSA data are used in this chapter to update the residential load shapes in the existing Load Composition Model (LCM). A total of 66 cities participated in the RBSA study. Each city contains

at least one representative surveyed house. There are totally 103 houses distributed in the 66 cities. Based on the geographical locations, the 66 cities are divided into 4 climate zones as shown in Table 3.2 and Figure 3.4. It is noted that each sampled house may not output a full set of end-use load information. The number of houses that contain each of the end-uses are listed in Table 3.3 if all the surveyed cities are selected in EPRI's LSL 4.0. The average load shape of an end-use in a house is generated based on the number of houses that have this end-use.

Table 3.2 Division of Surveyed Cities Based on Climate Zones

66 cities in Load Shape Library	
NWC Region (21 cities)	
WA: Seattle WA, Tacoma WA, Tenino WA, Burien WA, Bainbridge Island WA, Kirkland WA, Olympia WA, Arlington WA, Bothell WA, Mill Creek WA, Lynnwood WA, Bellingham WA, Oak Harbor WA, Puyallup WA, Mountlake Terrace WA, Bellevue WA, Renton WA, Fox Island WA OR: Bandon OR, Brookings OR, South Beach OR.	
NWV Region (13 cities)	
OR: Eugene OR, Lebanon OR, Albany OR, Jefferson OR, Monmouth OR, Salem OR, McMinnville OR, Carlton OR, Dundee OR, Hillsboro OR, Beaverton OR, Lake Oswego OR, Portland OR	
NWI Region (25 cities)	
WA: Kettle Falls WA, Okanogan WA, Newport WA, East Wenatchee WA, Wenatchee WA, Moses Lake WA, Cheney WA, Airway Heights WA, Spokane WA, Spokane Valley WA, Yakima WA, Grandview WA, West Richland WA, Kennewick WA, ID: Coeur d'Alene ID, Moscow ID, Lewiston ID, Emmett ID, Caldwell ID, Nampa ID, Kuna ID, Meridian ID, Boise ID, Mountain Home ID, Sandpoint ID	
RMN Region (7 cities)	
MT: Hamilton MT, Cascade MT, Helena MT, Whitehall MT, Bozeman MT ID: Shoshone ID, Jerome ID	

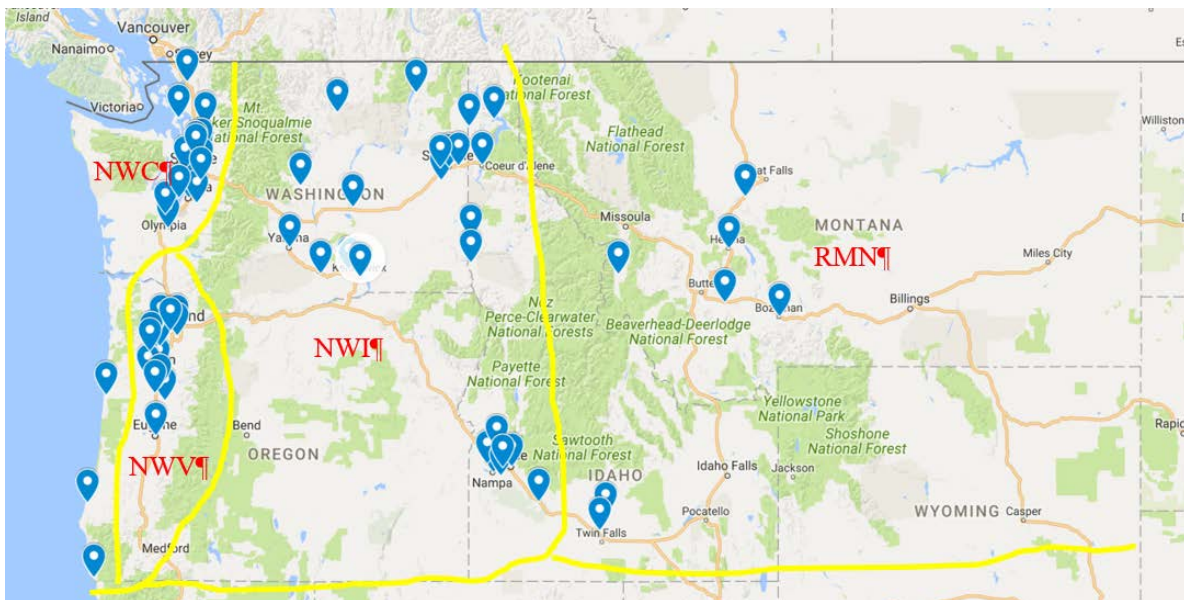


Figure 3.4 Geographical Segregation of Surveyed Cities

Table 3.3 Number of Sites (Houses) that Contain Each Specific End-Use
Month=12, Workday and Weekend, All Area (NWC+NWV+NWI+RMN)

RBSA Type	Appliance Type	Sites (Houses)
Premise Total	Premise kWh	103
HVAC	Central Heating	6
HVAC	Air Source HP	20
HVAC	Packaged Terminal HP	1
HVAC	Ductless Space HP	3
HVAC	Central AC	26
HVAC	Packaged Terminal AC	1
HVAC	Ground Source HP	1
HVAC	Air Handler	2
Water Heater	Electric Resistance WH	57
Water Heater	Heat Pump WH	2
Portable Heating and Cooling	Room Heater(s)	45
Refrigeration	Refrigerator	102
Refrigeration	Freezer	46
Cooking	Oven	68
Cooking	Microwave	2
Laundry & Dishwashing	Dryer	98
Laundry & Dishwashing	Washer	96
Laundry & Dishwashing	Dishwasher	63
Entertainment	Gaming Console	32
Entertainment	TV & Accessories	99
Entertainment	Cable Box & DVR	46
Entertainment	Home Audio	9
Computer	Computer & Accessories	86
Lighting and Other	Interior Lighting	93
Lighting and Other	Exterior Lighting	13
Lighting and Other	Other	58

3.3 Re-Categorization of LSL's RBSA End-Uses

The LSL's RBSA load shape data have more specific categories of end use than ELCAP data. In order to align RBSA data with ELCAP data, the RBSA end-uses need to be re-categorized to match the ELCAP end-use types. This re-categorization not only facilitates the update of load shape data but also preserves the structure of the load shape database that is linked to PNNL's Load Model Data Tool (LMDT). Table 3.4 displays some details of this re-categorization.

Table 3.4 Mapping from RBSA End-Uses to ELCAP End-Uses

RBSA End-Use Categories	RBSA Appliances	Mapped to ELCAP End-Uses
HVAC	Central Heating	Heating
HVAC	Air Source HP	Vent
HVAC	Packaged Terminal HP	Cooling
HVAC	Ductless Space HP	Vent
HVAC	Central AC	Cooling
HVAC	Packaged Terminal AC	Cooling
HVAC	Ground Source HP	Vent
HVAC	Air Handler	Vent
Water Heater	Electric Resistance WH	Water Heat
Water Heater	Heat Pump WH	Water Heat
Portable Heating and Cooling	Room Heater(s)	Heating
Portable Heating and Cooling	Window AC	Cooling
Refrigeration	Refrigerator	Refrigeration
Refrigeration	Freezer	Refrigeration
Cooking	Oven	Cooking
Cooking	Microwave	Cooking
Laundry & Dishwashing	Dryer	Appliance
Laundry & Dishwashing	Washer	Appliance
Laundry & Dishwashing	Dishwasher	Appliance
Entertainment	Gaming Console	Electronics
Entertainment	TV & Accessories	Electronics
Entertainment	Cable Box & DVR	Electronics
Entertainment	Home Audio	Electronics
Computer	Computer & Accessories	Electronics
Lighting and Other	Interior Lighting	Interior Lighting
Lighting and Other	Exterior Lighting	Exterior Lighting
Lighting and Other	Other	Misc.

3.4 Generation of ELCAP-format Load Shape Data Using LSL's RBSA Database

The RBSA load shape data of each climate zone is manually downloaded from EPRI's LSL 4.0 by selecting corresponding surveyed cities in that zone. The load shape data are prepared on a monthly basis to give some flexibility for choosing the type of season to be studied. An example of original RBSA 15-min interval load shape data is demonstrated in Figure 3.5. Column 2 of Figure 3.5 lists the types of RBSA end-use appliances that need re-categorization to match ELCAP end-use types.

Month=6								
RBSA Type	Appliance Type	Avg Value At 0:00	Avg Value At 0:15	Avg Value At 0:30	Avg Value At 0:45	Avg Value At 1:00	Avg Value At 1:15	Avg Value At 1:30
Premise Total	Premise kWh	0.211937086	0.203661249	0.199255774	0.193613345	0.183917878	0.176201882	0.172035928
HVAC	Central Heating	0.012473118	0.007777778	0.008444444	0.008777778	0	0.012777778	0
HVAC	Air Source HP	0.076	0.079199999	0.087733333	0.082266667	0.091666666	0.093266666	0.089599999
HVAC	Packaged Terminal HP	0.005483871	0.008	0.005666667	0.007666666	0.006	0.007333333	0.006666667
HVAC	Ductless Space HP	0.002688172	0.002888889	0.002888889	0.002111111	0.003	0.002555555	0.002777778
HVAC	Central AC	0	0	0	0	0	0	0
HVAC	Air Handler	0.000645161	0.001333333	0.001	0.000333333	0.000666667	0.002333333	0.001
Water Heater	Electric Resistance WH	0.046912443	0.043111111	0.046968254	0.043714286	0.032396825	0.033412698	0.030111111
Portable Heating and Cooling	Room Heater(s)	0.012404305	0.009555607	0.010055035	0.011065205	0.0104256	0.009406748	0.012344673
Portable Heating and Cooling	Window AC	0.012469226	0.014133514	0.011729703	0.011505978	0.012205089	0.011230169	0.009661497
Refrigeration	Refrigerator	0.01795422	0.017425723	0.017741214	0.017896694	0.016790043	0.016905015	0.016611531
Refrigeration	Freezer	0.013681619	0.012874213	0.012296297	0.012725148	0.012110077	0.012308456	0.013008136
Cooking	Oven	0.000705645	0.000354167	0.000375	0.000354167	0.000375	0.0003125	0.0003125
Laundry & Dishwashing	Dryer	0.007605381	0.006088971	0.003188137	0.005254866	0.004244671	0.002335496	0.001556997
Laundry & Dishwashing	Washer	0.000891057	0.0007068	0.00051701	0.000331219	0.000291414	0.000246349	0.000283407
Laundry & Dishwashing	Dishwasher	0.004738462	0.00327504	0.00391097	0.003847377	0.00290938	0.001955485	0.002750397
Entertainment	Gaming Console	0.00375475	0.003547146	0.003445204	0.003265761	0.003285724	0.003301479	0.003231021
Entertainment	TV & Accessories	0.006922724	0.006042602	0.005363461	0.004813651	0.004428593	0.003894714	0.003727413
Entertainment	Cable Box & DVR	0.005926759	0.005919691	0.005914428	0.005912703	0.005906739	0.005905324	0.00590327
Computer	Computer & Accessories	0.010239035	0.01013229	0.010089744	0.009973415	0.009813642	0.009575765	0.009645685
Lighting and Other	Interior Lighting	0.008837943	0.007697209	0.005653178	0.004018749	0.003149463	0.002729138	0.002460416
Lighting and Other	Exterior Lighting	0.003866156	0.003739052	0.003750286	0.003752246	0.003714397	0.003755187	0.003782841
Lighting and Other	Other	0.036539486	0.039953103	0.038084759	0.038518944	0.036629605	0.030588762	0.031283459

Figure 3.5 Original RBSA 15-min Interval Load Shape Extracted for NWC Climate Zone (in June)

The type of season is opted for by designating representative month as shown in Figure 3.6. An Excel Visual Basic for Applications (VBA) Macro called “Update Data” has been developed to convert the 15-min interval RBSA load shape data into hourly data and aggregate the same type of load shapes as shown in Column 3 of Figure 3.6.

The output of the Excel VBA Macro is an excel sheet in similar format to the ELCAP light model data sheet. A snapshot of the generated data sheet is shown in Figure 3.7. This generated excel sheet stores the hourly load shape data derived from LSL’s RBSA data for the entire year.

FirstColumn: RBSA Type	SecondColumn: Appliance Type	ThirdColumn: Mapped to ELCAP End-Uses	PreMap Enduse Index
HVAC	Central Heating	Heating	0
HVAC	Air Source HP	Vent	1
HVAC	Packaged Terminal HP	Cooling	2
HVAC	Ductless Space HP	Vent	3
HVAC	Central AC	Cooling	4
HVAC	Packaged Terminal AC	Cooling	5
HVAC	Ground Source HP	Vent	6
HVAC	Air Handler	Vent	7
Water Heater	Electric Resistance WH	Waterheat	8
Water Heater	Heat Pump WH	Waterheat	9
Portable Heating and Cooling	Room Heater(s)	Heating	10
Portable Heating and Cooling	Window AC	Cooling	11
Refrigeration	Refrigerator	Refrigeration	12
Refrigeration	Freezer	Refrigeration	13
Cooking	Oven	Cooking	14
Cooking	Microwave	Cooking	15
Laundry & Dishwashing	Dryer	Appliance	16
Laundry & Dishwashing	Washer	Appliance	17
Laundry & Dishwashing	Dishwasher	Appliance	18
Entertainment	Gaming Console	Electronics	19
Entertainment	TV & Accessories	Electronics	20
Entertainment	Cable Box & DVR	Electronics	21
Entertainment	Home Audio	Electronics	22
Computer	Computer & Accessories	Electronics	23
Lighting and Other	Interior Lighting	InteriorLighting	24
Lighting and Other	Exterior Lighting	ExteriorLighting	25
Lighting and Other	Other	Misc	26
1 = Normal summer	Month=6		
2 = Hot summer	Month=7		
3 = Cool summer	Month=9		
4 = Shoulder	Month=10		
5 = Winter	Month=12	Contents in yellow cells are changeable	

Figure 3.6 End-use Mapping Information and Representative Month for Each Type of Season

Day (1=NormalSummer, 2=HotSummer, 3=CoolSummer, 4=Shoulder, 5=Winter)	Hour Index	Heating	Cooling	Vent	WaterHeat	Cooking	Refrig	ExtLight	IntLight	Electronics	Appliances	Misc	Vehicle	Total
NWC	1	1 NWC_1_1	0.043080151	0.076655625	0.339088888	0.180706093	0.001788979	0.122595129	0.015107739	0.026207079	0.101263366	0.040355289	0.153096292	0 1.099945
NWC	1	2 NWC_1_2	0.049213028	0.049395252	0.26666667	0.438936507	0.050721917	0.116370468	0.012021091	0.056345639	0.107316473	0.08600822	0.073302997	0 3.106486
NWC	1	3 NWC_1_3	0.046929784	0.065591196	0.420844442	0.090825397	0.001375	0.118388113	0.01482381	0.006630526	0.087590926	0.007288411	0.101841917	0 0.96213
NWC	1	4 NWC_1_4	0.05860884	0.135404204	0.456777775	0.099286032	0.001854167	0.113346158	0.01482381	0.004990973	0.08241136	0.002931599	0.063812181	0 1.034247
NWC	1	5 NWC_1_5	0.080977963	0.054155644	0.5646	0.083507936	0.003083333	0.121447656	0.006479167	0.014747808	0.078535239	0.019405933	0.077247817	0 1.076505
NWC	1	6 NWC_1_6	0.083916807	0.074187915	0.622287592	0.121444766	0.006479167	0.111174488	0.014747808	0.01479728	0.077247817	0 1.224228		
NWC	1	7 NWC_1_7	0.078013307	0.040753836	0.653222221	0.335269841	0.007291667	0.117407796	0.014379753	0.0855368894	0.026549388	0.067160531	0 1.452831	
NWC	1	8 NWC_1_8	0.06033333	0.038153844	1.776466672	0.391523808	0.046208333	0.115923266	0.014285714	0.045566607	0.095149754	0.043651208	0.087349604	0 2.714591
NWC	1	9 NWC_1_9	0.049213028	0.049395252	0.26666667	0.438936507	0.050721917	0.116370468	0.012021091	0.056345639	0.107316473	0.08600822	0.073302997	0 3.106486
NWC	1	10 NWC_1_10	0.043886233	0.037805405	2.316444446	0.502365078	0.0466875	0.115307421	0.006633254	0.049736539	0.112637247	0.106224781	0.0466474761	0 3.384375
NWC	1	11 NWC_1_11	0.046702439	0.042387303	1.52631112	0.427492063	0.052854167	0.113572869	0.002242196	0.045245928	0.112638867	0.125054269	0.056078147	0 2.551029
NWC	1	12 NWC_1_12	0.030663681	0.099380923	0.745755552	0.453031745	0.059145833	0.117476681	0.00145106	0.047557502	0.113825313	0.161593753	0.071125156	0 1.894152
NWC	1	13 NWC_1_13	0.029799952	0.074121719	0.516244443	0.35711111	0.068916667	0.121130918	0.134795672	0.142600114	0.068906054	0 1.543953		
NWC	1	14 NWC_1_14	0.036203315	0.095348628	0.47708889	0.040645833	0.040645833	0.119739374	1.50595E-05	0.047791474	0.115201514	0.165985628	0.067214056	0 1.505657
NWC	1	15 NWC_1_15	0.035322082	0.064943183	0.448822222	0.332256012	0.02825	0.120127233	1.50632E-06	0.046027033	0.163007719	0.049282623	0 1.403336	
NWC	1	16 NWC_1_16	0.035072033	0.206111661	0.348888891	0.301802167	0.038145833	0.124199805	0	0.046175675	0.119189539	0.146597821	0.068552234	0 1.434736
NWC	1	17 NWC_1_17	0.022698685	0.024121861	0.338133334	0.338139904	0.055166666	0.126732597	0.003627788	0.053920248	0.123420877	0.130180008	0.051443847	0 1.388411
NWC	1	18 NWC_1_18	0.024510234	0.28171978	0.270688888	0.382957075	0.1266875	0.126720536	0.001163819	0.065594619	0.129859938	0.153250789	0.058784421	0 1.62209
NWC	1	19 NWC_1_19	0.034312153	0.401358093	0.365147802	0.154125	0.131563938	0.001934444	0.077339255	0.140253927	0.146432662	0.051170315	0 1.844097	
NWC	1	20 NWC_1_20	0.041285509	0.327323286	0.497977777	0.408619047	0.0888125	0.130526839	0.008613426	0.093400253	0.151225541	0.145263832	0.08600409	0 1.979052
NWC	1	21 NWC_1_21	0.038593727	0.28331461	0.404355557	0.39976026	0.027270833	0.132604727	0.03116619	0.104173019	0.162185763	0.133819406	0.087341735	0 1.804583
NWC	1	22 NWC_1_22	0.046882753	0.224253881	0.462644444	0.423571426	0.016375	0.131521242	0.041139841	0.107220025	0.16202505	0.146481567	0.064331348	0 1.826447
NWC	1	23 NWC_1_23	0.045402424	0.181898524	0.385977777	0.359206348	0.01275	0.130903104	0.025087318	0.091863443	0.142515735	0.10800682	0.084068109	0 1.56768
NWC	1	24 NWC_1_24	0.042168787	0.122772478	0.298488887	0.291539682	0.003458333	0.121123235	0.017459409	0.055765374	0.118806326	0.085146762	0.085029519	0 1.241759
NWV	1	1 NWV_1_1	0.043080151	0.049838421	0.3252	0.18070609	0.001908244	0.12242195	0.01762569	0.027001233	0.095120381	0.04710137	0.153096292	0 1.061932
NWV	1	2 NWV_1_2	0.045533062	0.043969178	0.363533332	0.124206349	0.001444444	0.117837983	0.01745144	0.010928091	0.088908224	0.020385569	0.128868051	0 0.963066
NWV	1	3 NWV_1_3	0.046929784	0.03892453	0.402733331	0.090825397	0.001466667	0.117952562	0.017294445	0.006831451	0.085364675	0.007264964	0.101841917	0 0.91743
NWV	1	4 NWV_1_4	0.05860884	0.033737539	0.437666664	0.099286032	0.001977778	0.113034907	0.017294445	0.005142215	0.079948619	0.002933265	0.063812181	0 0.913442

Figure 3.7 Generated Data Sheet Using RBSA Load Shape Database

Figure 3.8 demonstrates the fractional change of different components in the load composition model for a residential feeder in NWC climate zone after updating the residential end-use load shapes for the four northwest climate zones (NWC, NWV, NWI and RMN). It can be seen from Figure 3.8 that for a

residential feeder located in NWC zone the Motor-D component, which is the single-phase air-conditioner load, significantly increases after the data update.

ELCAP	PSLF LID	Motor A	Motor B	Motor C	Motor D	Power Electronic	DG	Static PF	Static P Resistive	Static P Current	Static P Power	Static Q Reactance	Static Q Current	Static Q Power	
		NWC_RES	0.07	0.10	0.04	0.25	0.14	0.00	-1.000	0.33	0.07	0.00	-0.50	1.50	0.00
RBSA	PSLF LID	NWC_COM	0.23	0.12	0.05	0.07	0.20	0.00	-0.994	0.12	0.22	0.00	-0.50	1.50	0.00
		NWC_MIX	0.16	0.11	0.04	0.15	0.19	0.00	-0.998	0.21	0.15	0.00	-0.50	1.50	0.00
		NWC_RAG	0.15	0.11	0.12	0.15	0.13	0.00	-0.999	0.25	0.09	0.00	-0.50	1.50	0.00
		NWC_RES	0.07	0.07	0.04	0.38	0.13	0.00	-0.999	0.24	0.07	0.00	-0.50	1.50	0.00
		NWC_COM	0.23	0.11	0.05	0.10	0.20	0.00	-0.993	0.10	0.22	0.00	-0.50	1.50	0.00

Figure 3.8 Change of Component Fraction in the Load Composition Model for a Residential Feeder in NWC Climate Zone, Hot Summer Day, Hour = 16 (4:00pm)

Figure 3.9 presents the comparison of load shapes of appliance and electronics end uses under old ELCAP and new RBSA dataset. It is observed that the efficiencies of these two plug-in end uses are improved by seeing reduced power consumption especially at the peak point over a day.

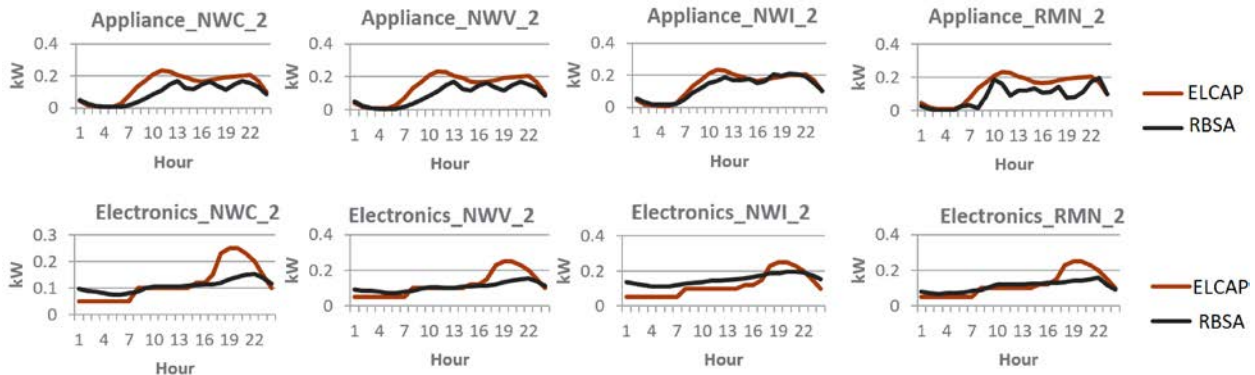


Figure 3.9 Load Shapes of Appliance and Electronics End Uses for the Pacific Northwest 4 Climate Zones on a Hot Summer Day (Study Type = 2)

3.5 Popularization of the RBSA Load Shapes

The up-to-date NEEA RBSA survey only covers 4 climate zones. The end-use load shapes for the other 8 climate zones in WECC can be derived by populating the RBSA load shape data into the rest of WECC region that does not have up-to-date load shape data sources available. Multiple strategies are proposed and implemented in this chapter and following chapters to leverage the up-to-date dataset of limited climate zones and the zonal correlations discovered from the old dataset to generate new dataset for the remaining climate zones in WECC system.

This chapter only presents a preliminary approach based on weighted difference to calculate load shapes of the other 8 WECC climate zones. It is presumed that the end-use load shapes change from the ELCAP dataset to the new RBSA dataset in a uniform pattern. This uniform change can be expressed by summing up the weighted differences between the RBSA and ELCAP load shape data for the four northwest climate zones. And this uniform change of load shapes will then be applied to the other 8 climate zones. Therefore, the updated end-use load shapes of the other 8 climate zones can be computed

by (3.1) and (3.2). Equation (3.1) computes the uniform change of the load shape of each end use in each study type (Normal Summer, Hot Summer, etc.). Since the RBSA data of the four northwest climate zones are available, the difference between the RBSA and ELCAP load shapes can be calculated for each climate zone. After that, the difference is weighed based on the number of surveyed cities in that climate zone to ensure data authenticity (more surveyed cities in a climate zone indicate more accurate data). The uniform change of load shape of each end use is computed by adding up the weighted differences as shown by (3.1). Equation (3.2) considers adding the load shape change to the ELCAP load shape data of the other 8 climate zones to achieve the new load shapes for these climate zones.

$$\Delta EndUse(i)_{ST(j)} = \sum_{k=1}^4 [WF(4CLZ(k)) * (EndUse(i)_{RBSA(ST(j), 4CLZ(k))} - EndUse(i)_{ELCAP(ST(j), 4CLZ(k))})] \quad (3.1)$$

$$EndUse(i)_{RBSA(ST(j), 8CLZ(k))} = EndUse(i)_{ELCAP(ST(j), 8CLZ(k))} + \Delta EndUse(i)_{ST(j)} \quad (3.2)$$

In which,

$$4CLZ(k) = "NWC", "NWW", "NWI", "RMN"$$

$$8CLZ(k) = "NCC", "NCV", "NCI", "SCC", "SCV", "SCI", "HID", "DSW"$$

$$ST(j) = "Normal Summer", "Hot Summer", "Cool Summer", "Shoulder", "Winter"$$

$$WF = Weighted Factor, proportional to the number of surveyed cities in each of the 4 climate zones$$

After extending the RBSA data to the other 8 climate zones, the cooling load shapes for all 12 climate zones are plotted in Figure 3.10.

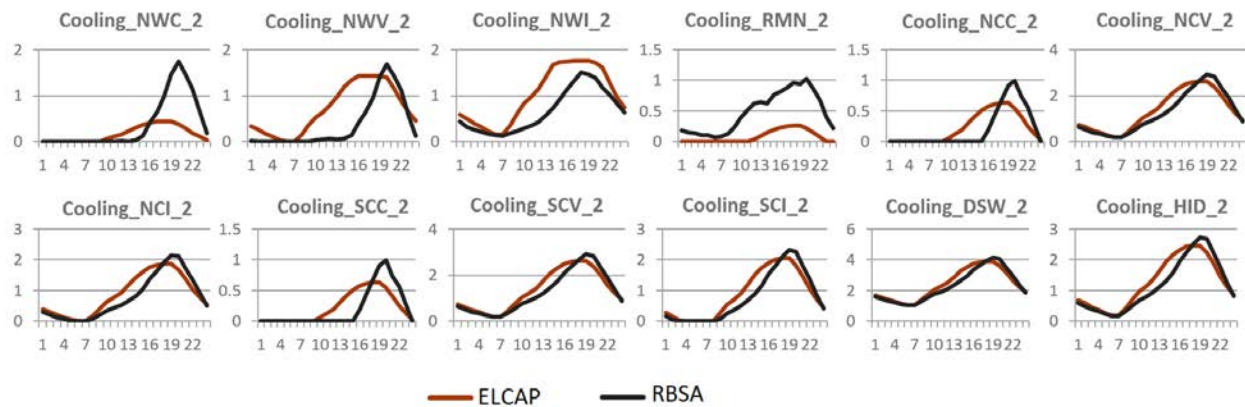


Figure 3.10 Cooling Load Shapes for All 12 Climate Zones under New RBSA Dataset

3.6 Summary

This section summarizes a preliminary approach based on weighted difference to update residential load shape data using the RBSA results. A flow chart shown in Figure 3.11 is drawn to better illustrate the process.

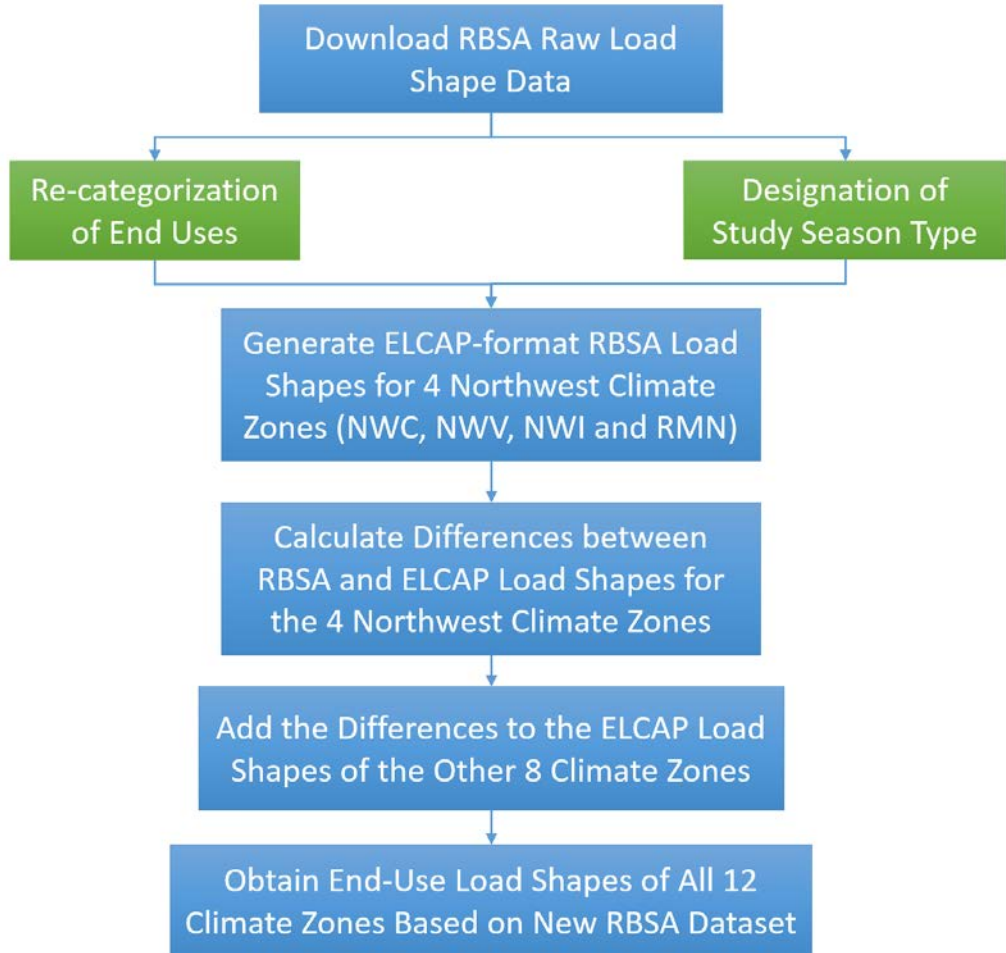


Figure 3.11 Flow Chart of the Process to Update Residential Load Shapes

4.0 Estimation of Residential Load Composition Using Cross-Correlation Method

The chapter discusses our efforts [21] to update the residential dataset of the load composition model (LCM) using the original RBSA load shape dataset collected and generated by NEEA rather than the processed RBSA data implemented in EPRI's LSL 4.0. The LCM residential dataset contains load profiles for 12 climate zones and 5 season conditions. The original LCM residential dataset was derived based on ELCAP load shape data, which is outdated. This chapter innovatively proposes a cross-correlation-based methodology [22] [23] to use the latest NEEA RBSA data to estimate load shapes for the other eight WECC climate zones by analyzing the correlations of power consumption patterns between the four Northwest climate zones and the other eight climate zones. Based on the NEEA database, this component-wise cross-correlation-based approach has been developed in this chapter to reconstruct the residential load profiles of the four Pacific Northwest climate zones and to populate the new load shape data into the other eight WECC climate zones.

4.1 NEEA RBSA Data

NEEA sponsored the RBSA program to develop an inventory and profile of existing residential building stock in the Northwest based on field data from a representative, random sample of existing homes. The RBSA study was conducted across four states (WA, OR, ID, MT) for three categories of residences: single-family homes, manufactured homes, and multifamily homes. A total of 66 cities participate in the RBSA study [20]. Each city contains at least one representative surveyed house (measurement site). There are a total of 103 houses distributed in the 66 cities [20]. Based on the geographical locations, the 66 cities are divided into four climate zones as shown in Table 3.1 and depicted by Figure 3.3.

NEEA RBSA metering data is comprised of detailed end-use loads measured at 15-minute intervals. In this chapter, we process and aggregate the metering data ranging from April 2011 through March 2012 to derive seasonal, hourly energy usage data characterized to LCM's 11 end-use categories [3].

4.2 Model Development

This section discusses the details about the initial data processing, including re-categorizing the 160 RBSA end-use types [20] into 11 LCM end-use types, defining season conditions, and aggregating the raw RBSA load shape data to form the hourly, seasonal and climate-zone-based data in the same format as the LCM residential data. This section also presents the mathematic model of the cross-correlation-based approach to apply the RBSA dataset to estimating load shape data for the eight WECC target climate zones. The entire process for updating the LCM residential load shape data is shown in Figure 4.1.

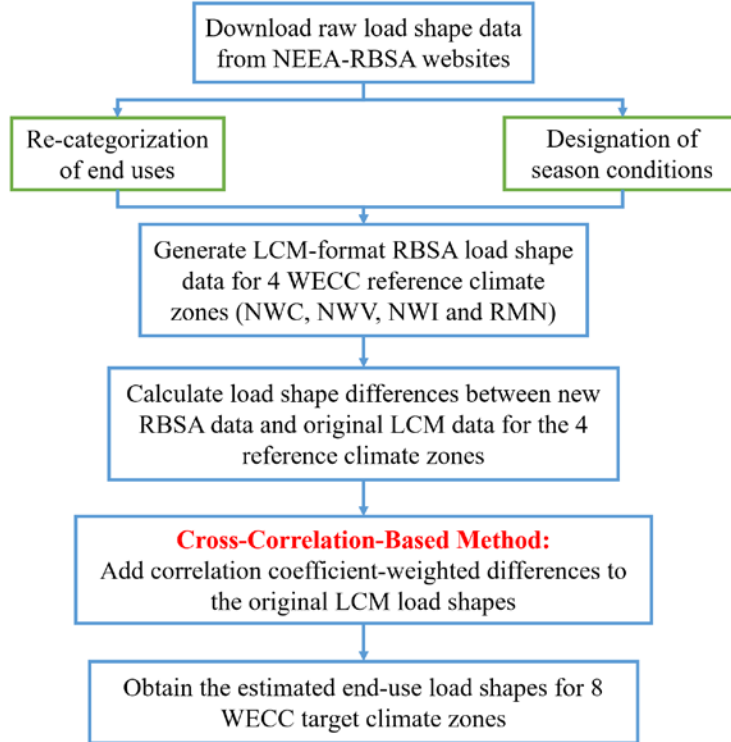


Figure 4.1 Flowchart of the Process for Updating LCM Residential Load Shape Data

4.2.1 End-Use Re-Categorization and Season Conditions

The RBSA study meters electric energy consumption for 160 end uses in a representative residential home. In this chapter, a mapping is developed to re-categorize the types of these end uses into the 11 LCM end-use categories to facilitate load aggregation. The end-use re-categorization is shown in Table 4.1. As previously mentioned, five season conditions are defined in LCM, with normal summer = 1, hot summer = 2, cool summer = 3, shoulder (fall or spring) = 4 and winter = 5. It is noted that the mapping in Table 4.1 is defined for all five season conditions except Group# 4. The RBSA heat pump end uses in Group# 4 function as heating load in the winter season and as cooling load during the other four seasons.

The raw RBSA data used in this section contain end-use load shapes measured at 15-minute interval for each day within the period April 2011 - March 2012. To aggregate the RBSA load shapes over the five season conditions defined by LCM, a relation between months and season conditions is developed in Table 4.2.

To aggregate the RBSA load shape data to form a dataset in the same format as the LCM data, the first step is to convert the RBSA 15-minute load shape data into hourly data by adding four 15-minute energy consumption readings within each specific hour. The second step is to aggregate the RBSA hourly data over the LCM end-use categories based on the defined mapping in Table 4.1. The hourly load shapes of RBSA end uses belonging to the same LCM end-use category are added. The last step is to aggregate the RBSA end-use hourly data aligned with LCM categories over the season conditions based on Table 4.2. For the same season condition, the RBSA hourly data of all the dates falling into this season are added up and averaged over the total number of dates. Ultimately, the new RBSA residential load shape dataset in the same format as LCM dataset is generated for the four Northwest climate zones (reference climate zones) and used as the foundational data source to evaluate the residential load shapes for the entire WECC climate zones.

Table 4.1 Mapping RBSA End Uses into LCM Categories

Group#	RBSA End-Use Types in Each Group	LCM End-Use Categories
1	Light fixtures in basement, bedroom, bathroom, closet, den, entryway, dining room, family room, garage, hallway, kitchen, laundry room, living room, office room and other room	Interior lighting
2	Exterior light fixture	Exterior lighting
3	Central, window air conditioners	Cooling
4	ductless heat pump, ground source heat pump units, air source heat pump systems, packaged terminal air conditioner, packaged terminal heat pump	Cooling (Heating in winter season)
5	Hydronic loop electric pump, electric resistance tank water heater, heat pump water heater, Electric furnace resistance heating element	Water heater
6	Cable box, digital video recorder, computer, computer accessory (printer, scanner etc.), computer tower, digital video disc player, gaming console, computer monitor, stereo, stereo accessory, TV, TV accessory	Electronics
7	Clothes washer, clothes drier, dish washer, standalone freezer,	Appliances
8	Zonal electric resistance heater	Heating
9	Microwave oven, Electric cooking stove (oven and range)	Cooking
10	Refrigerator	Refrigerator
11	Central forced air system air handler	Ventilation
12	Septic pump, hot tub, electrical subpanel, sump pump, unspecified device, well pump	Miscellaneous

Table 4.2 Relation Between Months and Season Conditions

Season Conditions	Months
Normal Summer (Day 1)	June
Hot Summer (Day 2)	July, August
Cool Summer (Day 3)	May, September
Shoulder (fall or spring) (Day 4)	March, April, October, November
Winter (Day 5)	December, January, February

4.2.2 Cross-Correlation-Based Methodology

To reconstruct the LCM load profiles, a cross-dependence analysis-based approach [22] [23] is developed. The differences between the aggregated RBSA and original LCM load profiles in the reference climate zones are calculated as the basis for LCM adjustment. Specific weighting factors are assigned to the load profile differences for each reference climate zone. For each end-use load component, the weights are assumed to be proportional to the correlation coefficient between a reference climate zone and a specific climate zone, if correlation coefficients exist. When correlation coefficients do not exist, equal weights of 0.25 are used to compute the adjusted load profile. Such adjusted LCM data maintain the original cross-dependence structure among the load profiles across the WECC climate zones, and combine both the old and new measurement-based datasets to generate a more genuine dataset reflecting realistic load profiles.

Total load of aggregated RBSA data is the summation of power consumption of the 11 end uses, expressed by (4.1). The difference between new RBSA and old LCM data for the four reference climate zones can be computed by (4.2).

$$RBSA_TotalLoad_{i,j,h} = \sum_{l=1}^{11} RBSA_EndUse_{i,j,l,h} \quad (4.1)$$

$$Difference_{k,j,h,l} = RBSA_{k,j,h,l} - LCM_{k,j,h,l} \quad (4.2)$$

where, $i=1,2,\dots,12$ represents the 12 climate zones (NWC, NWV, NWI, RMN, NCC, NCV, NCI, SCC, SCV, SCI, DSW, HID), $k=1,2,3,4$ represents the four reference climate zones (NWC, NWV, NWI, RMN), $j=1,2,3,4,5$ represents five different season conditions (normal summer, hot summer, cool summer, shoulder, winter), and $h=1,2,\dots,24$ represents 24 hours in a day, $l=1,2,\dots,12$ represents 11 end-use categories (appliance, cooking, cooling, electronics, extlight, heating, intlight, misc, refrig, vent and waterheat) and the total load. The correlation coefficients are computed between a specific climate zone (i) and a specific reference climate zone (k) for each end use for any climate condition. The formulas are expressed as (4.3) – (4.6).

$$\rho_{(LCM_{i,j,l})(LCM_{k,j,l})} = \frac{\text{cov}\left[\left(LCM_{i,j,l}\right), \left(LCM_{k,j,l}\right)\right]}{\sqrt{\sigma^2\left(LCM_{i,j,l}\right) * \sigma^2\left(LCM_{k,j,l}\right)}} \quad (4.3)$$

$$\text{cov}\left[\left(LCM_{i,j,l}\right), \left(LCM_{k,j,l}\right)\right] = \frac{1}{23} \sum_{h=1}^{24} \left[\left(LCM_{i,j,l,h} - \frac{1}{24} \sum_{h=1}^{24} LCM_{i,j,l,h} \right) * \left(LCM_{k,j,l,h} - \frac{1}{24} \sum_{h=1}^{24} LCM_{k,j,l,h} \right) \right] \quad (4.4)$$

$$\sigma^2\left(LCM_{i,j,l}\right) = \frac{1}{23} \sum_{h=1}^{24} \left(LCM_{i,j,l,h} - \frac{1}{24} \sum_{h=1}^{24} LCM_{i,j,l,h} \right)^2 \quad (4.5)$$

$$\sigma^2\left(LCM_{k,j,l}\right) = \frac{1}{23} \sum_{h=1}^{24} \left(LCM_{k,j,l,h} - \frac{1}{24} \sum_{h=1}^{24} LCM_{k,j,l,h} \right)^2 \quad (4.6)$$

When the correlation coefficients exist, the weights are proportional to the correlation coefficients and scaled to unit length (i.e., the total weights add up to 1). The correlation coefficient-based scaled weight $W_{i,k}$ is computed to be proportional to the correlation coefficient between a specific climate zone i and each of the four reference climate zones, and is expressed by (4.7).

$$W_{i,k} = \frac{\rho_{(LCM_{i,j,l})(LCM_{k,j,l})}}{\sum_{k=1}^4 \rho_{(LCM_{k,j,l})(LCM_{i,j,l})}} \quad (4.7)$$

The LCM data is adjusted by multiplying the scaled weights to the corresponding differences, and the results are added to the original LCM values.

$$\text{Adjusted_LCM}_{i,j,h,l} = \sum_{k=1}^4 \text{Difference}_{k,j,h,l} * W_{i,k} + \text{LCM}_{i,j,h,l} \quad (4.8)$$

Combining (4.7) and (4.8), the updated LCM data for all 12 climate zones can be calculated.

4.3 Results

The innovation of this part of work is to derive load profiles for the eight WECC target climate zones, which typically did not have up-to-date residential load shape data measured by utility. This LCM data update combines both the original LCM and the latest NEEA RBSA database to estimate load profiles for the eight WECC target climate zones using cross-correlation analysis. This section presents the graphic results of the updated LCM residential load shapes for selected end uses and climate zones. In addition, the final changes of load model composition are presented.

Figure 4.2 presents the load shapes of the cooling end use for the four reference climate zones under hot summer condition, including the original LCM data and the new NEEA RBSA data. Figure 4.3 shows the comparison of cooling load profiles between the original and updated LCM datasets for the eight target climate zones, considering both the normal summer and hot summer conditions. It can be seen from Figure 4.3 that the peak values of the cooling loads become larger in the updated LCM dataset than in the original LCM dataset, indicating expanded capacity of air-conditioner loads in the residential feeder. Figure 4.4 and Figure 4.5 demonstrate the vent load shapes and total load profiles for the eight target climate zones under normal summer condition.

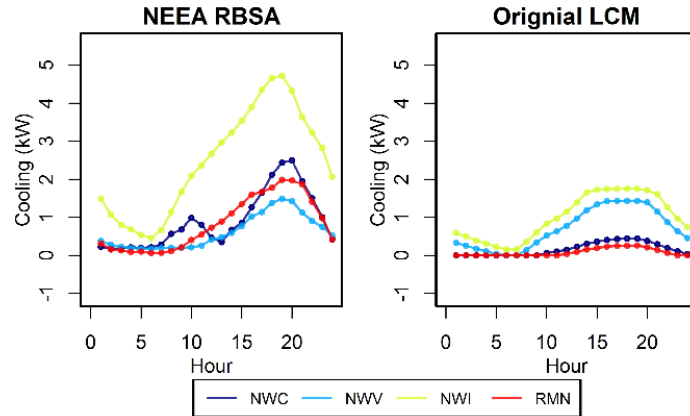


Figure 4.2 **Hot Summer**, Cooling Load Shapes for Four Reference Climate Zones

Table 4.3 presents the changes of load compositions for a residential composite load model in NWC climate zone with the original LCM residential load shape data replaced by the updated LCM data. The load composition data is extracted for hot summer season during the peak hour of cooling end use, which is roughly 19:00 - 20:00 in the evening. It can be seen from Table 4.3 that the Motor D fraction in the composite load model, representing the amount of air-conditioner load, increases from 21.3% in the original LCM to 33% in the updated LCM. The power electronics load drops slightly because of improved efficiency.

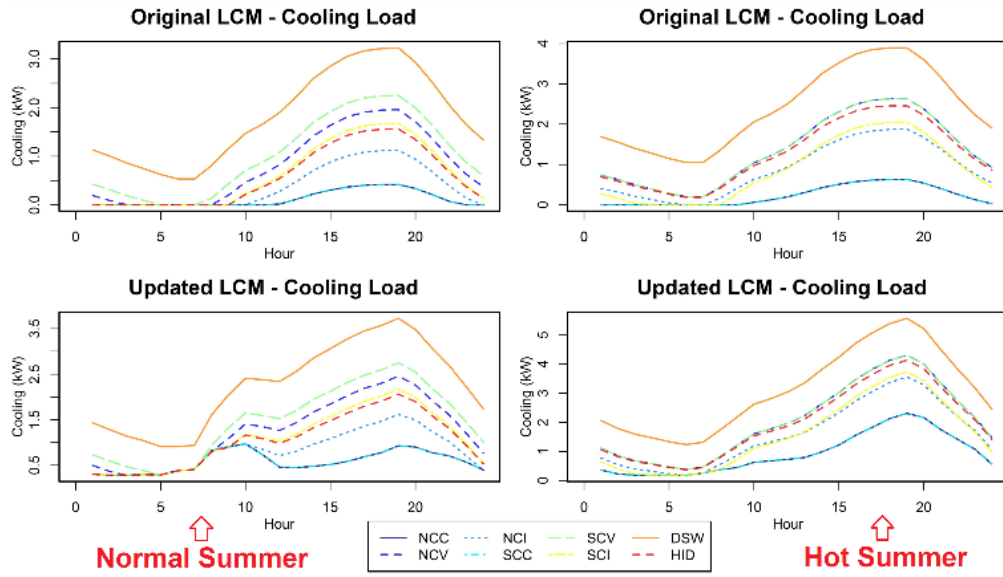


Figure 4.3 **Normal Summer** (Left Two Subplots) and **Hot Summer** (Right Two Subplots), Cooling Load Shapes for Eight Target Climate Zones

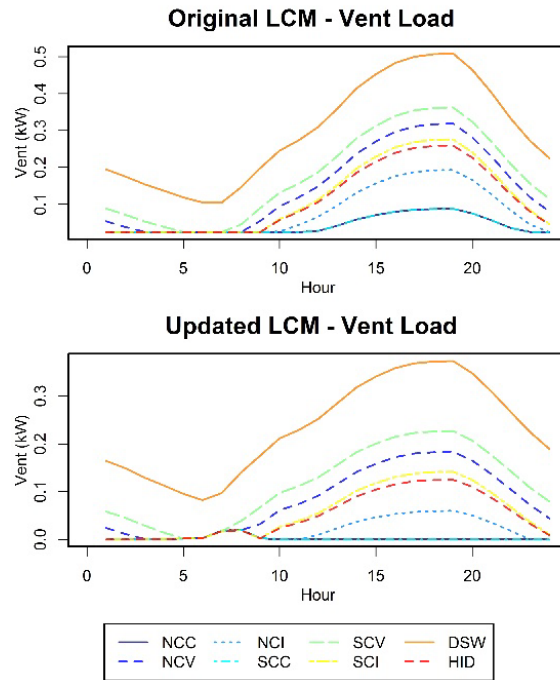


Figure 4.4 **Normal Summer**, Vent Load for Eight Target Climate Zones

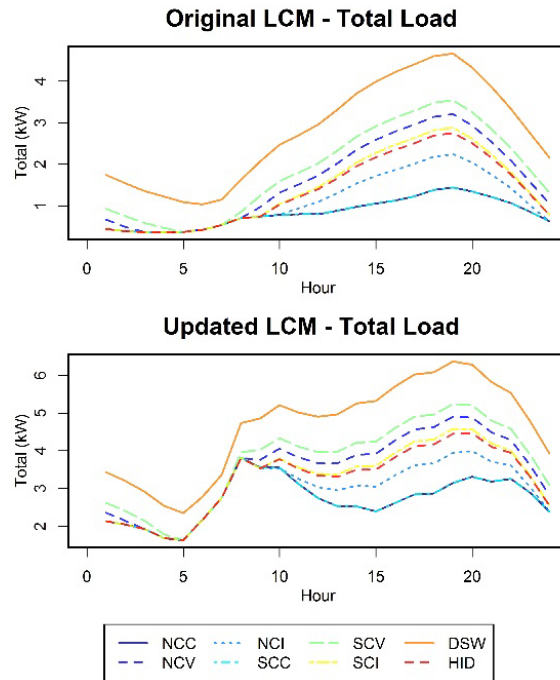


Figure 4.5 **Normal Summer**, Total Load for Eight Target Climate Zones

Table 4.3 Load Compositions in Per Unit for NWC Climate Zone Residential Composite Load Model

Original LCM				
Motor A	Motor B	Motor C	Motor D	Power Electronic
0.036	0.081	0.038	0.213	0.178
DG	Static P Resistive	Static P Current	Static P Power	Total
0.00	0.392	0.062	0.00	1.0
Adjusted LCM				
Motor A	Motor B	Motor C	Motor D	Power Electronic
0.034	0.053	0.074	0.33	0.159
DG	Static P Resistive	Static P Current	Static P Power	Total
0.00	0.29	0.06	0.00	1.0

4.4 Summary

In this chapter, we discussed the philosophy to aggregate load profiles of the up-to-date NEEA RBSA data to align with the existing LCM load shape dataset. A cross dependence structure analysis-based approach was applied to make adjustments to the original LCM load shape data. This cross-correlation approach studies the dependencies of power consumption patterns among the 12 WECC climate zones using the original LCM dataset, and combines both the original LCM and new RBSA datasets to estimate the residential load shape data for the eight WECC target climate zones, which typically don't have new

RBSA data available in the industry. In Chapter 5, weather conditions of those climate zones can be considered as additional factors for LCM adjustment.

5.0 Estimation of Residential and Commercial Load Composition Using Machine Learning Techniques

Chapter 4 aims at load profile approximation/correction without taking into account factors such as weather attributes which may well determine the load profiles or their cross-correlations. In this chapter, machine learning feature selection was conducted to understand the impact of various weather attributes on both residential and commercial electricity demand components in the western United States [24] [25], where residential/commercial load in various climate zones are available, as explained in the previous chapters. The load data has been processed to yield hourly load profiles with the same temporal resolution and duration as weather condition data from the National Oceanic and Atmospheric Administration (NOAA) at representative weather stations [26]. The data were divided into five seasonal conditions. For each condition and each load component, the influences of weather factors were evaluated and quantified using cross-correlation, principal component analysis, and mutual information evaluation. Then predictive models were developed based on the ranked/screened factors using the regression tree (RT) and random forest (RF) approaches. After multi-fold cross-validation, the optimal complexity/depth of the RT and RF models are determined and used for approximating load profiles in the climate zones with available weather data. Data from the western areas are used for training the models (i.e., WECC RT/RF models). The validated better-performing WECC RF models, together with the available weather data, are then used for approximating load profiles in the current focus areas of Eastern Interconnection (EI) and ERCOT.

5.1 Introduction

The electric demands are affected by not only human activities but also different weather condition [27] [28] [29]. In different seasonal conditions, the load demands of heating and cooling are significantly different [30]. Normally, heating load variations in different seasons are caused by temperature variations over a year, but daily heating load variations are caused by human activities and differences in temperature occurring over the diurnal cycle during cold weather [31]. Humidity is another common weather attribute that can affect electricity demands, as water vapor in the air may condense to its liquid phase and release heat when air conditioning reduces the indoor temperature; for similar reasons, more heating is needed for wetter days in the winter. In general, lower electricity demand comes with lower humidity [32].

The purpose of this study is to leverage machine learning to investigate the connection between load profile and weather conditions in the western United States (WECC) and then approximating load profiles in the EI and ERCOT systems. Although the load profile for the rest of the United States is either unavailable or unpublished, nationwide weather information is available online from NOAA. The weather-load connection studied in our research could be used to estimate the load profile data for the other regions in the nation where the weather information is available. The estimated load profile data would eventually be used by power system planners to make decisions.

Feature selection—selecting a subset of relevant features (variables, predictors) for use in model construction—is a common process in machine learning [33]. In this regard, feature selection is very important to high-dimensional models because it reduces overfitting and simplifies the models. In this study, three methods of feature selection are adopted: 1) cross-correlation analysis, 2) principal component analysis (PCA), and 3) mutual information evaluation [33] [34].

Many studies have looked into the impact of weather attributes, particularly temperature, on electricity load [35] [36] [37], and advanced machine learning approaches (e.g., artificial neural network, support vector machine, regression models, random forest models and Bayesian methods) have been used

to incorporate weather information in load forecasting [38] [39] [40] [41] [42] [43]. RT models combine regression models and decision trees and can be applied to linear or nonlinear regression models when the data has many features with complex nonlinear interactions [44]. Based on the work by Fan et al., RTs are one of the best performing approaches used in machine-learning-based load time series forecasting models [45].

Random forests (RFs) are an ensemble learning method by constructing a multitude of decision trees during the training phase and producing predictions based on the mode of the classes (for classification) or averaging (for regression) of the individual trees. RFs reduce decision trees' probability of overfitting the training set [46]. Radom forests methods have been introduced in the field of electricity load forecasting [47] [48].

We developed, validated, and tested both RT-based and RF-based predictive models that can be used to predict critical residential heating and cooling loads using multiple weather attributes.

5.2 Data

Both the processed WECC residential and commercial data contain measurement points for 24 hours, 12 climate zones, and five seasons, with variables including cooling, lighting, heating, ventilation, and so on. Other variables include climate zone, study day (season), hour of the day, and climate zone index, based on which weather data were collected from the National Oceanic and Atmospheric Administration website, with the same time spans, at one representative weather station for each climate zone. The weather attributes include six variables: visibility (%), temperature (deg C), dew point temperature (deg C), humidity (%), wind speed (mph), and precipitation (inch), for each climate zone, season, and hour of the day.

5.3 Methodology

PCA is a statistical procedure that uses an orthogonal transformation to convert a set of observations of possibly correlated variables into a set of values of linearly uncorrelated variables. PCA is one of the methods developed to deal with the multi-collinearity problem; it analyzes covariance and correlation structuring; and can be used to reduce dimensionality by eliminating trivial principal components.

Mutual information is another feature selection method used to find a suitable subset of features from a data set that has the largest joint dependency on target variables [34]. Mutual information ($I(x,y)$) between two continuous random variables x, y with joint probability density function $f(x,y)$ is given by the following relationship [34]:

$$I(x,y) = \iint f(x,y) \log \frac{f(xy)}{f(x)f(y)} d(x)d(y) \quad (4.1)$$

where $f(x,y)$ is the joint probability density function of x and y , and $f(x)$ and $f(y)$ are the marginal probability density functions of x and y , respectively. And for two variables, it is possible to represent the different entropic quantities with an analogy of set theory.

The above approaches help understand the impacts of the various factors on the differences. To obtain a predictive model of the response variable(s), multiple machine learning approaches are available. Here, considering the nature of the data, we adopted the RT approach [44]. An RT algorithm targets the best relationship between the factors (splitting variables) and the response variable, and is formed by a

collection of rules to achieve the best split to differentiate the data. The tree-based model can be written as follows:

$$f(x) = \sum_{m=1}^M c_m I(x \in R_m). \quad (4.2)$$

In the trees, the regions R_m are usually defined by means of binary split, and $I(\cdot)$ is an indicator function returning 1 if its argument is true and 0 if otherwise, and M is the number of partition regions. For a data set, we would like to pick the regions R_m and the constants c_m to minimize the squared error.

$$\text{Objective} = \min \left(\sum (f(x_i) - y_i)^2 \right) \quad (4.3)$$

The size of trees is reduced by removing sections that provide little power (e.g., in terms of mean squared errors) to distinguish instances (called pruning) to improve predictive accuracy by reducing overfitting.

An alternative approach using RF can be integrated to complement the RT models towards more robust analyses and findings. The RF models can randomly classify a group of individual decision trees and the final decision can be obtained by averaging the outputs of the selected individual trees, with the following algorithm [49]: (a) randomly select a bootstrap sample of the size N from the training data; (b) build a RF tree T_b ($b=1$ to B) to the bootstrapped data and get the minimum node size n_{min} ; and (c) repeat the following steps: (c1) randomly select m variables out of the original p variables; (c2) choose the best variable/split-point among the m variables; and (c3) split the node into two children nodes. The outputs are the ensemble of trees, and the prediction at a new point x of RF regression can be written as:

$$\widehat{f}_{rf}^B(x) = \frac{1}{B} \sum_{b=1}^B T_b(x) \quad (4.4)$$

5.4 Results

5.4.1 Development and Validation of Machine-Learning (ML) Models for Residential Load

First, ML models were developed for the NEEA RBSA data, which has 12 load components, and the corresponding NOAA weather data has six attributes. Figure 5.1 shows the variables with at least one absolute correlation coefficient between weather attributes and load components over 0.5. The selected variables are temperature, dew point temperature, visibility, humidity, heating, refrigeration, and miscellaneous. Figure 5.1 shows statistical summaries of the load components and weather attributes for the overall data across the four climate zones, including distributions of the selected variables, their Pearson cross-correlation coefficients, and scatter plots of any two different variables. The histogram of temperature is slightly bimodal but its distribution is symmetric. The visibility, dew point temperature, and humidity are right-skewed while heating, refrigeration, and miscellaneous are left-skewed. Heating has a negative linear relationship with temperature, visibility, and dew point temperature, and the Pearson correlation values are -0.64, -0.61, and -0.59, respectively.

The feature scatter plots show that not all the relationships between the variables are linear. To explore the nonlinearity more comprehensively, mutual information is used to provide a supplementary perspective of the relationships.

The *x*-axes in Figure 5.1 show the ranges of the variables. For example, temperature is from -4 °C to 32 °C, and the dew point temperature is from -10 °C to 12 °C.

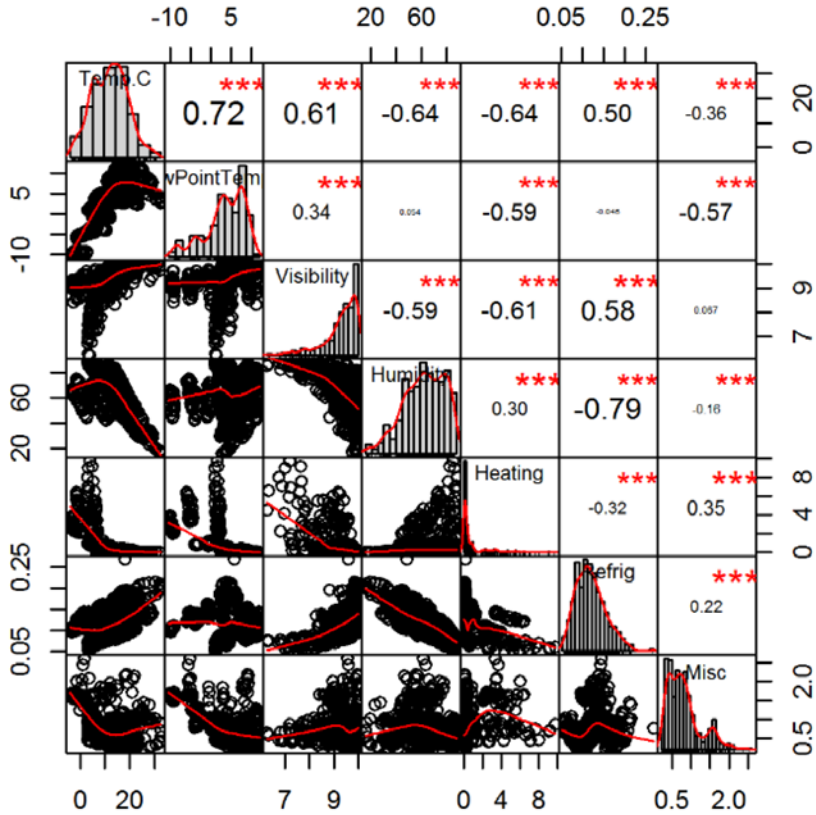


Figure 5.1 Marginal Distribution, Scatter Plots, and Cross-Correlation Coefficients between the NEEA RBSA Load Components and Weather Condition Variables. Pairs with Absolute Correlation Values <0.5 are Not Shown.

Dew point temperature relates to temperature and humidity. The climate zones have different weather conditions. Figure 5.2 illustrates the correspondences between load components (e.g., heating) and weather conditions during different seasonal conditions (study days).

The panels for normal summer (Day 1), hot summer (Day 2), and cool summer (Day 3) in Figure 5.2 show that during the summer, the average use of heating is very low, especially for Day 2, when the heating is less than 0.05 kW. The dew point temperatures of NWC and NWI are similar in their shapes and magnitudes during different days. Except for Day 3, dew point temperatures have similar patterns between NWV and RMN. During the normal and hot summer, RMN has a higher dew point temperature, but during the shoulder and winter, NWV has higher dew point temperatures. During the cool summer, the dew point temperatures of RMN and NWV are very close to each other.

Electricity usage for heating during Day 5 is notable: peak usage for NWC is at 9:00 a.m., and the value is near 10 kW. The peak usage for NWV is near 8 kW at 7:00 a.m., and the peak usage for NWI is near 6.5 kW at 6:00 a.m. For RMN, the peak usage occurs at 9:00 a.m., and the value is near 4 kW. Dew point temperature patterns for NWC and NWV are similar, but their heat usages are different. One of the reasons is the different average temperatures of those two climate zones, although their heating usage variations are similar. Both of them have dual peaks. We also found the heating usage patterns of NWI and RMN to be similar but with different magnitudes.

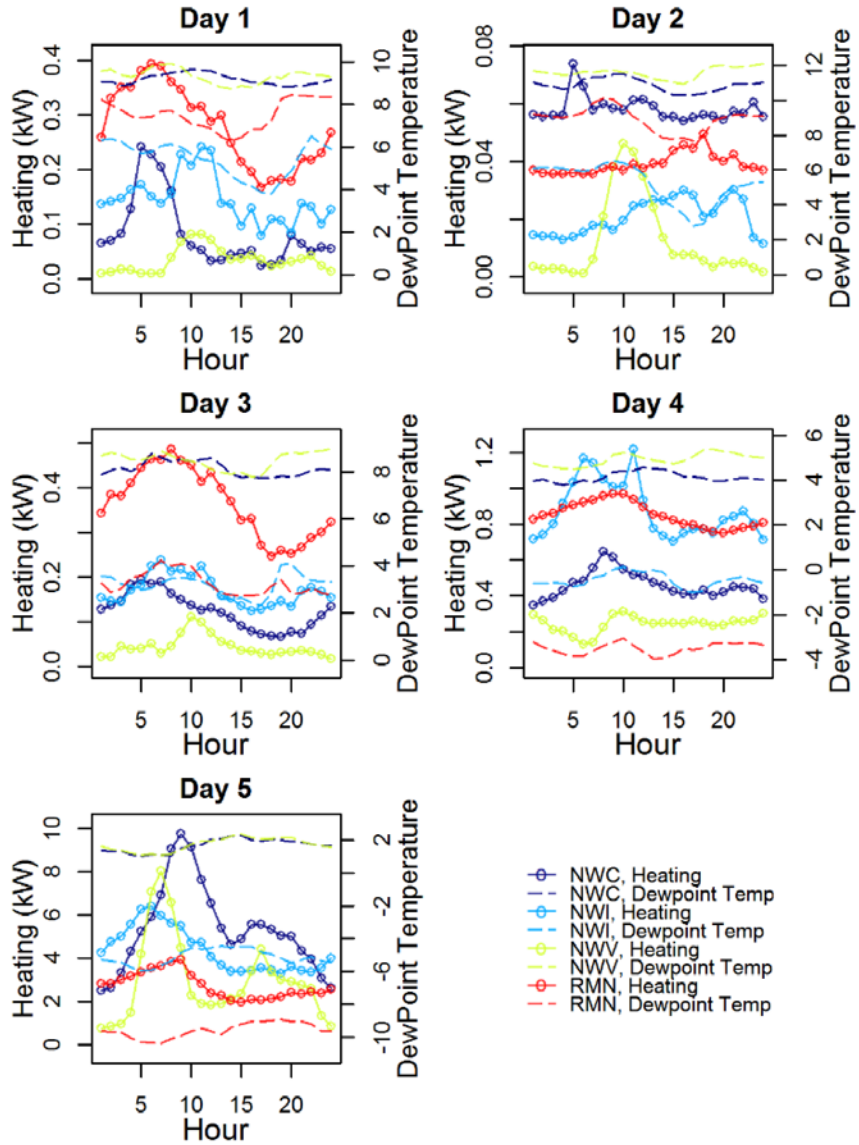


Figure 5.2 Time Series of Heating and Dew Point Temperature on Different Seasonal Conditions (Study Days, Day 1 = normal summer, Day 2 = hot summer, Day 3 = cool summer, Day 4 = shoulder (fall or spring), Day 5 = winter).

The absolute value of a correlation coefficient shows the magnitude of the relationship between two variables. The greater absolute value of a correlation coefficient, the stronger the linear relationship. Figure 5.3 is the heat map of absolute Pearson correlation coefficients among load components and weather attributes. It is clear that the variables of load components and weather attributes can be grouped based on absolute correlation coefficients. Temperature, visibility, dew point temperature, and wind speed among the weather attributes, and heating, water heat, total load, and miscellaneous of the load components are grouped together. This indicates that heating, water heat, and total load can be explained linearly by some of those weather attributes. The rest of the load components, such as cooling, electronics, appliances, cooking, internal light, refrigerator, external light, and ventilation are grouped with humidity and precipitation.

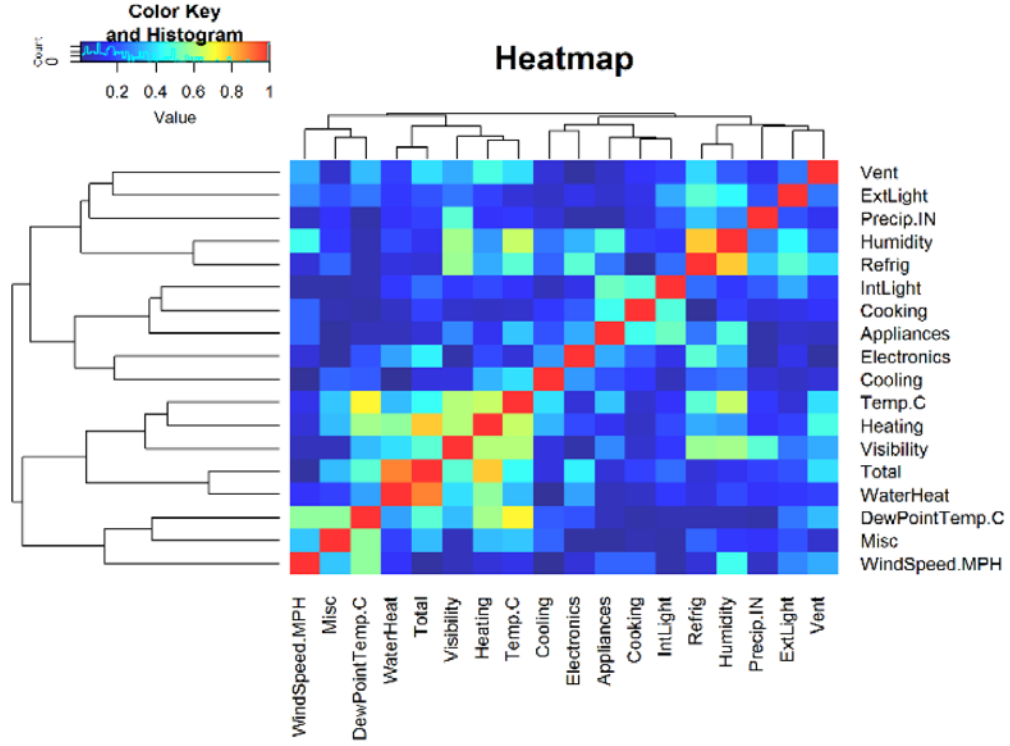


Figure 5.3 Heat Map of Absolute Pearson Correlation Coefficients among Load Components and Weather Attributes.

Figure 5.4 shows the PCA bi-plots, where the first two principal components are used to visualize the similarities among load components and weather conditions. The first component accounted for ~27.2% and the second component accounted for about 17.4% of the total variance of load components and weather attributes. The bi-plots show that the total load, water heat, and heating negatively correlate to temperature and dew point temperature. Panel 1 of Figure 5.4 shows the points with different colors for each of the four climate zones. Note that points that are close to each other correspond to observations with similar scores/projections onto the principal components. Figure 5.4 shows that NWI (green points) is behaving differently from NWC (orange points) and NWV (blue points). NWC and NWV are behaving similarly because of their geographic vicinity. RMN observations are mixed with all the other three climate zones. Panel 2 shows the measurement points with different colors on different days, and they seem to be distinct without much overlap. Observations for Day 2 (hot summer) and Day 5 (winter) are far apart. The arrows in Figure 5.4 indicate the projections of the variables onto the first two principal components PC1 and PC2. Temperature mostly contributes to PC1 while electronics and wind speed contribute mainly to PC2. Humidity and external light align well in the similar direction indicating certain similarity, but humidity contributes more than external light to both PC1 and PC2.

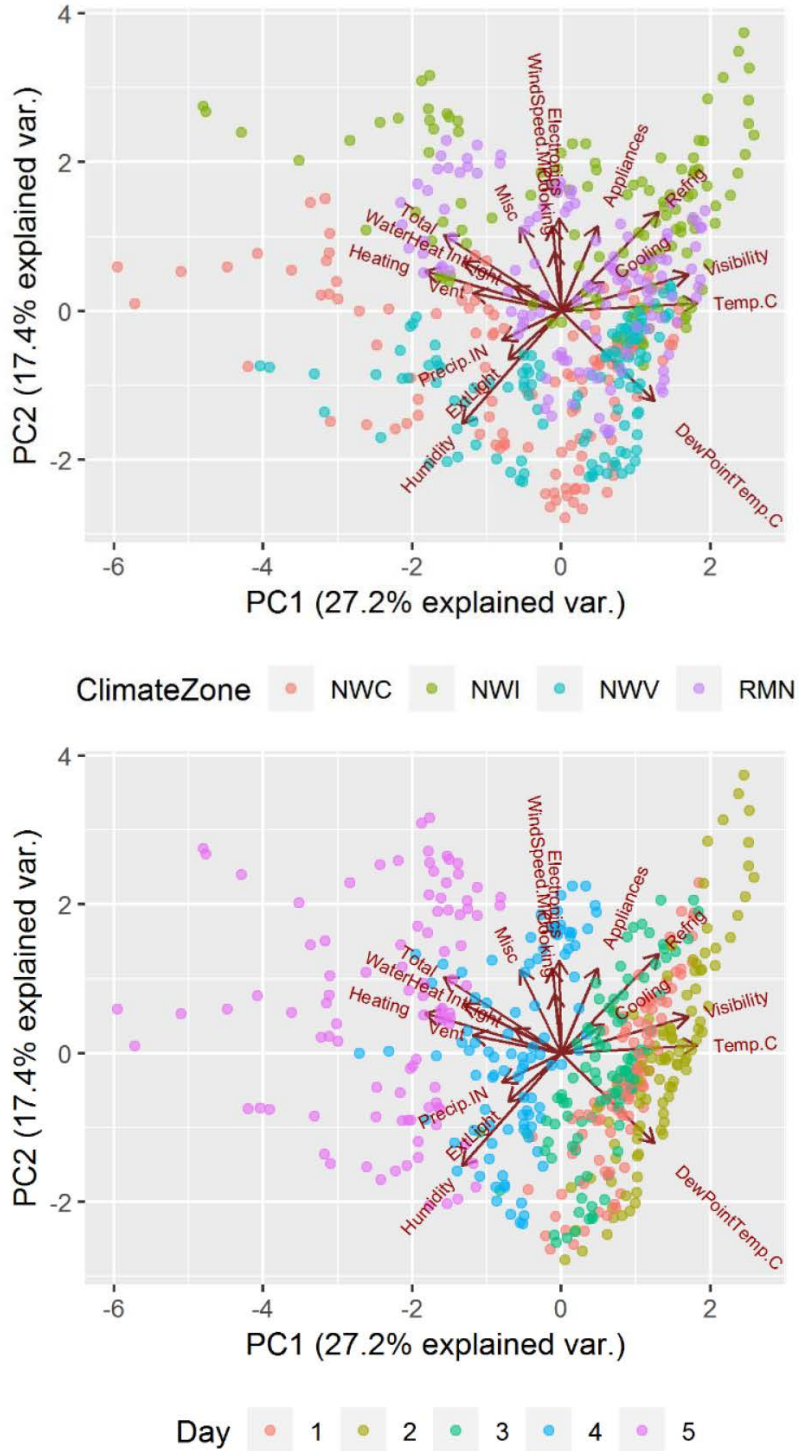


Figure 5.4 PCA Biplot of All Load Components and Climate Condition Variables. Top: Observations Colored per Climate Zone; Bottom: Observation Points Colored by Seasons.

The mutual information of the load components and weather attributes is summarized in Table 5.1. Unlike correlation coefficients that only provide linear relationship, mutual information can describe the

joint distributions among load components and weather attributes (e.g., it is possible for two variables to have zero linear relationship but a strong curvilinear relationship).

Table 5.1 Mutual Information among Load Components and Weather Attributes

	Visibility	Temp	DewPoint Temp	Humidity	Wind Speed	Precip	Day
Appliances	0	0.306	0.226	0.352	0.162	0.014	0.057
Cooking	0	0.128	0.193	0.204	0.231	0.093	0.014
Cooling	0.284	0.538	0.722	0.238	0.17	0.101	0.502
Electronics	0.149	0.578	0.958	0.506	0.42	0.109	0.159
ExtLight	0.151	0.316	0.645	0.363	0.4	0.159	0.046
Heating	0.484	0.798	1.343	0.27	0.363	0.37	0.969
IntLight	0.064	0.321	0.345	0.287	0.218	0.142	0.141
Misc	0.112	0.519	0.618	0.282	0.359	0.15	0
Refrig	0.498	0.721	1.009	0.686	0.404	0.36	0.27
Vent	0.152	0.321	0.536	0.214	0.317	0.117	0.146
WaterHeat	0.22	0.353	0.492	0.181	0.179	0.183	0.242
Total	0.208	0.482	0.634	0.289	0.284	0.102	0.389

Table 5.1 shows that cooling is highly dependent on temperature and dew point temperature. Heating and total load highly depend on temperature, dew point temperature, and seasonal day, while refrigeration highly depends on temperature, dew point temperature and humidity. Water heat strongly relates to temperature and dew point temperature. The mutual information among appliances, cooking and visibility is zero. When using weather attributes to explain appliance and cooking, the visibility attribute can be ignored. On the other hand, when the mutual information between heating and all the weather attributes is greater than 0.2, none of the weather attributes should be ignored when predicting heating usage.

In a further study, we used an RT model to quantitatively relate the 12 load components to the weather attributes and temporal factors such as seasons and hours of a day. We conducted multi-fold validation in the load component and weather attributed data set is randomly split into a training subset (75%) and a testing subset (25%). To find the optimal complexity of an RT, validations for trees with various depths are done and compared. The highest test score of each load component and its maximum depth of RT are shown in Table 5.2.

Table 5.2 The Highest Accuracy Scores of RT Models and the Corresponding RT Model Complexity (i.e., Depths) for Each Load Component.

	Optimal Depth	Optimal Test Score
Appliances	10	0.33
Cooking	7	0.215
Cooling	7	0.584
Electronics	8	0.752
ExtLight	10	0.578
Heating	4	0.851
IntLight	3	0.361
Misc	5	0.657
Refrig	6	0.826
Vent	2	0.242
WaterHeat	4	0.722
Total	2	0.493

The prediction accuracy of the RT models for heating can be as high as 85% with an optimal depth of four layers (see Figure 5.6). The optimal test scores for RTs for appliance and external lighting are 0.33 and 0.578, respectively, when the depth is around 10 (see Table 5.2). However, note that the larger the depth (higher complexity), the more likely the model is overfitting and not transferable to other regions of study.

Based on Table 5.2, the RT model for heating with an optimal depth of four is taken as an example, as shown in Figure 5.5. The tree represents the interaction between heating load and weather attributes and temporal factors. The season factor (day) first splits heating into two parts (winter vs. non-winter). Dew point temperature also plays an important role.

Season, dew point temperature, and temperature altogether can account for more than 50% of the heating load.

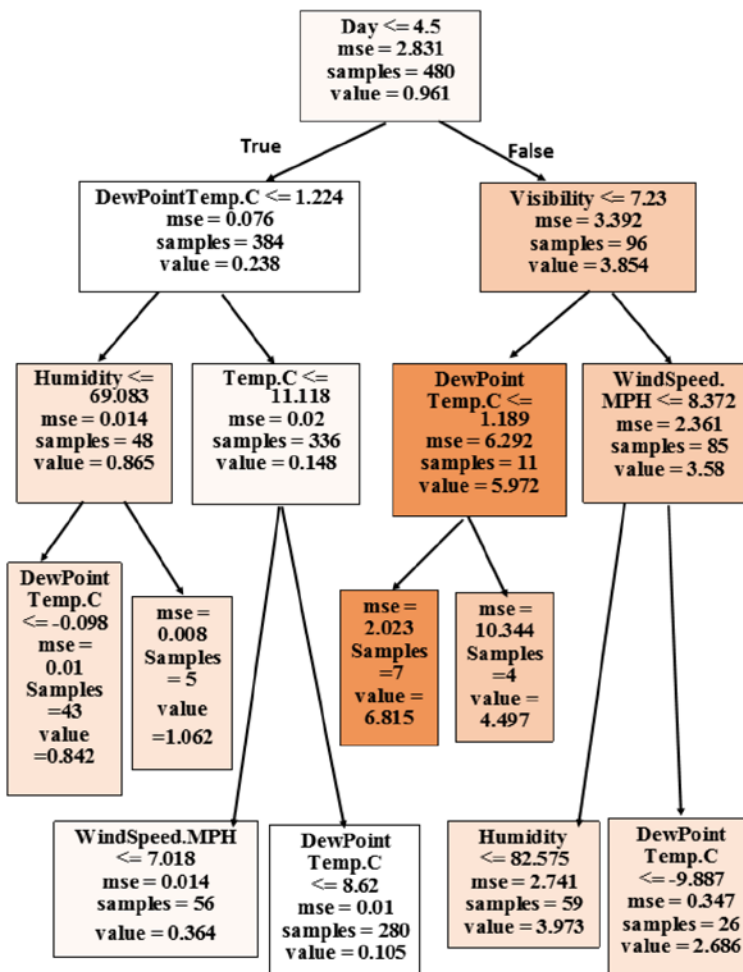


Figure 5.5 The RT Model for Heating

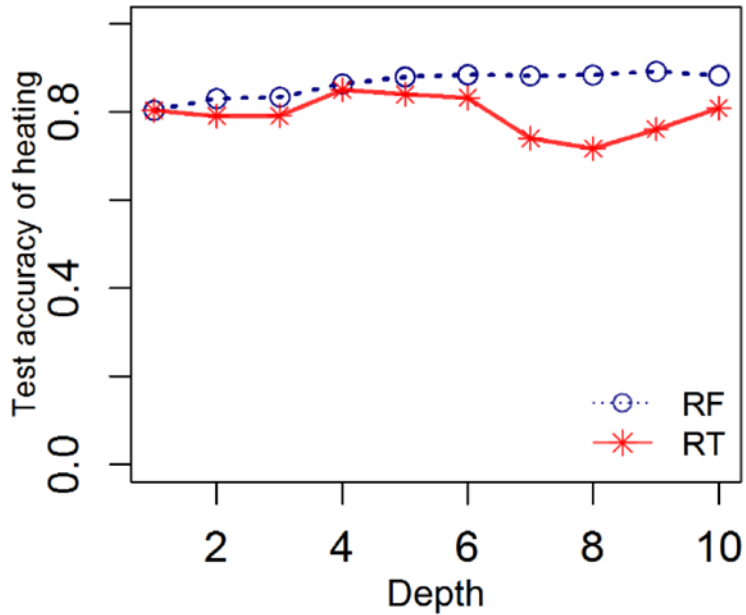


Figure 5.6 Test Accuracy of Heating by RF and RT Models

Figure 5.6 shows the testing accuracy for the heating components as a function of model depth using the RF and RT approaches. When the depth is smaller than or around four, the accuracy values of the RF and RT models are comparable. With the increase of the RF and RT model depths, the RF models yield higher accuracy and consistency in the predictions. A very complex RT model is not necessarily better than a simple RT model due to significant overfitting of the training data. RF models, on the other hand, can take care of the overfitting issues very well, and the testing accuracy can go up to 85% or above in our study. Still it is more straightforward to visualize the impacts of important variables based on the RT model fitting, and therefore it can be used as a guidance on the model complexity and factor importance.

5.4.2 ML Models for Residential and Commercial Cooling

In this section, we focus on the development and validation of ML models for the cooling components in both the residential and commercial datasets of the WECC system. The models will be used for approximating load profiles in the target zones (e.g., eastern interconnection and ERCOT).

In order to obtain reliable relationships among load components and weather attributes as well as seasonal conditions, both RT and RF methods were developed with multi-fold validation, where the load component and weather attribute dataset was randomly split into training (75%) and testing subsets (25%). The analyses were done for all load components, and the results on the cooling component in the summer time (July and August) is the focus of this section.

Table 5.3 shows the feature importance based on the RT and RF models for commercial and residential cooling. For commercial cooling, temperature is the top factor as expected. Dew point temperature also plays an important role according to the RT and RF models. The factor ranks are consistent between RT and RF models for commercial cooling. For residential cooling, the relationships are much more complicated, season (Day) is a critical factor based on the RT model, and dew point temperature and humidity are also important. Humidity and visibility (related to humidity in the Northwestern region) are also non-negligible in the RF model.

Table 5.3 Feature Importance in RT and RF Models for Cooling

	Commercial		Residential	
	RT	RF	RT	RF
Visibility	0.049	0.033	0.066	0.243
Temperature	0.658	0.745	0.011	0.037
Dew point Temperature	0.206	0.161	0.064	0.092
Humidity	0.014	0.022	0.056	0.405
Wind Speed	0.064	0.03	0.048	0.042
Precipitation	0.01	0.009	0.015	0.04
Day	0	0	0.739	0.141

Figure 5.7 and Figure 5.8 show the RT models for commercial and residential cooling, respectively. The prediction accuracy (the goodness of fit on the testing data) of RT can be as high as 82% with an optimal depth of three layers for commercial cooling, and temperature, dew temperature and visibility are the major factors for fitting variability in commercial cooling. Fitting variability in the residential cooling needs larger depths. The accuracy of the RT model for residential cooling is about 50% with a depth of four and up to 60% with a depth of seven. Humidity, dew point temperature, day (seasonal condition), visibility, precipitation, wind speed and temperature all contribute to this RT model.

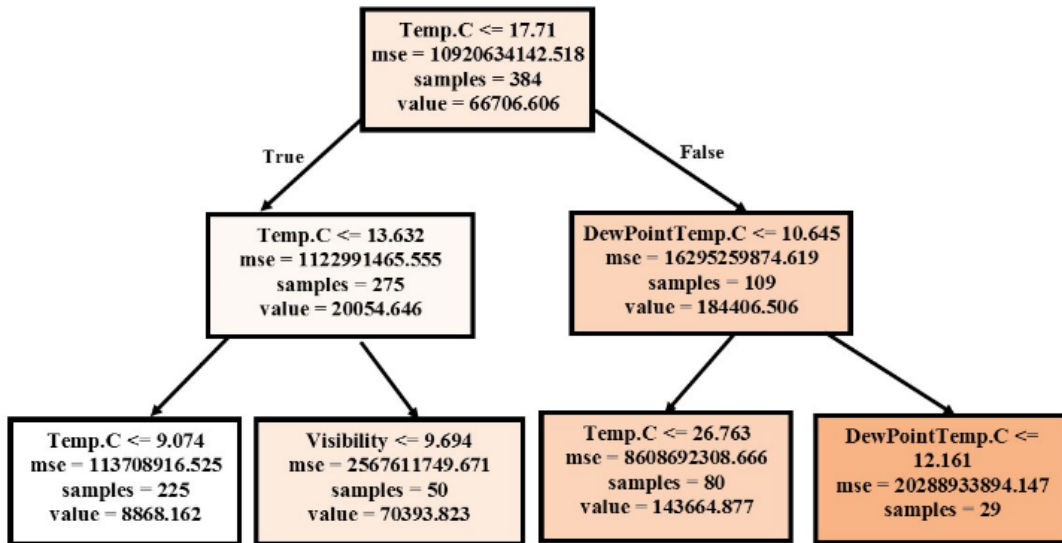


Figure 5.7 RT Model for Commercial Cooling

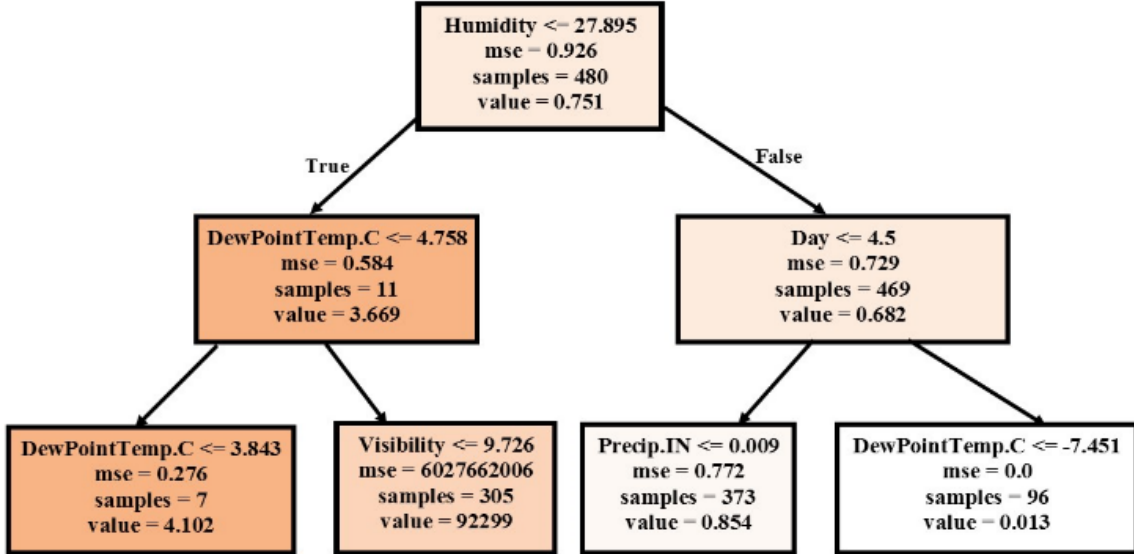


Figure 5.8 RT Model for Residential Cooling

Figure 5.9 shows the testing accuracy for commercial and residential cooling as a function of RT and RF model complexity (i.e., depths) for the four climate zones. The dotted lines represent the accuracy values of the RF models and the solid lines represent those from the RT models. In general, the prediction accuracy of commercial cooling (red) are higher than those for residential cooling (blue) with either RT or RF models. A simpler RT or RF model is needed for the commercial data as the prediction accuracy can go beyond 80% with a depth of three, and there is not much gain by adding layers in the models. More complicated models are needed for residential cooling, a depth of four can help RT to achieve an accuracy of up to 60%, and a depth of eight for RF yields an accuracy comparable to the commercial cooling predictions.

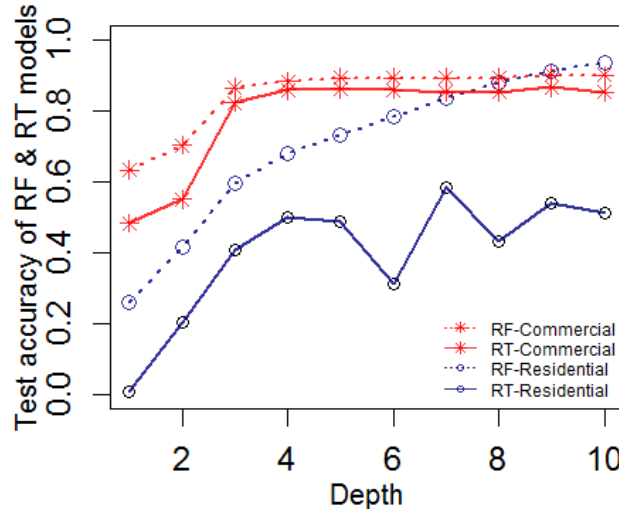


Figure 5.9 Testing Accuracy of RT and RF Models of Cooling.

The accuracies of the RF models are always higher than those of the RT models. For example, when the model depth is three, the accuracy of the RT model is about 82% and the accuracy of the RF model is over 86% for commercial cooling. For residential cooling, when the RT model depth is seven, the

maximum accuracy is about 58%, while the RF model can achieve an accuracy to beyond 80% by adding model layers. Much more layers did not help RT due to overfitting.

5.4.3 Summary

In this study, we applied two machine learning approaches to our unique commercial and residential load datasets and the corresponding weather information. Reliable machine learning models were developed and evaluated under different climate conditions in the Northwestern US.

In general, commercial data has rather straightforward relationships with weather attributes, and therefore needs simpler models than for residential data. The temperature is highly important to the commercial cooling while the residential cooling is affected by temperature and several other factors.

Both RT and RF models have good performance on commercial cooling predictions achieving accuracy over 82% with a depth of three layers. Residential load models are more complex than the commercial load models, and need more layers for acceptable accuracy. Based on the accuracy of the fitted RT and RF models, the RF model is preferable as it can handle overfitting problems and yield lower testing errors under all conditions in the study.

Overall, weather-based machine learning approaches can be reasonably used to predict commercial and residential cooling and other load components to produce load profiling for power system planning and operation purposes. In the next section, transfer learning methods will be evaluated to predict load shapes using available weather attributes for the locations where load data are unavailable.

5.5 Load Shape Estimation for Eastern Interconnection (EI) and Electric Reliability Council of Texas (ERCOT)

5.5.1 Background

In Chapter 5.4, RF models were developed using weather attributes and commercial/residential load data of the WECC system. The RF models have good performance on commercial cooling predictions by achieving an accuracy over 82% with a depth of three layers. This is remarkable since it is well known that the western zones cover a large geographic region with diverse weather and temperature conditions. Since the major weather attributes in the western United States, such as the temperature and humidity, has comparable ranges to the entire United States, we assume that developed models have transferability to the eastern target zones. In this work, the weather data of the same time span was downloaded from the NOAA website and Canada government website. The weather data is then used as inputs to the RF models for approximating the commercial load for EI and ERCOT systems.

5.5.2 Target Zones: Eastern Interconnection and ERCOT

Eastern United States has two large interconnections - Eastern interconnection and ERCOT, which can be divided into 11 climate zones as shown in Figure 5.10. For each climate zone, a representative city was selected and shown in Table 5.4.

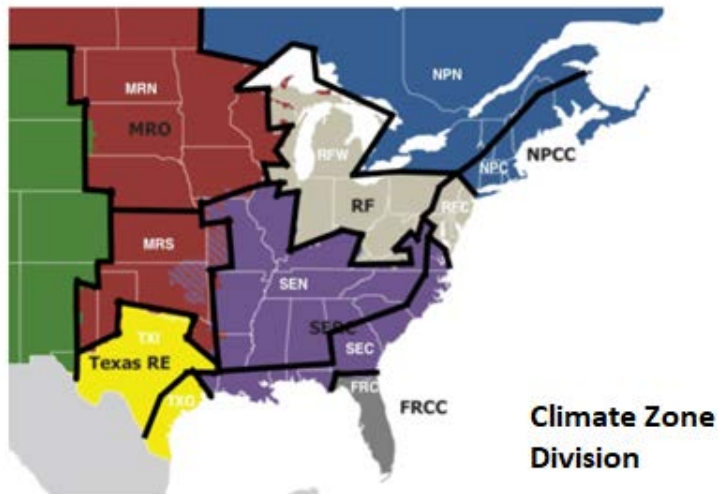


Figure 5.10 Map Depicting Geographic Region for Each Climate Zone [50]

Table 5.4 Eastern Climate Zones with Representative Cities

Climate Zones	Representative Cities
MRN	Duluth, MN
MRS	Wichita, KS
RFW	Chicago, IL
SEN	Nashville, TN
NPN	Toronto, ONT
NPC	Boston, MA
RFC	Baltimore, MA
SEC	New Orleans, LA
FRC	Tampa, FL
TXG	Houston, TX
TXI	Dallas, TX

5.5.3 Weather Data of Eastern Climate Zones

For consistency, weather data of each eastern climate zone during the same time period (2002.1-2003.12) as commercial load shape data was downloaded from the NOAA website and Canada government website. Figure 5.11 and Figure 5.12 show the temperature time series on Day 2 (hot summer). Comparing these two figures, the temperature range in the western region is wider than that of the eastern region. Moreover, the temperature patterns of the eastern zones are simpler than those of the western ones. Favorable conditions exist to make the developed ML models more likely to be transferrable, which support our assumption that the WECC RF models and eastern weather information can be used to estimate eastern load profiles.

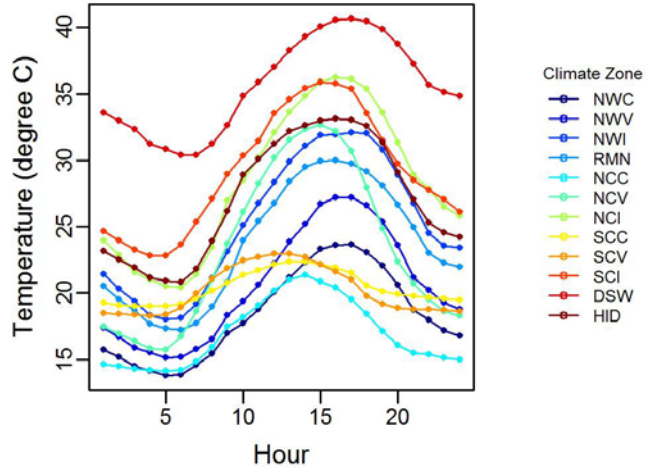


Figure 5.11 Western Temperature Time Series Plot

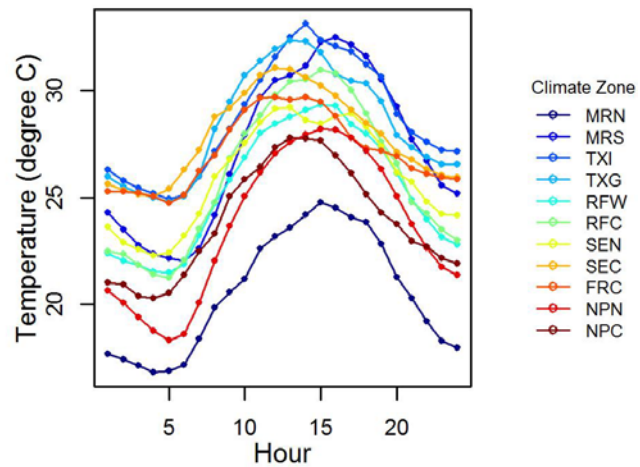


Figure 5.12 Eastern Temperature Time Series Plot

5.5.4 Results

Figure 5.13 presents the estimation of commercial cooling usage on hot summer (Day 2) by using the developed RF model and eastern weather data. For most of those climate zones, the peak usage of cooling match the peak temperature since temperature is the roughly the most influential factor. The climate zone with higher temperature in general has higher cooling usage. It is noted that the estimated load seems to be low in several zones (e.g., TXI, TXG and FRC) with concurrent high temperature and high humidity. Such conditions are not often seen in the training climate zones in the western US. As a result, the model transferability might be relatively low. In future development, a scaling factor might need to be introduced, or an alternative solution is to include more data with such high-temperature and high-humidity conditions in the model training.

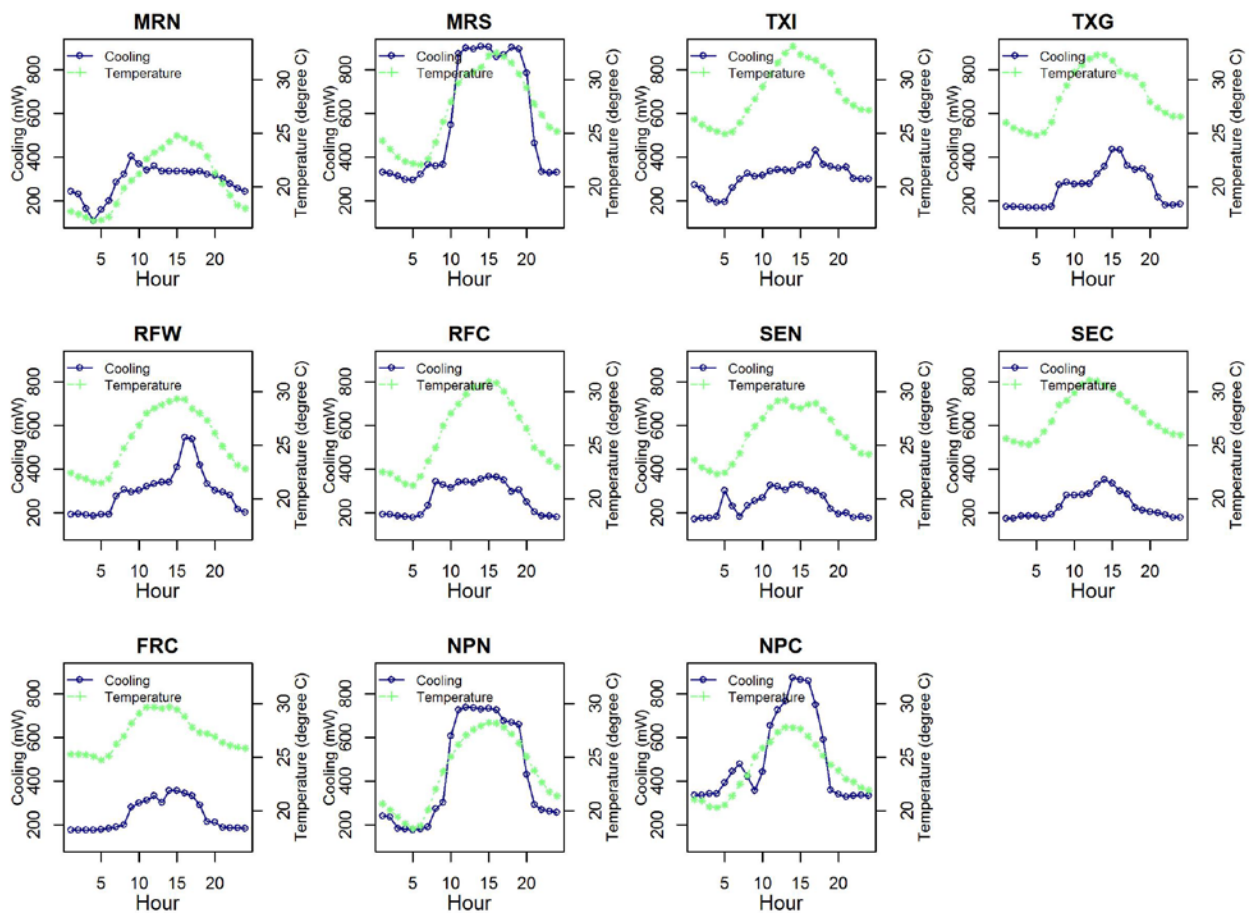


Figure 5.13 Cooling Estimation of Eastern United States for Day 2 (Hot Summer)

6.0 Aggregate Motor Protection Modeling

6.1 Background

Four types of aggregate motor model are implemented in the WECC composite load model, referred to as the motor type A, B, C and D. Brief description of the different types of motors are given below:

- Motor A: Three-phase induction motors that operate under constant torque. Examples of such motors include commercial air-conditioners and refrigerators.
- Motor B: Three-phase induction motors with high inertia, operating under speed-dependent torque. Examples include fan motors.
- Motor C: Three-phase induction motors with low inertia, operating under speed-dependent torque. Examples include pump motors.
- Motor D: Single-phase induction motors represented by aggregate performance-based model. Examples of single-phase motors include residential air-conditioners and heat pumps.

Motors are typically protected by different protection methods, such as relays, contactors, thermal protection, etc. During a fault, as the voltage drops below a certain limit for longer than a certain duration, then the protection mechanism gets triggered to trip the associated motor load. Figure 6.1 illustrates how an aggregate motor load may respond during voltage event due to the various protection schemes activated over the duration of the fault (the figure ignores the motor dynamics, but focuses only on the effect of the protection). Understanding the behavior of motor loads under the action of different protection schemes is of paramount importance. The goal of this task is to develop aggregate motor protection models for commercial-sector composite load models.

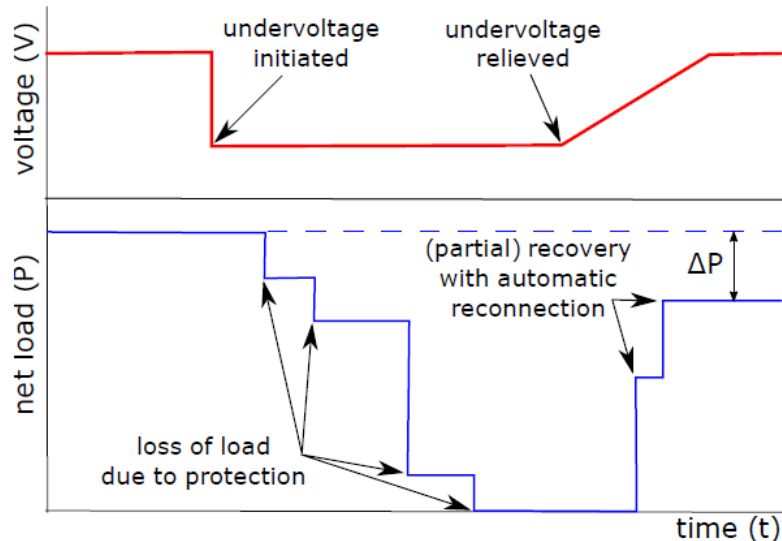


Figure 6.1 Typical Load Tripping Profile

6.2 Protection Methods

The protection equipment presented in different motors vary widely in their operating parameters (i.e. tripping and reconnection behavior). Furthermore, the response parameters of a protection may not be static, and can also depend on factors such as the loading on the motor (e.g. fully loaded motors will likely trip earlier than lightly loaded motors), which may in turn depend on conditions such as the outside air temperature, occupancy of a buildings, etc. Modeling the protection schemes in a generic sense, therefore, is a challenging task.

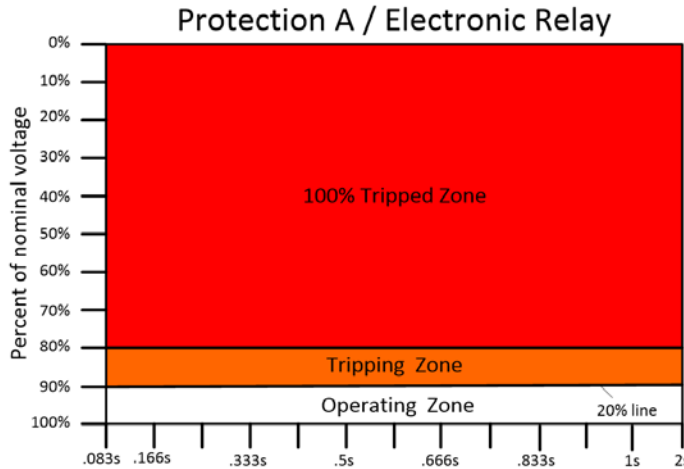


Figure 6.2 Protection Parameters for Electronic Relays

To illustrate the modeling of the protection schemes, we introduce Figure 6.2 which depicts the parameters of electronic relays. The red area labeled as “100% Tripped Zone” is where it has been identified that the motor protection would most likely be activated and the motor taken offline. The white area labeled “Operating zone” is where it has been identified that the motors will continually operate through the voltage variance with no protection activated. The orange area labeled “Tripping Zone” indicates the area in which the protections on some fraction of the motors, such as the ones that are heavily loaded, are likely to be activated. The number/fraction of heavily loaded motors vary at any given time, and could be estimated at, say, 5-10% during unoccupied hours or shoulder months, and 15-20% during occupied hours or peak summer time. The figure shows that if the voltage falls below 80% the protection trips almost 100% of the motors that have electronic relays, while the heavily loaded motors (estimated at 20%) can start tripping when the voltage drops below 90%.

For this work, we categorize the different motor protection schemes found into five different types, each of which is characterized by a (range of) voltage depth and duration for tripping, and a (range of) voltage depth and duration for reconnection (upon recovery). The different categories of protection are as follows:

- (1) **Protection 1 (or, Electronic Relays):** These devices monitor incoming voltage to the motor. When a critical fault condition (phase loss or phase reversal) is present, the relay will immediately de-energize the contactor thus dropping the motor voltage. These devices have user defined trip parameters but the device default settings apply to most applications and most devices are left to the recommended manufacturer trip settings. This protection trips the motor operating in under-voltage conditions at the terminal. This protection is usually accompanied with reconnection logics.
- (2) **Protection 2 (or, Current Overload Relays):** When excessive current flows through the motor circuit, the relay opens due to increased relay temperature or sensed overload current, depending

on the relay type. This protection trips the motor if the motor terminal current exceeds a threshold and lasts for a delayed period of time.

- (3) **Protection 3 (or, Thermal Protection):** These devices rely on excessive motor winding or motor case heat to trip a mechanical bimetal disk. These devices may be mounted internally next to the motor windings or externally on the motor or compressor casing. These are used in single phase applications only, such as residential air-conditioner motor.
- (4) **Protection 4 (or, Contactors):** These devices play a role in how and when a motor may disconnect and reconnect from the grid. This protection trips the motor running in extremely low voltage conditions. This type of protection is usually configured for fast response to severe voltage depression conditions. Contactor protection also has reconnection logics.
- (5) **Protection 5 (or, Building Management System):** These devices are generally computerized and when supply power or voltage is varied enough, the control system will proceed through a reboot process. During that time the motors under its control will be shut down (This is generally building wide). Testing conducted by the Bonneville Power Administration has shown that the BMS can ride though severe voltage sags down to 65% of nominal voltage [51]. BMS controllers have reconnection logics.

Our previous study [51] carried out a research on the different protection schemes found on various commercial building types. The findings of that report were used to generate a “Protection Table” listing the available motor protections into the five different types defined above.

Building	Space [sf]	Appliance	Equipment	Type	Protection					Rating [kW]	
					P1	P2	P3	P4	P5 Aggregate		
Small Retail	10000	RTU	Fan	MB	0	1	0	1	1	P2P4P5	6.15
Small Retail	10000	RTU	Compressor	MA	0	1	0	1	1	P2P4P5	21.25
Small Retail	10000	RTU	Frac_Condensor	MD	0	0	1	1	1	P3P4P5	6.50
Small Retail	10000	Exhaust	Frac_Fan	MD	0	0	1	1	1	P3P4P5	0.46
Small Retail	10000	RiRF	Frac_Compressor	MD	0	1	0	1	0	P2P4	8.50
Small Retail	10000	RiRF	Frac_Fan	MD	0	0	1	0	0	P3	3.40
Small Retail	10000	WiRF	Compressor	MA	1	1	0	1	0	P1P2P4	10.63
Small Retail	10000	WiRF	Frac_Fan	MD	1	0	1	1	0	P1P3P4	4.25
Medium Retail	25000	RTU	Fan	MB	0	1	0	1	1	P2P4P5	15.38
Medium Retail	25000	RTU	Compressor	MA	0	1	0	1	1	P2P4P5	53.13
Medium Retail	25000	RTU	Frac_Condensor	MD	0	0	1	1	1	P3P4P5	16.25
Medium Retail	25000	RTU	Frac_Ind_Draft	MD	0	0	1	1	1	P3P4P5	10.41
Medium Retail	25000	Exhaust	Frac_Fan	MD	0	0	1	1	1	P3P4P5	0.92
Large Retail	75000	RTU	Fan	MB	0	1	0	1	1	P2P4P5	46.15
Large Retail	75000	RTU	Compressor	MA	0	1	0	1	1	P2P4P5	159.38
Large Retail	75000	RTU	Frac_Condensor	MD	0	0	1	1	1	P3P4P5	48.75
Large Retail	75000	RTU	Frac_Ind_Draft	MD	0	0	1	1	1	P3P4P5	31.22
Large Retail	75000	Exhaust	Frac_Fan	MD	0	0	1	1	1	P3P4P5	1.38

Figure 6.3 Snapshot of Building Motor Loads and Protection Schemes.

Figure 6.3 shows a snapshot of such a table, shown for retail buildings, where the P1 to P5 refers to the protection types and the numbers 0 and 1 are used to represent absence and presence of that protection, respectively. In this example, the small retail building (with a typical floor-space of 10,000 square feet) has different appliances – roof-top units (RTU), reach-in refrigerators and freezers (RiRF), walk-in refrigerators and freezers (WiRF) and exhaust fans, with various motors (e.g. fan motors, compressors, fractional compressors and condensers, etc.). Each such motor is equipped with a set of protection methods (assigned a value 1). Such tables are built for the following types of commercial buildings: (1) Retail: small, medium, large, (2) Supermarket, (3) Fast food, (4) Office: small, large, (5) Hotel/Lodging, (6) Warehouse, (7) School, and (8) Hospital

6.3 Typical Commercial Building Prototypes and Controls

The next step in the process of generating the aggregate motor protection model is to estimate the fractions of the commercial net end-use motor load consumption that is subjected to each type of protection. To do so, we need to estimate the loading on the different appliances in each building type, over a range of operating conditions defined by the seasons (summer, winter, etc.), time of day, and climatic region the building is located in. This is done in two ways:

- EnergyPlus (E+) [52] simulations allow us to generate power consumption profiles of certain appliances in prototype building models, which will be explained in Chapter 6.4.
- For appliances and/or building types for which EnergyPlus not available, we estimate the loading on the appliance motors, based on factors such as occupancy and outside air temperature.

Once the loading of the appliance motors is estimated at every time instant of any given day of the year the net load fractions associated with each protection type can be computed for each building. For example, if a building has ‘ n ’ different motors, each of which is drawing a certain power $P_i(t)$, $\forall i \in \{1, \dots, n\}$, then the fractions of net building load at any given time ‘ t ’ that are assigned to any protection can be computed as:

$$\alpha_j^{building}(t) = \frac{\sum_{i=1}^n s_{j,i} P_i(t)}{\sum_{i=1}^n P_i(t)}, \quad \forall j \in \{1, 2, \dots, 5\} \quad (6.1)$$

where the variables $s_{j,i} \in \{0, 1\}$, $\forall i \in \{1, \dots, n\}$, $\forall j \in \{1, 2, \dots, 5\}$, denote whether or not a particular protection type- j is present in a the motor- i . Note that this fraction is a time-varying value.

The key here is to estimate the power consumption of the motors and the appliances. EnergyPlus simulations help us get these power consumption for most of the appliances in the prototype buildings, such as the roof-top units compressors and supply fans. For other smaller motors, such as those in exhaust fans, dedicated outdoor air systems (DOAS) and make-up air units (MAUs), the power consumptions are estimated based on buildings design protocols [53] [54] [55]. A couple of examples are given below:

- 1) The exhaust fans used in the toilets are generally designed for air movement of 75 cubic-ft-per-meter (cfm) per fixture. The fan motors are typically rated at 1300 cfm/hp. Thus assuming a medium retail building of 25000sf of floor-space has 20 toilet fixtures, the exhaust fans are rated at 1.15hp (or, 0.92kW, with an efficiency of 0.8kW/hp). Furthermore, the exhaust fans are expected to be running during the occupancy hours, which yield the desired power consumption profile for the exhaust fans.
- 2) The dedicated outdoor air systems (DOAS) that are found in hospital or large office buildings are designed to supply 5 cfm/person. Estimating the occupancies in a large office building of 500000sf at 2500 persons, and in a hospital of 100000sf at 1000 persons, the total air-movement

through the DOAS can be estimated at 12500cfm and 5000cfm, respectively. An energy conversion factor of 300cfm/hp yield the ratings of the DOAS fans in large office and hospital buildings as 41.67hp and 16.67hp, respectively. The DOAS also run during occupancy hours.

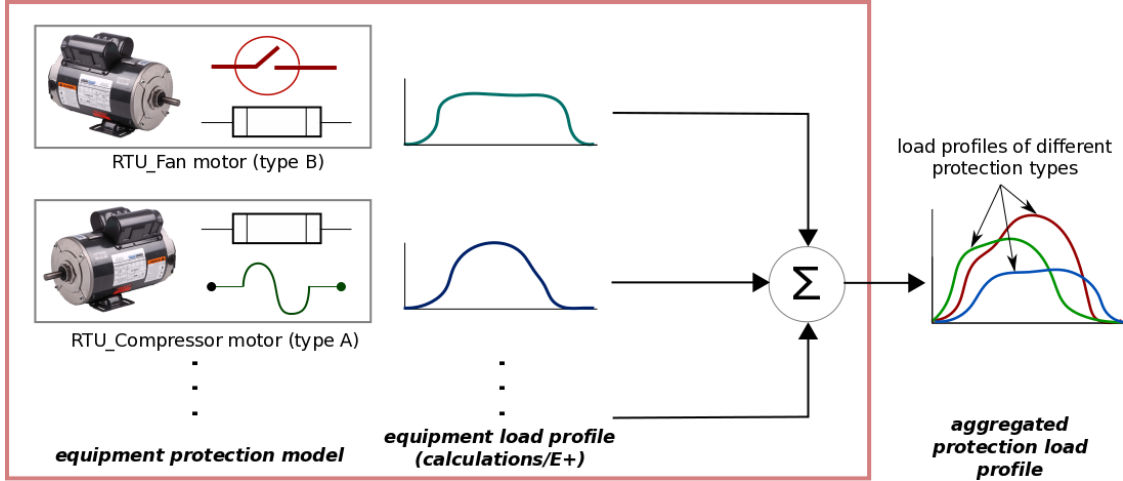


Figure 6.4 Load Protection Profile for a Building Proto-type

Once the aggregation of appliance protection profiles is computed for each building (see Figure 6.4), the next step is to build the aggregate protection profile across all the building types. To do this, the presence of different buildings types across a (geographic/climatic) region is needed, either in terms of number or the total floorspace. The EIA Commercial Buildings Energy Consumption Survey [56] data provides us the total floorspace of each building type present in different geographic regions across the United States of America. This is done as illustrated in Figure 6.5. For each building type, we scale the protection profiles by a factor equal to:

$$\omega_{\langle \text{building} \rangle} := \frac{\text{total floorspace of } \langle \text{building} \rangle}{\text{floorspace of a prototype of } \langle \text{building} \rangle} \quad (6.2)$$

and then take the sum across all building types weighted by this ratio.

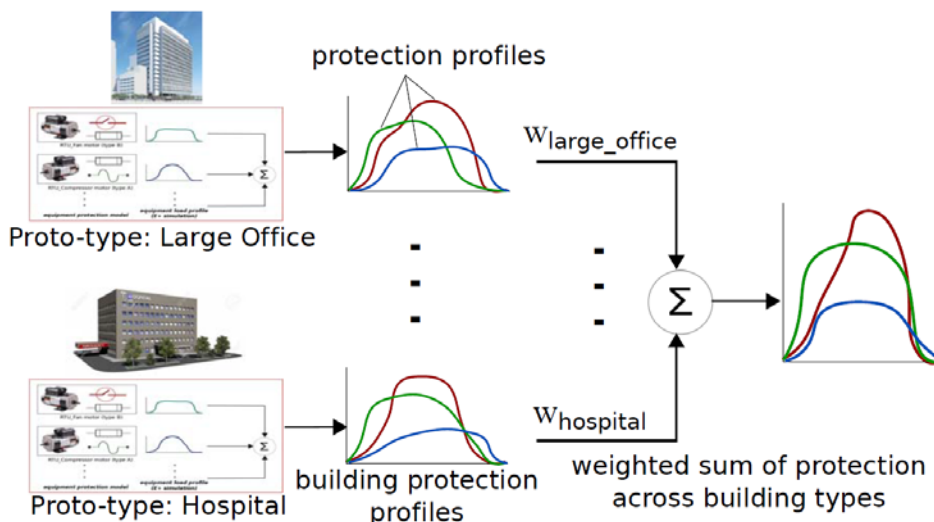


Figure 6.5 Aggregation of Protection Profiles across All Building Types, Based on Floor-Space Ratios.

Using the proposed method, the aggregated protection profiles have been generated for commercial buildings in representative cities from different climate zones. These results are presented in a tabular form where the fractions of total load subjected to each protection method are calculated at an hourly basis for five typical days chosen to represent each different season of the year. Figure 6.6 shows a snapshot of such a table, for the commercial buildings in Phoenix, AZ, for a typical day in the month of January (winter season).

Time	MA					MB					MC					MD				
	P1	P2	P3	P4	P5	P1	P2	P3	P4	P5	P1	P2	P3	P4	P5	P1	P2	P3	P4	P5
mo=1 hr=1	5%	11%	1%	15%	3%	3%	43%	0%	46%	41%	0%	7%	0%	3%	6%	1%	1%	31%	23%	20%
mo=1 hr=2	5%	11%	1%	15%	3%	3%	43%	0%	46%	42%	0%	7%	0%	3%	5%	1%	2%	31%	23%	20%
mo=1 hr=3	5%	11%	1%	14%	3%	3%	43%	0%	46%	42%	0%	7%	0%	3%	5%	1%	2%	31%	23%	20%
mo=1 hr=4	5%	11%	1%	14%	3%	3%	44%	0%	47%	42%	0%	7%	0%	3%	5%	1%	2%	31%	23%	20%
mo=1 hr=5	5%	10%	0%	14%	3%	3%	45%	0%	47%	43%	0%	7%	0%	3%	5%	1%	2%	31%	23%	20%
mo=1 hr=6	5%	8%	0%	12%	3%	3%	46%	1%	50%	46%	0%	6%	0%	3%	5%	1%	3%	30%	22%	20%
mo=1 hr=7	5%	7%	0%	11%	4%	3%	53%	1%	56%	53%	0%	5%	0%	2%	4%	1%	3%	25%	19%	17%
mo=1 hr=8	5%	7%	1%	12%	4%	3%	53%	1%	56%	54%	0%	5%	0%	2%	4%	1%	3%	25%	18%	16%
mo=1 hr=9	5%	7%	1%	12%	4%	3%	54%	1%	57%	54%	0%	5%	0%	2%	4%	1%	2%	24%	18%	16%
mo=1 hr=10	8%	7%	1%	14%	7%	2%	51%	1%	54%	51%	0%	6%	0%	2%	5%	1%	2%	23%	17%	15%
mo=1 hr=11	9%	8%	1%	16%	9%	2%	49%	1%	52%	49%	0%	7%	0%	2%	6%	1%	2%	22%	17%	15%
mo=1 hr=12	11%	9%	1%	19%	12%	2%	46%	1%	49%	47%	0%	8%	0%	2%	7%	1%	2%	22%	16%	14%
mo=1 hr=13	13%	10%	1%	22%	15%	2%	44%	1%	47%	45%	0%	8%	0%	2%	7%	1%	2%	21%	16%	14%
mo=1 hr=14	14%	11%	1%	24%	17%	2%	43%	1%	45%	43%	0%	8%	0%	2%	7%	1%	2%	21%	16%	14%
mo=1 hr=15	15%	12%	1%	25%	18%	2%	41%	0%	44%	42%	0%	8%	0%	2%	7%	1%	2%	21%	16%	14%
mo=1 hr=16	14%	12%	2%	25%	18%	2%	41%	0%	43%	41%	0%	8%	0%	2%	7%	0%	2%	21%	17%	14%
mo=1 hr=17	14%	12%	2%	25%	17%	2%	41%	0%	43%	41%	0%	8%	0%	2%	7%	0%	2%	22%	17%	15%
mo=1 hr=18	14%	10%	2%	24%	16%	2%	42%	1%	44%	42%	0%	9%	0%	2%	8%	1%	2%	22%	17%	14%
mo=1 hr=19	10%	10%	2%	20%	11%	2%	45%	1%	48%	45%	0%	8%	0%	2%	7%	1%	2%	23%	17%	15%
mo=1 hr=20	10%	9%	2%	19%	10%	2%	45%	1%	48%	45%	0%	8%	0%	2%	7%	1%	2%	23%	18%	15%
mo=1 hr=21	9%	9%	2%	18%	9%	2%	46%	1%	49%	46%	0%	7%	0%	2%	6%	1%	2%	24%	18%	15%
mo=1 hr=22	9%	11%	2%	20%	8%	3%	42%	0%	45%	42%	0%	9%	0%	3%	7%	1%	1%	26%	20%	16%
mo=1 hr=23	6%	11%	2%	17%	5%	3%	41%	0%	44%	40%	0%	8%	0%	3%	6%	1%	1%	29%	22%	19%
mo=1 hr=24	6%	11%	1%	16%	4%	3%	42%	0%	45%	41%	0%	8%	0%	3%	6%	1%	1%	30%	22%	19%

Figure 6.6 Aggregated Protection Profile for Phoenix, AZ, for a Typical Day in January.

6.4 EnergyPlus Simulation

DOE's Commercial Prototype Building Models [57] were used in this study to generate building electric load profiles. The suite of prototypes consists of 16 building types, covering 80% of the commercial and multifamily building floor area in the United States for new constructions. A list of the prototypes is given in Table 6.1.

Table 6.1 Building Prototypes

Building Activity	Building Prototype	Prototype Floor Area (ft ²)
Office	Small Office	5,500
	Medium Office	53,630
	Large Office	498,640
Retail	Standalone Retail	24,690
	Strip Mall	22,500
Education	Primary School	73,970
	Secondary School	210,910
Healthcare	Outpatient Healthcare	40,950
	Hospital	241,410
Lodging	Small Hotel	43,210
	Large Hotel	122,120
Warehouse	Warehouse	52,050
Food Service	Quick-Service Restaurant	2,500
	Full-Service Restaurant	5,500
Apartment	Mid-Rise Apartment	33,740
	High-Rise Apartment	84,360

The energy efficiency design of the prototypes meets the minimum requirements of national model energy code ASHRAE Standard 90.1-2004 [58], which is assumed to represent existing buildings that were constructed in the past decade. Whole building energy simulations were conducted by using DOE's EnergyPlus program for 111 representative weather locations in 50 states in the U.S. The electric loads are outputted in 10-minute interval for an entire year. The load profile is generated at individual equipment level when possible. In some cases, multiple pieces of equipment are combined in the prototype models and their combined load profile is generated.

Altogether, the suite of prototype buildings covers a large range of electric equipment and appliances including interior and exterior lighting, fans, pumps, direct expansion heating and cooling coils, electric resistance heating coils, chillers, cooling towers, humidifiers, service water heaters, and plug and process loads (such as elevators, commercial kitchen appliances, commercial reach-in and walk-in refrigerators and freezers). The rated power of the equipment and appliances is also reported.

6.5 Optimization-Based Protection Aggregation Algorithm

Induction motors are usually equipped with several types of protection with different operation mechanisms, making it challenging to develop adequate yet not overly complex protection models and determine their parameters for aggregate induction motor models. This sub-chapter proposes an optimization-based framework to determine protection model parameters for aggregate induction motor loads in commercial buildings [59]. Introducing a mathematical abstraction, the task of determining a

suitable set of parameters for the protection model in composite load models is formulated as a nonlinear regression problem. Numerical examples are provided to illustrate the application of the framework.

6.5.1 Protections: Mathematical Modeling

Motors are typically protected by multiple devices, such as relays, contactors, thermal protection, etc. During a fault, as the voltage drops below a certain limit for longer than a certain duration, multiple protection mechanisms could be triggered to trip the associated motor load. The protection action has been illustrated in Figure 6.1, which illustrates how an aggregate motor load may respond during a voltage event due to the various protection schemes activated over the duration of the fault (Note that Figure 6.1 ignores the motor dynamics, but focuses only on the effect of the protection). Understanding the behavior of motor loads under the action of different protection schemes is of paramount importance. The focus of the work presented in this section is on the commercial sector, however the application to residential and industrial sectors should be similar.

Modeling protection schemes, in general, is a challenging task. The protection equipment present in different motors vary widely in their operating parameters (i.e. tripping and reconnection behavior). Furthermore, the response parameters of a protection device may not be static, and can also depend on factors such as the loading on the motor (e.g. fully loaded motors will likely trip earlier than lightly loaded motors), which may in turn depend on conditions such as the outside air temperature, occupancy of a buildings, etc. A probabilistic framework is required to capture this behavior. However, for simplicity in the mathematical modeling and the optimization framework presented in this section, we would assume a deterministic model of the protection, i.e., given a fault, the protection is either tripped or is in the operational region based on some static trip conditions. To facilitate the mathematical construction of model, let us define the protection ‘trip-zone’ as:

Definition 1: Trip-zone for a given protection scheme- i , denoted by T^i , is defined as the set of pairs of voltage levels at fault (v_f) and the fault duration values (τ_f) such that the protection- i is tripped if and only if $(\tau_f, v_f) \in T^i$, i.e.

$$(\tau_f, v_f) \in T^i \Leftrightarrow \text{protection-}i \text{ is tripped} \quad (6.3)$$

Each protection scheme can be modeled mathematically in the form of a discrete-valued function $f^i: \mathbb{R}_{\geq 0}^2 \mapsto \{0, 1\}$ defined as follows:

$$f^i(\tau_f, v_f) = \begin{cases} 0, & (\tau_f, v_f) \in T^i \\ 1, & \text{otherwise} \end{cases} \quad (6.4)$$

where the value of the function is 0 whenever the protection is triggered (i.e. the motor is disconnected from the network), and 1 when the protection has not been triggered (i.e. the motor is still connected to the network). It is noted that the shape of the trip-zone is different for different protections.

Remark 1: In this work, we focus only on the tripping of the protection and not on the reconnection event.

Motor protection schemes commonly found in commercial buildings in United States can be categorized into five different types including 1) electronic relays (P1), 2) current overload relays (P2), 3) thermal protection (P3), 4) contactors (P4) and 5) building management system (P5), each of which is characterized by a range of voltage deviations and durations for tripping after the fault. For more details readers are referred to [51] [60]. Most often the motors are protected not by a single mechanism, but by a combination of the different protection schemes, in a series combination. In a series combination of protections, each protection needs to be in operational state in order for the motor to be connected to the

network. Let us consider some protection- k which is a series combination of protection- i and protection- j . Then the following holds:

$$T^k = T^i \cup T^j \quad (6.5a)$$

$$\text{(or, equivalently)} \quad f^k(\tau_f, v_f) = f^i(\tau_f, v_f) \cdot f^j(\tau_f, v_f) \quad (6.5b)$$

i.e. the trip-zone of a series combination is a union of the trip-zones of each of the protections in the combination. In other words, the motor is disconnected from the network whenever any of the protections in the series combination trips. Figure 6.7 shows examples of the protection diagrams of the five individual protection schemes outlined above, as well as a series combination P1-P4-P5 with a trip-zone that is a union of the trip-zones for P1, P4 and P5. Other combinations can be constructed likewise.

In a distribution system different motors are protected by various (series combinations of) protection schemes. For example, a total of 31 series combinations can be constructed out of the five individual protections outlined in this section (excluding the unprotected case). Let us denote the set of all available (series) combinations of protection schemes by P (set of all available protection combinations) such that each member of the set P is unique. aggregate protection modeling is about constructing a reduced order protection model that can predict the fractions of total motor load tripped during a fault.

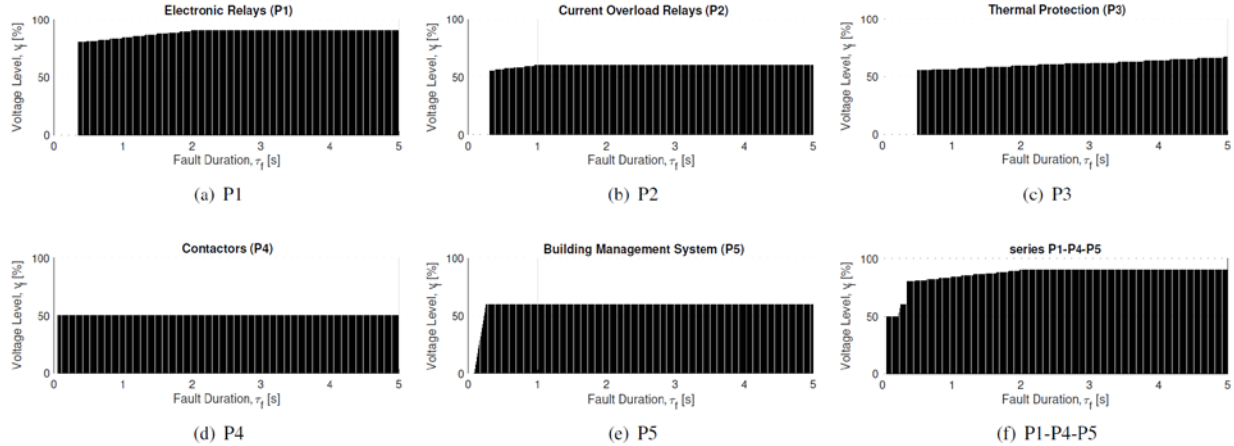


Figure 6.7 Examples of Protection Diagrams for Various Protection Schemes. Black Region Denotes the Trip Zone.

Definition 2: The aggregate protection scheme of a collection of motors served by (combinations of) protection schemes belonging to the set P can be mathematically modeled in the form of the (discrete-valued) function $F: \mathbb{R}_{\geq 0}^2 \mapsto \{0, 1\}$ defined as follows:

$$F(\tau_f, v_f) = \sum_{i \in P} \pi^i f^i(\tau_f, v_f) \quad (6.6)$$

where $\pi^i \in [0, 1]$ is the fraction of the motor load served by protection- i , i.e. $\sum_{i \in P} \pi^i = 1$. Henceforth F is referred to as the ‘aggregate protection function’.

Remark 2: Note that the fractions of the motor load served by a particular protection type is a time-varying quantity. Thus, the aggregate protection function will also be time-varying. For the purpose of this work, we do not explicitly model the time variability, while noting that the approach extends to the time-variable aggregate protection functions as well.

Since P is a finite set, F takes discrete values between 0 and 1, with the value of 0 referring to all the motor loads are disconnected, while the value of 1 refers to all motor loads being connected. In recent work [61], the authors presented a methodology to approximate the motor load fractions (π^i) for each protection combination based on typical commercial buildings' (hourly) energy consumption profiles, in different climate-zones. In the following example, we show how the aggregate protection scheme can be used to predict what fraction of motor loads will be tripped during a fault.

Example 1: Consider the protections shown in Figure 6.7. Let us assume a scenario where various motors are protected by the schemes P1, P2, P3, P5 and P1-P4-P5 (series combination), with equal fractions of motor loads associated with each protection scheme. The resulting protection diagram is shown in Figure 6.8. The aggregate protection diagram is shown (on the top), along with a plot (on the bottom) of the fractions of non-tripped (operational) motor loads under two voltage dips at 50% and 55% of nominal values.

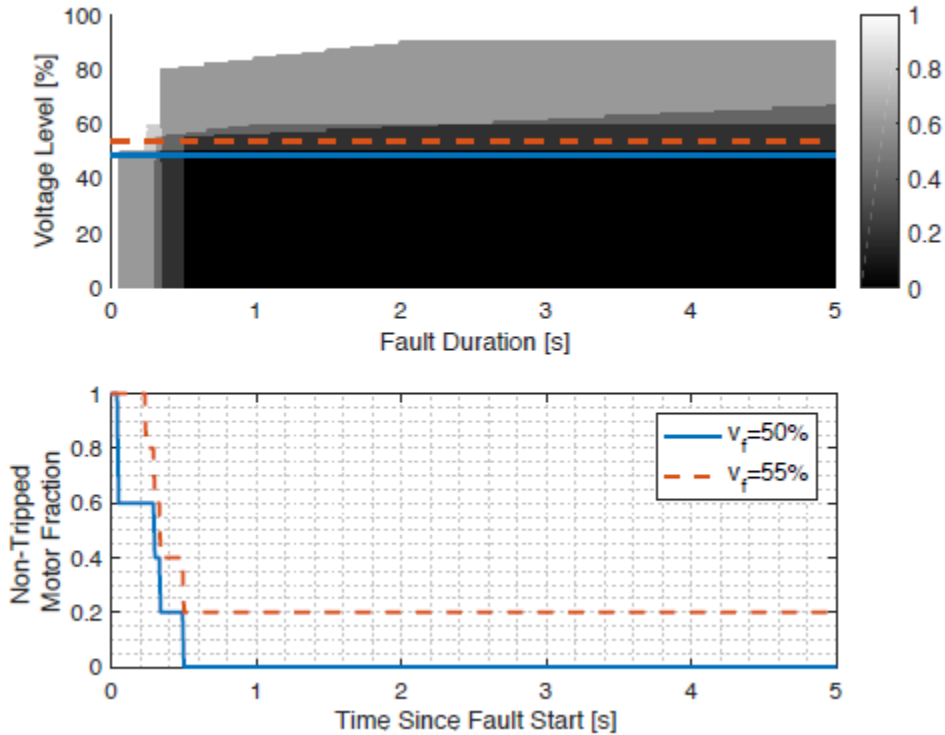


Figure 6.8 Aggregate Protection Diagram and Load Tripping

6.5.2 Aggregate Protection Modeling

As can be seen from the example (Figure 6.8), the aggregate protection scheme can be quite complex with rather arbitrarily shaped trip-zones. While such detailed models can be quite useful for understanding the behavior in the distribution networks, these are not very easy to integrate with transmission-level simulation tools. A simplified model with reduced complexity appears to be necessary, which approximates the detailed aggregate protection model as best as possible. More details can be found in the WECC composite load modeling efforts [14]. In this section, our goal is to approximate the aggregate protection model using the simplified form as follows (Figure 6.9).

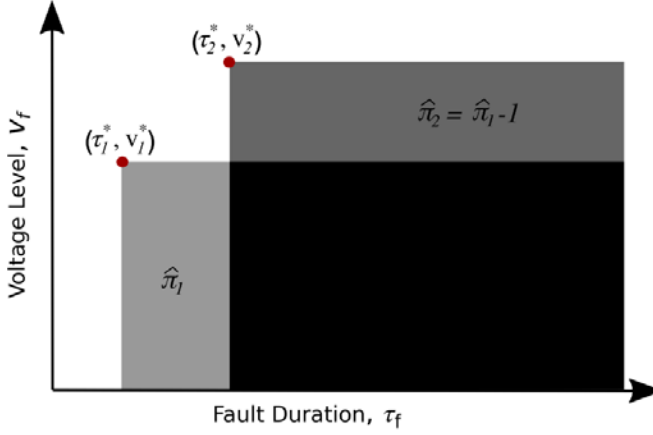


Figure 6.9 Simplified Model of the Aggregate Protection Scheme

$$\hat{F}(\tau_f, v_f) := \hat{\pi}_1 \hat{F}_1(\tau_f, v_f) + \hat{\pi}_2 \hat{F}_2(\tau_f, v_f) \quad (6.7a)$$

$$\forall i \in \{1, 2\}: \hat{F}_i(\tau_f, v_f) := \begin{cases} 0, & \tau_f \geq \tau_i^* \text{ and } v_f \leq v_i^* \\ 1, & \text{otherwise} \end{cases} \quad (6.7b)$$

$$1 = \hat{\pi}_1 + \hat{\pi}_2 \quad (6.7c)$$

Here \hat{F}_1 (\hat{F}_2) denotes the protection scheme that serves $\hat{\pi}_1$ ($\hat{\pi}_2$) fraction of motor loads, with a trip zone that is parameterized by a trip voltage v_i^* (v_2^*) and trip duration τ_i^* (τ_2^*). The goal is to find the parameters

$$\Phi = \{\hat{\pi}_1, \tau_1^*, v_1^*, \hat{\pi}_2, \tau_2^*, v_2^*\} \quad (6.8)$$

such that the simplified protection scheme \hat{F} in (6.7) approximates the true protection scheme F in (6.6). We set up a nonlinear regression problem to find the parameters in Φ that gives the best approximation (\hat{F}) of the true aggregate protection (F). This is done in the following steps:

1) Randomly select N points from the (τ_f, v_f) -space and note down the values of the true aggregate protection function F at those points (from (6.6)). Let us denote these points by (τ_f^j, v_f^j) and the corresponding value of F as $y^j = F(\tau_f^j, v_f^j)$, for each $j \in \{1, 2, \dots, N\}$.

2) Construct the cost function as

$$J(\Phi) := \frac{1}{2N} \sum_{j=1}^N \left[\hat{F}(\tau_f^j, v_f^j) - y^j \right]^2 \quad (6.9)$$

3) Solve the following optimization problem:

$$\min_{\Phi} [J(\Phi)] \quad (6.10a)$$

$$\text{s.t. } v_i^* \in [0, 100], \tau_i^* \in [0, 5] \quad \forall i \in \{1, 2\}, \quad (6.10b)$$

$$\hat{\pi}_1 + \hat{\pi}_2 = 1 \quad (6.10c)$$

Note that the optimization problem (6.10) cannot be solved directly in the present form, since it involves functions ($\hat{F}_{1,2}$) that are described in conditional forms (6.7). We overcome this problem by using logistic functions to model the protection functions $\hat{F}_{1,2}$. Logistic functions $h: \mathbb{R} \mapsto [0,1]$ are approximations of step functions and are defined as follows:

$$(\text{logistic}) \quad h(x; \alpha) := \frac{1}{1 + \exp(-\alpha x)} \quad (6.11)$$

where $\alpha > 0$ is a steepness parameter related to the slope of the function at $x = 0$. The function $\hat{F}_{1,2}$ are approximated using logistic function as follow:

$$\hat{F}_i(\tau_f, v_f) = 1 - h(\tau_f - \tau_i^*; \alpha_\tau) \left[1 - h(v_f - v_i^*; \alpha_v) \right] \quad (6.12)$$

for each $i \in \{1,2\}$, for some chosen $\alpha_\tau, \alpha_v > 0$. The optimization problem (6.10) is solved via IPOPT [62] using the logistic functional representation of $\hat{F}_{1,2}$ in (6.12).

Ideally, one would like to solve (6.10) with as many data points as possible (large N), however, due to computational limitations N has to be reasonably small. Thus, the data points need to selected judiciously so that the approximation is sufficiently accurate. It can be argued from the protection diagrams in Figure 6.7 that the protection function changes value rapidly when τ_f is near 0s. Moreover, during faults v_f is typically close to 50 %. Therefore we select the data points by assigning some weights $\omega(\cdot) \in [0,1]$ to every point on the (τ_f, v_f) -axis as follows:

$$\omega(\tau_f, v_f) = 1 - \left(1 - e^{-\beta_\tau \tau_f} \right) \left(1 - e^{-\beta_v (v_f - 50)} \right) \quad (6.13)$$

for some $\beta_\tau, \beta_v > 0$, and selecting N points randomly from all points that have larger than a chosen weight. Finally, we measure the accuracy of the approximation using the following mean absolute error metric:

$$\varepsilon := \frac{1}{M} \sum_{i=k}^M \left| \hat{F}(\tau_f^k, v_f^k) - F(\tau_f^k, v_f^k) \right| \quad (6.14)$$

where the $M (\gg N)$ points (τ_f^k, v_f^k) are selected randomly (and separately from the data points used in (6.10)) using, say, Latin hypercube sampling technique from the (τ_f, v_f) -space.

6.5.3 Numerical Results

We apply the aforementioned optimization framework to the problem in Example 1 in Chapter 6.5.2 to obtain the simplified aggregate protection diagram. The result is shown in Figure 6.10, where the top plot shows the selected data-points for (6.10) and the bottom plot shows the resulting simplified protection scheme with a mean absolute approximation error (ε) of 0.06.

Next, we consider the test cases developed in [63]. In particular, we apply the optimization framework to obtain simplified aggregate protection functions for motor loads in a hotel, large retail, medium retail, school, warehouse and supermarket. The protection schemes and the associated motor load fractions used in the study are listed in Table 6.2. Note that, out of a possible 31 combinations of protection schemes, only seven were found in the buildings considered (based on the study done in [51], [61]). The optimization problem was separately for the motor types A, B, C and D to obtain their simplified aggregate protection schemes. The results are shown in Figure 6.11 (due to similarity between the protection schemes of motor A and B, only A is shown in the plot). In this particular case, it turned out that the $\hat{\pi}_1 = 0$ for all the motors (but not expected in general, e.g. Figure 6.10).

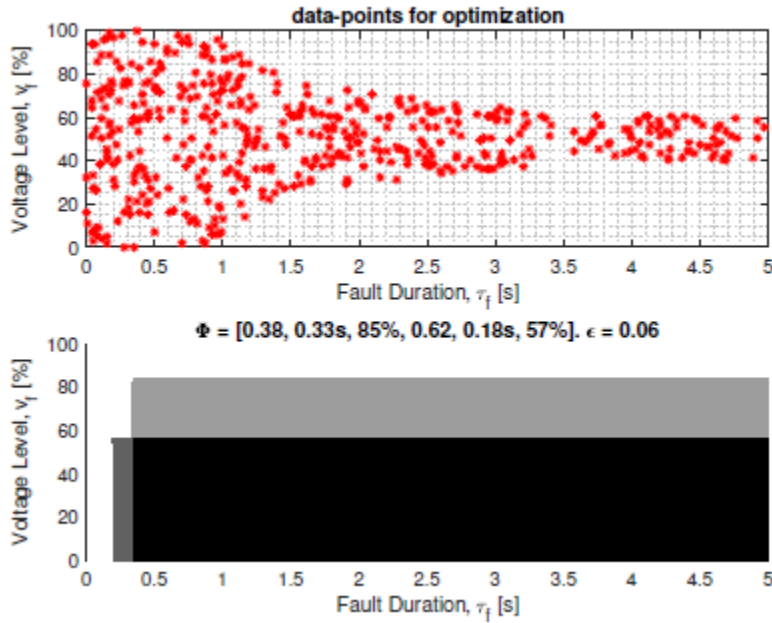


Figure 6.10 Simplified Aggregate Protection for Example 1.

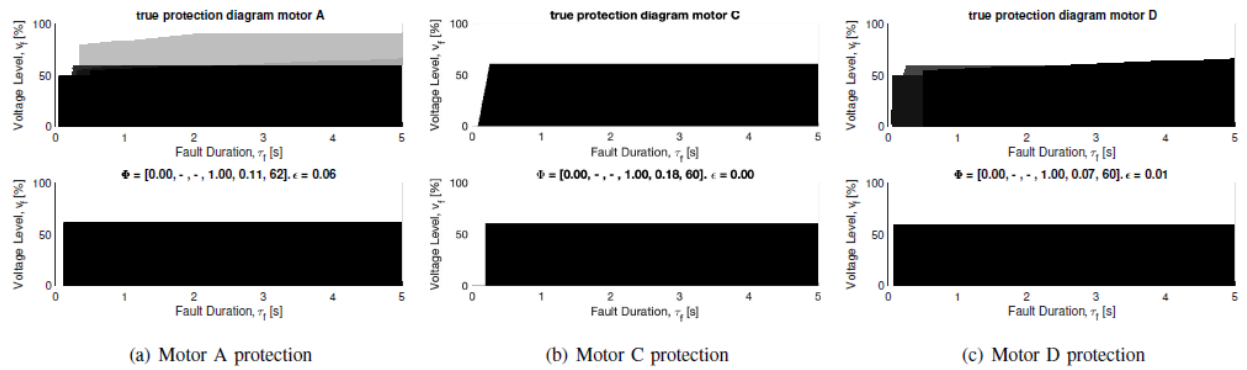


Figure 6.11 True and Simplified Aggregate Protection Schemes for the Test Case in [63].

Table 6.2 Test Case Protection Parameters

P	π (for motors A, B, C & D)
P3	{0.00, 0.00, 0.00, 0.08}
P2-P4	{0.09, 0.08, 0.00, 0.00}
P3-P4	{0.08, 0.00, 0.00, 0.20}
P2-P5	{0.00, 0.00, 1.00, 0.00}
P1-P4-P5	{0.25, 0.21, 0.00, 0.00}
P2-P4-P5	{0.58, 0.69, 0.00, 0.00}
P3-P4-P5	{0.00, 0.02, 0.00, 0.72}

6.5.4 Summary

There is a need for high-fidelity composite load protection models for induction motor loads to better represent the aggregate dynamic behavior of distribution systems in the transmission system dynamic simulations and studies. This work builds on recent developments on the aggregate protection modeling, to propose an optimization framework to generate simplified aggregate protection schemes. Introducing a mathematical abstraction of the protection schemes, a nonlinear regression problem is formulated to suitably approximate complex protection schemes in a simple parametric form. Numerical results are presented to illustrate the application of the framework.

6.6 Cross-Categorical Transfer Learning Algorithm

6.6.1 Transfer Learning Problem Definition

This sub-chapter discusses a cross-categorical transfer learning algorithm to model the aggregate motor protection [64]. In this problem, we have one source S and one target T space. Source space is defined as the data space used to train part of the proposed deep learning based framework offline (specifically transferable layers), while target space is a much smaller disjoint space ($S \cap T = \emptyset$) where the pre-trained architecture can be transferred with minimal amount of retraining (training involving the rest of the proposed deep network based architecture, i.e., the non-transferable layers). In our learning problem, we have two training datasets and two testing datasets. Furthermore, we define a feature space \mathcal{F} where all the instances are represented.

For this application, source system S comprises of simulated fault scenarios (without modeling uncertainties) generated for four different class of electric motors (Domain \mathcal{D}_i), with instances which denotes the tuple with measurements of fault duration, voltage level and fraction of motor load tripped at fault, happened at discrete time step k . On the other hand, target system T comprises of simulated fault scenarios with different level of uncertainties in the simulation model parameters (specifically we have made two different uncertainty cases, one with uncertainty variation between $\pm 10\%$ and the other one between $\pm 20\%$ of the nominal values of the modeling parameters). Feature space \mathcal{F} comprises of the detected features, output from the transferable layers. The non-transferable layers will work on the feature space \mathcal{F} to identify simplified model parameters as shown in Figure 6.9.

6.6.2 Transferable Layers

Dataset Preparation: Both source S and target system spaces T , consists motor specific dataset. For each type of motor, dataset consists of fault duration (τ_f^j), voltage level at fault (v_f^j), and the fraction of motor load tripped by the fault (π^j), of different fault category. Each row of this dataset contains one fault incident, with the repeating tuple of fault duration, voltage level of fault and fraction of motor load tripped by fault, at each discrete time step until the duration of this particular fault type.

Dataset Splitting: We have used a 10-fold cross validation for training and validation of the transferable layers, using the source S , specific dataset (without model uncertainties). We have kept the testing set separated as an indicator of generalized performance. 30% of the source specific dataset are separated and kept as test dataset, and 70% have used in the random cross validation, of the transferable layers of the proposed network.

Transferable Layers Architecture: Proposed transferable layers are shown in Figure 6.12, with respective dimensions of each transferable layers along with the selected activation functions. As shown in Figure 6.12, the transferable layer consists of an Autoencoder and a Classifier. Addition of classifier enforces,

these Autoencoder layers to turn properties related to different type of motor in the dataset. These properties in the feature space \mathcal{F} are not fault event specific and are transferable. The inner most encoding dimension is important, as it represents the dimension of the feature space \mathcal{F} . The higher the dimension of the feature space \mathcal{F} , the more computation time is required to convert the feature space output, to the simplified model parameters. Based on this motivation, effort needs to be taken to reduce the feature space \mathcal{F} dimension. We have tested different feature space \mathcal{F} dimension starting from 100 to 10, with a constant decrement of 10. Figure 6.13 shows the variation of the reconstruction error from the autoencoder along with the true positive accuracy from the classifier, with the reduction in feature space \mathcal{F} dimension. We have selected feature space dimension, i.e., inner most encoding dimension to be 30, as below that true positive accuracy from the classifier significantly drops, which implies loss of motor type specific information. Moreover, we have plotted the confusion matrix for the feature space dimension 30, as shown in Figure 6.14. As we can see, we get a total true positive accuracy (TPR) of 94% for feature space dimension 30, which is adequate for our purpose.

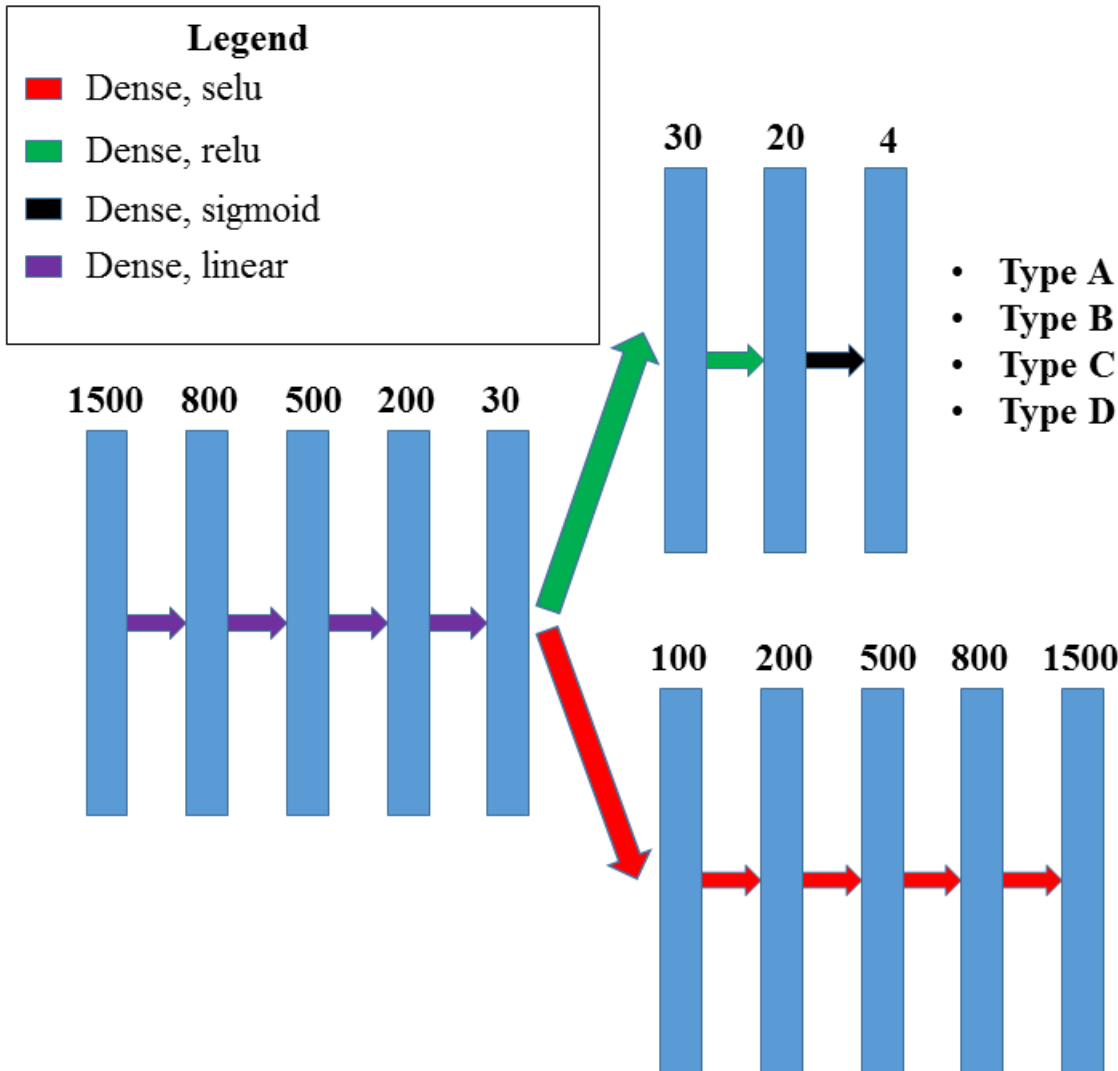


Figure 6.12 Architecture of the Transferable Layers

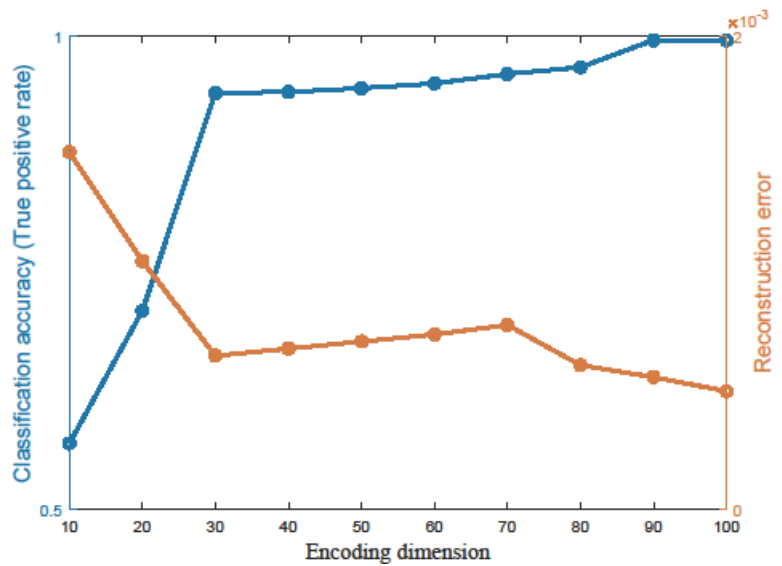


Figure 6.13 Change in Reconstruction Error and True Positive Rate (TPR) with Change in Encoding Dimension

Confusion Matrix for Encoding dimension 30					
Output Class	Type A	3175 24.1%	51 0.4%	151 1.1%	46 0.3%
	Type B	51 0.4%	3048 23.1%	0 0.0%	143 1.1%
	Type C	151 1.1%	0 0.0%	3089 23.4%	0 0.0%
	Type D	0 0.0%	143 1.1%	46 0.3%	3098 23.5%
	94.0% 6.0%	94.0% 6.0%	94.0% 6.0%	94.3% 5.7%	94.1% 5.9%
Type A Type B Type C Type D					

Figure 6.14 Confusion Matrix of Feature Space of Dimension 30

Model Exploration: Now we will discuss the different network architecture we have tried to design rest of the transferable layer architecture, after fixing the inner most encoding. We have tested different combinations of intermediate layer dimensions for the encoder and the decoder part, and tabulated the reconstruction error. Table 6.3 shows the four different network architectures that we have tried to design the transferable autoencoder layers, within which we have selected the bold-faced architecture, as shown in Figure 6.12.

Table 6.3 Variation of Reconstruction Error with Different Tried Transferable Layer Architectures

Encoder Structure	Decoder Structure	Reconstruction error (ϵ)
(,1000,30)	(30,1000,)	0.00153
(,1000,30)	(30,200, 1000,)	0.00117
(,900,200, 30)	(30,200, 900,)	0.00108
(,800,500, 200,30)	(200, 500,800,)	0.00071

Training and Validation: Proposed transferable network is trained using Tensorflow backend [65] using 2 GPU nodes on a NVIDIA P100 GPU cluster. We have used Adam algorithm to train the transferable layers, for 2000 epochs using the settings, learning rate=0.001, $\beta_1 = 0.9$, $\beta_2 = 0.999$, $\epsilon = \text{None}$, decay= 10^{-6} , amsgrad=False. Furthermore, we have used a batch size of 100 data points and have implemented an early stopping protocol to avoid overfitting. This protocol consists of monitoring the loss of the validation set, and if there is no improvement of the validation loss after 100 epochs, the training is stopped and restarted with a different initial weights and biases. After successful training of the proposed transferable architecture, the encoded (30) dimensional output from the trained Autoencoder, should be able to capture motor type specific information.

6.6.3 Non-Transferable Layers

Proposed Architecture: For this part of selected architecture, both training and evaluation involves only target space (T) specific dataset (dataset with uncertainties as discussed before). Similar dataset preparation and dataset splitting methods are used for target space dataset, as mentioned before. Proposed network architecture combining the transferable and non-transferable layers is shown in Figure 6.15. The non-transferable layers comprise of two dense layers, as shown in Figure 6.15.

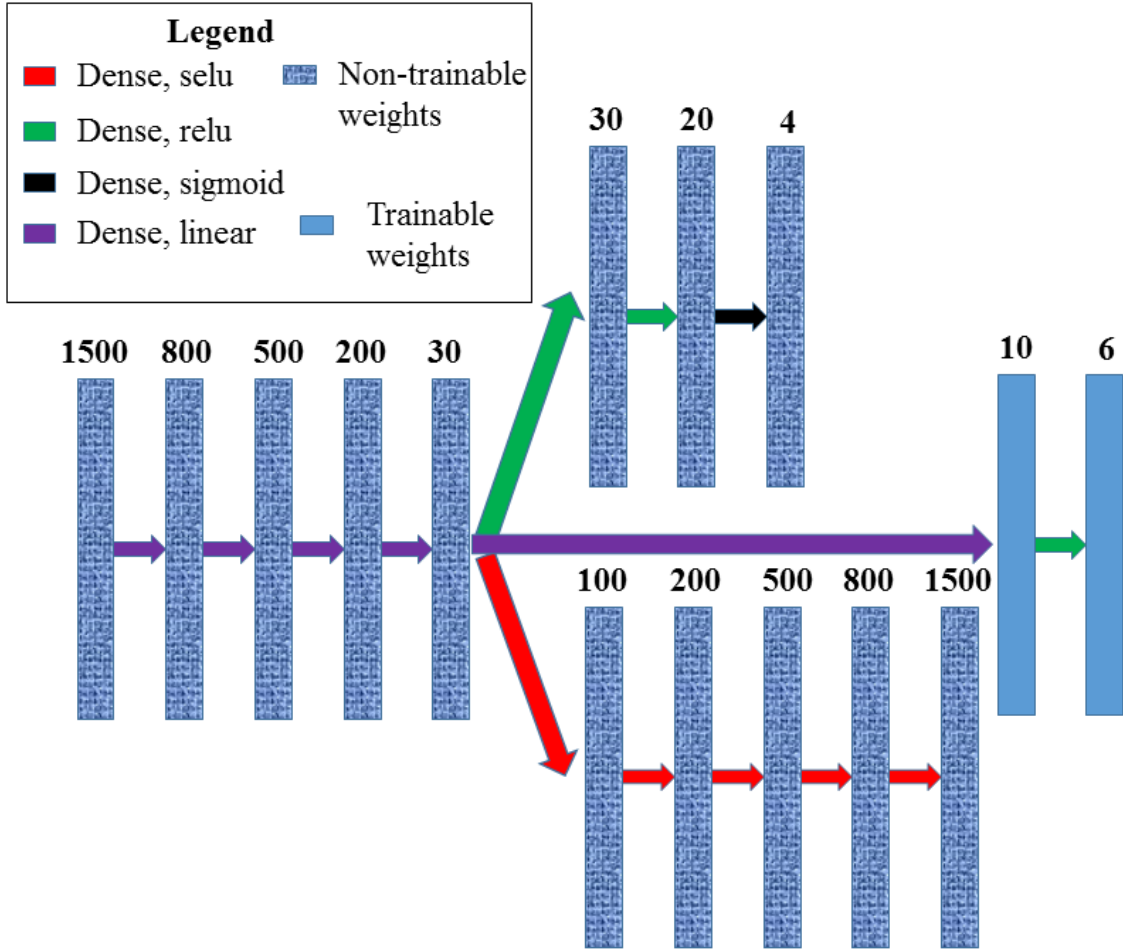


Figure 6.15 Architecture of the Whole Proposed Framework (Combination of Transferable and Non-Transferable Layers)

Training and Validation: Proposed stack of non-transferable layers is trained using Tensorflow backend [65] using 2 GPU nodes on a NVIDIA P100 GPU cluster. We have used stochastic gradient descent algorithm to train the proposed architecture, for 1000 epochs using the settings, learning rate=0.1, decay= 10^{-6} , momentum=0.9, nesterov=True. Furthermore, we have used a batch size of 100 data points and have implemented an early stopping protocol to avoid overfitting.

6.6.4 Numerical Results

Figure 6.16 shows the advantage of using our proposed transfer learning based framework. While our transfer learning based framework achieves similar reconstruction error, as in a framework without the transferable layers (complete retraining of Figure 6.15), saves computation time in the order of more than 80% in average, between all the different type of fault scenarios. Figure 6.17 shows the error histograms, of the relative percentage error ($((\text{Actual}-\text{Reconstruction of actual})/\text{Actual}) \times 100$) for both voltage level and motor load fraction, applied to four different types of motor. From Figure 6.17, more than 85% error points lie within $\pm 10\%$ of the relative percentage error. Finally, Figure 6.18 - Figure 6.20 show the simplified protection diagrams

In conclusion, we have proposed a stacked Autoencoder based framework to find a simplified load model, for a given occurrence of fault for a given motor type. Furthermore, we have identified specific layers in our framework, which is transferable between different category of faults, and reduced the

number of non-transferable layers (parameters need to be tuned online), which results in a significant savings in computation time. Moreover, we have incorporated probabilistic moments, to calculate the correct mean and variance in the final layer of the stacked Autoencoder, which results in an accurate estimation of the simplified protection model.

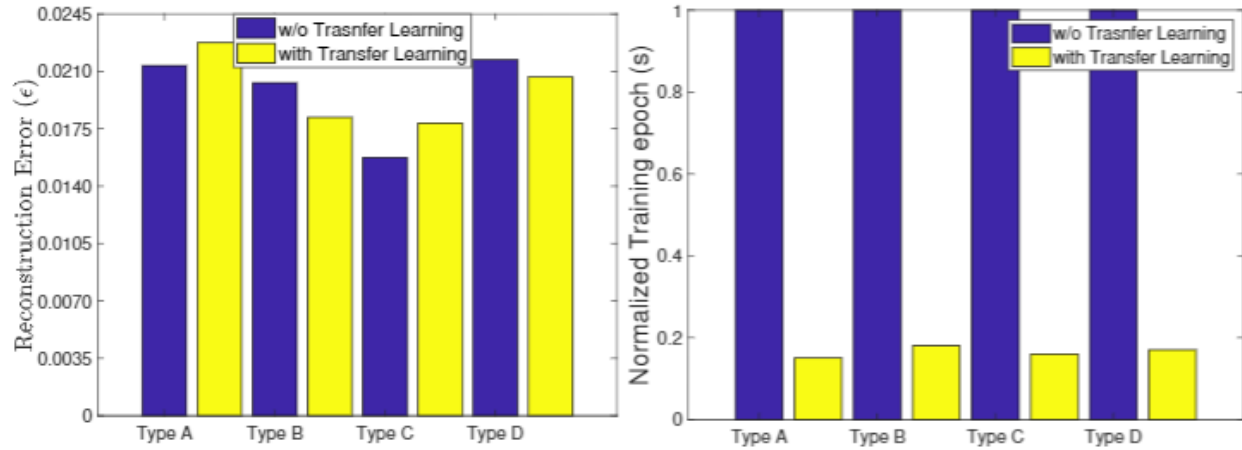


Figure 6.16 Comparison of Reconstruction Error and Training Epoch, with and without Transfer Learning

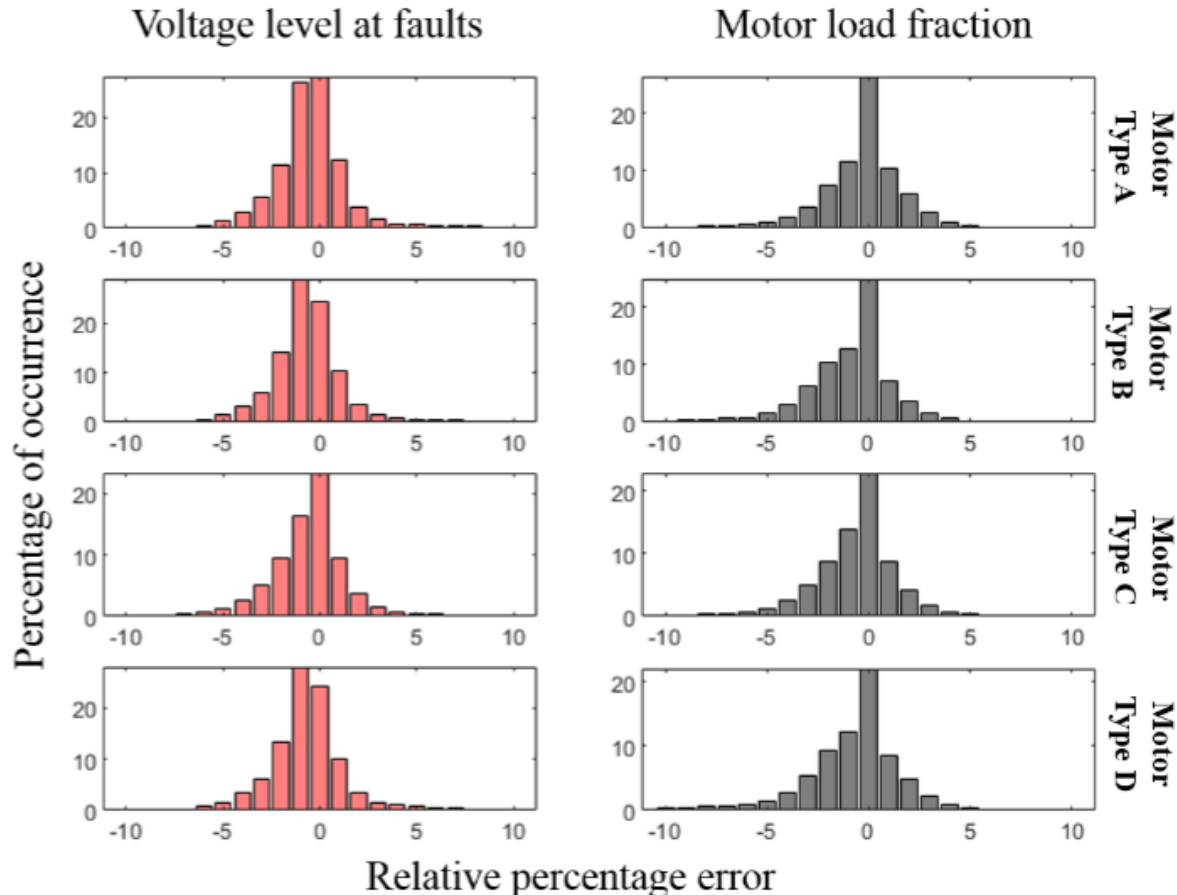


Figure 6.17 Error Histogram of Voltage Level at Faults and Motor Load Fraction

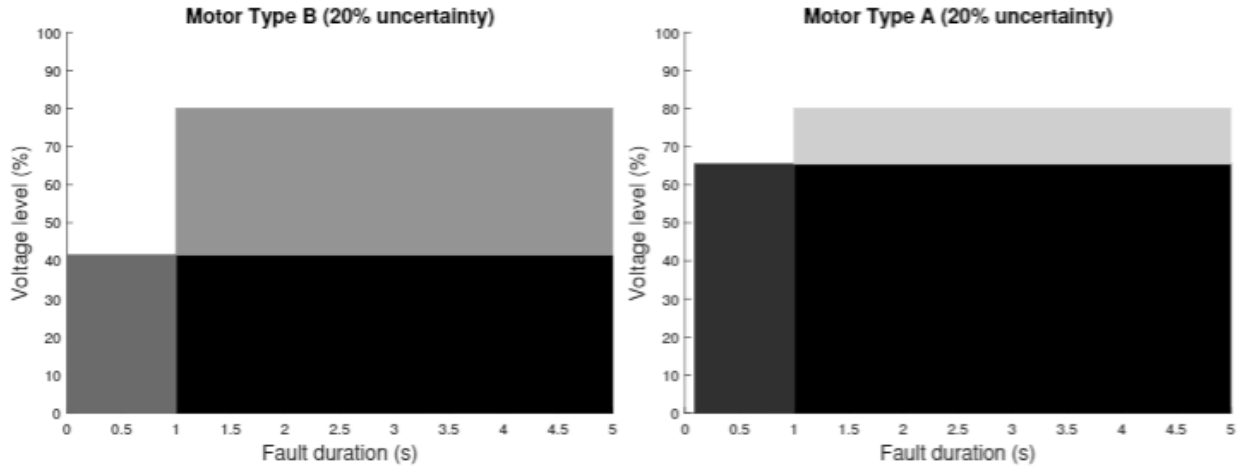


Figure 6.18 Simplified Protection Diagrams for Case1 with 20% Uncertainty

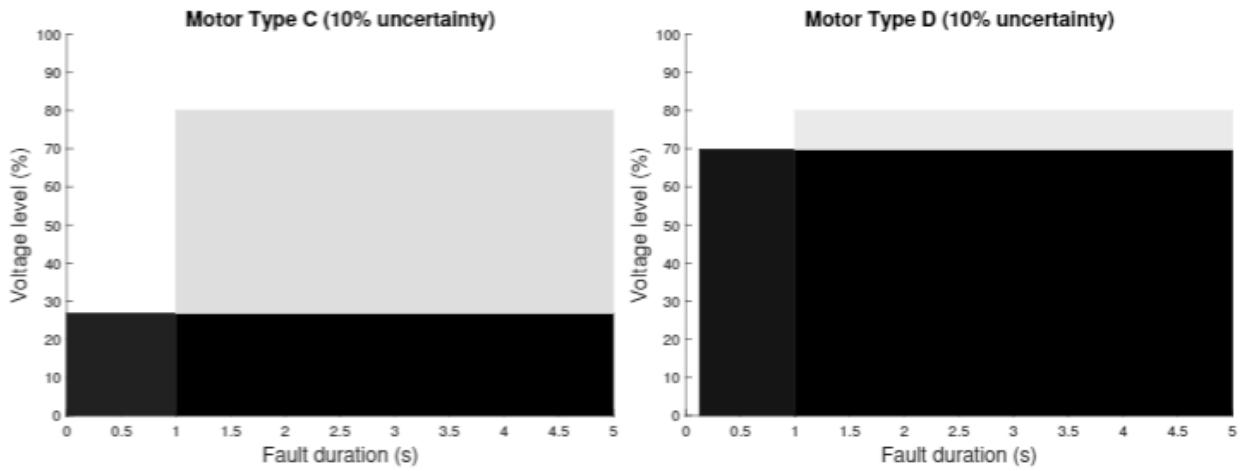


Figure 6.19 Simplified Protection Diagrams for Case2 with 10% Uncertainty

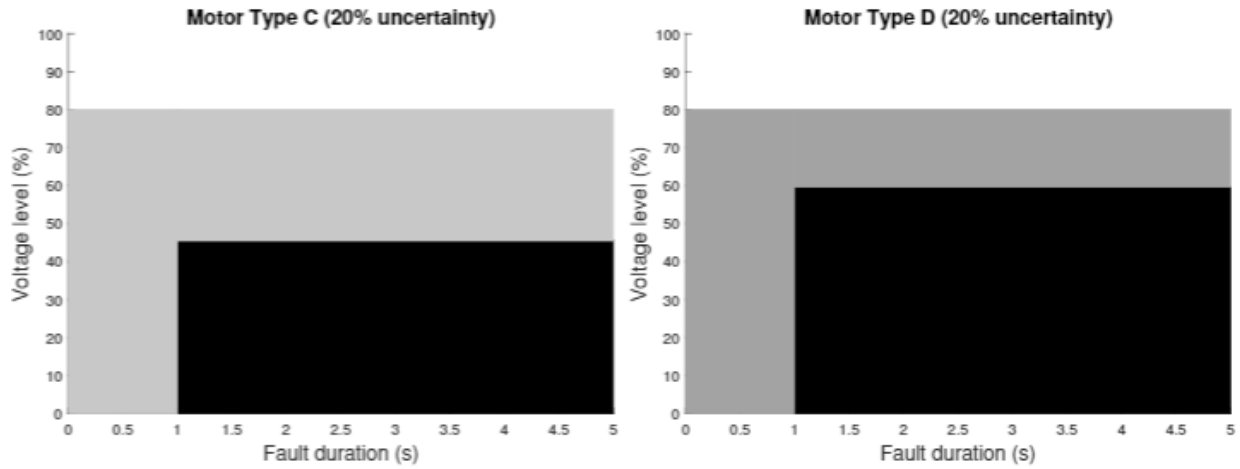


Figure 6.20 Simplified Protection Diagrams for Case3 with 20% Uncertainty

7.0 Simulation Platform Development for Performance Data Extraction

7.1 Transmission and Distribution (T&D) Simulations

7.1.1 Introduction

There are mainly three categories of parameters for the WECC composite load, i.e., composition, operation and protection parameters for each class of loads. For motor loads, composition can be derived from the regional end-use load survey and operational parameters such as the electrical impedances and the time constants for the motors are well-understood and well-defined. While motor protections play a significant role in determining the behavior of the motors, as it dictates whether motors connected to the grid continue running when subjected to voltage sag and recovery. So far, the aggregate protection models and parameters have not been well understood, and they are loosely determined based on past experiences and limited number of measurements for actual disturbances. Furthermore, it was pointed out in [66] that the four classes of motors in existing composite load model are categorized based on driven loads and thus are quite broad. Within each class of motors, there are various types of protection and controls, which makes it challenging to derive suitable aggregated protection models.

To develop adequate aggregate motor protection models, we first need to have better understanding of the detailed responses of the protections in typical motor loads. In this section, integrated transmission and distribution (T&D) system dynamic co-simulation will be employed to obtain detailed responses, particularly the responses of the protections, of loads in the distribution systems to disturbances in the transmission system. The detailed responses and their collective performance will subsequently be used to study the aggregated protection behaviors of different classes of loads (the classification of loads is based on the components in existing WECC composite load model). A flowchart of the proposed process of developing enhanced aggregate motor protection model is illustrated in Figure 7.1.

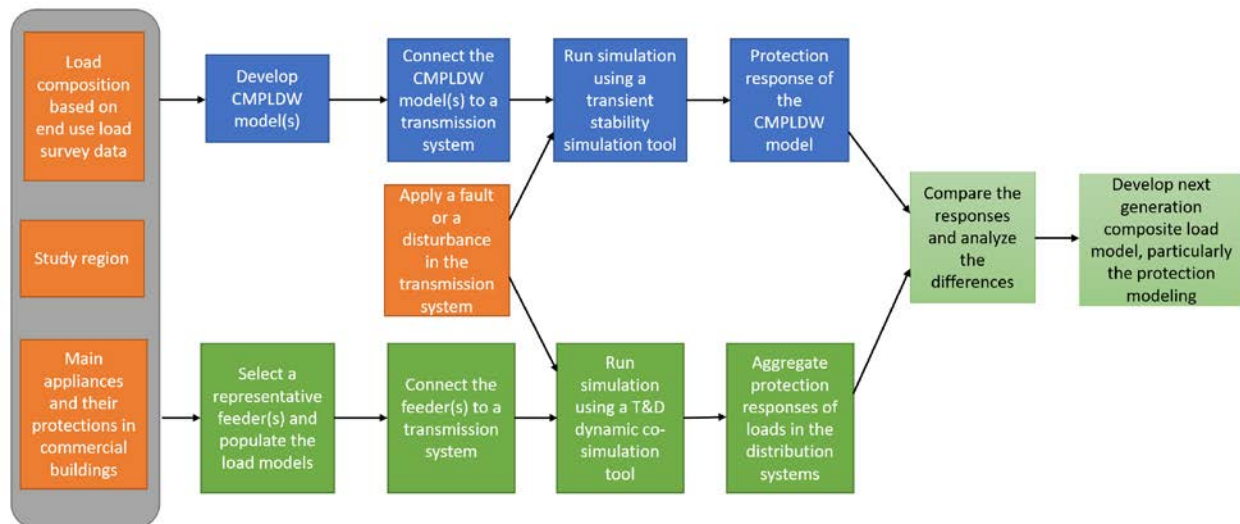


Figure 7.1 A Flowchart of Developing Enhanced Motor Protection Models Based on Integrated T&D Dynamic Simulation

7.1.2 Integrated T&D Dynamic Co-Simulation

Due to the traditional separate modeling and simulation practice, existing transmission-level and distribution-level simulation tools (e.g., PSLF, PSS/E for transmission systems and OpenDSS, GridLAB-D for distribution systems) cannot be used to study the detailed responses of end use loads in the distribution systems when subjected to a disturbance or fault in the transmission system. With integrated T&D dynamic co-simulation, both systems can be modeled and studied simultaneously so that their interactions can be adequately captured. Thus, it serves the purpose of obtaining detailed responses of the protections in typical motor loads in distribution systems when there is a fault or disturbance in the transmission system. The interactions between the transmission and distribution systems during the co-simulation include two stages: 1) power flow for initializing the dynamic simulation will be solved, and 2) the dynamic simulation stage where the dynamic responses of the motor loads to voltage sag and recovery will be analyzed in detail. The two stages are illustrated in Figure 7.2.

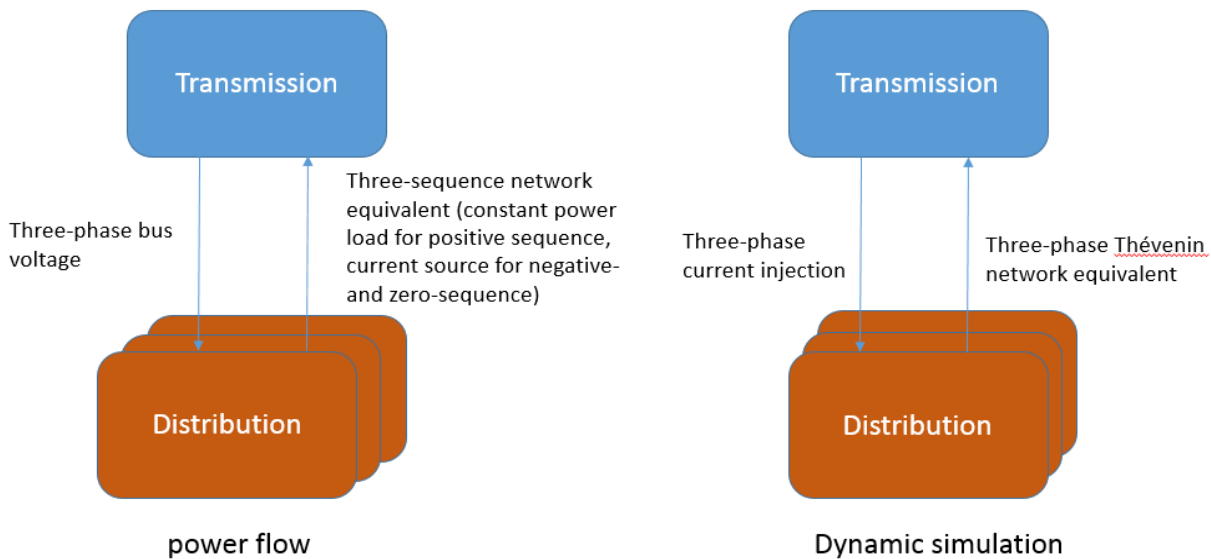


Figure 7.2 The Interactions between the T&D Solvers: (Left) at Each Iteration Step of Power Flow Calculation; (Right) at Each Step of Network Solution during Dynamic Simulation

After the T&D power flow successfully converges, the simulation is then transitioned to integrated T&D dynamic simulation. In dynamic simulation, network solution and integration steps will be solved iteratively at each time step. The iterative information exchange at each time step is illustrated in Figure 7.3. It should be noted that the number of iterations is not predefined. The algorithm has been developed on InterPSS, an open-source power system simulation tool. More details can be found in [67].

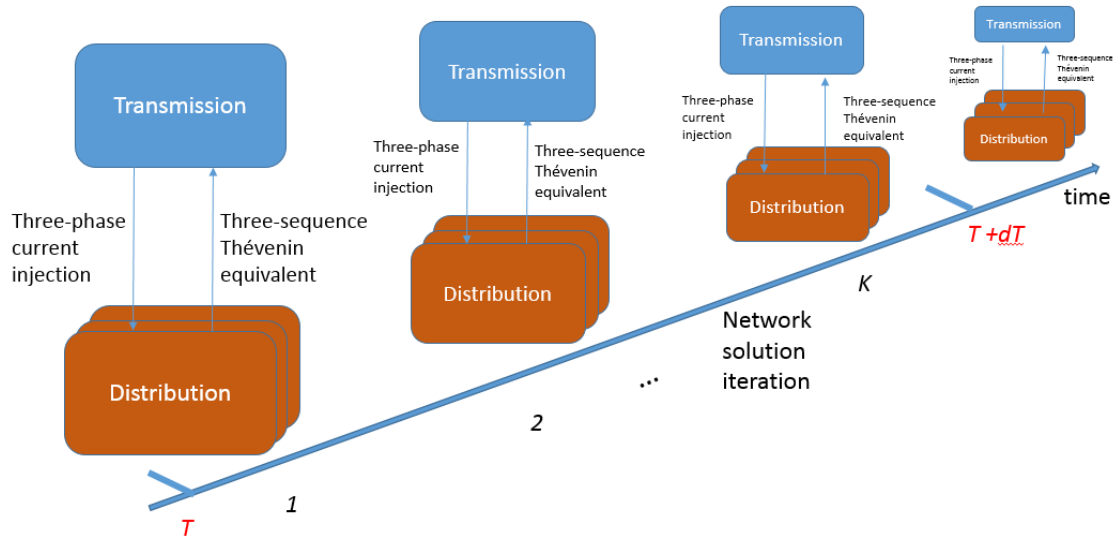


Figure 7.3 Iterative Information Exchange at Each Time Step.

7.1.3 Test System

Transmission System

In this study, the IEEE 39 bus test system [68], which is shown in Figure 7.4, is used to represent the transmission system. Basic information about the system is summarized in Figure 7.5.

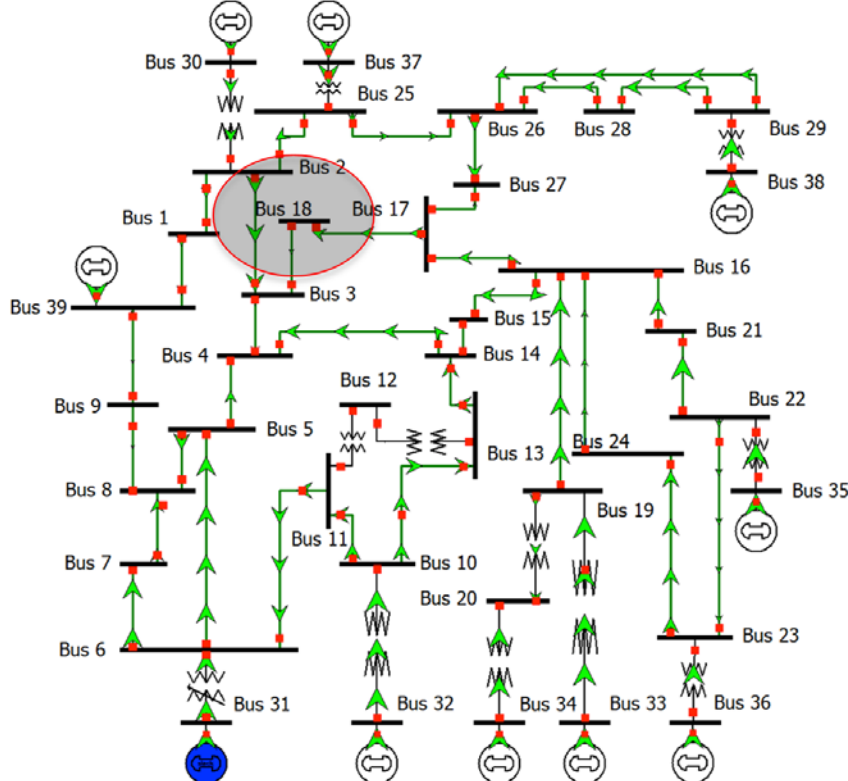


Figure 7.4 One-Line Diagram of the IEEE 39-Bus Test System

Number of Devices in Case		Case Totals (for in-service devices only)	
		MW	Mvar
Buses	39	Trans. Lines (AC)	34
Generators	10	Series Capacitors	0
Loads	31	LTCs (Control Volt)	1
Switched Shunts	2	Phase Shifters	0
2 Term. DC Lines	0	Mvar Controlling	0
Multi-Term. DC	0		
Breakers	0	Fuses	0
Disconnects	0	Load Break Disc.	0
ZBRs	0	Ground Disconnects	0
Areas	1	Islands	1
Zones	1	Interfaces	0
Substations	0	Injection Groups	0
Generator Spinning Reserves		Positive [MW] Negative [MW]	
		93831.7	6167.3
Negative MW Loads and Generators		MW Mvar	
Load		0.0	0.0
Generation		0.0	0.0
Slack Buses:		31 (31); in Area 1 (1)	

Figure 7.5 Case Summary of the IEEE 39-Bus Test System

Distribution Feeder

A part of the original load directly connected to bus 18 of the transmission system is replaced by PNNL taxonomy feeder GC-12.47-1 [69] (shown in Figure 7.6). The basic information of the feeder is shown in Table 7.1. This feeder is representative of serving a block of dense commercial or industrial loads, such as a very large shopping mall or a lumber mill. These feeders may supply the load through a single large transformer or a group of smaller units.

Table 7.1 Basic Information of the Feeder GC-12.47-1

Nodes	27
Voltage (kV)	12.47
Load (kW)	5,200
Voltage Regulators	0
Reclosers	0
Residential Transformers	0
Commercial Transformers	0
Industrial Transformers	3
Agricultural Transformers	0

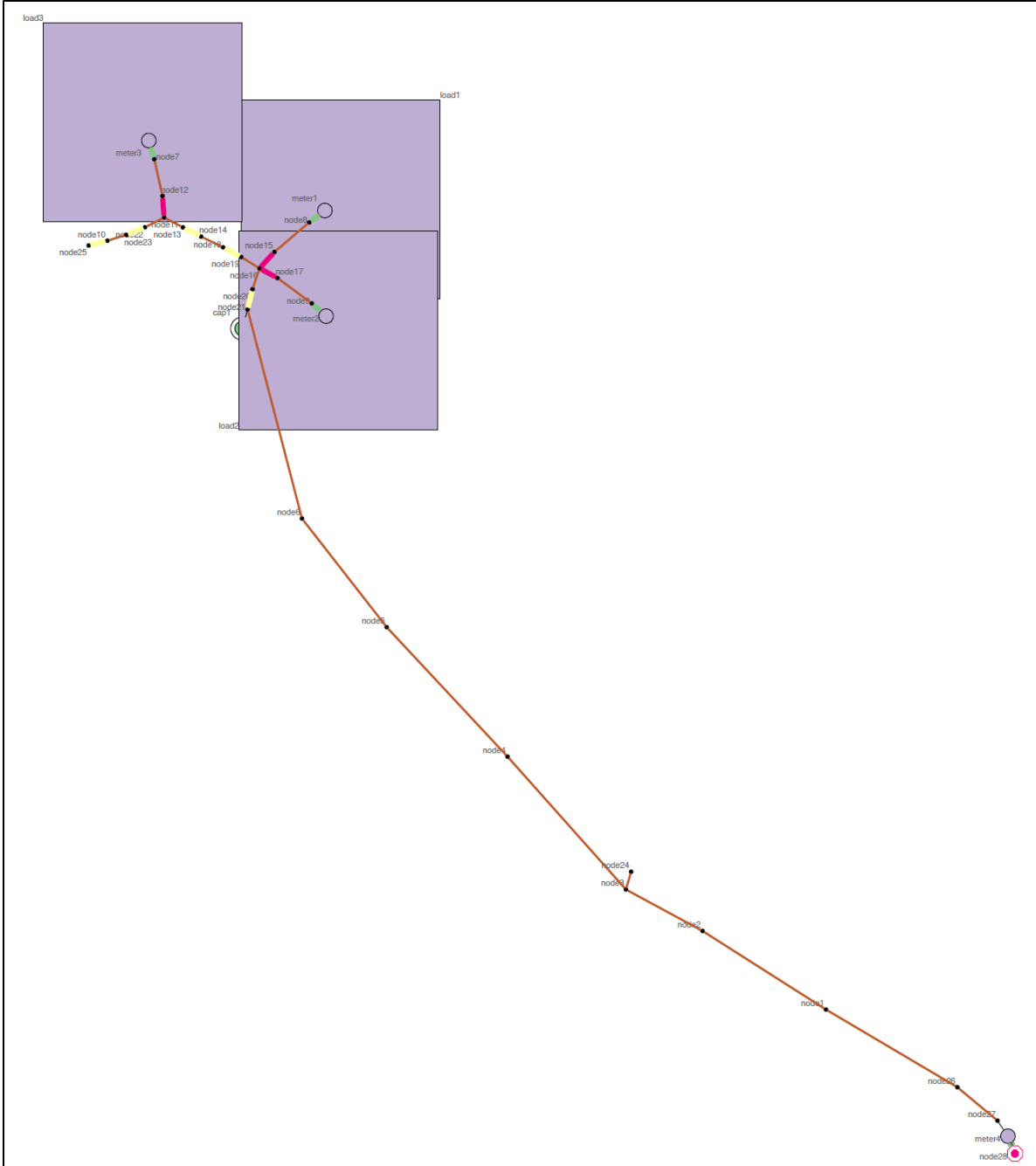


Figure 7.6 One-Line Diagram of the Feeder GC-12.47-1

In this study, to represent a typical feeder in a city downtown area, one large office, five small offices and one hotel are modeled to represent commercial buildings connected to the feeder. All commercial buildings are connected to the three transformers at the end of the feeder shown in Figure 7.6. Modeling of the main motor loads in each of the three buildings are shown in Table 7.2. It is assumed that the motor loads account for 70%, 70% and 75%, respectively, of the total loads (in terms of real power) in the large office, small offices and hotel. The remaining loads are assumed to be static load model represented by constant impedances.

Table 7.2 Main Motor-Driven Appliances in the Large Office, Small Offices and Hotel.

Building	Appliance	Equipment	Type	Protection	Rating (kW)	Percentage of building motor load
Large Office	AHU	Fan	MB	P2P4P5	308	13%
Large Office	VAV	Frac_Fan	MD	P3P4P5	51	2%
Large Office	DOAS	Fan	MB	P2P4P5	33	1%
Large Office	Chiller	Compressor	MA	P1P4P5	875	38%
Large Office	Chiller	Pump	MC	P2P5	245	11%
Large Office	Cool_Tower	Fan	MB	P2P4P5	105	5%
Large Office	Boilers	Ind_Draft	MB	P1P4P5	208	9%
Large Office	Boilers	Pump	MC	P2P5	245	11%
Large Office	CRAC	Compressor	MA	P1P4P5	106	5%
Large Office	CRAC	Fan	MB	P1P4P5	31	1%
Large Office	CRAC	Frac_Condensor	MD	P3P4P5	51	2%
Small Office	AHU	Compressor	MA	P1P2P4P5	106	55%
Small Office	AHU	Fan	MB	P1P2P4P5	31	16%
Small Office	VAV	Frac_Fan	MD	P3P4P5	15	8%
Small Office	Boilers	Ind_Draft	MD	P3P4P5	21	11%
Small Office	CRAC	Compressor	MA	P1P4P5	11	6%
Small Office	CRAC	Fan	MB	P1P4P5	3	2%
Small Office	CRAC	Frac_Fan	MD	P3P4P5	5	3%
Hotel	PTAC	Compressor	MA	P3P4	425	32%
Hotel	PTAC	Fan	MD	P3	123	9%
Hotel	Exhaust	Fan	MD	P3	23	2%
Hotel	Split	Fan	MB	P2P4	123	9%
Hotel	Split	Compressor	MA	P2P4	425	32%
Hotel	Split	Frac_Condensor	MD	P3P4	130	10%
Hotel	Split	Frac_Ind_Draft	MD	P3P4	83	6%

Motors are typically protected by different protection methods, such as relays, contactors, thermal protection, etc. During a fault, as the voltage drops below a certain limit for longer than a certain duration, the protection mechanism gets triggered to trip the associated motor load. As discussed in Chapter 6, the motor protection schemes commonly found in the commercial buildings in United States can be categorized into five types i.e., 1) electronic relays (P1), 2) overload relays (P2), 3) thermal protection (P3), 4) contractors (P4) and 5) building management system (BMS) control (P5). Each motor is usually

equipped with multiple types of protection devices. Each protection is characterized by a (range of) voltage depth and duration for tripping, and a (range of) voltage depth and duration for reconnection (upon recovery). The protection triggering zones of the five types of protection are illustrated in Figure 7.7. For the tripping zone illustrated on the top subplot of Figure 7.7, if the sustained low voltage magnitude and duration fall into the region under the characteristic curve of specific protection scheme, the motor will be tripped by this scheme. For the reconnection zone depicted on the bottom subplot, if the voltage magnitude and duration recover to the region above the characteristic curve, the motor will be reconnected. The fact that P2 and P3 have no traces on bottom subplot of Figure 7.7 means they will not automatically reconnect in the time frame of interest.

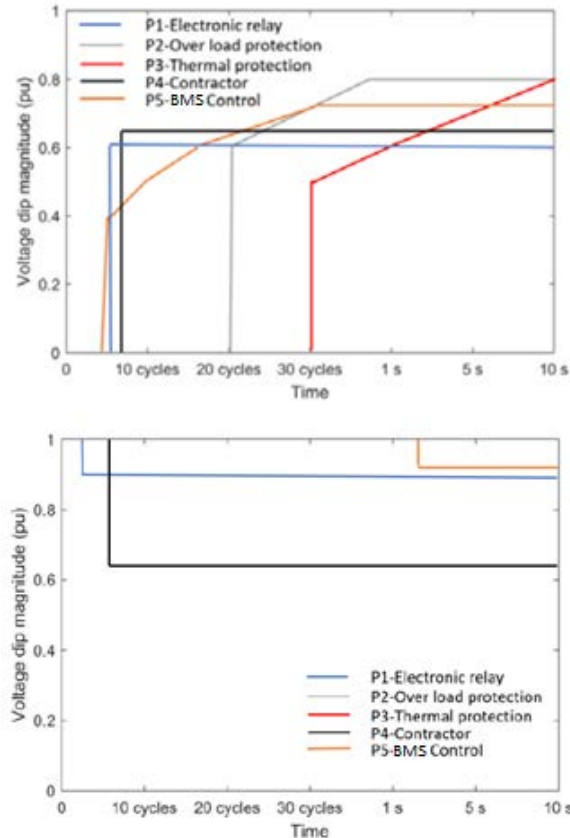


Figure 7.7 Illustration of Protection Parameter Setting of the Five Protection Types: (Top) Tripping Voltage and Time Delay; (Bottom) Reconnection Voltage and Time Delay

7.1.4 Simulation Results

A three-phase fault close to bus 18 in the transmission system results in a voltage drop to 0.4 pu at bus 18, lasting for 0.0833 second (5 cycles) and followed by normal recovery. The voltages at nodes meter_1, meter_2 and meter_3 of the feeder are shown in Figure 7.8.

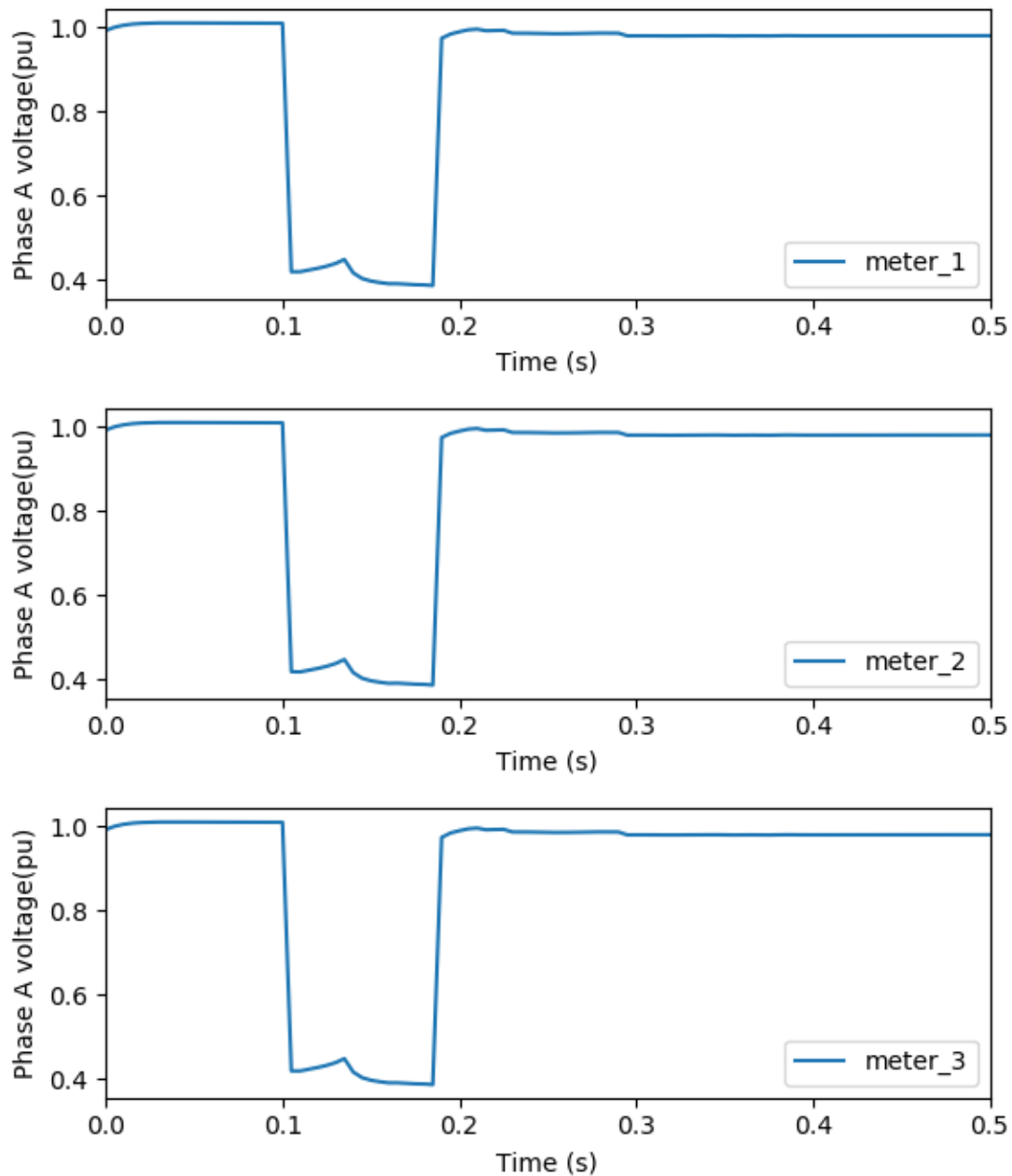


Figure 7.8 Phase A Voltages at Nodes meter_1, meter_2 and meter_3 in the Feeder

The individual protection trip and reconnection responses of all motors are shown in Figure 7.9. If the trip time or reconnection time is zero, it means the motor was not tripped by its protections.

It can be observed from the scatter plot that the protection performance of MA type motors follows a similar pattern, while there is not a clear pattern for the MB and MC types of motors. This suggests that it is more challenging to perform aggregation for the MB and MC type motors. It should be noted that these are preliminary results, more simulations should be performed to better identify the trends and patterns in the protections.

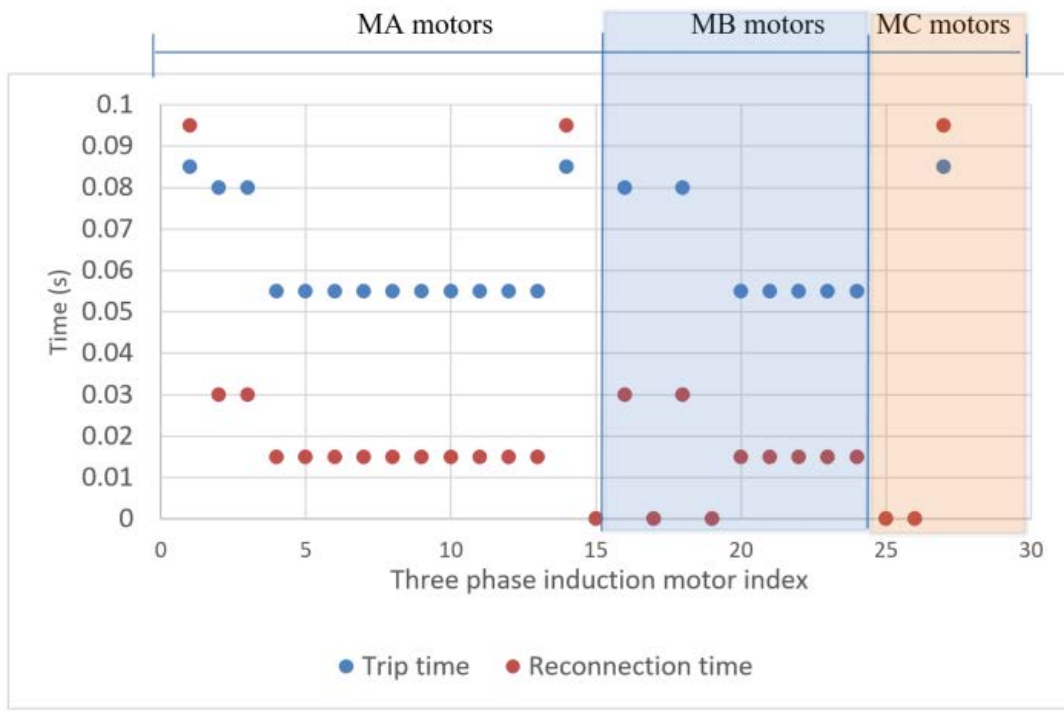
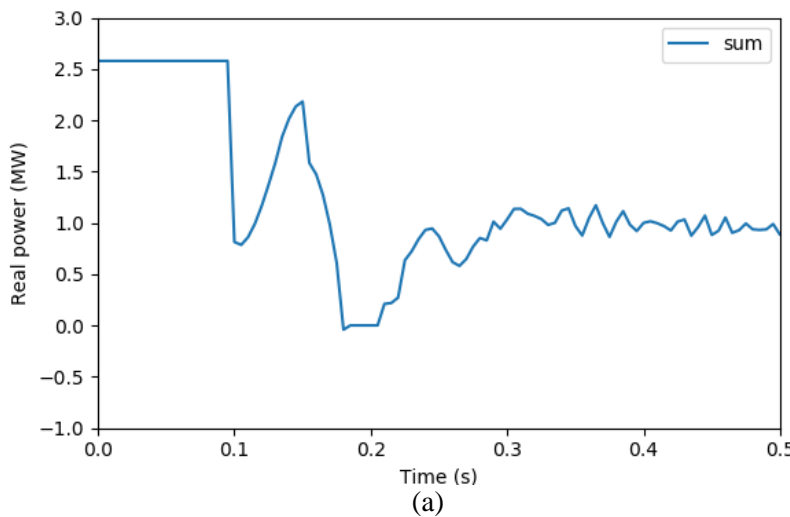


Figure 7.9 Trip Time and Reconnection Time for All Three Phase Motors

The aggregated power of different class of three phase induction motors are shown in Figure 7.10. The non-tripped fractions of each class of motors in terms of total MVA and the normalized fraction are shown in Figure 7.11 and Figure 7.12, respectively. The results in Figure 7.12 show that normalized non-tripped fractions are significantly different for the three motor classes, which is significantly different from the fact that very similar protection default settings are recommended for current WECC composite load model.



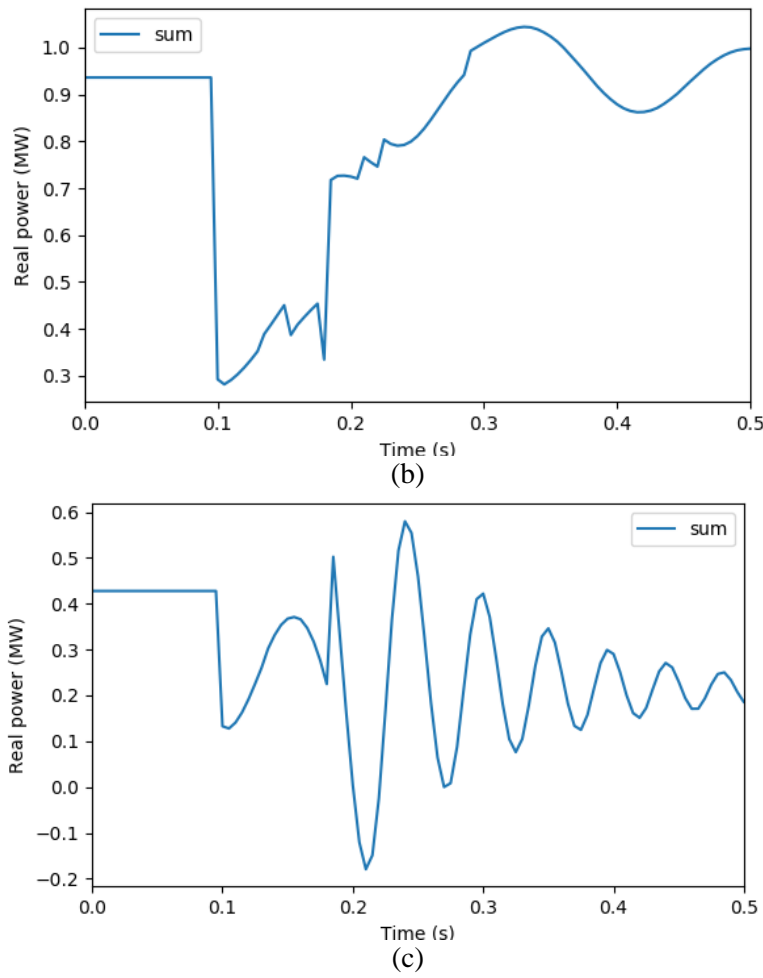
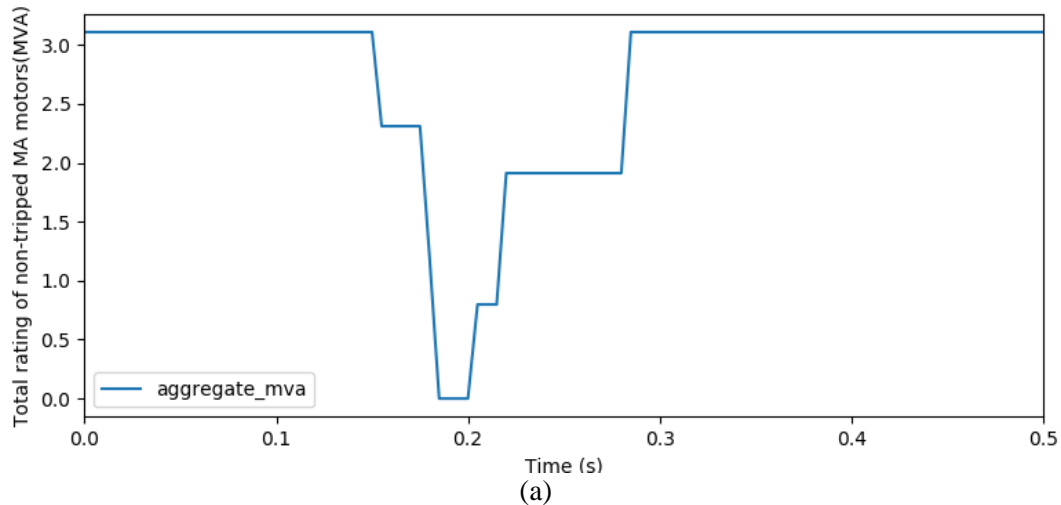
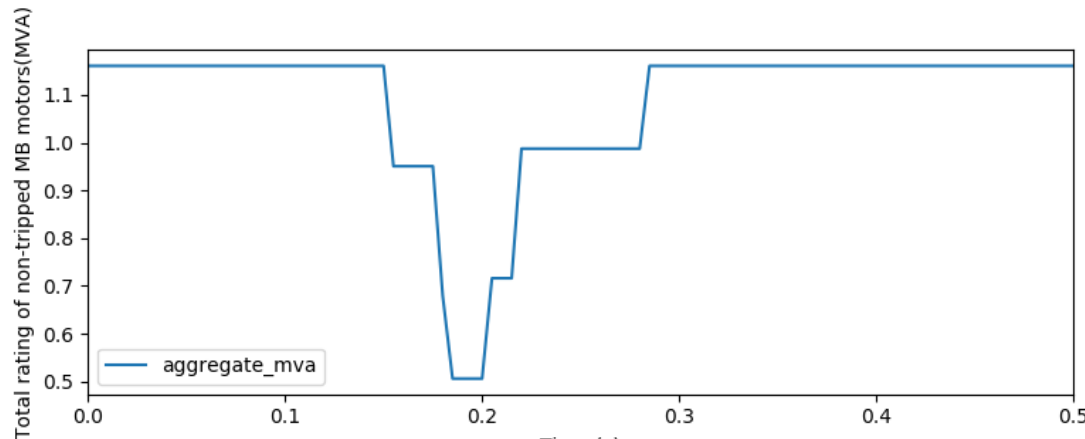
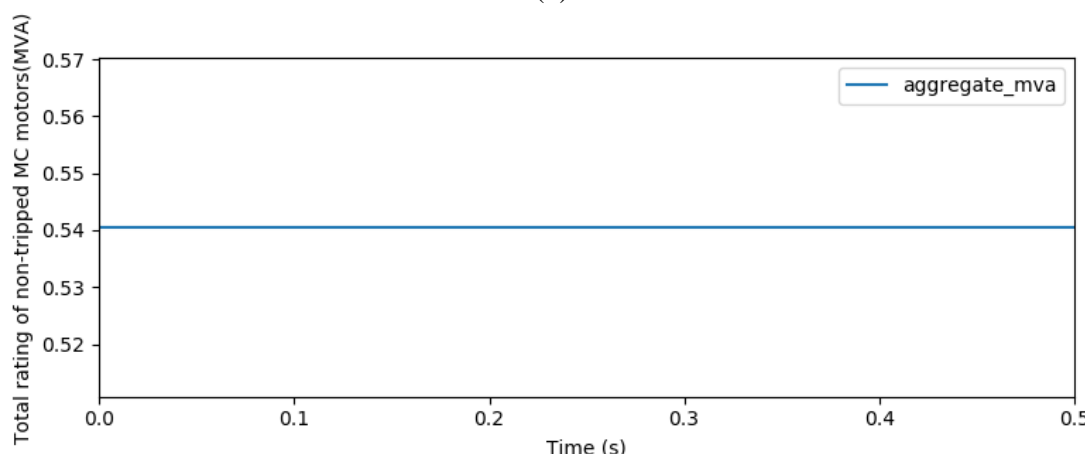


Figure 7.10 Aggregate Real Power of Three-Phase Induction Motors: (a) MA;(b) MB; (c) MC



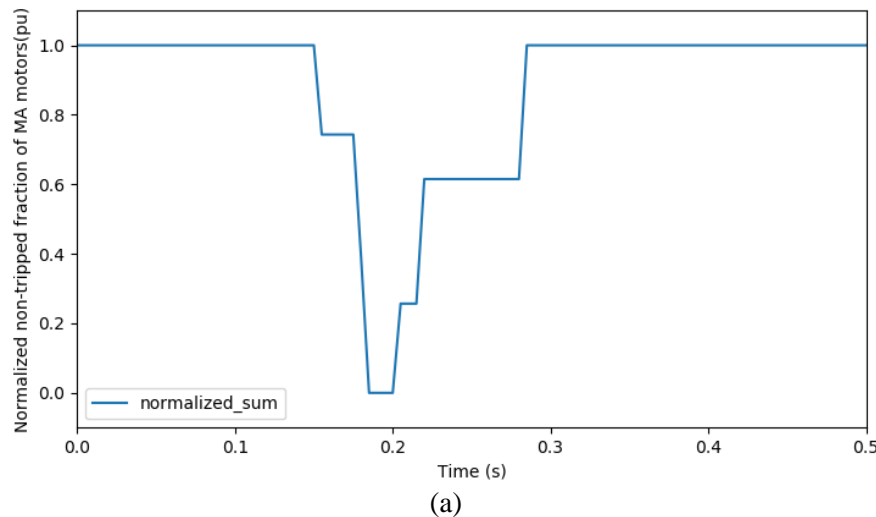


(b)

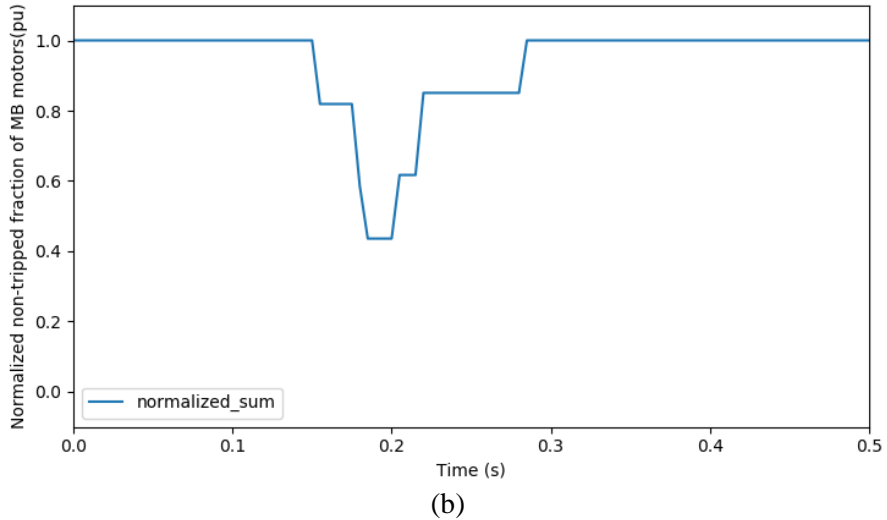


(c)

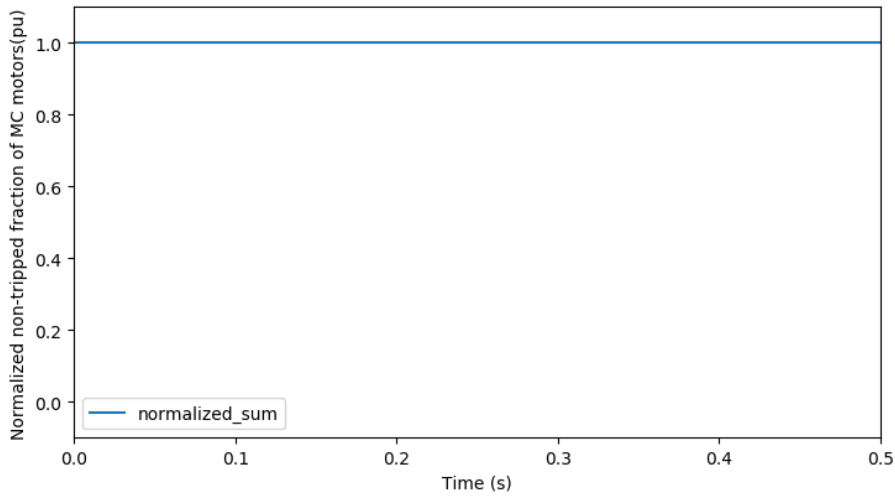
Figure 7.11 Aggregate MVA of Non-Tripped Three-Phase Induction Motors: (a) MA;(b) MB; (c) MC



(a)



(b)



(c)

Figure 7.12 Normalized Fraction of Non-Tripped Three-Phase Induction Motors: (a) MA; (b) MB; (c) MC

7.2 Commercial Feeder Modeled in GridLAB-D

In this section, the five types of protection schemes for commercial buildings are developed in GridLAB-D [70]. Both SPIM and TPIM utilize the same set of protection schemes. A total of 5 protection types (relay, overload, thermal, contactor, building management system (BMS)) share the same trip and reconnection functions, which are based on under-voltage protection logics.

In this task, four Matlab functions are written to read from a .xlsx file containing motor information in representative commercial buildings connected to a commercial feeder, and to write the information into .glm files for GridLAB-D simulation. One .glm file will be generated for each building, containing the motor objects for all the motors in this building. All the building model .glm files will be included in the feeder model .glm file to connect buildings to the feeder.

7.2.1 Input Parameters

The protection parameters as shown in Figure 7.13 contain the types of available protections and their parameters. Column "Trip" and "Reconnect" list the protection parameters for each type of protection. The number before the semicolon is the trip (or reconnect) voltage, and the number after the semicolon is the trip (or reconnect) time. For example, P1 (electronic protection) has parameters "0.6;0.08" under "Trip", which means that if the voltage falls below 0.6 pu for 0.08 seconds, electronic protection should kick in and trip the motor. Similarly, the parameters "0.9;0.033" indicates that if the motor is tripped, but the voltage recovers to be above 0.9 pu for 0.033 seconds, electronic protection should reconnect the motor to the grid.

Protection	Type	Trip	Reconnect
P1	Electronic	0.6;0.08	0.9;0.033
P2	Overload	0.6 0.7 0.8;0.33 0.5 1.0	Manual
P3	Thermal	0.55 0.6 0.65 0.7 0.75 0.8;0.5 1.0 2.0 4.0 8.0 10.0	Manual
P4	Contactors	0.65;0.1	0.75;0.1
P5	BMS	0.0 0.4 0.5 0.6 0.7;0.083 0.1 0.166 0.25 0.5	0.95;2.0

Figure 7.13 Commercial Building Protection Parameters

The building types as shown in Figure 7.14 indicate the number of each type of buildings connected to this feeder. Thus, it also determines the number of .glm files generated as output files with the naming rules as: if there is only one building like "Hotel" in Figure 7.14, the output file name is "hotel.glm". If there are more than one building of the same type, for example "Small Retail", the output files are named as "small_retail_1.glm" and "small_retail_2.glm".

Small Retail	2
Medium Retail	0
Large Retail	0
Supermarket	0
Fast Food	0
Small Office	5
Large Office	1
Warehouse	0
Lodging	0
School	0
Hotel	1
Hospital	0

Figure 7.14 Types of Commercial Buildings

The motor loads and protection schemes of typical commercial buildings (e.g. retail buildings) are summarized in an excel file and a snapshot of this file is shown in Figure 6.3**Error! Reference source not found.**. The motor loads table of each building contains the following information for each motor: building type, appliance, equipment, motor type, protection schemes and motor rating. For type D motors (MD), as they are single phase motors, one motor is assumed to connect to each phase to ensure phase balance. The naming rules for a motor object are: "Building_Appliance_Equipment" for three-phase induction motors, and "Building_Appliance_Equipment_Phase" for single-phase motors. "Phase" can be A, B, or C.

The motor parameters as shown in Figure 7.15 list the motor electrical and mechanical parameters. Note that motor type D is using GridLAB-D default values. Different parameters for each motor can be used by explicitly modifying the parameter values in motor information .xlsx file.

Type	H	Rs	Xs	Xm	Rr	Xr
MA	0.363	0.0041472	0.078336	3.350016	0.00466176	0.0768
MB	0.363	0.0041472	0.078336	3.350016	0.00466176	0.0768
MC	0.363	0.0041472	0.078336	3.350016	0.00466176	0.0768
MD	default	default	default	default	default	default

Figure 7.15 Motor Parameters

7.2.2 Matlab Codes

Four Matlab functions are developed to read the input .xlsx file and write the output .glm files.

- *motorGlmGenerator.m*: Main function. The user should only execute this function once.
- *xls2cell.m*: Read in the .xlsx input file containing motor information and convert it to cell arrays. actXserver technique [71] is used to accelerate the process.
- *glmFileGenetator.m*: Write motor models of different buildings into .glm files.
- *writeMotorObject.m* Subfunction of *glmFileGenerator.m* that writes a motor object into .glm file. Should be run for each motor.

7.2.3 Output Files

Figure 7.16 illustrates snapshot of a sample output file. This file contains multiple motor objects in a commercial building (small office building). A recorder object is associated with each motor object. To link this building to the feeder model for GridLAB-D simulation, the users should add "#include "small_offices_1.glm"" to the feeder model .glm file.

```

//Motors
//This file is small_offices_1.glm
//Generated at 6/25/2018, 16:21:26
object motor {
    name small_offices_1_AHU_Compressor;
    parent GC-12-47-1_meter_2;
    phases ABCN;
    frequency_measure_type PLL;
    base_power 106250.00000; // [W]
    nominal_voltage 277;
    flags DELTAMODE;

    TPIM_type TPIM_A;

    H 0.363000; // [s]
    Rs 0.004147200; // [pu]
    Xs 0.078336000; // [pu]
    Xm 3.350016000; // [pu]
    Rr 0.004661760; // [pu]
    Xr 0.076800000; // [pu]

    groupid small_offices_1;

    relayProtectionTrip "0.6;0.08";
    relayProtectionReconnect "0.9;0.033";

    overLoadProtectionTrip "0.6 0.7 0.8;0.33 0.5 1.0";

    contactorProtectionTrip "0.65;0.1";
    contactorProtectionReconnect "0.75;0.1";

    emsProtectionTrip "0.0 0.4 0.5 0.6 0.7;0.083 0.1 0.166 0.25 0.5";
    emsProtectionReconnect "0.95;2.0";

    object recorder {
        property "ws, rotor_speed, Vas.real, Vas.imag, Vbs.real, Vbs.imag, Vcs.real, Vcs.imag, mechanical_power";
        interval 0;
        file output/small_offices_1_AHU_Compressor.csv;
        flags DELTAMODE;
    };
};

object motor {
    name small_offices_1_AHU_Fan;
    parent GC-12-47-1_meter_2;
}

```

Figure 7.16 Sample Output File

7.2.4 Simulation Results

A voltage depression test is applied at the head of GC-12.47-1 feeder (used in Chapter 7.1). Three types of commercial buildings, including large office, small office, and hotel, are placed at meter_1, meter_2, and meter_3 of the GC-12.47-1 feeder respectively. It is assumed that the motor loads account for 70%, 70% and 75%, respectively, of the total loads (in terms of real power) in the large office, small offices and hotel. The remaining loads are modeled as constant impedance loads. Figure 7.17 shows the zoomed-in diagram of GC-12.47-1 feeder. Table 7.3 shows the connection of the three types of buildings to specific nodes of the feeder.

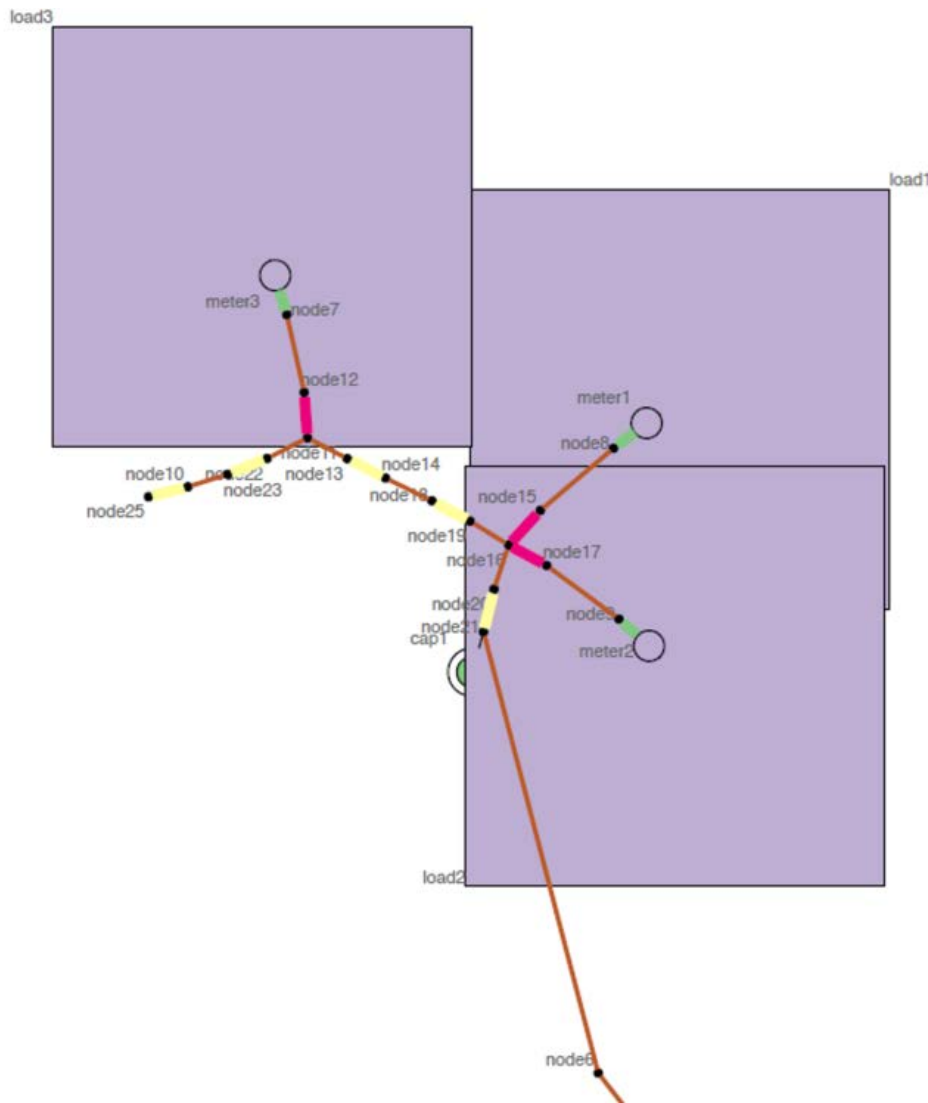


Figure 7.17 Zoomed-in Diagram of GC-12.47-1 Feeder

Table 7.3 Connection of the Three Types of Commercial Buildings

Meter	Building	Number of buildings	Total motor power per building	Impedance load at the meter
meter1	Large office	1	$3000 * 0.7 \text{ kW}$	$900 + j546 \text{ kVA}$
meter2	Small office	5	$300 * 0.7 \text{ kW}$	$450 + j273 \text{ kVA}$
meter3	Hotel	1	$3000 * 0.75 \text{ kW}$	$500 + j303 \text{ kVA}$

The motor types, protection schemes and motor ratings for each type of building are demonstrated in Figure 6.3. The rotor speed plots of all the motors in large office and hotel buildings are simulated and presented in Figure 7.18 and Figure 7.19.

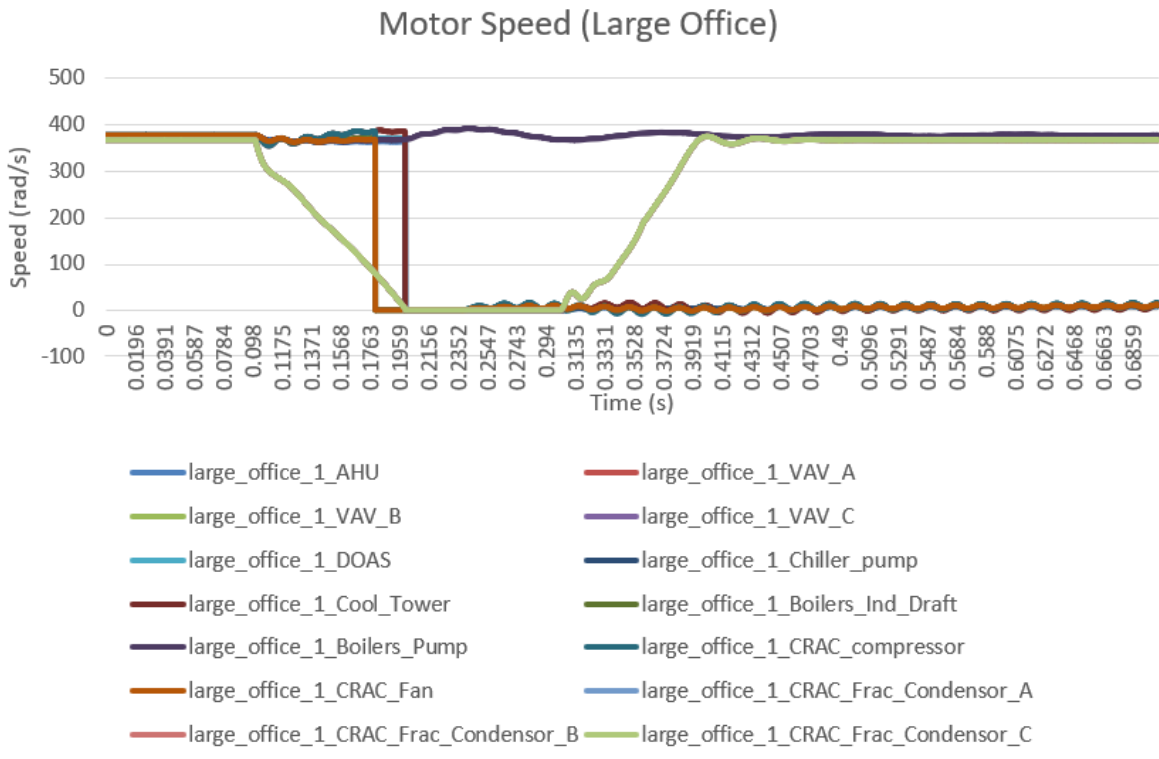


Figure 7.18 Rotor Speed of Motors in Large Office Building

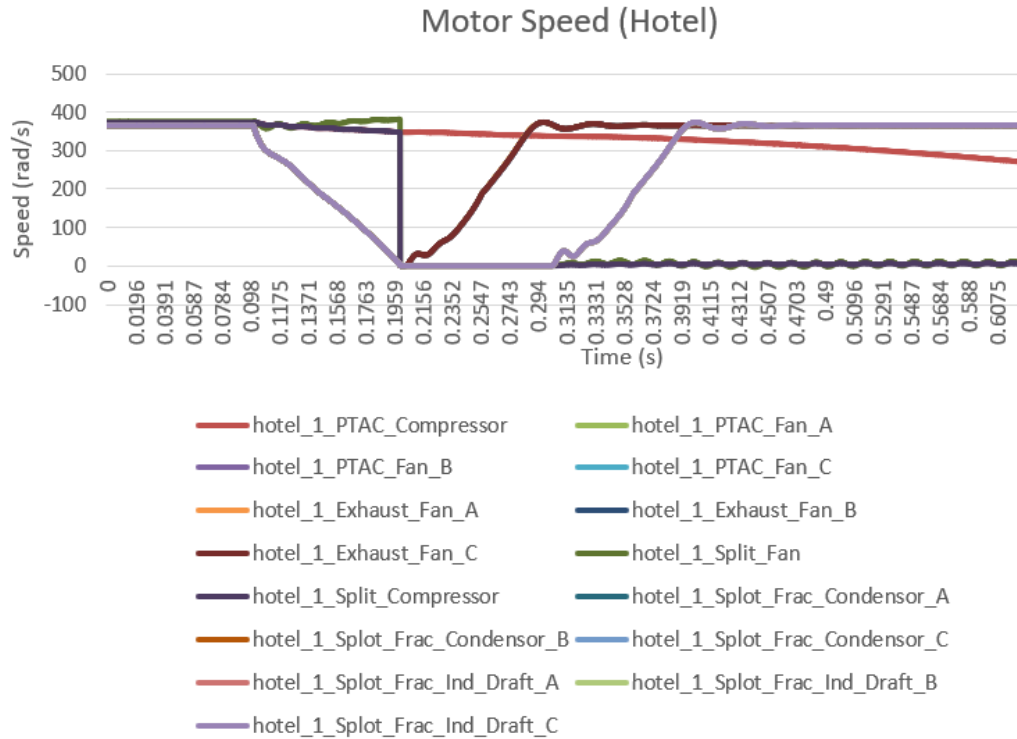


Figure 7.19 Rotor Speed of Motors in Hotel Building

7.3 Commercial Feeder Model Modeled in PSCAD

The intent of this section is to provide implementation guidelines for several critical motor protection models at the distribution end-use level and to investigate the impacts of end-use motor protections on system transient behaviors in electro-magnetic transient (EMT) simulation. The heterogeneous collection of motors present in the system is represented for several typical commercial buildings connected to different nodes of a distribution feeder. Each of the commercial buildings contains a combination of motor loads and ZIP loads [72]. The composition and protection parameters of the heterogeneous motors in each building are based on reviews of previous research publications. Several representative motor protection schemes are described and implemented in detail. The feeder model, motor composition model, and five types of protection models with examined parameters are explicitly developed in the PSCAD simulator [73]. The dynamics of the realistically modeled feeder are observed in the PSCAD simulation by feeding various voltage depressions at the head of the feeder. Transmission and distribution (T&D) hybrid modeling is carried out intentionally to explore the impacts of individual motor protections on transmission-scale system dynamics.

7.3.1 Categorization of Motor Loads

The common types of three-phase or single-phase induction motors found in typical commercial buildings were investigated through reviews of previously reported work [3] [51] and identified in Chapters 6 and 7. Six buildings are selected and represented in PSCAD feeder model, including two retail stores (medium and large), a supermarket, a school, a hotel, and a warehouse. The identified motors in these buildings are categorized into the four CMPLDW motor types based on inertia and torque characteristics. The four motor types in WECC composite load model, referred to as Motors A, B, C, and D, and are summarized in Chapter 6.1.

The ratings of the identified motors were determined from reviews of DOE-conducted survey reports, including an Energy Information Administration commercial building survey [56] and DOE commercial prototype building models [57] used in EnergyPlus simulations [52]. For motor-rated data that was not found in DOE reports, a common calculation was applied to find the typical rated motor load for each particular building set. If specified motors fell outside the common calculations, a top-down approach [57] was used to roughly estimate the rated motor load within that building set.

7.3.2 Five Types of Protection

Motor protections are categorized into five typical types and discussed in detail in Chapter 6.2. Some performance metrics of these five protection schemes associated with voltage levels are presented in Figure 7.7 and Figure 7.13. The motor loads and associated protections for the six commercial buildings have been studied in previous works [51] [61], and are summarized in Table 7.4. According to the investigation, some identified motors are equipped with more than one types of protection. It is noted that protections P1, P4, and P5 are triggered by transient low voltage conditions, and each has a reconnection logic. These three voltage-dependent protections can be defined identically and implemented with different parameter settings. Unlike the voltage-dependent implementation presented in Chapters 7.1 and 7.2, the current overload and thermal protections are implemented individually based on real physical models in this sub-chapter. The development of the five protection logics is accomplished in PSCAD using the master library components and user-defined models.

Table 7.4 Static Loads, Motor Loads and Associated Protections

Building	Appliance	Equipment	Motor Type	Protections	Rating (kW)
Medium Retail	RTU	Fan	MB	P2P4P5	15.38
	RTU	Compressor	MA	P2P4P5	53.13
	RTU	Frac. Condenser	MD	P3P4P5	16.25
	RTU	Frac. Ind. Draft	MD	P3P4P5	10.41
	Exhaust	Frac. Fan	MD	P3P4P5	0.92
	Static Loads				41.18
Large Retail	RTU	Fan	MB	P2P4P5	46.15
	RTU	Compressor	MA	P2P4P5	159.38
	RTU	Frac. Condenser	MD	P3P4P5	48.75
	RTU	Frac. Ind. Draft	MD	P3P4P5	31.22
	Exhaust	Frac. Fan	MD	P3P4P5	1.38
	Static Loads				122.95
Supermarket	RF	Compressor	MA	P2P4	42.5
	RF	Frac. Fan	MD	P3	17
	Exhaust	Frac. Fan	MD	P3P4P5	1.38
	RTU	Fan	MB	P2P4P5	30.77
	RTU	Compressor	MA	P2P4P5	106.25
	RTU	Frac. Condenser	MD	P3P4P5	32.5
	RTU	Frac. Ind. Draft	MD	P3P4P5	20.81
	Static Loads				107.66
Warehouse	Gas_Heater	Fan	MD	P3P4	1.2
	Exhaust	Frac. Fan	MD	P3P4	24.62
	Static Loads				11.07
School	Chiller	Compressor	MA	P1P4P5	350
	Chiller	Pump	MC	P2P5	98
	Cool_Tower	Fan	MB	P2P4P5	42
	Fan_Coil	Fan	MB	P4P5	6.15
	Exhaust	Fan	MB	P2P4P5	1.29
	Boilers	Ind. Draft	MB	P1P4P5	83.25
	Boilers	Pump	MC	P2P5	98
	RTU	Fan	MB	P2P4P5	123
	RTU	Compressor	MA	P2P4P5	425
	RTU	Frac. Condenser	MD	P3P4P5	130
	RTU	Frac. Ind. Draft	MD	P3P4P5	83.25
	Static Loads				617.12
Hotel	PTAC	Compressor	MA	P4	425
	PTAC	Fan	MD	P3	123
	Exhaust	Fan	MD	P3	23
	HWP	Pump	MD	P3	1.2
	Split	Fan	MB	P2P4	123
	Split	Compressor	MA	P2P4	425
	Split	Frac. Condenser	MD	P3P4	130
	Split	Frac. Ind. Draft	MD	P3P4	83.25
	Static Loads				571.48
Static		MA	MB	MC	MD
1471.45	1986.26	470.99	196.00	780.14	4904.84
30.00%	40.50%	9.60%	4.00%	15.91%	100.00%
Note: Frac. → Fractional, Ind. → Induced					

7.3.3 Voltage-Dependent Protection Schemes

The voltage-dependent protection schemes include the electronic relay (P1), contactor (P4), and BMS (P5). These three protection logics are defined in the same subroutine of the PSCAD user-defined component with options of enabling or disabling each type. Each protection logic receives the same voltage signal from the motor terminal sensor. If the voltage drops below the trip voltage level of a specific protection, an individual timer will begin to count the length of time the voltage stays below the trip level. If the voltage recovers sooner than the delayed time is reached, the motor does not trip, and the timer would be reset to zero. If the voltage does not recover, a trip signal will be sent. The reconnection for this specific protection type follows similar rules under the pre-conditions that the motor has been disconnected by this protection and voltage recovers above the reconnection threshold. Because some motors have more than one voltage-dependent protection, the outputs of these three protection controllers are logically connected in parallel as inputs of an OR gate to ensure that the final output of the OR gate will be based on a “first-come–first-trip” mechanism. The implementation algorithm of the voltage-dependent protection scheme is outlined in Table 7.5.

Table 7.5 Algorithm of Voltage Dependent Protection

Algorithm 1 Voltage Dependent Protection	
1:	Subroutine MyProtection
2:	<i>ProtActivated</i> \leftarrow True or False (user specified)
3:	<i>ProtWorkTime</i> \leftarrow time protection begins to work (user specified)
4:	<i>Vtr</i> \leftarrow trip voltage (user specified)
5:	<i>Ttr</i> \leftarrow trip delay (user specified)
6:	<i>Vrec</i> \leftarrow reconnection voltage (user specified)
7:	<i>Trec</i> \leftarrow reconnection delay (user specified)
8:	<i>MaxTripCount</i> \leftarrow maximum allowed tripping count (user specified)
9:	Initialize Variables:
10:	<i>Time</i> \leftarrow 0.0, <i>TripTimer</i> \leftarrow 0.0, <i>RecTimer</i> \leftarrow 0.0, <i>TripCounter</i> \leftarrow 0
11:	Loop:
12:	If (<i>ProtActivated</i> = True) AND (<i>Time</i> \geq <i>ProtWorkTime</i>) Then
13:	If <i>Vmeasured</i> < <i>Vtr</i> Then //Tripping logic initiated
14:	<i>TripTimer</i> \leftarrow <i>TripTimer</i> + Δt
15:	If <i>TripTimer</i> > <i>Ttr</i> Then
16:	If <i>ProtTrip</i> = False Then
17:	<i>TripCounter</i> \leftarrow <i>TripCounter</i> + 1
18:	End if
19:	<i>ProtTrip</i> \leftarrow True
20:	Else
21:	<i>ProtTrip</i> \leftarrow False
22:	End if
23:	Else
24:	<i>TripTimer</i> \leftarrow 0.0
25:	End if
26:	If <i>ProtTrip</i> = True Then //Reconnection logic initiated
27:	If <i>Vmeasured</i> > <i>Vrec</i> Then
28:	<i>RecTimer</i> \leftarrow <i>RecTimer</i> + Δt
29:	If <i>RecTimer</i> > <i>Trec</i> Then
30:	<i>ProtTrip</i> \leftarrow False
31:	<i>TripTimer</i> \leftarrow 0.0
32:	End if
33:	Else
34:	<i>RecTimer</i> \leftarrow 0.0
35:	End if
36:	End if
37:	If <i>TripCounter</i> \geq <i>MaxTripCount</i> Then //Check trip counter
38:	<i>ProtTrip</i> \leftarrow True
39:	End if
40:	End if
41:	<i>Time</i> \leftarrow <i>Time</i> + Δt , goto Loop
42:	Output: <i>ProtTrip</i>

7.3.4 Current Overload Protection

Current overload protection is implemented using similar tripping logic (lines 13–25 in Table 7.5) to the voltage-dependent protection scheme presented in Table 7.5. The current measurement ($I_{measured}$) is sent in as an input and compared with trip current threshold (I_{tr}). The motor is tripped by the current overload protection after a time delay if ($I_{measured} > I_{tr}$). The difference is that there is no reconnection logic for overload protection. Thus, the maximum allowed tripping number ($MaxTripCount$) is hard coded to be 1.

7.3.5 Thermal Protection

The standard thermal protection model used in the PSLF performance-based model of an air-conditioner (ld1pac) [14] [5] is implemented for all the single-phase motors identified as MD in Table 7.4.

The thermal protection logic, which is connected to the third input port of the OR gate, is shown in Figure 7.20. When the motor is stalled, the current drawn by the stalled motor is represented by a constant impedance load ($R_{stall} + jX_{stall}$). The temperature of the motor is computed by integrating ($R_{stall}I^2_{measured}$) through the thermal time constant (T_{therm}) in the first-order transfer function in Figure 7.20. The integrated result, which represents the motor temperature, is compared with a threshold temperature (T_{th}). The motor is tripped when the motor temperature exceeds the threshold.

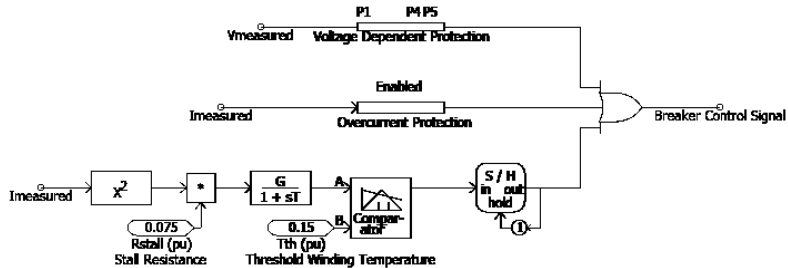


Figure 7.20 Schematic of Protection Logics

7.3.6 Capacitor Bank Over-Voltage Tripping

A capacitor bank is deployed at the high-voltage side of each building transformer to provide VAr support. The over-voltage tripping mechanism is implemented for these capacitor banks during a cascaded motor tripping event caused by voltage depression. The status of the capacitor bank does not change if the terminal operating voltage V_{op} stays within a range. The capacitor bank is tripped when V_{op} rises above the upper bound, and is reconnected when V_{op} drops below the lower bound. The mechanism is expressed by (7.1)–(7.4).

$$\text{Initialize: } Status \leftarrow on \quad (7.1)$$

$$\text{If } V_{op} \geq V_{max} \text{ then, } Status \leftarrow off \quad (7.2)$$

$$\text{Else if } V_{min} < V_{op} < V_{max} \text{ then, } Status \leftarrow \text{Not Changed} \quad (7.3)$$

$$\text{Else, } Status \leftarrow on \quad (7.4)$$

7.3.7 Study Cases

In this study, the six commercial buildings are supplied by two distribution taxonomy feeders GC-12.47-1 [60], as shown in Figure 7.21. The feeders consist of 30% static (ZIP) loads and 70% motor loads [60] [74]. The percentage of each motor type is shown in Table 7.4. The feeders are connected to Bus 18 of the IEEE 39 bus system [60] to replace the original ZIP load, as illustrated by Figure 7.22.

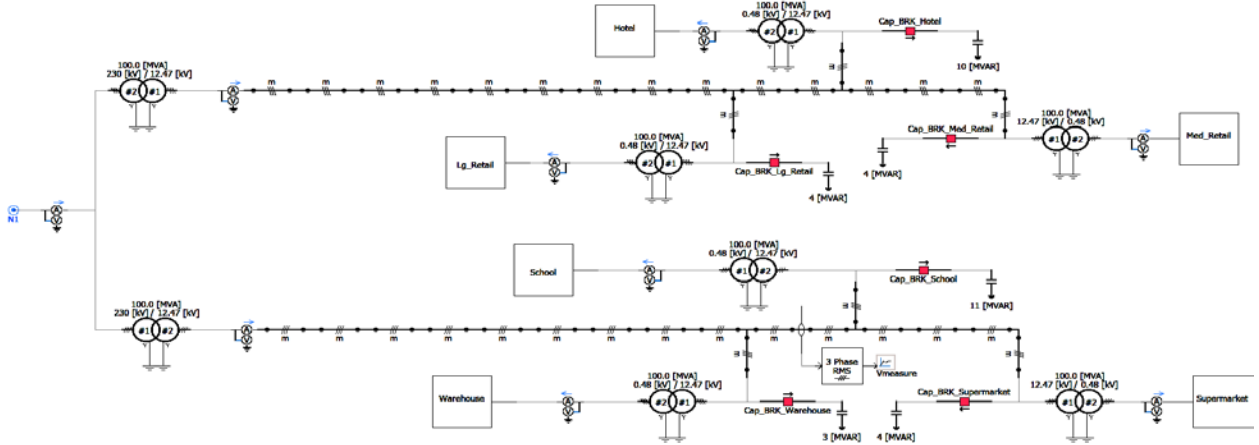


Figure 7.21 Distribution Feeder Schematic

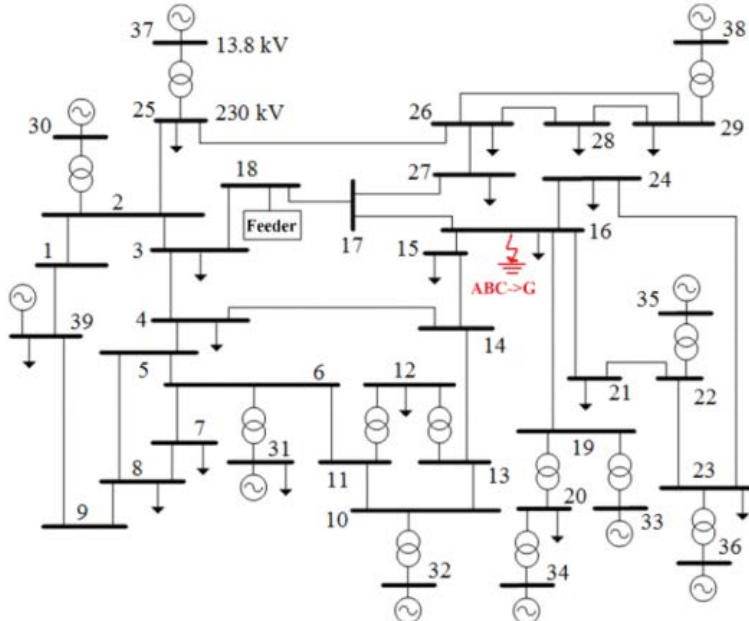


Figure 7.22 IEEE 39 Bus Transmission System

The building load ratings in Table 7.4 are identically scaled to match the original load at Bus 18. A six-cycle, three-phase-to-ground fault is applied at Bus 16 of the transmission system, thus depressing the voltage at Bus 18 to 0.35 pu. The simulation considers two scenarios: Scenario A when all of the described protections for each motor in Table 7.4 are activated and Scenario B when only the thermal protection (P3) is activated and the other protections are deactivated. The parameters of the five protections used in the simulation are generated from the specific numbers or randomly picked up from the ranges described below [51] [66] [75]:

- P1: $V_{tr} = 0.8 \sim 0.9 \text{ pu}$, $T_{tr} = 20 \text{ cycles} \sim 20 \text{ s}$, $V_{rec} = 1.0 \text{ pu}$, $T_{rec} = 6 \sim 300 \text{ s}$
- P2: $I_{tr} = 8.5 \text{ pu}$, $T_{tr} = 10 \text{ s}$
- P3: $T_{th} = 0.15 \text{ pu}$, $T_{therm} = 10 \text{ s}$, $R_{stall} = 0.054 \sim 0.086 \text{ pu}$
- P4: $V_{tr} = 0.5 \text{ pu}$, $T_{tr} = 1 \sim 5 \text{ cycles}$, $V_{rec} = 0.65 \sim 0.7 \text{ pu}$, $T_{rec} = 2 \sim 8.5 \text{ cycles}$

- P5: $V_{tr} = 0.6 \text{ pu}$, $T_{tr} = 2 \text{ s}$, $V_{rec} = 1.0 \text{ pu}$, $T_{rec} = 2\sim300 \text{ s}$

The parameters of over-voltage protection for all the capacitor banks are given as

- $V_{max} = 1.15 \text{ pu}$, $V_{min} = 0.55 \text{ pu}$

The voltage between the warehouse and school buildings is measured by a three-phase RMS voltage meter, as shown in Figure 7.21. The measured voltages in Scenarios A and B are compared in Figure 7.23.

Figure 7.23 shows the voltages at the head of the feeder (Bus 18) and at the measurement point. It can be seen that with all protections activated, the post-event voltage is slightly higher than the scenario in which only thermal protection is enabled because some motors are tripped offline by fast-reacting contactor protection (P4). However, most motors equipped with P4 are reconnected because the contactor protection has a relatively low reconnection voltage. It can be seen from Figure 7.23 (b) that a slow voltage drop, caused by motor reconnection, occurs after the clearance of the fault. In Scenario B, for which only the thermal protection is activated, the stalled single-phase motors are tripped offline with delays of seconds.

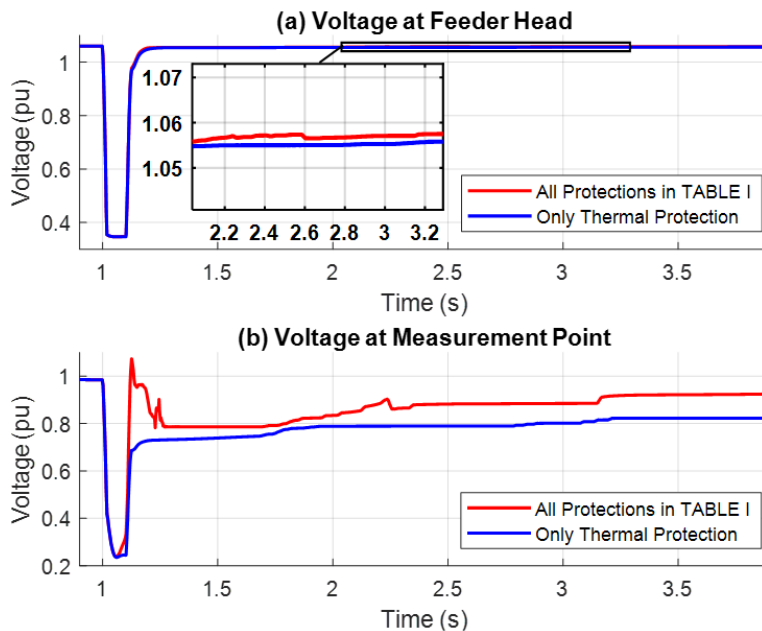


Figure 7.23 Voltages at Bus 18 (Feeder Head) and Measurement Point

Figure 7.24 shows the comparison of protection actions in Scenarios A and B. In Figure 7.24 (a), the motor is first tripped by contactor (P4) and then reconnected after the voltage recovers. The stalled motor draws high current and the stator winding heats up after the motor is reconnected. When the winding temperature reaches a threshold value, the motor is tripped by thermal protection (P3). In Figure 7.24 (b), because the motor is equipped with only the thermal protection, the stator winding starts to heat up once the voltage recovers.

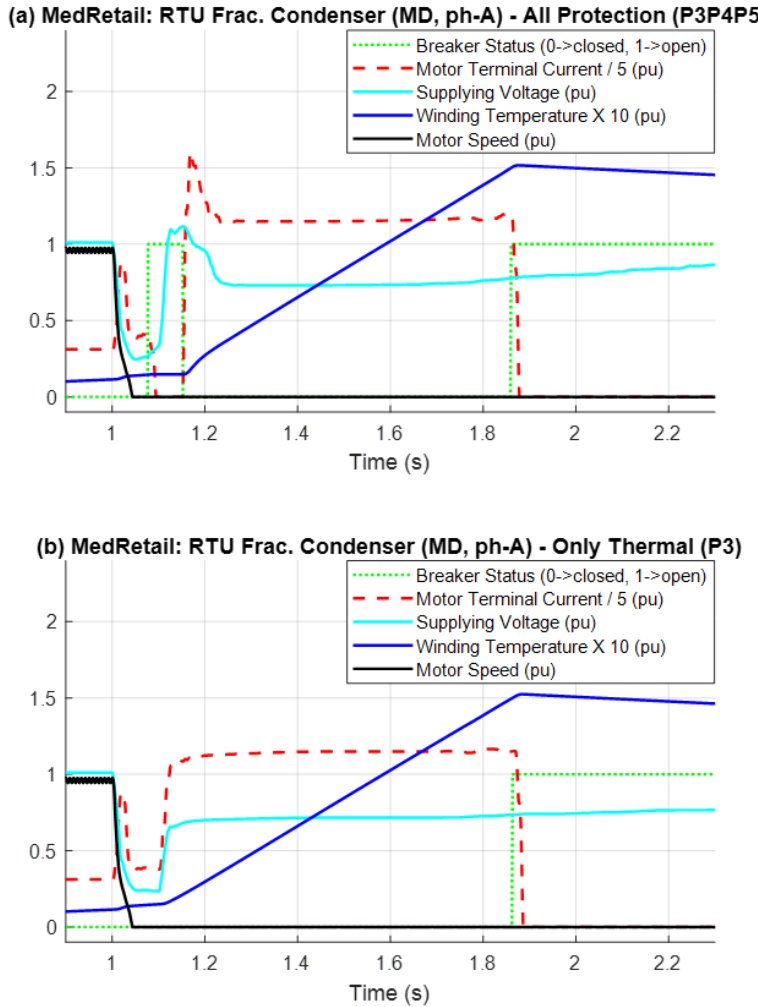


Figure 7.24 (a) Performance of thermal protection (P3) and contactor (P4) for Scenario A. (b) Performance of thermal protection (P3) for Scenario B, in a roof top unit fractional condenser motor in a medium size retail building

7.3.8 Summary

In this section, we discuss the results of our study of the impacts of end-use motor loads with protections on power system transient behaviors. The motor loads and their protections in six types of commercial buildings are categorized and modeled in Electro-Magnetic Transient Program T&D co-simulations. The IEEE 39 bus system and a typical distribution taxonomy feeder are used in the PSCAD simulation. The realistic system dynamics can be properly simulated by modeling the motor loads and protections in detail. It can be concluded from our study that with all motor protections properly configured the fault-induced delayed voltage recovery could be improved. The protection parameters have a great impacts on the system dynamics.

7.4 Residential Feeder Modeled in GridLAB-D

This sub-chapter focuses on modeling a generic residential distribution feeder with detailed representation of residential end-use loads and motor protection schemes [76]. The feeder and motor

models are implemented in GridLAB-D simulator, which supports model development based on dynamic-phasor techniques and effectuates distribution system simulation in mini-seconds timescale. The power ratings of the end-use loads are determined based on the consideration of residential home types, device nameplate values, home floor space and climate zones. Two common protection models residing in residential motor loads are elaborately developed. Three profiles of mechanical torque are explicitly modeled for the residential motors serving different functions. With the triangular-wave mechanical torque modeled for reciprocating air-conditioner (A/C) compressor motor, the point-on-wave effects impacting motor stalling and recovery can be innovatively investigated in the dynamic-phasor simulation program, while previously the effects could only be simulated in electro-magnetic transient (EMT) simulation tools [1]. An individual motor test is performed to explore the mechanism of motor recovery, and a feeder-level test is carried out to investigate the impacts of motor protections on system voltage profile. The feeder-level simulation results can be further used to calibrate the aggregate protection parameters of the residential composite load model in the WECC network.

7.4.1 Identification of End-Use Loads in Residential Houses

Typical residential houses can be classified as single-family home (SFH) and multi-family home (MFH). Single-family homes usually consist of one property unit that houses only one family, Multi-family homes have more than one unit, which can ultimately house more than one family. The types of end use in single-family and multi-family homes are identical, while the power ratings are different. Table 7.6 shows a list of common end uses in single-family and multi-family homes.

Table 7.6 End Uses in Single-Family and Multi-Family Homes

Residential Home	Enduse	Type	Voltage [V]	Base Power [W]	Protection/Power Factor	Scaling Factor
Single-Family Home	A/C Compressor	MDT	240	Floor-Area Related	P1P2	7
	A/C Fan	MDS	240	Floor-Area Related	P1P2	7
	Dryer	MDS	240	3000	P2	7
	Clothes Washer	MDS	120	1000	P2	7
	Dish Washer	MDS	120	1500	P2	7
	Fridge	MDC	120	60	P2	7
	Freezer	MDC	120	52	P2	7
	Water Heater	ZIP	240	4500	0.8	7
	Oven	ZIP	120	1200	0.85	7
	Microwave	ZIP	120	1000	0.98	7
	Lighting	ZIP	120	Floor-Area Related	0.7	7
	Electronics	ZIP	120	Floor-Area Related	0.6	7
Multi-Family Home	A/C Compressor	MDT	240	Floor-Area Related	P1P2	4
	A/C Fan	MDS	240	Floor-Area Related	P1P2	4
	Dryer	MDS	240	2400	P2	4
	Clothes Washer	MDS	120	800	P2	4
	Dish Washer	MDS	120	1200	P2	4
	Fridge	MDC	120	50	P2	4
	Freezer	MDC	120	45	P2	4
	Water Heater	ZIP	240	4500	0.8	4
	Oven	ZIP	120	1200	0.85	4
	Microwave	ZIP	120	1000	0.98	4
	Lighting	ZIP	120	Floor-Area Related	0.7	4
	Electronics	ZIP	120	Floor-Area Related	0.6	4

All the motor loads in residential houses are single-phase induction motors, noted as *MD* in Table 7.6. The A/C compressor and A/C fan motors are equipped with thermal protection (*P1*) and contactor protection (*P2*). All the other motors are only equipped with contactor protection. The power factors of all

ZIP type loads [77] are provided in the same column of the motor protection type, as shown in Table 7.6. The mechanical torque of these motors is different based on their functionality. Three types of mechanical torque are represented for the single-phase motors (*MD*), with *T* indicating triangular-wave torque for reciprocating A/C compressor [1], *S* indicating speed dependent torque, and *C* indicating constant torque. In Table 7.6, some end uses consume a certain amount of power regardless of the floor space of a house. The base powers of these end uses are computed based on the best estimates and online resources [78] [79]. The power ratings of the A/C compressor and associated A/C fans are computed according to the floor space of a house. To reflect the actual power consumption at each node of the feeder, a scaling factor will be applied to scale up the total power of a house to represent multiple identical houses connected in parallel.

For the A/C compressor, the compressor motor base power in W [80] [81] is calculated as:

$$P_{comp} = \frac{HRR \times C}{EER} \quad (7.5)$$

where, *HRR* is the heat remove ratio, which is a constant defined as the heat removed by a 1 ton A/C in 1 hour, and its value is 3516 W/ton [80]; *C* is the A/C capacity in number of tons, which is related to the unit area and climate zone [81]; and *EER* is the abbreviation for energy efficiency ratio, which is defined to be the ratio of amount of heat removed in W over the power consumed in W [80].

For the A/C fan motor, the base power can be calculated using a ratio between A/C fan power and A/C compressor power. Typically, this ratio is 15:85 [82]. Thus,

$$P_{fan} = \frac{15}{85} P_{comp} \quad (7.6)$$

For lighting and electronics loads, referring to the statistical data released by Energy Information Administration [83], the values of power rating in W can be estimated by

$$P_{lighting} = \frac{S}{2}, P_{electronics} = \frac{S}{3} \quad (7.7)$$

where *S* represents the square-feet floor space per property unit.

7.4.2 Protection Models for Residential End-Use Motors

There are two types of protection modeled for residential end-use motors [66], including contactor protection and thermal protection. The contactor protection is an undervoltage protection. If the voltage drops below a specific level for a specific length of time, contactor protection will trip the motor. If the voltage recovers to another level for a specific length of time, contactor protection will reconnect the motor to the system. The thermal protection is triggered by high temperature on stator winding. The stator current of motor is monitored and used to evaluate the temperature inside the motor. If the temperature exceeds a pre-defined threshold, the thermal protection will trip the motor. Usually the thermal protection requires manual reconnection.

Figure 7.25 illustrates the flowchart implementation of contactor protection, where *Ttrip* and *Trec* are time delay thresholds for contactor tripping and reconnection, respectively; and *TripTimer* and *ReconnectTimer* are the elapsed time after voltage drops below trip threshold (*Vtrip*) and recovers above reconnect threshold (*Vrec*), respectively.

The implementation of thermal protection is described by Figure 7.26. The standard thermal protection model used in the PSLF performance-based model of an air-conditioner (ld1pac) [14] is implemented for A/C compressor and A/C fan motors.

In Figure 7.26, I represents the stator current of motor; T_{th} is the thermal time constant of a first-order lag transfer function; and Γ indicates the motor temperature. When the motor is stalled, the current drawn by the stalled motor is represented by a constant impedance load ($R_{stall} + jX_{stall}$). The temperature of the motor is computed by multiplying ($I^2 R_{stall}$) with the first-order lag transfer function in Fig. 2. The integrated result, which represents the motor temperature, is compared with a threshold temperature (Γ_{th}). The motor is tripped when the motor temperature exceeds the threshold.

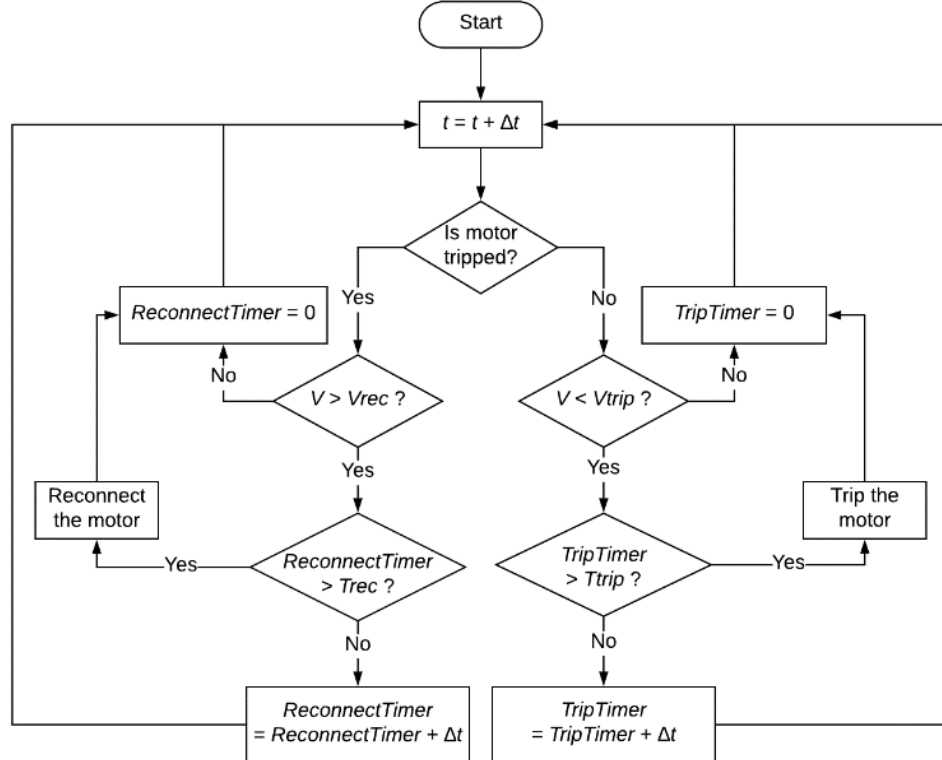


Figure 7.25 Implementation of Contactor Protection

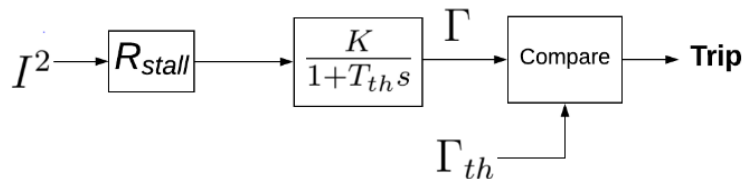


Figure 7.26 Implementation of Thermal Protection

7.4.3 Motor Model and Mechanical Torque

The motor model used in the simulation is the dynamic-phasor model of single-phase induction motor, which was initially developed for use in the positive-sequence transmission system simulator [84], and later adopted in the GridLAB-D simulation program [85]. Three types of mechanical torque, including constant torque, speed-dependent torque and triangular-wave torque, are represented based on the functionality of motor, as shown in Table 7.6. The triangular-wave torque is modeled uniquely for reciprocating A/C compressor, which is prone to stalling [1]. Figure 7.27 depicts the mechanical torque of

the A/C compressor in steady state, comprising a speed-dependent component T_{spd} and a rotor-angle-dependent component T_{tri} .

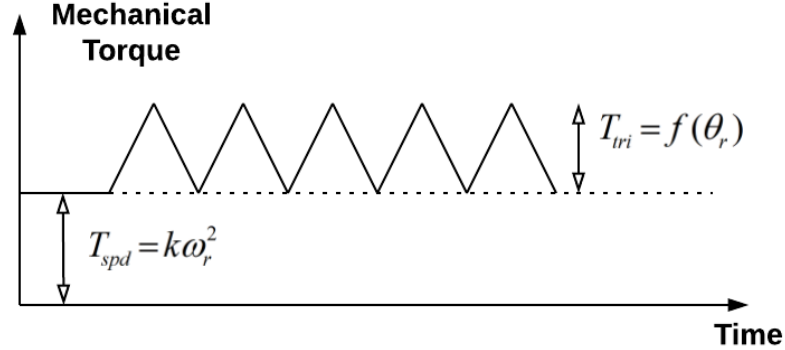


Figure 7.27 Triangular-Wave Mechanical Torque for A/C Compressor

7.4.4 Simulation Cases

The simulation considers two scenarios in this study. In the first scenario, the point-on-wave analysis is performed to investigate the motor recovery behavior of an individual A/C compressor. The second scenario examines the dynamic responses of a feeder supplying multiple residential homes to the voltage depressions at the feeder head.

Scenario I: Test of an Individual A/C Compressor

The purpose of this test is to verify the feasibility that the dynamic-phasor model of single-phase induction motor with proper modeling of mechanical torque could emulate the point-on-wave effects discovered in the simulation of EMT model of A/C compressor motor [1]. In this scenario, an individual A/C compressor motor without protection is tested by altering supplying voltage at the motor terminal. In the test, two voltage depressions are applied at the motor terminal with the same depression level, duration, and recovery level, but are initiated at different time instants. The results are shown in Figure 7.28 and Figure 7.29.

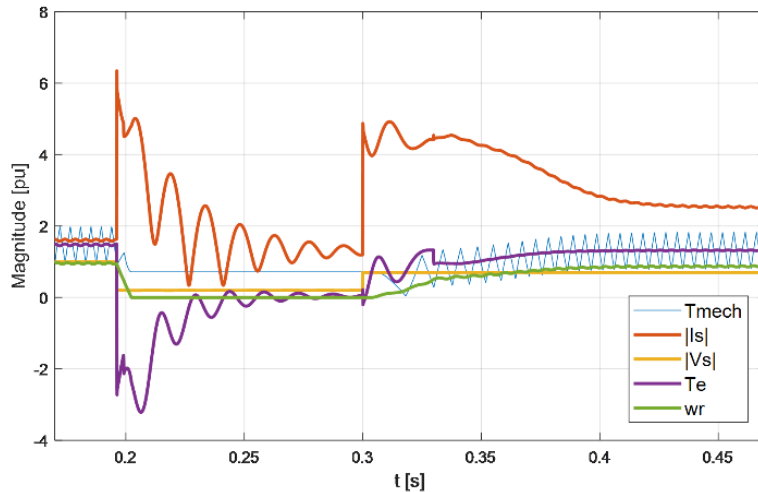


Figure 7.28 Case 1: Mechanical Torque (T_{mech}), Terminal Current Magnitude ($|I_s|$), Terminal Voltage Magnitude ($|V_s|$), Electrical Torque (T_e) and Rotor Speed (w_r)

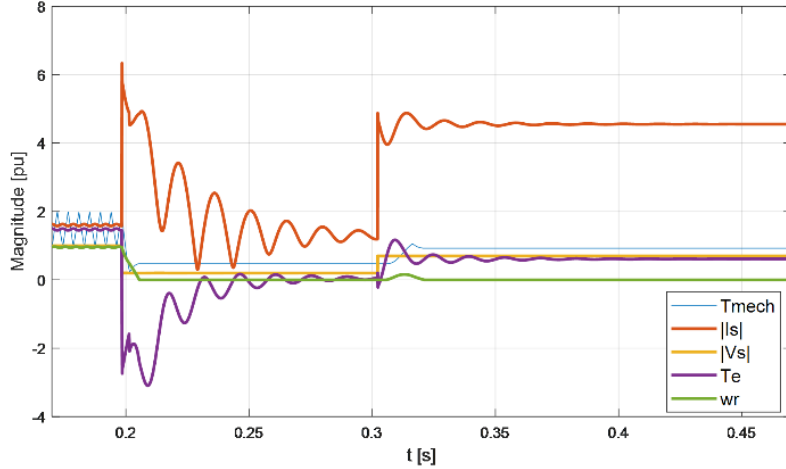


Figure 7.29 **Case 2:** Mechanical Torque (T_{mech}), Terminal Current Magnitude ($|I_s|$), Terminal Voltage Magnitude ($|V_s|$), Electrical Torque (T_e) and Rotor Speed (w_r)

For both Case 1 and Case 2, the voltage drops from 1.0 pu to 0.2 pu, lasts for 0.1038 s, then recovers to 0.7 pu and keeps at this level afterwards. In Case 1, the voltage depression starts at 0.1962s, at which time the triangular mechanical torque is at its minimum value. In Case 2, the voltage drops at 0.1984s, at which time the motor mechanical torque is at its maximum value. It is seen from the results in Figure 7.28 and Figure 7.29 that, after the voltage recovery, the motor re-accelerates in Case 1 and remains stalled in Case 2. The determining factor for motor recovery is not the level of mechanical torque during voltage depression. However, the change of mechanical torque following voltage recovery determines whether a motor recovers or not. It is seen from Figure 7.28 (Case 1) that the mechanical torque following the voltage recovery tends to decrease to the bottom point of the triangular wave, which gives the electrical torque enough time to overcome the mechanical torque and reaccelerate the motor. In Figure 7.29 (Case 2), the mechanical torque tends to increase after $t = 0.3$ s, preventing the recovery of the motor. The point-on-wave analysis in [1] discovered the mechanism of motor stalling. In this section, the behavior of motor recovery from stalled status is captured through a similar point-on-wave study.

Scenario II: Test of Residential Feeder

This scenario considers the simulation of a typical residential feeder supplying 21 residential homes, including 15 single-family homes and 6 multi-family homes. The feeder *R1-12.47-3* from the GridLAB-D taxonomy feeder list [86] is chosen to be the testing feeder, with the schematic shown in Figure 7.30. Table 7.7 shows the base floor space and the connection of the 21 residential homes to specific nodes of the feeder. In this section, it is assumed that each single-family home represents one property unit, thus contains one group of end use, and each multi-family home consists of three units and contains three groups of end use.

To add a certain level of randomization to the residential homes to reflect reality, the actual space of each unit is uniformly distributed within $\pm 10\%$ of the value specified in the last column of Table 7.7 so that the A/C compressor and fan powers that are area-related will have some randomness. For those end uses whose base powers are not area-related, the base power itself is assumed to be uniformly distributed within 10% of the base power values specified in Table 7.6.

Table 7.7 Connection of 21 Residential Homes

Name	Node	Phase	# of Units / Home	Space (sqft)/Unit
single_family_home_1	11	AS	1	2000
single_family_home_2	22	BS	1	2000
single_family_home_3	6	CS	1	2000
single_family_home_4	20	AS	1	2500
single_family_home_5	24	BS	1	2500
single_family_home_6	12	CS	1	2500
single_family_home_7	28	AS	1	2800
single_family_home_8	27	BS	1	2800
single_family_home_9	14	CS	1	2800
single_family_home_10	29	AS	1	2250
single_family_home_11	37	BS	1	2250
single_family_home_12	42	CS	1	2250
single_family_home_13	30	AS	1	2650
single_family_home_14	38	BS	1	2650
single_family_home_15	47	CS	1	2650
multi_family_home_1	44	AS	3	800
multi_family_home_2	39	BS	3	800
multi_family_home_3	48	CS	3	800
multi_family_home_4	33	AS	3	1000
multi_family_home_5	18	BS	3	1000
multi_family_home_6	10	CS	3	1000

In this scenario, the two types of protection as given in Table 7.6 are enabled for all the motor end uses. A voltage depression is applied at the feeder head (Bus 53) to dip the voltage from 1.0 pu to 0.4 pu at $t = 0.1\text{s}$ and recover the voltage to 0.74 pu at $t = 0.3\text{s}$. The simulation is performed to explore the device-level functionality of the two protections and the aggregate system-level impacts of motor protections on voltages. Table 7.8 shows the parameters of the two protections. The results are shown in Figure 7.31 and Figure 7.32.

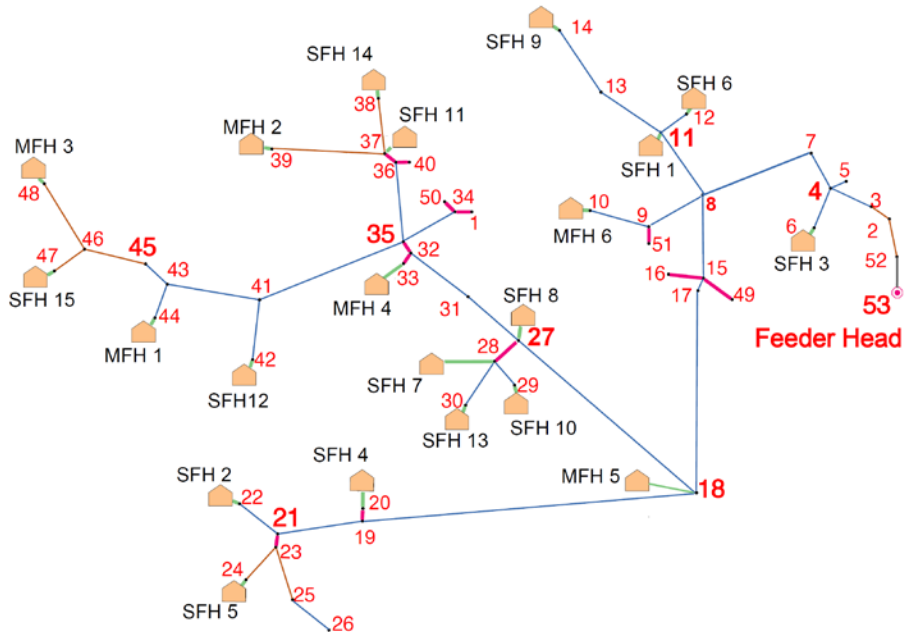


Figure 7.30 Residential Feeder Model (SFH Stands for Single-Family Home; MFH Indicates Multi-Family Home)

Table 7.8 Protection Parameters

Protection	Type	Trip Parameters	Reconnect Parameters
P1	Thermal	$R_{stall} = 0.124 \text{ pu}$ $T_{th} = 10 \text{ s}$ $K = 1.0$ $I_{th} = 0.8 \text{ pu}$	Manual Reconnection
P2	Contactor	$V_{trip} = 0.6 \text{ pu}$ $T_{trip} = 0.1 \text{ s}$	$V_{rec} = 0.7 \text{ pu}$ $T_{rec} = 0.1 \text{ s}$

It can be seen from Figure 7.32 that when voltage drops at $t = 0.1\text{s}$, the motor stalls instantly and is tripped by contactor after 0.1s delay, at which point the terminal current drops steeply to zero. After the terminal voltage recovers to a level above $V_{rec} = 0.7 \text{ pu}$, the motor is reconnected to the system after 0.1s delay, remains stalled and draws high-magnitude current, resulting in the rise of stator winding temperature. When the temperature hits the pre-determined threshold, the stalled motor is tripped by thermal protection.

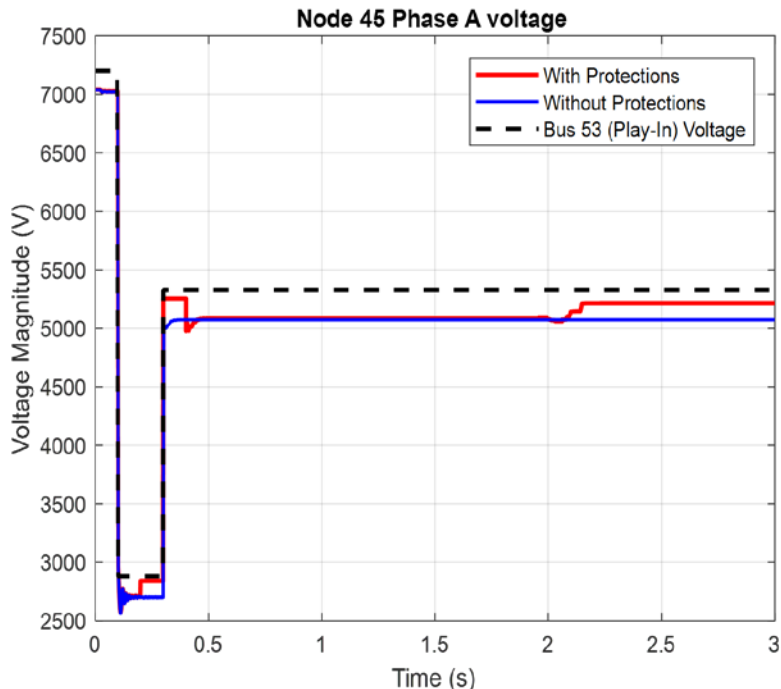


Figure 7.31 Phase-A Voltage at Node 45

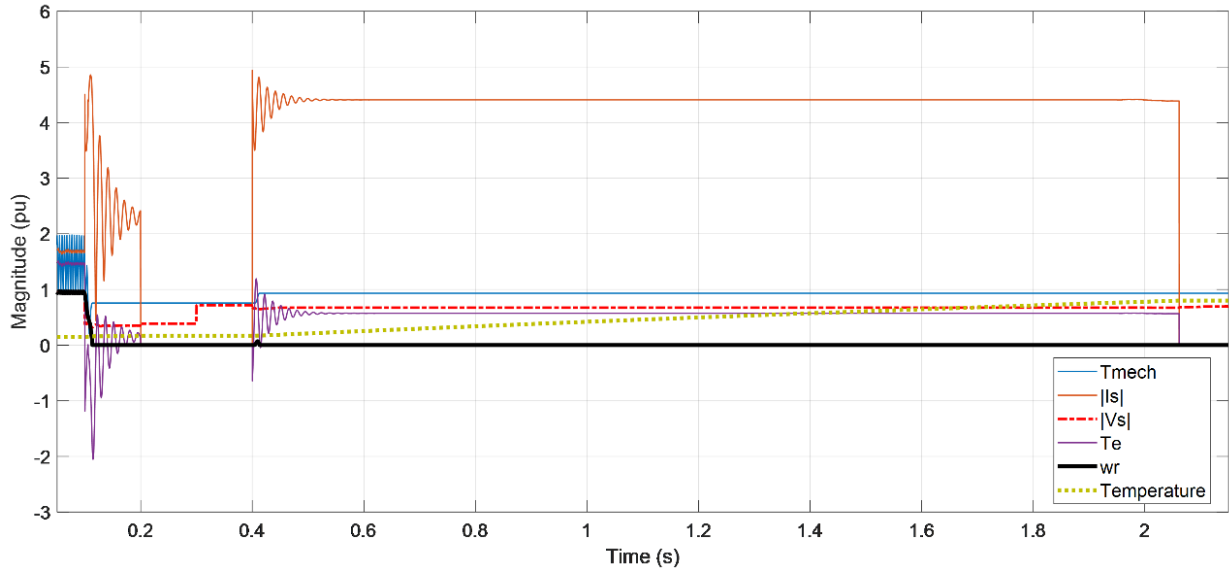


Figure 7.32 A/C Compressor in Multi-Family Home 1: Motor Mechanical Torque (T_{mech}), Terminal Current Magnitude ($|I_s|$), Terminal Voltage Magnitude ($|V_s|$), Electrical Torque (T_e), Rotor Speed (w_r) and Stator Winding Temperature

Figure 7.31 shows the Phase-A voltage at Node 45, which is far away from the feeder head. With all protections enabled, the voltage level after $t = 2.0\text{s}$ is higher compared to the situation of no protections, attributing to the action of thermal protections that trips all stalled motors.

7.4.5 Summary

This part of work presents guidelines and relevant details to realistically model residential end-use motor loads and associated protections. The mechanism of A/C compressor stalling and recovery can be studied in the dynamic-phasor simulation with appropriate implementation of triangular-wave mechanical torque. The contactor and thermal protections, if properly coordinated, can help to reduce the fault-induced delayed voltage recovery (FIDVR) problem by tripping stalled motors. In the future, the dynamic-phasor models of variable frequency drives [87] [88] [89] will be implemented for distribution system simulations. The characteristics of motor behind drive [90] and associated protection behaviors will also be investigated.

8.0 Next Generation Load Model Data Tool

The Load Model Data Tool (LMDT) has been developed by PNNL in cooperation with Bonneville Power Administration (BPA), NERC load modeling task force (LMTF), and WECC modeling and validation working group (MVWG). The LMDT is a standalone Windows application and it helps to generate composite load model parameters taking into account climate zone and seasonal information, operating hour and feeder type. The LMDT reads in the necessary long identifier (LID) information, and supplements that with the base case power flow conditions and supplemental load shape data to generate the dynamics records in GE PSLF and Siemens PTI PSS/E format. The LMDT application has been released under an open-source license and can be downloaded at [91].

The first version of the tool (LMDT 1.0) was released in 2013. The first version of the tool is a relatively simple application (Figure 8.1), it does not have built-in load model database and it requires to generate composite load data using external tools (e.g. WECC composite load spreadsheet). The LMDT 1.0 is still maintained and available for downloading on the LMDT web site. Recently, the PSS/E CMLDBLU2 model support has been added to the first generation LMDT (version 1.1)

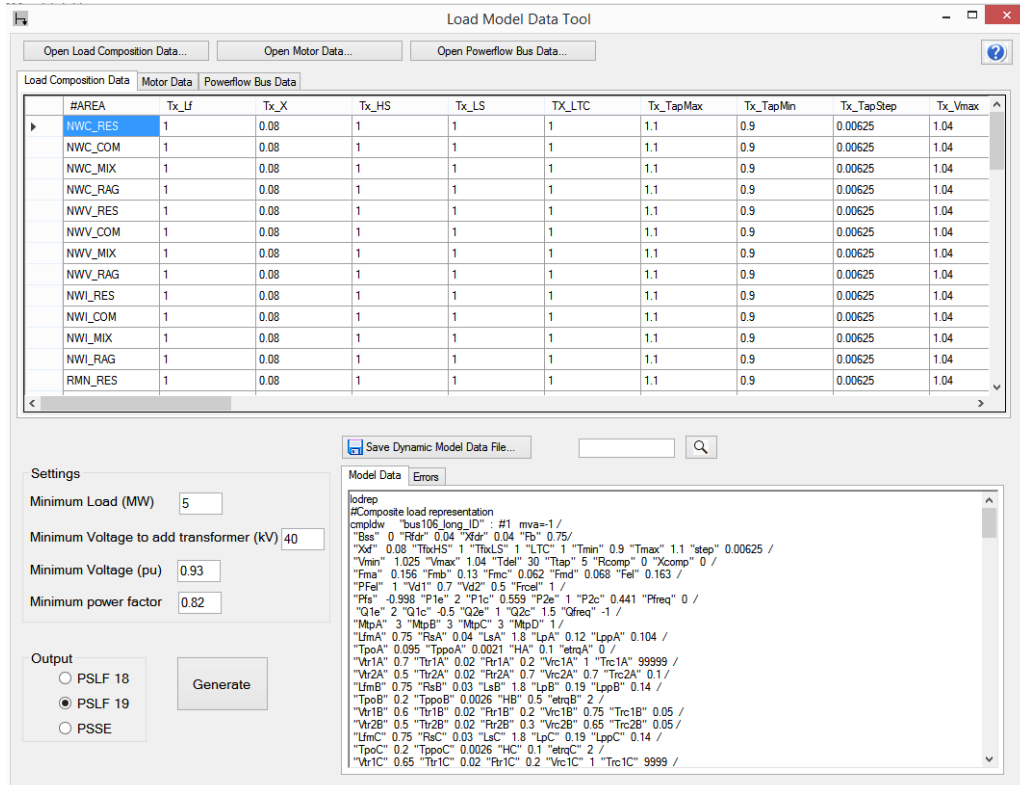


Figure 8.1 LMDT 1.0 Main Graphical User Interface (GUI).

8.1 LMDT 2.0

New version of the tool (LMDT 2.0) was released in 2016. The LMDT 2.0 has a built-in database of load models for different climate zones and also has an advanced analytical and visualization capabilities. The LMDT 2.0 graphical user interface (GUI) consists of the toolbar and four major panels (Figure 8.2):

- 1) **Toolbar** - includes buttons to specify the program settings and to display/hide additional panels (map, hourly plots, etc.).

- 2) **Database panel** – The database includes information for commercial, residential, industrial, agricultural, and data load.
- 3) **Composite load model panel** – to setup the composite load parameters
- 4) **Hourly plots panel** – to display dependence of the composite load model parameters on the operating hour
- 5) **Map panel** – to show the climate zone location and composite load model parameters distribution using a heat map.

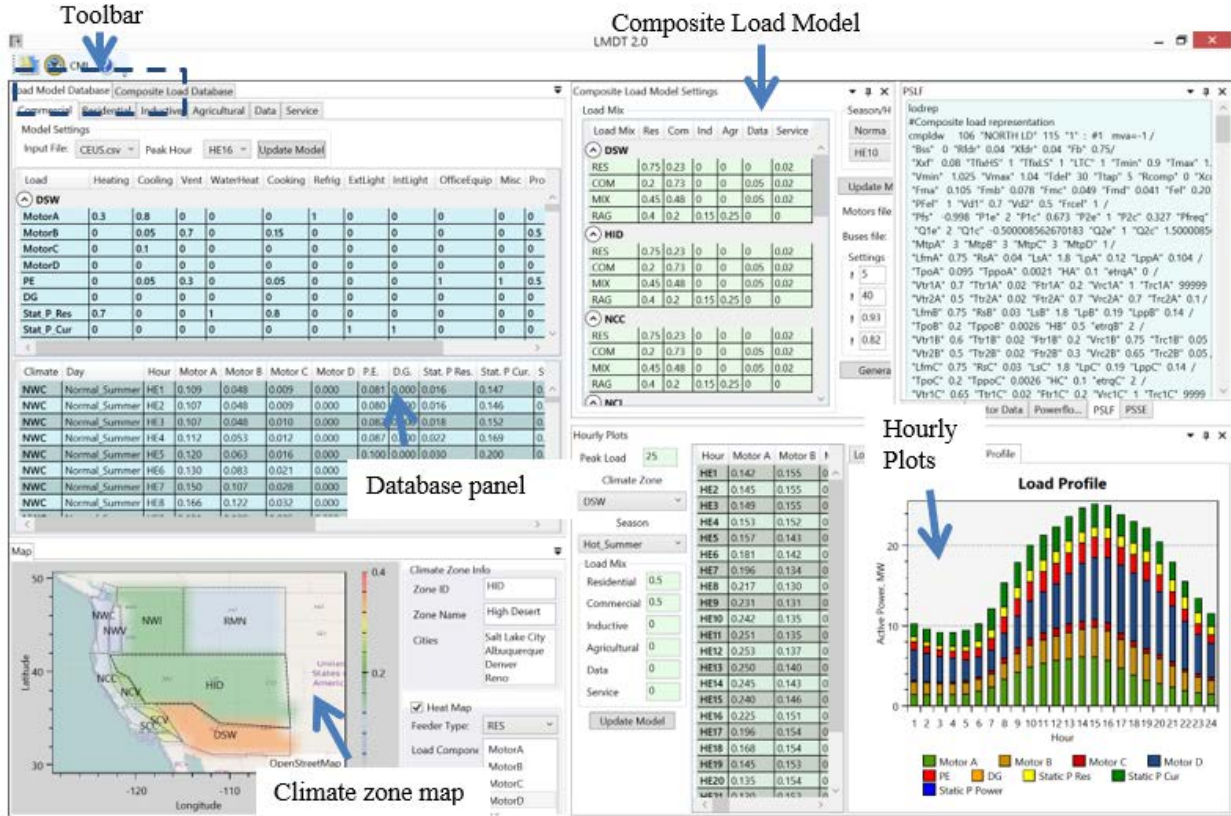


Figure 8.2 LMDT 2.0 Main Graphical User Interface (GUI).

8.1.1 Load Model Database

The LMDT tool has a built-in database of the load shapes (end use data) for different load types, including: (1) Commercial, (2) Residential, (3) Industrial, (4) Agricultural, (4) Data, and (5) Service. This information is collected for different seasons and climate zones. Example of commercial and residential end use data is shown in Figure 8.3.

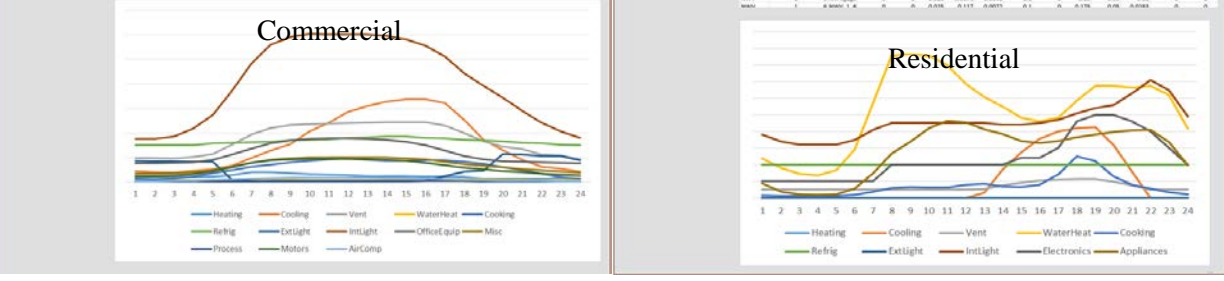


Figure 8.3 Example of Commercial and Residential End Use Data.

8.1.2 Rules of Association

Rules of association are used by LMGT to link end use data with composite model fractions (e.g., Motor A or Motor B). Rules of association are defined for each climate zone and stored in LMGT settings (Figure 8.4)



Figure 8.4 Rules of Association Screen.

8.1.3 Feeder Configuration

Four types of feeders are supported by LMDT (RES – residential feeder, COM – commercial feeder, MIX – mixed use feeder, RAG – rural feeder). Feeder parameters can be defined for each climate zone and stored in the program settings (Figure 8.5). LMDT also supports custom industrial feeders (e.g., petro-chemical, paper mill, steel mill, semiconductor).



Figure 8.5 Feeder Configuration Setup.

8.1.4 Motor Parameters Screen

Motor parameters can be selected in “Motor data” screen (Figure 8.6). Parameters are stored in csv files and can be chosen using the file selector. The set of parameters includes: different three phase motors (motors A, B and C), single phase motor (Motor D), and power electronic load.

Figure 8.6 Motor Parameters.

8.1.5 Bus Data

Bus information is needed to generate composite load records for individual buses. CSV files are used as a bus data input and should include climate zone ID information to map bus with corresponding climate zone (Figure 8.7). To add distributed generation (DG) to composite load record, bus data file should also include DG information.

File Selector

Buses file: loads_with_DG.csv

Settings

- Minimum Load(MW)
- Minimum voltage to add transformer (kV)
- Minimum voltage (p.u.)
- Minimum power factor

PSLF

- CMPLDW(G)
- CMPLDW
- CMPLDW2

PSSE

- CMLD**U1
- CMLD**U2

Generate

Climate Zone ID (optional)

BusNumber	BusName	BasekV	LoadID	Area	Zone	Owner	P	Q	Voltage	Climate Zone	LID	Pgen	DGID
106	NORTH LD	115	1	1	1	0	1000	0	1.023064	NWC_MIX	bus106_long_ID	1.56	DG1
202	MIDWAY	115	1	1	1	0	300	150	1.018719	NWC_RES	bus202_long_ID	15	DG1
306	SOUTH LD	115	1	1	1	0	2700	0	1.030095	HID_MIX	bus306_long_ID	12	-100
102	NORTH G1	18	1	1	1	0	100	50	1	PPA_AUX	bz102_long_ID	25	DG2
104	NORTH G2	18	1	1	1	0	100	50	1	PPA_AUX	bz104_long_ID	1.56	DG1
302	SOUTH G1	18	1	1	1	0	100	50	1	PPA_AUX	bz302_long_ID	1.56	-101
304	SOUTH G2	18	1	1	1	0	100	50	1	HID_RES	bz304_long_ID	31	DG1
307	SOUTH G2B	18	1	1	1	0	100	50	1	HID_COM	bz307_long_ID	13	-100
1111	Texas1111	18	1	1	1	0	100	50	1	TXG_COM	bz1111_long_ID	20	DG1

Composite Load Model **Motor Data** **DG Data** **Area Data** **Powerflow Bus Data** **PSLF** **ISSE** **Error Log**

Thresholds

DG information (optional)

Figure 8.7 Bus Data.

8.1.6 Area/Zone/Owner Data

Area (zone or owner) information is needed to generate composite load records for a group (area/zone/owner). CSV files are used as an area data input and should include climate zone ID information to map area/zone/owner with corresponding climate zone (Figure 8.8).

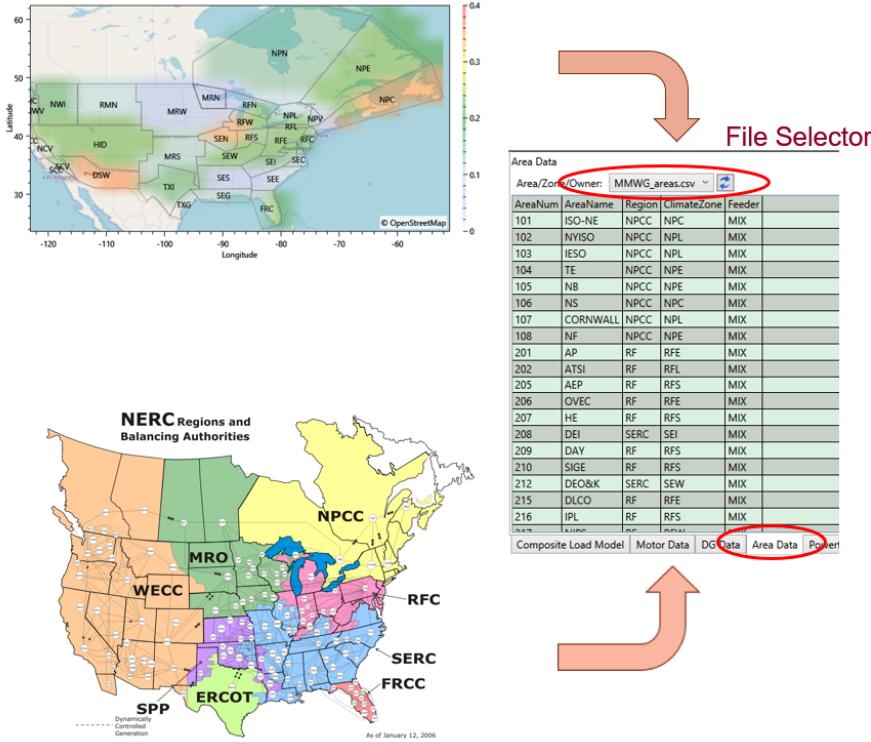


Figure 8.8 Area Data.

8.2 Load Model Creation Process Using Second-Generation LMDT

To create composite load dynamics records, several steps need to be done. The users can elect to generate composite load records by bus level or by group.

The first 4 steps are described below and shown in Figure 8.9.

- Step 1: Select season
- Step 2: Select operating hour
- Step 3 (*optional*): Specify percentage of different types of loads connected to the feeders:
 - RES – residential feeder
 - COM – commercial feeder
 - MIX – mixed use feeder
 - RAG – rural feeder
- Step 4: Click “Update Model” button

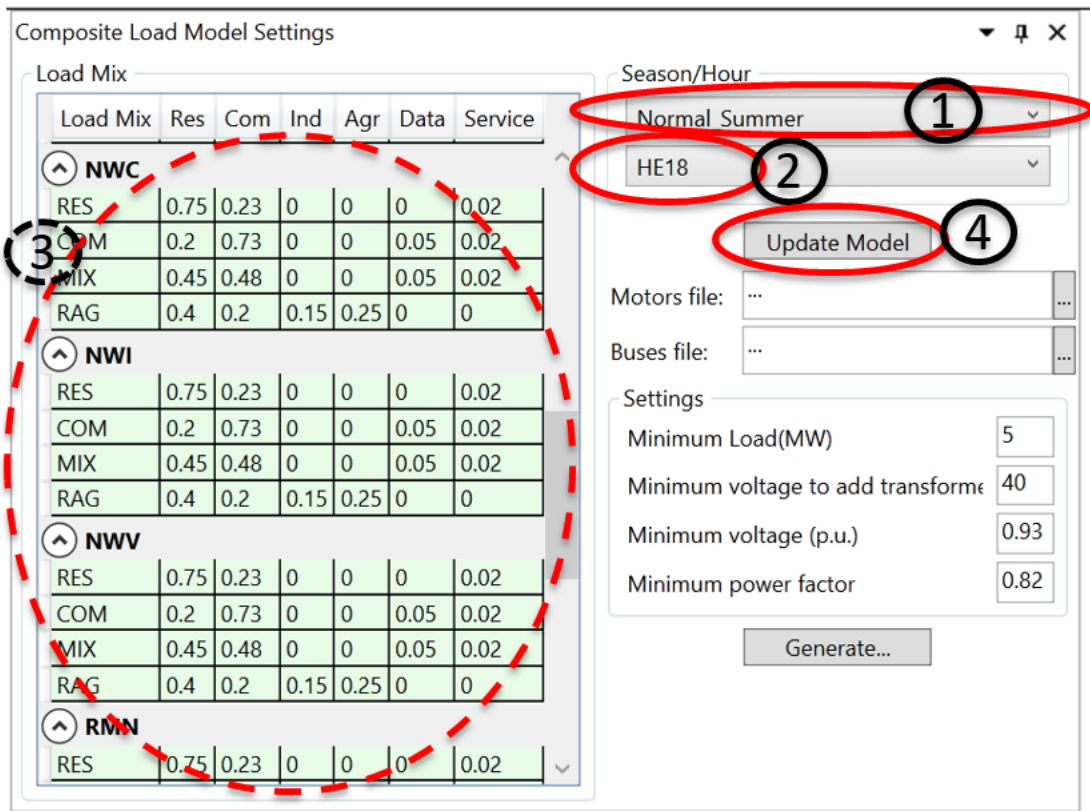


Figure 8.9 Composite Load Model Records Creation (Steps 1-4)

8.2.1 Generate Load Records by Bus Level

If the users choose to generate load records by bus level, the following Steps 5-9 need to be executed and are illustrated by Figure 8.10 and Figure 8.11.

- Step 5: Select bus data
- Step 6: Select PSLF/PSSE load model
- Step 7: Select by “Bus” option
- Step 8: Click “Generate” button
- Step 9: Copy and add composite load model dynamic records to the dynamic records file

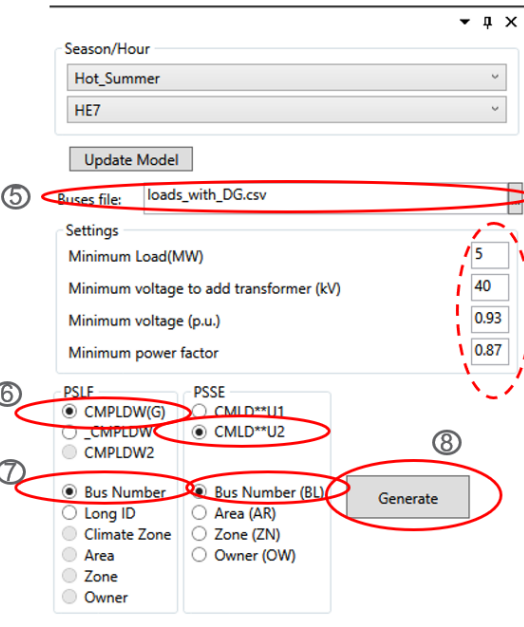


Figure 8.10 Composite Load Model Records Creation by Bus (Steps 5-8)

PSSE

DYRE Data Record:

```
I, 'USRLOD', LID, 'CMILDBU2', 12, IT, 2, 133, 27, 146, 48, 0, 0,
CON(1) to CON(2+132) /
```

LID is an explicit load identifier or may be * for application to loads of any ID associated with the subsystem type.

Model	IT ¹	Description	IT ²	Description
BL	1	Bus number		
OW	*	Owner number		
ZN	3	Zone number		
AR	4	Area number		
AL	5	0		

PSLF

Model Name: cmpldwg

Description: WECC Composite load model with distributed generation (DG)

Prerequisites: Load in load flow solved case

Inputs: Voltage at bus to which the composite load is connected

Invocation: cmpldwg [<n>] [<name> <bv>] <id> : #1 mva=mvarbase>

PSSE and **PSLF** panes showing the command line inputs for generating composite load model records.

Figure 8.11. Composite Load Model Records Creation by Bus (Step 9)

8.2.2 Generate Load Records by Group

If the users choose to generate load records by group, the following Steps 5-9 need to be executed and are illustrated by Figure 8.12 and Figure 8.13.

- Step 5: Select area data
- Step 6: Select PSLF/PSSE load model
- Step 7: Select “Area”, “Zone”, or “Owner” option
- Step 8: Click “Generate” button
- Step 9: Copy and add composite load model dynamic records to the dynamic records file

The screenshot shows a software interface for generating composite load model records. The interface is divided into several sections:

- Area Data:** A table titled "Area Data" with columns: AreaNum, AreaName, Region, ClimateZone, and Feeder. A red circle labeled ⑤ highlights the dropdown menu "MMWG_areas.csv" and the refresh icon.
- Settings:** A section containing input fields for "Minimum voltage (kV)" (5), "Minimum voltage (p.u.)" (0.93), and "Minimum power factor" (0.87). A red dashed box labeled "PSLF only" encloses these settings.
- Load Model Selection:** Two groups of radio buttons for selecting the load model type.
 - PSLF:** Options include CMPLDW(G) (unchecked), CMPLDW (checked), CMPLDW2 (unchecked).
 - PSSE:** Options include CMLD**U1 (unchecked), CMLD**U2 (checked), CMLD**U3 (unchecked).
 A red circle labeled ⑥ highlights the selected CMPLDW option in the PSLF group.
- Group Selection:** A section with radio buttons for selecting the grouping criteria.
 - PSLF:** Options include Bus Number (unchecked), Long ID (unchecked), Climate Zone (unchecked), Area (checked).
 - PSSE:** Options include Bus Number (BL) (unchecked), Area (AR) (checked), Zone (ZN) (unchecked), Owner (OW) (unchecked).
 A red circle labeled ⑦ highlights the selected Area option in the PSLF group.
- Generate:** A large grey button labeled "Generate" with a red circle labeled ⑧ highlighting it.

Figure 8.12 Composite Load Model Records Creation by Group (Steps 5-8)

PSSE

DYRE Data Record:

```
I, 'USRLOD', LID, 'CMLDxxU2', 12, IT, 2, 133, 27, 146, 48, 0, 0,
CON(J) to CON(J+132) /
```

LID is an explicit load identifier or may be * for application to loads of any ID associated with the subsystem type.

Model suffix "xx"	"IT" Description	"I" Description
BL	1	Bus number
SW	2	Owner number
ZN	3	Zone number
AR	4	Area number
AL	5	

PSLF

Model Name: _cmpldw

Description: WECC Composite load model for a group (load zone, area, zone, owner).

Prerequisites:

Inputs: Voltage at bus to which the composite load is connected

Invocation: `cmpldw num "group name" <group type> : # mva=-load Factor`

Parameters:

LPCL Variable	Default Data	Description
Pmin	0.0	Minimum load P, MW
PQmin	0.0	Minimum load P / Q ratio
Vmin	0.0	Minimum bus voltage, p.u.

Settings:

- Minimum Load(MW) 5
- Minimum voltage to add transformer (kV) 40
- Minimum voltage (p.u.) 0.93
- Minimum power factor 0.87

Figure 8.13 Composite Load Model Records Creation by Group (Step 9)

8.3 LMDT Version History

8.3.1 LMDT 2.1

In 2017 new features were implemented in the LMDT tool and updated version of the tool has been released (LMDT 2.1). New features include:

- Configurable presets for each climate zone (based on XML file). Users can modify and store load composition and feeder configuration in the program setting file for future use.
- Improved errors diagnostics and errors log.
- Search within output files.

Configuration file structure is shown in Figure 8.14. It allows to store multiple presets with different configurations. Each preset includes an individual configuration for each climate zone and consist of feeder parameters and information for commercial and residential loads.

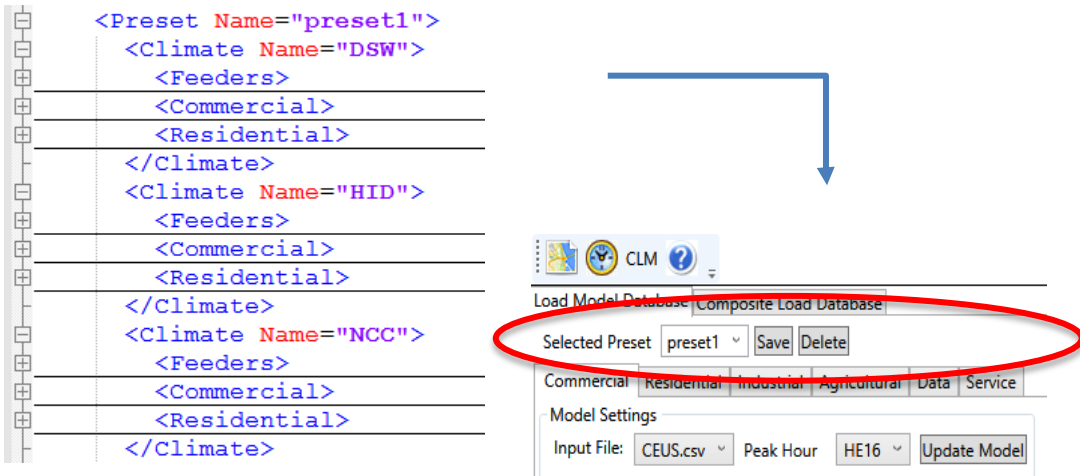


Figure 8.14 Configuration xml File Structure.

Feeder configuration xml schema is shown in Figure 8.15. LMDT tool supports four types of feeders (residential, commercial, mix use and rural). Each feeder composition of different types of loads can be specified and saved in the program settings file.

Load Mix							
	Load Mix	Res	Com	Ind	Agr	Data	Service
DSW	RES	0.75	0.23	0	0	0	0.02
	COM	0.2	0.73	0	0	0.05	0.02
	MIX	0.45	0.48	0	0	0.05	0.02
	RAG	0.4	0.2	0.15	0.25	0	0
HID	RES	0.75	0.23	0	0	0	0.02
	COM	0.2	0.73	0	0	0.05	0.02
	MIX	0.45	0.48	0	0	0.05	0.02
	RAG	0.4	0.2	0.15	0.25	0	0
NCC	RES	0.75	0.23	0	0	0	0.02
	COM	0.2	0.73	0	0	0.05	0.02
	MIX	0.45	0.48	0	0	0.05	0.02
	RAG	0.4	0.2	0.15	0.25	0	0
NCI	RES	0.75	0.23	0	0	0	0.02
	COM	0.2	0.73	0	0	0.05	0.02
	MIX	0.45	0.48	0	0	0.05	0.02
	RAG	0.4	0.2	0.15	0.25	0	0

Figure 8.15 Feeders xml Schema.

Commercial and residential loads configuration file structures are shown in Figure 8.16 and Figure 8.17. Users can specify and store parameters of the loads in different presets and use them in the future studies.

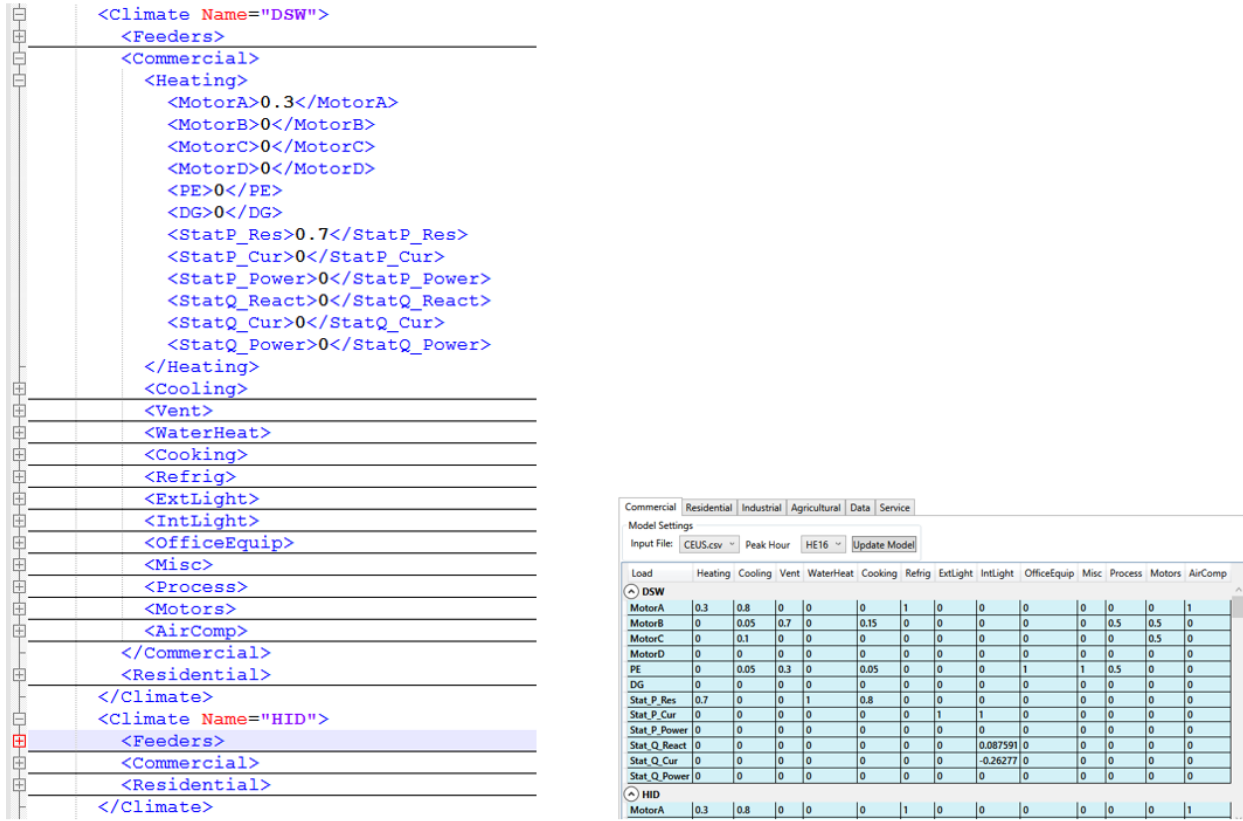


Figure 8.16 Commercial Load xml Schema.

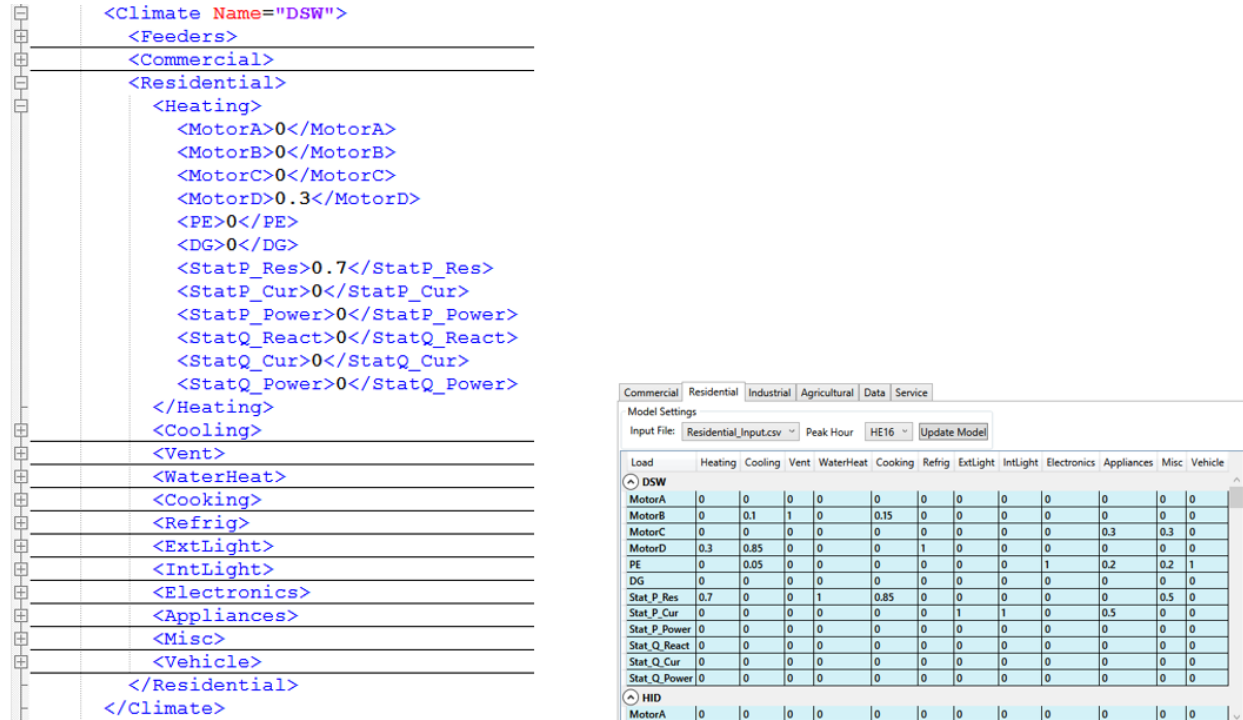


Figure 8.17 Residential Load xml Schema.

8.3.2 LMDT 2.2

New version of the LMDT tool was released in 2019. The tool's load shapes database was extended to the Eastern interconnection and ERCOT. Support of distributed generation (DG) was added for PSLF data records. Also torque-slip motors characteristics calculation (Figure 8.18) and new visualization (pie chart for load composition, see Figure 8.19) was added.

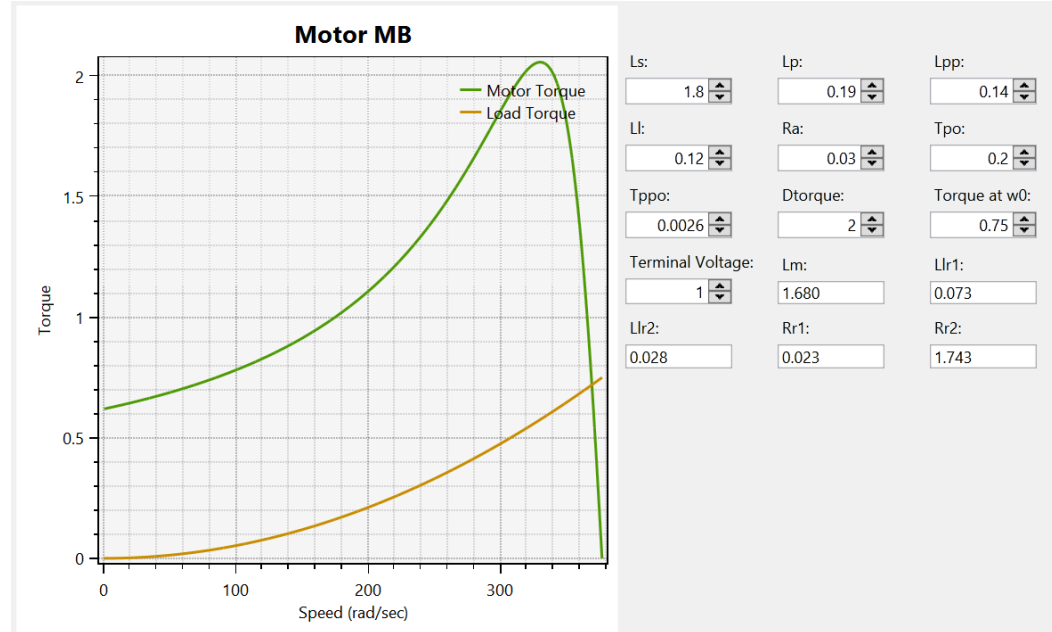


Figure 8.18 Motor Torque-Slip Characteristic Screen.

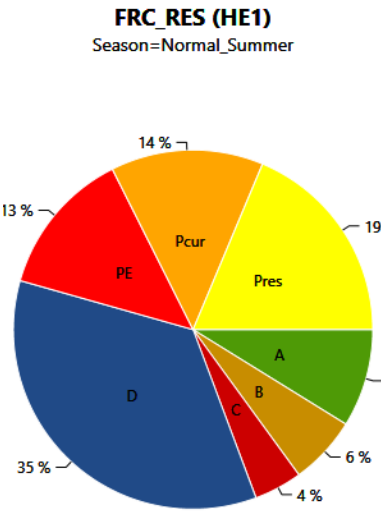


Figure 8.19 Load Composition Pie Chart.

Climate zone definition map is shown in Figure 8.20 [50]. User can select presets and use datasets for “whole” county or use datasets configured for WECC or Eastern interconnection (Figure 8.21).

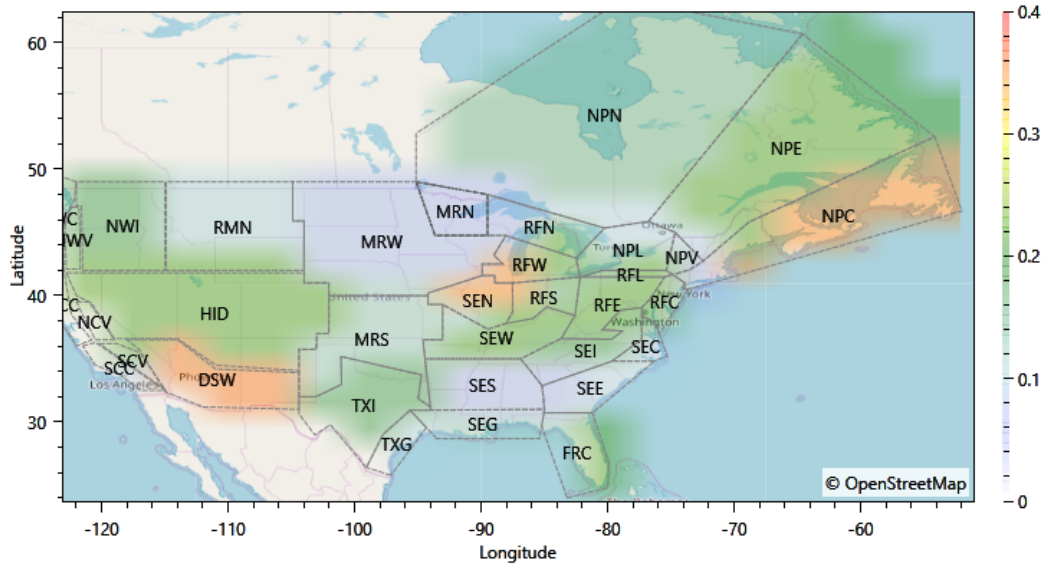


Figure 8.20 Climate Zone Definition Map.

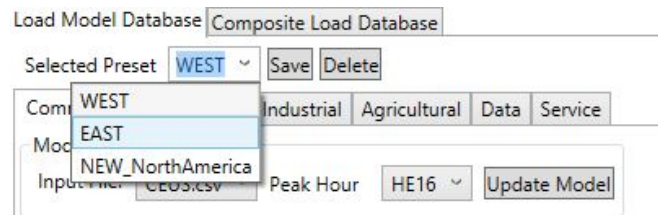


Figure 8.21 Presets for West, East and North America.

Distributed generation (DG) screen of LMDT 2.2 is shown in Figure 8.22. Two types of DG models are supported: PVD1 and DER_A. The tool uses csv format to store DG information and supports multiple presets for DG settings. Bus and group composite load model records are linked with DG parameters through DG ID identifier.

DG Data

DG data: DG_data.csv

#	Type	ID	DGtype	pflgdg	Pdg	Pfdg	Imax	Vt0	Vt1	Vt2	Vt3	Vrec	ft0	ft1	ft2	ft3	frec							
PVD1	DG1	1	2	0	1	1.1	0.45	0.75	1.1	1.2	0.5	57	59.4	60.6	61.7	0								
PVD1	DG2	1	2	0	1	1.2	0.46	0.76	1.1	1.21	0.5	57	59.5	60.8	61.7	0								
#	Type	ID	DGtype	trv	dbd1	dbd2	kqv	vref0	tp	pfflag	tiq	ddn	dup	fdbd1	fdbd2	femax	femin	pmax	pmin	frqflg	dPmax	dPmin	tpord	ima
DER_A	-100	2		0.00416	-0.1	0.1	1	1.02	0.025	1	0.02	0	0	0	0	999	-999	1.1	0	0	9	-9	0.1	1.2
DER_A	-101	2		0.005	-0.11	0.1	1	1.02	0.025	1	0.02	0	0	0	0	999	-999	1.1	0	0	9	-9	0.1	1.2

Composite Load Model Motor Data DG Data Powerflow Bus Data PSLF PSSE Error Log

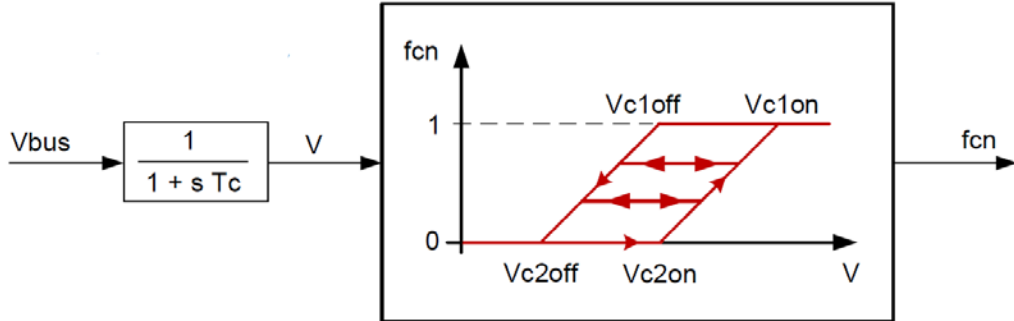
Figure 8.22 DG Screen.

9.0 Investigation on Motor Progressive Tripping

9.1 Motor Progressive Tripping

Within the traditional WECC composite load model (e.g. CMPLDW model in PSLF), the three-phase induction motor models (MOTORW model in PSLF) are protected by a 2-level voltage-dependent protection scheme which trips or reconnects specific fractions of the aggregate motor loads when the terminal voltage drops below or rises above pre-determined thresholds. However, this protection scheme neglects the fact that the realistic distribution feeder, which is simplified by a composite load model in PSLF, is in a radial or meshed configuration. The motor loads distributed along the feeder do not trip simultaneously given a voltage depression at the feeder head. Typically, motors approaching to the feeder head are more vulnerable to tripping than that connected downstream the feeder. To replicate this phenomenon, PSLF released a new three-phase induction motor model “MOTORLD” with progressive tripping implemented. However, the MOTORLD model is a standalone model that has not been merged into WECC composite load model. In this study, the progressive tripping mechanism will be explained and validated in an individual unit test case. This chapter also proposes a WECC composite load model formulated by individual components, in which all three-phase induction motors are represented by MOTORLD model rather than the traditional MOTORW model. A system-level test is performed to evaluate system voltage responses under different aggregate protection models.

There are two protection schemes implemented in MOTORLD, including contactor model and controller model. The model for the contactor is shown in Figure 9.1. It is intended to represent the tripping (and reconnection) of a fraction of an aggregation of motors over a range of voltage levels. If using the model to represent a single motor, V_{c2off} should be set equal to V_{c1off} , and V_{c2on} should be set equal to V_{c1on} [5]. The output of the contactor model indicates the fraction of motor connected to the grid.



V_{c1off}	0.0	Contactor voltage at which motors start tripping, p.u.
V_{c2off}	0.0	Contactor voltage at which all motors are tripped, p.u.
V_{c1on}	0.0	Contactor voltage at which all motors are reconnected, p.u.
V_{c2on}	0.0	Contactor voltage at which motors start reconnecting, p.u.
T_c	0.0	Voltage sensing time constant for contactor, sec.
fr_with_c	0.0	Fraction of motors with contactors

Figure 9.1 Contactor Protection [92]

The model for the “control trip” is shown in Figure 9.2. It is intended to represent the tripping of motors by a “controller” such as an energy management system, with a range of time delays that are a

function of voltage. If using the model to represent a single motor, one should set $V2 = V1$, $T2a = T1a$, and $T2b = T1b$. When the voltage dips below $V0$, a timer (dT) is started. For single motor trip curve, when timer exceeds $T1$, the motor is tripped. For the dual (fastest and slowest) trip curves, at each time step, the points on the two characteristics corresponding to the present value of V are calculated, call them $T1$ and $T2$. When dT becomes $> T1$, a fraction of the load is tripped equal to $(dT - T1) / (T2 - T1)$, that is, the relative fraction of the distance between the two characteristics. As V changes, the values of $T1$ and $T2$ will change, which may result in the trip fraction shifting to higher or lower values. However, once a given fraction has been tripped, it is not allowed to be “untrip”. When V recovers above $V0$, the timer is reset and the fraction tripped is stored. If a subsequent voltage dip below $V0$ occurs, the calculations are repeated to determine what additional amount may be tripped, i.e. tripping amounts on successive voltage dips are cumulative. Reconnection of tripped load is assumed to require operator action or a time delay beyond the range of the simulation, so no reconnection is modeled [5].

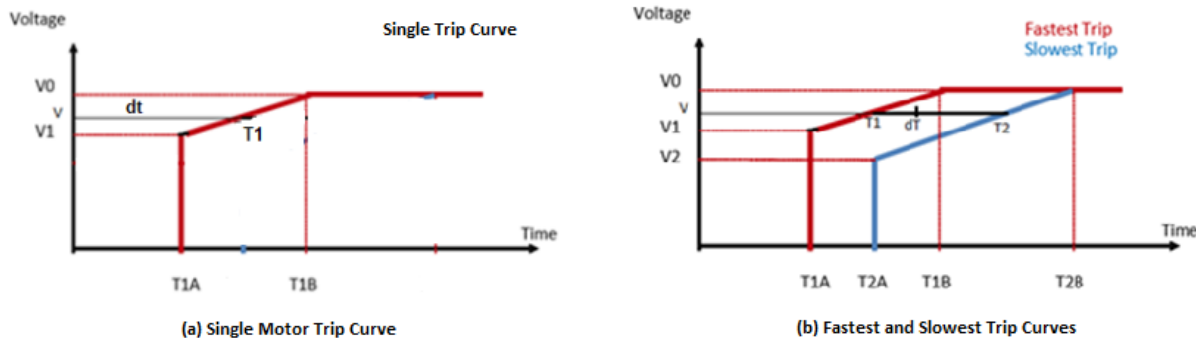


Figure 9.2 Controller Protection

It is noted that the fractions of motors with contactors and with controller are not additive but overlapping. Therefore, tripping of fractions of the motor by contactor, controller, and load shedding relays is multiplicative, that is, the total fraction not tripped is the product of the fraction not tripped by each of these devices. Tripping by these devices also trips a corresponding fraction of the compensating capacitor, if present [5].

9.2 Individual Unit Test

In this sub-chapter, single MOTORLD model is tested in a two-bus system. The scenarios exclusively consider a) contactor protection (no other protections) and b) controller protection (no contactor). In Scenario b), a single voltage dip and two consecutive voltage dips are created to examine the performances of single trip curve (representing single motor) and dual (fastest and slowest) trip curves (representing a number of motors) in controller protection model. The two-bus system schematic is given in Figure 9.3.

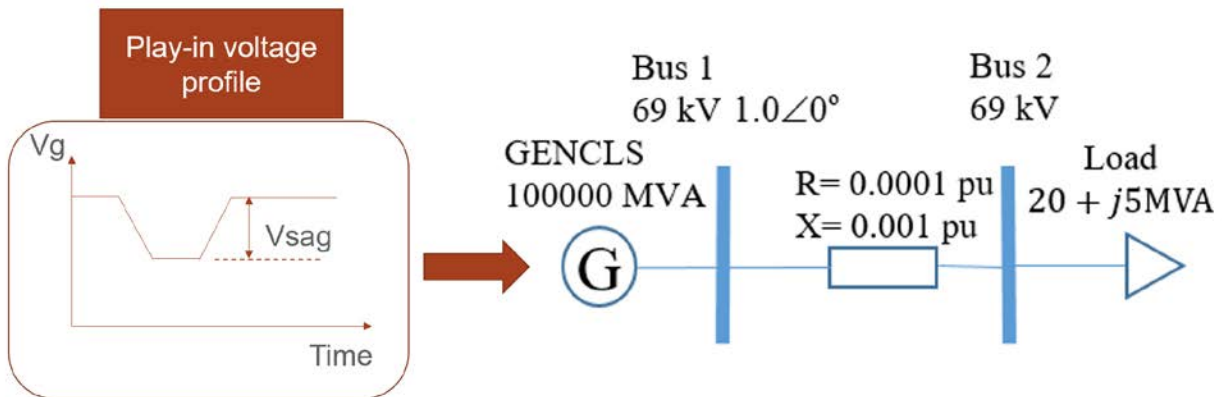


Figure 9.3 Two-Bus System for Testing Individual MOTORLD Model

The motor parameters of MOTORLD model is given in Figure 9.4.

pul	0.500000
ls	3.500000
lp	0.190000
lpp	0.165000
ll	0.120000
ra	0.020000
tpo	1.830000
tppo	0.020000
h	0.900000
dt	2.000000
sel	0.010000
se2	0.100000
acc	0.500000
ndelt	10.000000
wdelt	0.800000

Figure 9.4 Motor Parameters

Firstly, the contactor protection is tested. The protection parameters are summarized in Table 9.1. The simulation considers three scenarios: a). $V_{sag} > V_{c1off}$, b). $V_{c1off} > V_{sag} > V_{c2off}$, and c). $V_{sag} < V_{c2off}$. The results are presented in Figure 9.5.

Table 9.1 Protection Parameters for Contactor Test

Parameters	V_{c1off}	V_{c2off}	V_{c1on}	V_{c2on}	T_c
	0.6 pu	0.5 pu	0.7 pu	0.65 pu	0.02 s

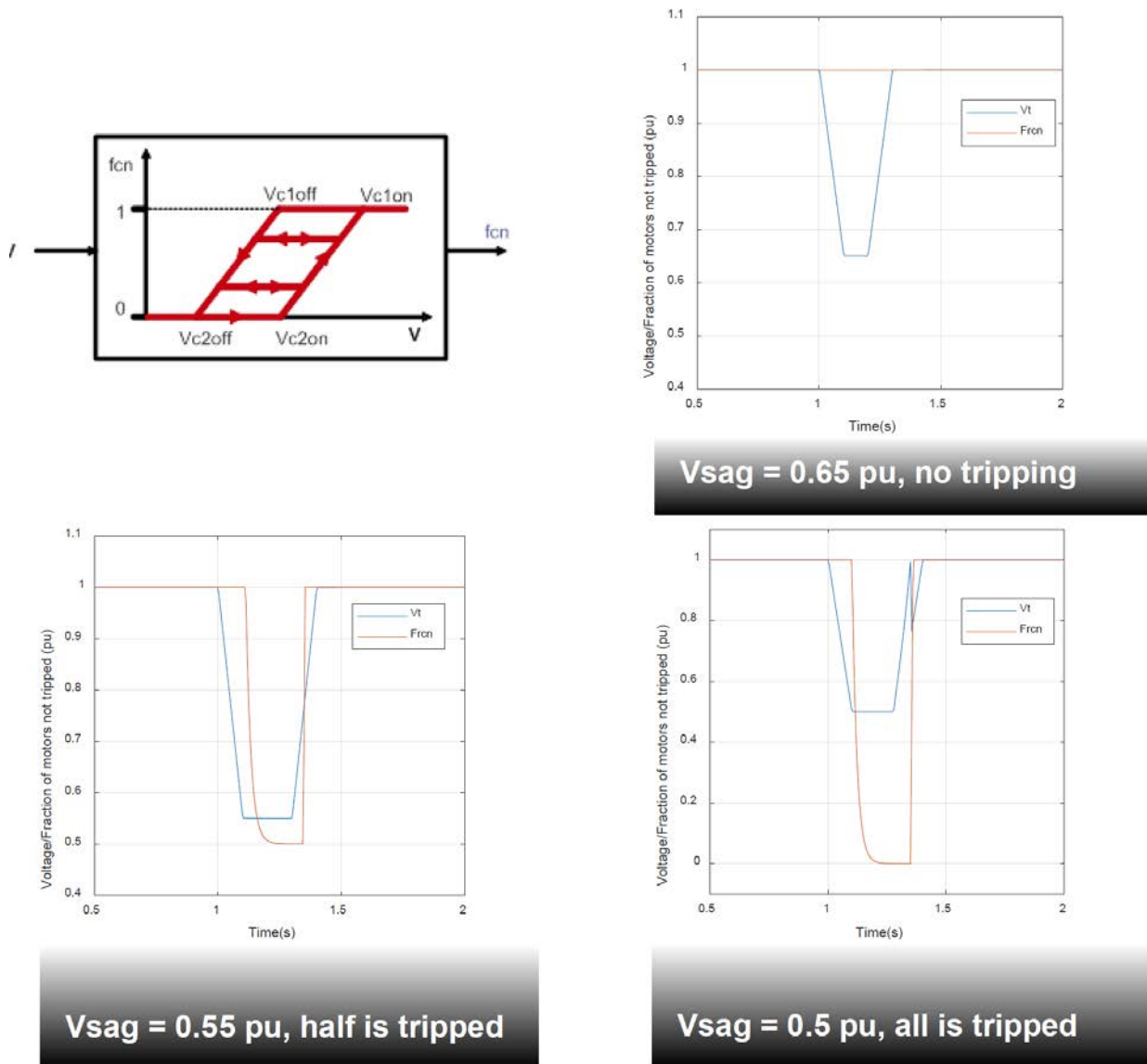


Figure 9.5 Contactor Test Results

The controller protection is tested considering the single motor trip curve depicted in Figure 9.2. The protection parameters are summarized in Table 9.2. This simulation involves three voltage dip scenarios: a). $V_{sag} > V_0$ (0.7 pu), b). $V_0 > V_{sag} > V_1$ (0.6 pu), and c). $V_{sag} < V_1$ (0.6 pu). The results are presented in Figure 9.6.

Table 9.2 Controller Protection Parameters for Single Motor Trip Curve

Parameters	V_1	V_2	$T1A$	$T2A$	$T1B$	$T2B$
	0.6 pu	0.6 pu	0.067 s	0.067 s	0.1 s	0.1 s

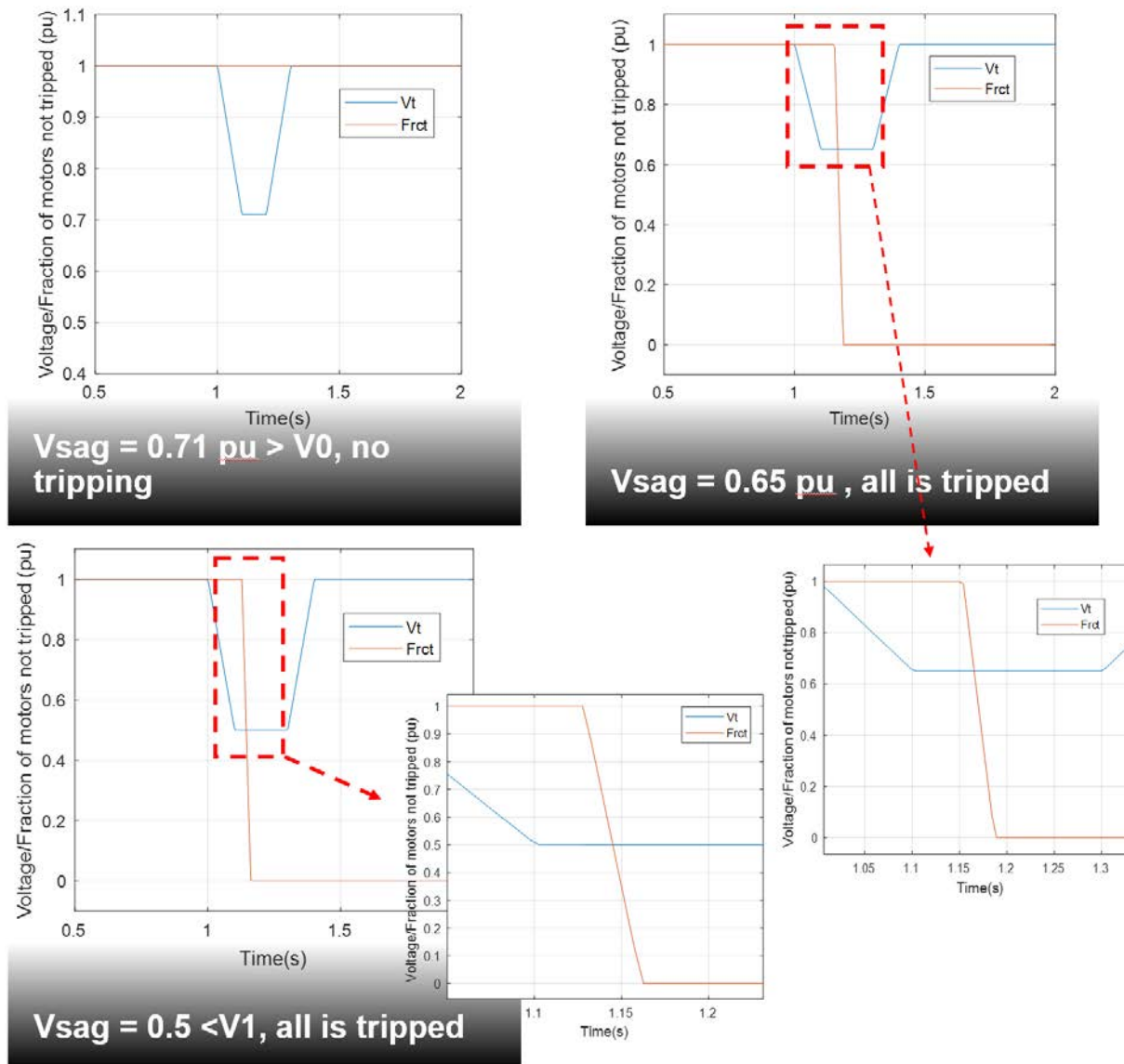


Figure 9.6 Test Results of Controller Protection with Single Motor Trip Curve

In the second test case of controller protection, the dual (fastest and slowest) trip curves are implemented. The protection parameters are summarized in Table 9.3. Four voltage dip conditions are considered, including a). $V_{sag} > V_0$ (0.7 pu), b). $V_0 > V_{sag} > V_1$ (0.6 pu), c). $V_{sag} < V_1$, and d). $V_{sag} < V_2$ (0.5 pu). The simulation results are shown in Figure 9.7.

Table 9.3 Controller Protection Parameters for Dual (Fastest and Slowest) Motor Trip Curves

Parameters	V_1	V_2	$T1A$	$T2A$	$T1B$	$T2B$
	0.6 pu	0.5 pu	0.06 s	0.08 s	0.1 s	0.15 s

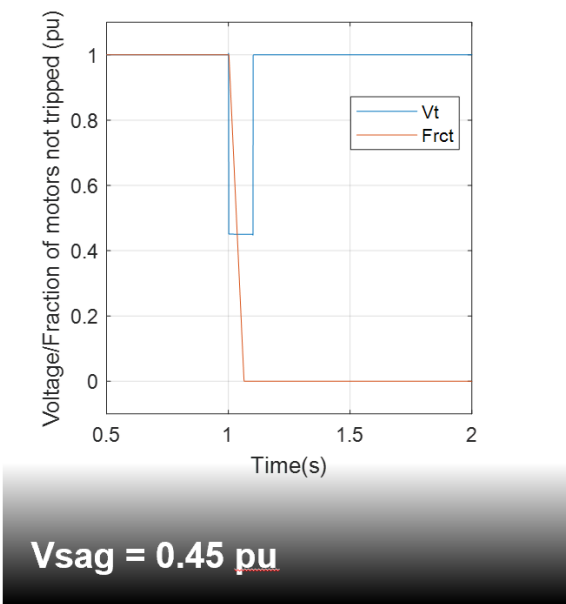
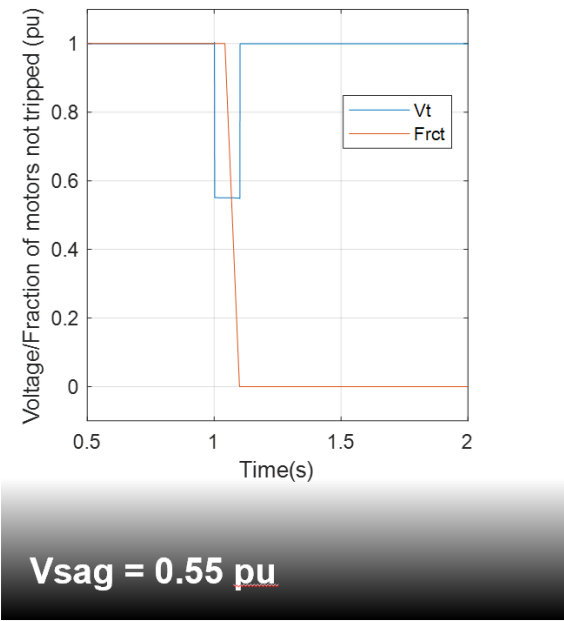
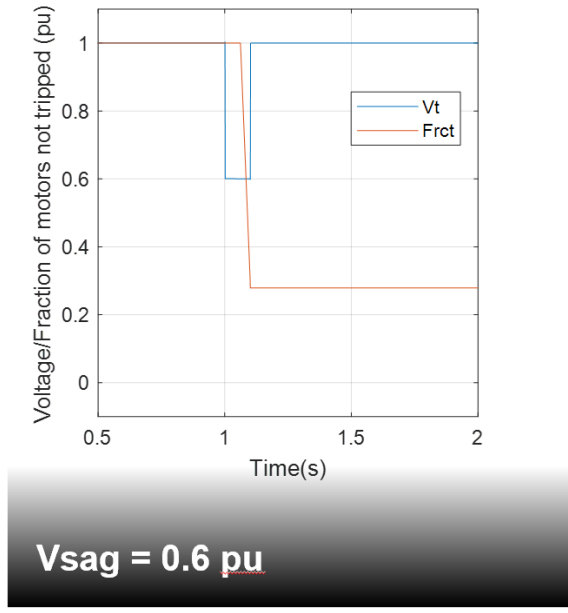
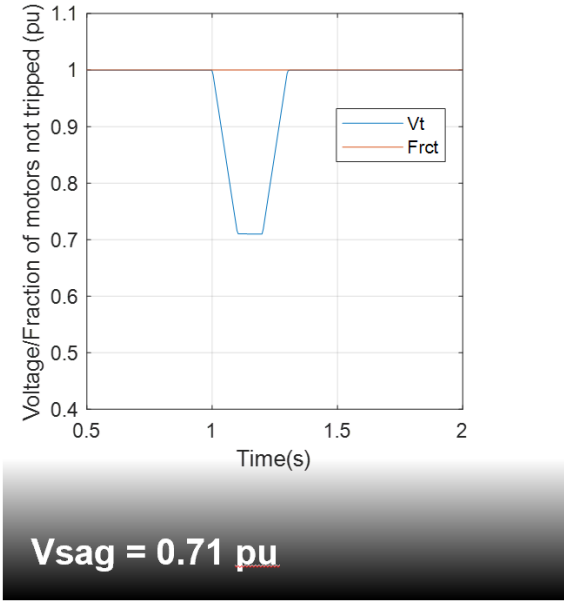


Figure 9.7 Test Results of Controller Protection with Dual (Fastest and Slowest) Trip Curves

Lastly, two successive voltage dips are applied to test the performances of dual-curve controller protection (see Table 9.3 for parameter setting). The simulation result is shown in Figure 9.8.

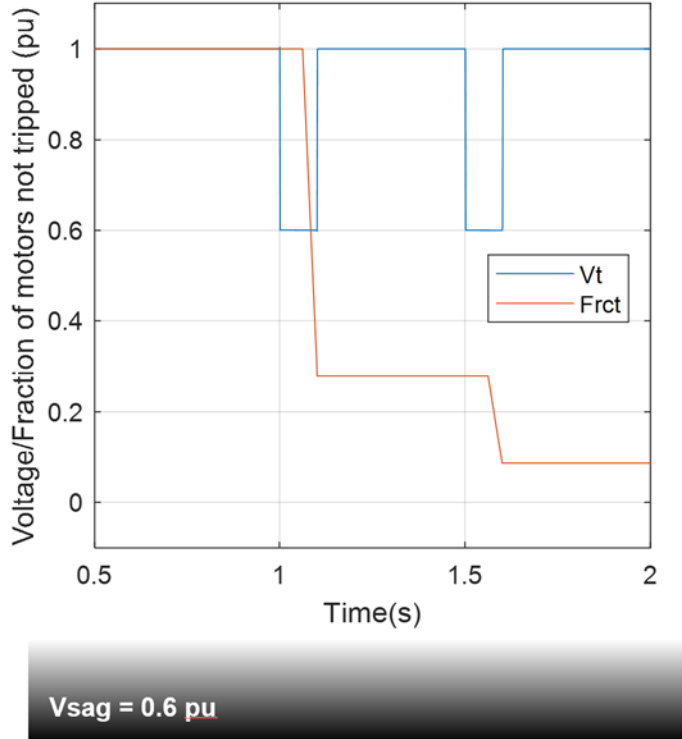


Figure 9.8 Test Results of Controller Protection with Dual Trip Curves under Two Successive Voltage Dips

The test results of single MOTORLD model showed that the contactor and controller protection responded to voltage sags of various magnitudes as expected (i.e., in agreement with the model specification and documentation).

9.3 System-Level Test

In this sub-chapter, a minni-WECC 120-bus transmission system [93] is utilized to represent the detailed WECC system in a smaller scale. The one-line diagram of mini-WECC system is shown in Figure 9.9. All the static load models in the minni-WECC system are replaced by WECC composite load models in two forms, including PSLF internal CMPLDW model and composite load model built with individual components as shown in Figure 9.10. The system-level responses of the two forms of models are compared in this study.

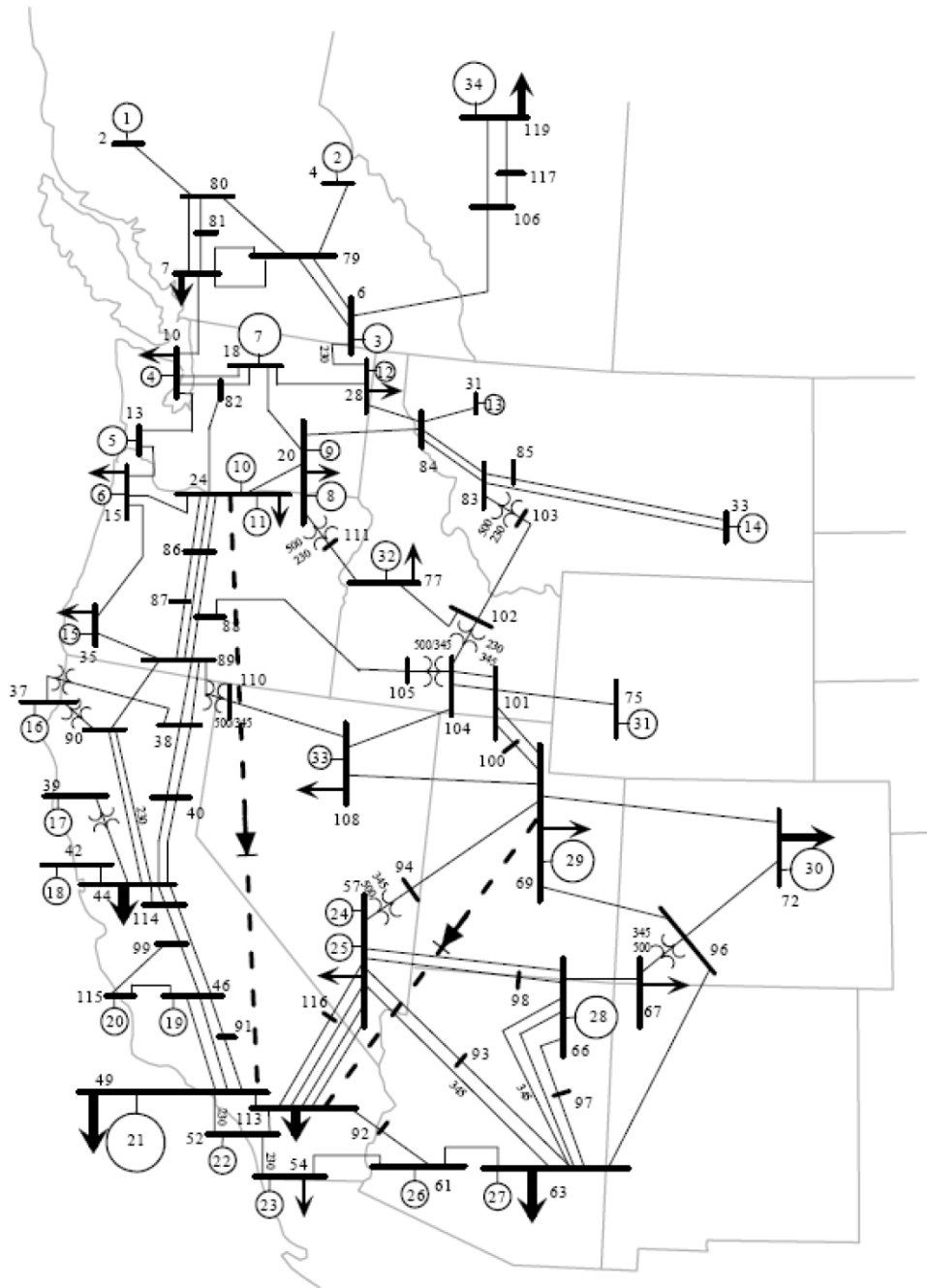
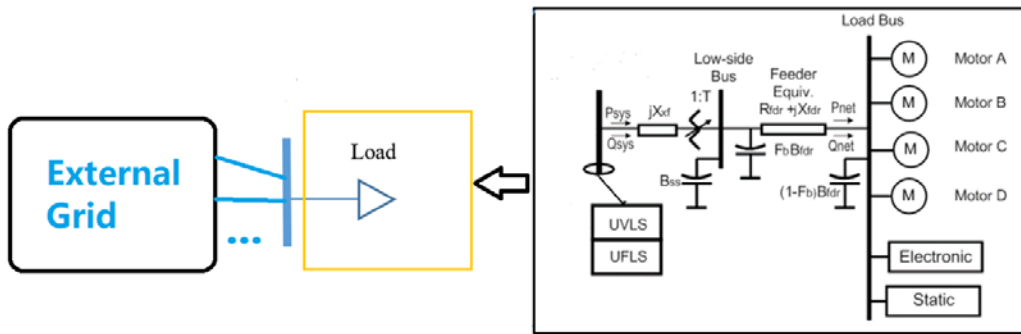
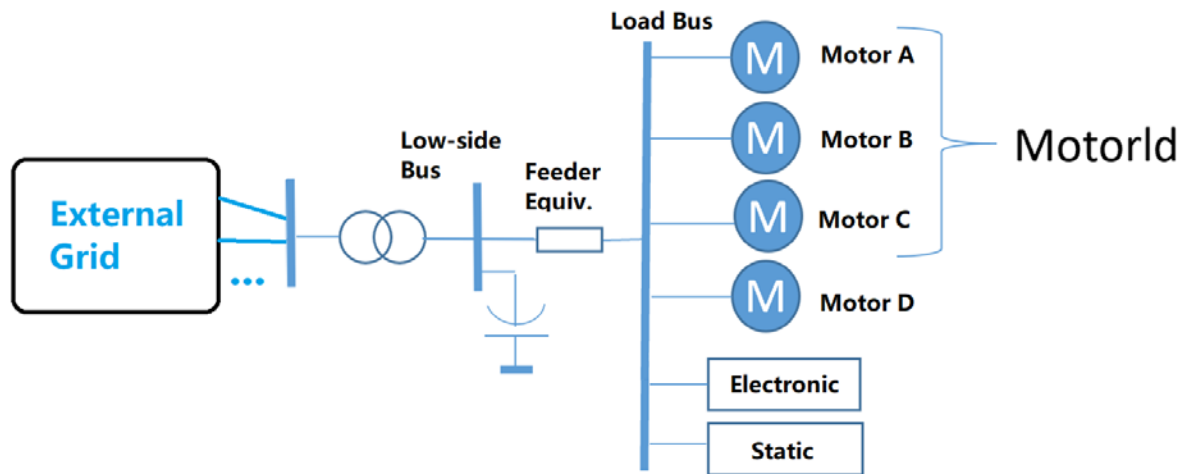


Figure 9.9 One-Line Diagram of Minni-WECC. All Generators and High-Voltage Buses Shown [93]



(a) PSLF Built-in WECC Composite Load Model (CMPLDW)



(b) WECC Composite Load Model Built by Individual Components

Figure 9.10 Two Forms of WECC Composite Load Model Formation

To more authentically mimic the real WECC grid, the load profile of the mini-WECC system, tabulated in Table 9.4, is created by referring to WECC climate zone definitions and load composition data from load model data tool (LMDT). A WECC 2020 Heavy Summer planning case (at 6pm) is considered for load model generation and simulation.

Table 9.4 Load Composition for Minni-WECC Load Models

Bus No.	Bus Name	Load P (MW)	Load Q (MVAr)	FmA	FmB	FmC	FmD	Fel	Fst
8	"BCH-8"	4,400	1,100	0.12	0.14	0.05	0.17	0.16	0.36
11	"SEA-LOAD"	5400	1,350	0.2	0.25	0.3	0.01	0.2	0.04
16	"ORE-16"	3,600	900	0.19	0.14	0.03	0.2	0.15	0.29
21	"ORE-21"	900	225	0.2	0.35	0.35	0.01	0.05	0.04
26	"ORE-26"	450	113	0.2	0.35	0.35	0.01	0.05	0.04
29	"BDY-GEN"	1,575	394	0.2	0.35	0.35	0.01	0.05	0.04
36	"ORE-36"	900	225	0.23	0.15	0.06	0.25	0.12	0.19
43	"SFO-LOAD"	13,240	4,060	0.19	0.14	0.03	0.2	0.15	0.29
50	"SC-LOAD"	11,050	2,763	0.19	0.14	0.03	0.2	0.15	0.29
55	"SDG-55"	3,485	871	0.06	0.09	0.04	0.2	0.21	0.4
56	"LAS-LOAD"	6,800	1,700	0.06	0.09	0.04	0.2	0.21	0.4
64	"PHX-LOAD"	12,060	3,015	0.17	0.16	0.06	0.27	0.11	0.23
70	"SLC-LOAD"	5,850	1,463	0.15	0.16	0.06	0.25	0.12	0.26
73	"COLO-73"	8,100	2,025	0.15	0.16	0.06	0.25	0.12	0.26
78	"IDA-78"	2,700	675	0.2	0.15	0.06	0.21	0.13	0.25
95	"FC-G1"	2,700	675	0.13	0.12	0.06	0.12	0.2	0.37
109	"NEV-109"	1,400	350	0.08	0.16	0.03	0.47	0.09	0.17
112	"SC-112"	13,175	3,294	0.17	0.16	0.06	0.27	0.11	0.23
120	"ALB-LOAD"	8,200	1,925	0.2	0.15	0.06	0.21	0.13	0.25

A three-phase-to-ground fault is applied at Bus 82 and lasts for 0.12 s. The simulation results are presented in Figure 9.11 - Figure 9.13. For the composite load model formulated by individual components, Motor A is represented by PSLF Motorld model and has two progressive protection schemes, which are contactor and controller protections. In the upper subplots of Figure 9.11 and Figure 9.12, the fractions of Motor A not tripped by contactor or controller are plotted. The aggregate fraction of untripped Motor A in the individual component-based composite load model is depicted by green line in the lower subplots of Figure 9.11 and Figure 9.12, while the black line represents the untripped Motor A in PSLF cmpldw model.

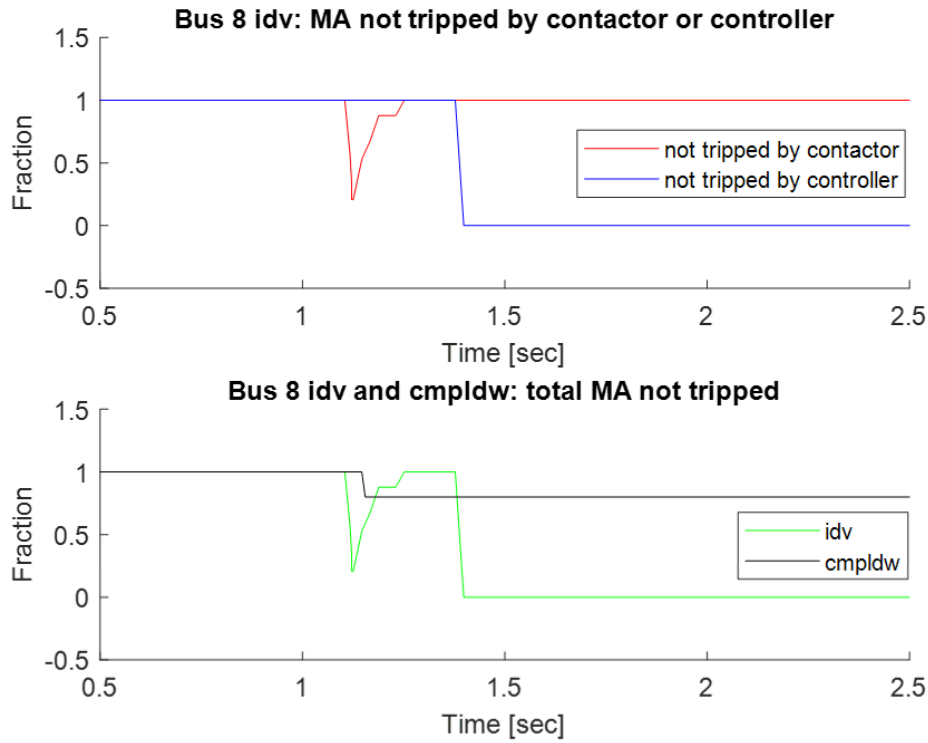


Figure 9.11 Fraction of Motor A Not Tripped in the Formulated Composite Load Model (idv) and PSLF Built-In Composite Load Model (cmpldw) at Bus 8

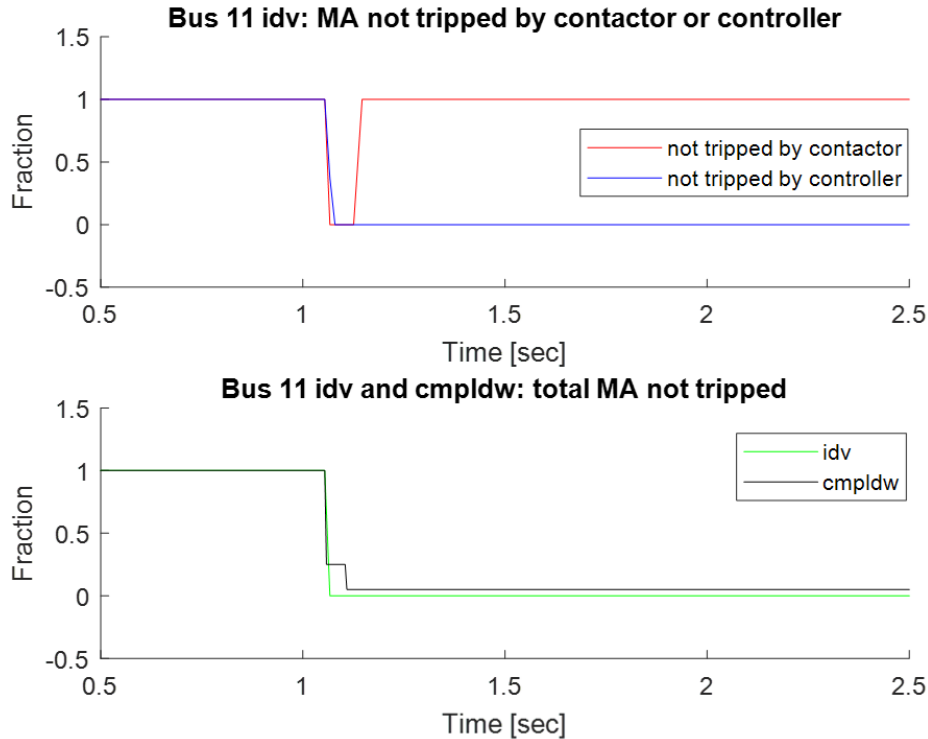


Figure 9.12 Fraction of Motor A Not Tripped in the Formulated Composite Load Model (idv) and PSLF Built-In Composite Load Model (cmpldw) at Bus 11

Figure 9.13 shows the voltages at Bus 82 and two adjacent buses (Buses 8 and 11), it can be seen that with the composite load model formulated by individual components, the post-fault voltage magnitudes are higher than that with PSLF built-in composite load model (cmpldw). This is because the progressive tripping mechanism featured by aggregate contactor and controller protection demonstrates higher level of load tripping compared to traditional 2-level voltage-dependent tripping mechanism in PSLF CMPLDW model (see lower subplots of Figure 9.11 and Figure 9.12).

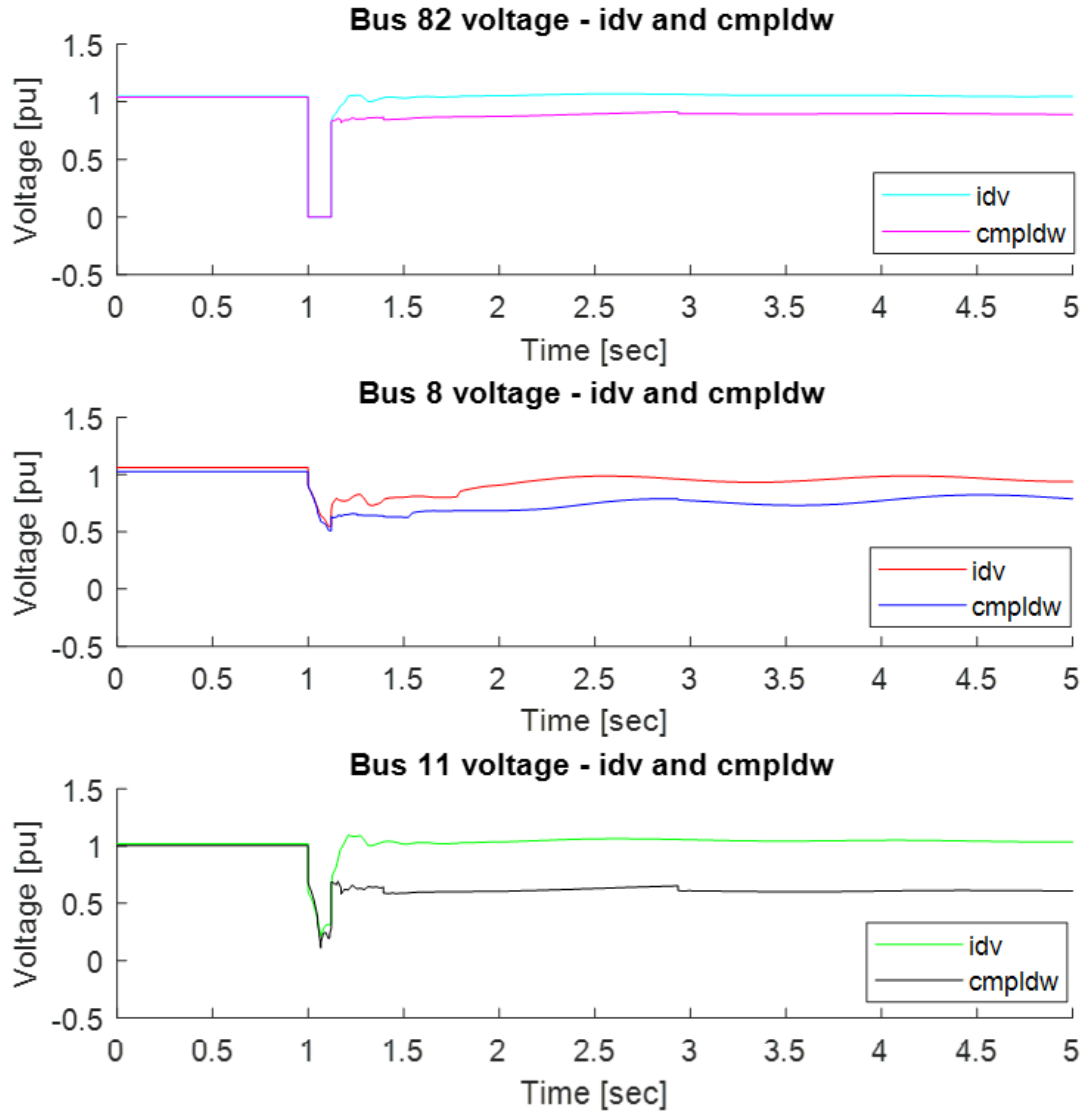


Figure 9.13 Voltages at Buses 82, 8, and 11 for Simulation Scenarios with the Two Forms of Composite Load Model Formation

10.0 Price Responsive Aggregate Load Model Development Plan

The earliest type of demand response in the electricity sector came in the form of time-based rates (TBR) which were heavily debated at the dawn of the industry [94]. However, because of the cost of metering to capture electricity consumption at the necessary level of time differentiation was so high, offering such time-based rates to customers and achieving the desired level of demand response was simply not cost effective. It wasn't until the 1970s when utilities in the Western United States saw metering costs come down enough to implement time-of-use rates for their largest commercial and industrial customers. For example, in 1976 the California Public Utility Commission ordered their three major investor-owned utilities to implement mandatory time-of-use for customers with demands greater than 500 kW [95].

As an alternative to time-based rates, utilities began to consider in the 1950s and 60s the merits of providing rate discounts for the ability to directly interrupt large industrial customer's load [96]. These incentive-based programs began to be offered by utilities to commercial customers starting in the 1980s. The first Pacific Northwest Power Plan (1983) explicitly identified demand response as a load modifying resource used by a number of utilities in the region to provide demand response for resource adequacy purposes [97].

With recent utility investments in Advanced Metering Infrastructure (AMI) and interval meters, more and more customers are becoming empowered to make decisions that will influence how the grid is operated in response to price and/or control demand response (DR) signals. California regulators recently ordered the state's investor owned utilities to transition their residential customers to a time-of-use rate by 2019 [98]. In addition, regulators, system planners and system operators throughout the Western Interconnection are increasingly appreciating the role that AMI-enabled demand response resources can play in providing both bulk and distribution system services by responding to these signals.

As more and more customers participate in time-based rates and incentive-based programs, the underlying composition of load will likely change. Electricity customers respond to such DR opportunities by using end-use devices differently. For example, research has shown that customers with programmable communicating thermostats exhibit substantially greater per customer load reductions to critical peak events than those without such control technology [99]. As such, models that forecast the consumption patterns of end-use devices based on observed load levels will need to evolve. Namely, they must account for differences in the level and timing of electricity consumed by end-uses in response to these new demand response opportunities.

In this Grid Modernization Lab Consortium (GMLC) project, PNNL is responsible for developing a model on how the power system experiences Fault Induced Delayed Voltage Recovery (FIDVR) events. LBNL is responsible for developing a component of this model that will serve as an input. This model component of response needs to focus on DR opportunities that are coincident during times when the power system is experiencing FIDVR events.

Within the Western Electricity Coordinating Council (WECC) footprint, there are a myriad of different time-based rates (TBR) and incentive-based programs (IBP) currently available to customers from different classes (i.e., residential, commercial and industrial) that fall under the umbrella of DR Opportunities (see Table 10.1 and Table 10.2).

Table 10.1 Count of Participants by Customer Class, DR Opportunity and State in WECC [100]

State	Commercial & Industrial Customers					Residential Customers				
	DLC	INT	LACR, EDR, & PTR	DBBB	TOU	RTP	TOU	CPP	DLC	LACR, EDR & PTR
	AZ	35	496	3,138		10,116		761,629	711	
CA	21,943	1,704	5,839	1,377	257	131	2,479	91	498,360	93,924
CO	439	307			2,217		8,747		155,923	
ID		2296	104						37,259	
MT					27			267		
NE	1,231									
NM			70		630		4012			35,000
NV			0		2				75,000	
OR		46	7						764	
SD	3,423								223	
UT	950	98					4		107,054	
WA		8			241				563	
WY					49		1,161			
Total	28,021	4,955	9,158	1,377	13,539	131	778,032	1,069	875,146	128,924

DLC = Direct Load Control; INT = Interruptible; LACR, EDR & PTR = Load Acting as a Capacity Resource, Emergency Demand Response and Peak-Time Rebate; DBBB = Demand Bidding Buy Back; CPP = Critical Peak Pricing Rate; TOU = Time-of-Use Rate; RTP = Real-Time Pricing Rate

Table 10.2 Potential Peak Demand Reduction (MW) by Customer Class, DR Opportunity, and State in WECC [100]

State	Commercial and Industrial Customers					Residential Customers				
	DLC	INT	LACR, EDR, & PTR	DBBB	TOU	RTP	TOU	CPP	DLC	LACR, EDR, & PTR
	AZ	13		190				157	1	
CA	76	660	1,057	80	1	15	3		536	110
CO	32	56	44		8		17		161	
ID		314	380						24	
MT					2					
NE	77									
NM			52		2		2			38
NV									130	
OR		6	14						1	
SD	4								2	
UT	339	4							110	
WA		20	1		1				1	
WY					11		14			
Total	542	1,061	1,770	80	25	15	193	1	964	148

DLC = Direct Load Control; INT = Interruptible; LACR, EDR & PTR = Load Acting as a Capacity Resource, Emergency Demand Response and Peak-Time Rebate; DBBB = Demand Bidding Buy Back; CPP = Critical Peak Pricing Rate; TOU = Time-of-Use Rate; RTP = Real-Time Pricing Rate

When this historical perspective is joined with DR Opportunity potential data developed on a prospective basis by the Northwest Power and Conservation Council to inform their own long-term planning efforts (i.e., Seventh Power Plan), it is possible to winnow down the list of DR Opportunities that will likely have the highest penetration and impact during FIDVR events over the next several years (see Table 10.3).

Table 10.3 Major WECC Regional DR Opportunities for Price Responsive Load Model [100] [101]

DR Opportunity	Residential	Commercial	Municipal, Agricultural & Industrial
TOU	●	●	●
LACR & PTR & EDR	●	●	●
DLC – PCT, A/C, WH	●	●	
INT			●

TOU = Time-of-Use Rate; DLC = Direct Load Control; PCT = Programmable Communicating Thermostat; A/C = Air Conditioning; WH = Water Heater; INT = Interruptible; LACR, EDR & PTR = Load Acting as a Capacity Resource, Emergency Demand Response and Peak-Time Rebate

The interest is ultimately to determine what end-uses are likely impacted by these different DR Opportunities during FIDVR events (see Table 10.4). The regional assessment of DR Opportunities in the Western Interconnection [101] along with a bottom-up DR Potential study undertaken recently by LBNL for the California Public Utility Commission provide just this type of data [102]. In the latter case, what that report revealed was that for many of these DR Opportunities going forward, the recent trend towards exercising more utility control over customer devices (e.g., PCT) has been significantly challenged by communications problems between the utility's demand response management system (DRMS) and the end-use device to be controlled. If the utility is responsible for communicating with a device for which customer payment is predicated on successful delivery of a control signal, then the customer has a viable argument for getting paid if it is the utility's communication problem that precluded a customers from participating in an event. As such, Alstone et al. [102] assumed that Direct Load Control programs with utility-controlled end-uses via radio, not WiFi, will increasingly become the standard program – a shift back to programs our industry has largely moved away from for the past 10 years or so.

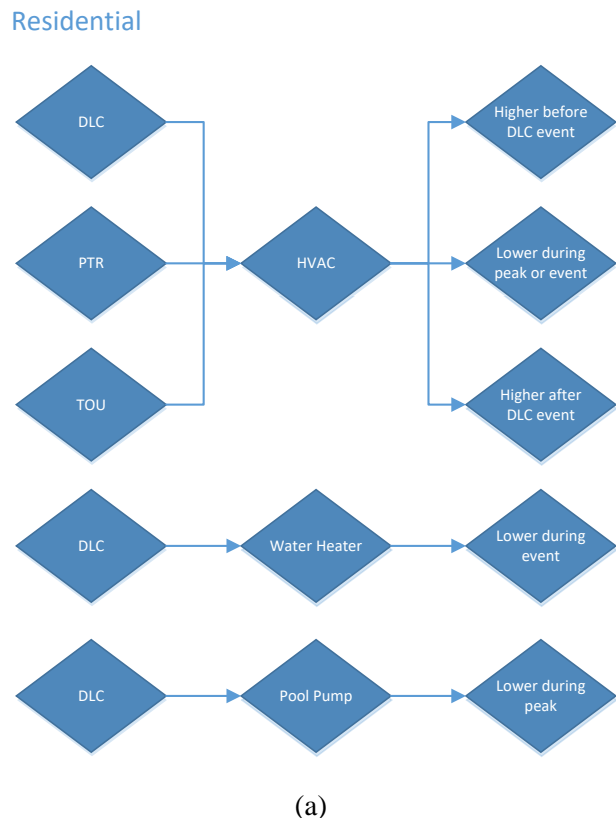
Table 10.4 Major End-Uses Affected by DR Opportunities by Customer Class [101] [102]

Residential	Commercial	Municipal, Agricultural & Industrial
Space Cooling	Space Cooling	Irrigation Pumping
Space Heating	Space Heating	Water Distribution Pumping
Water Heating	Indoor Lighting	Wastewater Pumping & Processing
Pool Pump	Ventilation	Industrial Processes

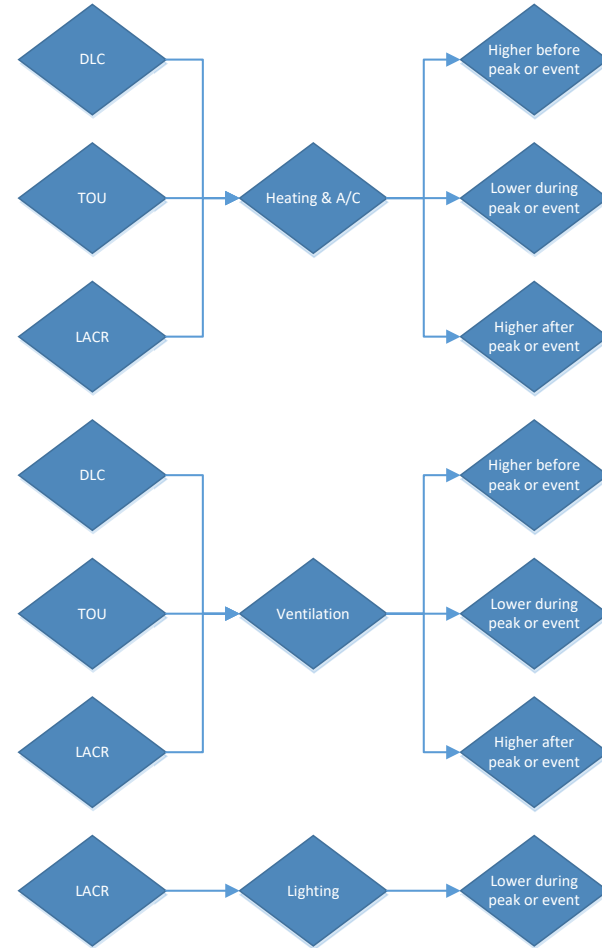
The end result of this trend is that it is our assessment that the response to each DR Opportunity will either be exclusively from utility-control of customer end-uses or from customer-control of these same end-uses. As such, we assume that utility-control of residential and commercial customers' end-uses will occur via DLC programs, utility-control of industrial customers' process loads will happen via Interruptible programs, whereas all other DR rates and programs will have customer-control of end-uses.

Under utility-control, we will assume there will be little to no opportunity for override. Such will not be the case for customer-control end-uses, where override of any control signal is likely and should result in a reduction (i.e., derating) in the total number of end-uses actually responding to a price, event or control signal.

Figure 10.1 (a)-(c) capture the relationship between customer class, major DR opportunity and the end-use or process load that will be affected. In addition, the figure shows how the electricity consumption of that end-use is likely to be affected before, during or after the peak (rate) or event period.

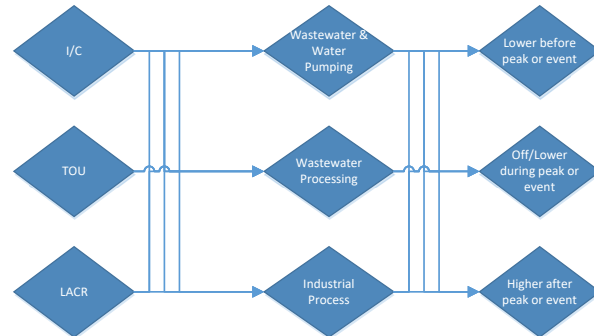


Commercial



(b)

Industrial



(c)

Figure 10.1. Relationship between Major DR Opportunity and Change in End-Use Electricity Consumption by Customer Class

The peer-reviewed literature on customer price response to TOU, both at the residential, commercial and industrial level is rather sparse; although there have been a number of pricing pilots more recently which have been evaluated and reported but have not gone through the peer review process. Berkeley Lab focused the literature review on North American experience with time-of-use rates, but where the literature was thin (e.g., industrial customers) more international experience was considered.

With recent utility investment in advanced metering infrastructure (AMI) and the associated benefits often cited in the business case concerning the ability to introduce more time-based rates, there is a fair amount of recent literature on residential customer response to time-of-use rates. However, most of it does not differentiate by end-use, as is suggested by Figure 10.1 which we would like to have. As will be discussed in more detail below, Berkeley Lab has an ability to analyze the results of a residential TOU pricing pilot that was active during the summer to derive elasticity estimates for those predicted to have central air conditioning as well as those without central air conditioner (CAC).¹ As for the other customer classes and end-uses identified in Figure 10.1, we will use the existing literature to inform how the Price Responsive Load model will need to accept inputs and how it should apply those inputs to derive impact estimates in response to time-of-use rates.

The most recent analyses of price response by small commercial customers to time-of-use rates comes from Ontario [103], Connecticut [104], and California [105]. All three sets of analyses found no statistically significant elasticity estimates in response to TOU.² The California Statewide Pricing pilot [105] also included medium sized commercial customers, where they did find a statistically significant response to TOU. However, the analysis did not differentiate by customers with and without end-uses, like HVAC systems. With respect to the largest commercial customers, the only literature that could be found comes from a pricing experiment back in the mid-1980s [106] which found no statistically significant elasticity estimates.

At the industrial customer level, there is substantial diversity in the business practices and end-uses that could be modified in response to a time-of-use rate. ICF International [107] summarized the recent empirical evidence of industrial customers' response to TOU showing there is a range of elasticity estimates which have emanated from evaluations over the past several decades. However, the report does not provide detailed breakouts by business type (e.g., North American Industry Classification System).

Overall, what this literature review also found is that the Price Responsive Load model will need to accept inputs for two different types of elasticities: Own-Price and Substitution. Since their definition is different, each will need to be used differently to derive impact estimates of price-responsive load in the model.

An **own-price elasticity** focuses on electricity consumption in one period and how a customer will alter that consumption based on a change in the price of electricity in that same period, as follows:

¹ Faruqui and Sergici (2010) [114] is the only reference LBNL could find that provided any elasticity estimates for residential customer response to time-based rates during the winter. However, it is from a 2006 study out of Australia and the original source material is unavailable. So its applicability to the US experience may be dubious.

² One has to go back to the late 1990s (Aigner et al., 1994 [133]; Ham et al., 1997 [115]) or into the mid 1980s (Aigner and Hirschberg, 1985 [106]) to find the last domestic instance of statistically significant estimates of price elasticities for this customer class. Even within the former experiment, the authors only found statistically significant elasticities for customers without electric HVAC systems or without electric water heating. In the latter case, they only found statistically significant elasticity estimates during the summer but not during the winter.

$$\sigma = \frac{\left[\frac{(q_{peak}^{TOU} - q_{peak}^{Base})}{q_{peak}^{Base}} \right]}{\left[\frac{(p_{peak}^{TOU} - p_{peak}^{Base})}{p_{peak}^{Base}} \right]} \quad (10.1)$$

Where q is the quantity consumed during either a single hour in the peak period (kWh/hr) or throughout all the hours in the peak period (kWh), and p is the price of electricity charged during the peak period $$/kWh$). Depending on what rate the customer is facing, the analysis could be performed to simulate either; a) what the customer's load would have been had they faced the TOU rate since they are facing some other (Base) rate; or b) what the customer's load would have been had they faced the Base rate since they are facing the TOU rate. It is simple enough to rearrange the above equation to derive estimates of either value for q .

A **substitution elasticity** focuses on measuring how the ratio of electricity consumed in two periods changes based on a change in the price ratio in those two same periods, as follows:

$$\eta = \frac{\left[\frac{\left(\frac{q_{peak}^{TOU}}{q_{offpeak}^{TOU}} - \frac{q_{peak}^{Base}}{q_{offpeak}^{Base}} \right)}{\left(\frac{q_{peak}^{Base}}{q_{offpeak}^{Base}} \right)} \right]}{\left[\frac{\left(\frac{p_{peak}^{TOU}}{p_{offpeak}^{TOU}} - \frac{p_{peak}^{Base}}{p_{offpeak}^{Base}} \right)}{\left(\frac{p_{peak}^{Base}}{p_{offpeak}^{Base}} \right)} \right]} \quad (10.2)$$

In this case, q represents total energy (kWh) consumed in the peak or off-peak period. So, for simulation purposes, one needs to rearrange the formula to derive estimates of the ratio of peak-to-off-peak electricity consumption forecasted in response to TOU (if the customer is currently facing some other Base rate design) or Base (if the customers is currently facing a TOU rate design).

The challenge with using a substitution elasticity is that the analyst doesn't know if the change in the electricity consumption ratio is due to changes (i.e., reductions) in peak period electricity, changes (i.e., increases) in off-peak period electricity, or some combination of the two. More recently the substitution elasticity has been jointly estimated with a daily elasticity to assess if some quantity of electricity is changed over the entire day in response to the change in price (e.g. [105]). This allows for an ability to allocate the change in the ratio of electricity use between peak and off-peak consumption. However, recent empirical evidence suggests there is no statistically significant daily response to the change in price for commercial customers [105]. As such, an analyst would assume that the change in the peak electricity consumption (kWh) is equal to the change in the off-peak electricity consumption (kWh). This can be easily derived by replacing the value of q^{TOU} in the above formula with $q^{Base} +/- \Delta q^{TOU}$, where the latter represents the identical kWh change in peak or off-peak electricity consumption from the Base consumption. From there, the analyst can rearrange terms to solve for Δq^{TOU} .

Using the results of the literature review, coupled with our own analysis detailed below, Berkeley Lab will provide own-price or substitution elasticity estimates by April 1, 2018 for as many of the customer class and end-use combinations found in Table 10.5, as possible. These will serve as inputs to PNNL's Price Responsive Load model. Where unique estimates cannot be found in the literature by customer class, season, end-use, etc., Berkeley Lab will collapse the categories to best reflect the analysis which was performed to produce those elasticity estimates in the first place.

Table 10.5. Elasticity Estimates by Customer Class, Retail Rate, Season and End-Use

Customer Class	Retail Rate	Season	End-Use
Residential	TOU	Summer	HVAC
Residential	TOU	Non-Summer	HVAC
Residential	TOU	Summer	Non-HVAC
Residential	TOU	Non-Summer	Non-HVAC
Commercial - Small (<50 kW)	TOU	Summer	HVAC
Commercial - Small (<50 kW)	TOU	Non-Summer	HVAC
Commercial - Small (<50 kW)	TOU	Summer	Non-HVAC
Commercial - Small (<50 kW)	TOU	Non-Summer	Non-HVAC
Commercial - Medium (50-200 kW)	TOU	Summer	HVAC
Commercial - Medium (50-200 kW)	TOU	Non-Summer	HVAC
Commercial - Medium (50-200 kW)	TOU	Summer	Non-HVAC
Commercial - Medium (50-200 kW)	TOU	Non-Summer	Non-HVAC
Commercial - Large (>200 kW)	TOU	Summer	HVAC
Commercial - Large (>200 kW)	TOU	Non-Summer	HVAC
Commercial - Large (>200 kW)	TOU	Summer	Non-HVAC
Commercial - Large (>200 kW)	TOU	Non-Summer	Non-HVAC
Industrial	TOU		

10.1 Berkeley Lab Residential Hourly Impact Analysis

As discussed above, Berkeley Lab will be performing its own analysis to derive elasticity estimates for residential customer response to time-of-use rates. This section discusses the work that has been done to date to inform how those elasticities should be estimated.

The hourly average load impact for treatment groups in the Sacramento Municipal Utility District's (SMUD) Smart Grid Investment Grant funded consumer behavior study that differed by enrollment approach (i.e., default or voluntary) and retail rate design (i.e., TOU or CPP) were estimated using a difference-in-differences (DID) instrumental variables (IV) regression employing a Two-Stage Least Squares (2SLS) joint estimation technique. While whether or not a household actually experienced the study's TOU or CPP electricity rates was not random (i.e., because of self-selection in or out of treatment), the assignment to a treatment group was random. We can therefore use *assignment* to treatment (or "encouragement" as it's known in the literature) as an instrument for *actual* treatment (i.e., exposure to the treatment time-of-use rate).

A separate regression is run for each rate and enrollment approach treatment group as follows:

$$Treat_i = \alpha + \vartheta Encouraged_i + \gamma Post_t + \varepsilon_{it} \quad (10.3)$$

$$y_{it} = \beta_t \widehat{Treat}_i + \gamma_i + \tau_t + \varepsilon_{it} \quad (10.4)$$

Where y_{it} represents hourly electricity consumption for household i in hour t ; $Post_t$ takes the value 1 for any time after the first date that the treatment rate went into effect (regardless of whether household i was

in treatment or control); $Encouraged_i$ takes the value 1 for any customer who was randomly chosen to be encouraged to take up treatment; $Treat_i$ takes the value 1 for any customer who was encouraged and decided to take up the treatment; and β_t is the variable of interest - the local average treatment effect for the average household during the estimated hour t of the treatment period $Post$. ε_{it} is the error, clustered at the household level.

The hourly average load impact estimates generated using this methodology for the different treatment groups are shown in Figure 10.2 (voluntary TOU all weekday non-holidays).³

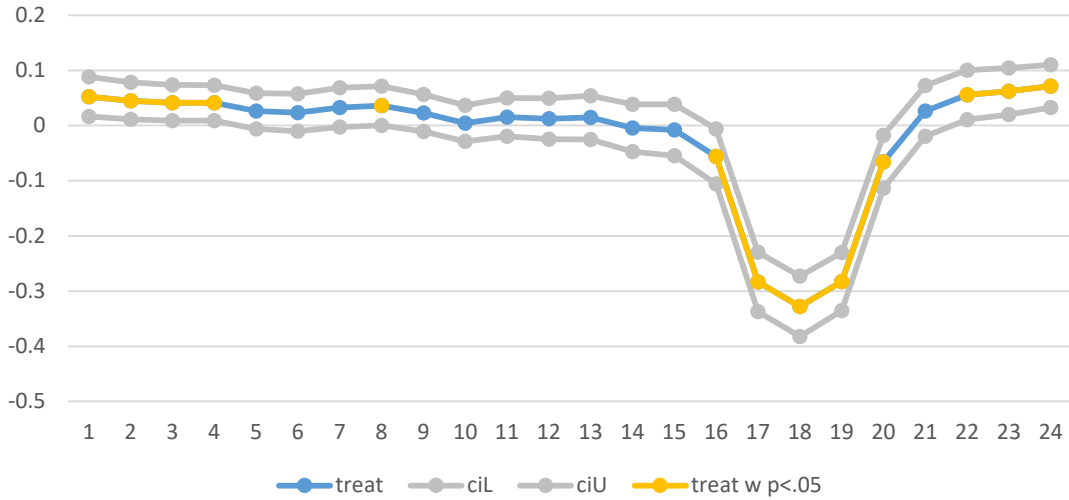


Figure 10.2 Hourly Average Load Impact Estimates for Voluntary TOU Treatments over all Weekday Non-holidays

10.2 Residential Demand Model Specification

The literature is replete with examples where residential demand models for electricity under a time-of-use rate design are estimated with a Constant Elasticity of Substitution (CES) specification, that assumes substitution between peak and off-peak electricity consumption, under non-or quasi-experimental conditions (e.g., [108] [109] [110] [111] [112]). However, given our experimentally derived load impact results in Figure 10.2 during the off-peak period which are very small and only statistically significant during a few of the overnight hours, we do not believe an application of a demand model that employs such an assumption (i.e., substitution between peak and off-peak electricity) is warranted. In fact, it is an assessment that imposing such an assumption (i.e., there exists substitution between peak and off-peak electricity) will result in a biased elasticity estimate.⁴

³ All points on the graph in yellow represent statistically significant load impact estimates.

⁴ In the work of Goldman et al [134], the authors develop a model based on Patrick's work [135] that adjusts the estimated substitution elasticity, derived from a CES specification, to account for behaviors that suggest foregoing of peak period electricity consumption instead of shifting that consumption to the off-peak period in order to derive more accurate peak period impact estimates. Numerical analysis using a simple bench model indicates such an approach produces identical load impact estimates as those that would be derived using a demand model specification that does not assume substitution but does so with a more accurate elasticity estimate.

Instead, we propose to leverage our RCT experimental design to estimate own-price demand elasticities. We do not assume anything about cross-hourly substitution. As such, we use a log-log specification, which implies a constant own-price elasticity of demand (i.e., a percentage change in price at a low price level would result in the same percentage change in quantity as for a high price level).

As with the average load impacts estimates, our efforts to estimate the own-price demand elasticity for treatment groups that differed by enrollment approach (i.e., default or voluntary) and retail rate design (i.e., TOU or CPP) were estimated using a difference-in-differences (DID) instrumental variables (IV) regression employing a Two-Stage Least Squares (2SLS) joint estimation technique and using *assignment* to treatment as an instrument for *actual* treatment.

There was a price change between the summer of 2011 (i.e., pre-treatment period) and 2012 (i.e., the first of two summers of the study). Since we are interested in using pre-treatment data to account for starting differences in electricity consumption between treatment and control cells, the demand model specification must first account for this change in price before attempting to isolate the specific change in price that occurred when treatment customers were exposed to the TOU or CPP rates during the study. To do so, a dummy variable is used to account for any marginal impact associated with the price increase that occurred between 2011 and 2012 and then directly measure the price difference between the tier and TOU or CPP rate in any given hour of 2012 and 2013. The final specification is as follows where a separate regression is run for each treatment group and time period:

Table 10.6 Own-Price Elasticity Estimation Groupings

Voluntary Enrollment Approach		Default Enrollment Approach	
TOU	Peak Period (weekday, non-holidays)		Peak Period (weekday, non-holidays)

$$Treat_i = \alpha + \vartheta Encouraged_i + \gamma Post_t + \varepsilon_{it} \quad (10.5)$$

$$\ln(y_{it}) = \alpha + \gamma Post_t + \varphi \widehat{Treat}_t + \beta \ln(\Delta Encouraged Price_{it}) * \widehat{Treat}_t * Post_t + \varepsilon_{it} \quad (10.6)$$

Where y_{it} represents hourly electricity consumption for household i in hour t ; $Post_t$ takes the value 1 for any time after the first date that the treatment rate went into effect (regardless of whether household i was in treatment or control); $Encouraged_i$ takes the value 1 for any customer who was randomly chosen to be encouraged to take up treatment; $Treat_i$ takes the value 1 for any customer who was encouraged and decided to take up the treatment; $\Delta Encouraged Price_{it}$ represents the difference in the price of electricity that each household i was encouraged to take up during time period t and the price of electricity that the control group experienced during the time period t ; and β is the variable of interest – the own-price demand elasticity during the treatment period $Post_t$. ε_{it} is the error, clustered at the household level.

The tiered nature of SMUD's residential rates results in a simultaneity problem that must be addressed during the estimation process for control customers in all hours. We assessed the average electricity consumption of the relevant control group to determine the applicable tier for the average control customer. The end result is that the average control customer faces only the Tier 1 usage price since their average consumption ($kWh/month$) is below the base usage threshold of 700 kWh. As such, the Tier 1 usage price for control group customers is applied in the estimation process of Equation (10.4) based on their status of Low Income (EAPR) or not.

Demand elasticities will be further estimated based on predictions of whether or not the customer owns and operates an electric air conditioning system using a predictive model developed in [113].

$$\begin{aligned} \ln(y_{it}) = & \alpha + \gamma Post_t + \varphi \widehat{Treat}_t + \eta \widehat{CAC}_{it} + \beta^{Treat} \ln(\Delta Encouraged Price_{it}) * \widehat{Treat}_t * Post_t + \\ & + \beta^{CAC} \ln(\Delta Encouraged Price_{it}) * \widehat{Treat}_t * Post_t * \widehat{CAC}_{it} + \varepsilon_{it} \end{aligned} \quad (10.7)$$

Where CAC_{it} takes a value of 1 if the customer is predicted to own a central air conditioning system, 0 otherwise; β^{Treat} is the own-price elasticity for those not predicted to own a central air conditioning system, and β^{CAC} is the marginal effect on the estimated own-price elasticity from being predicted to own a central air conditioning system.

10.3 LBNL Recommended Values for Price Elasticities

The LBNL recommended values for price elasticities are listed in Table 10.7.

Table 10.7 LBNL Recommended Values

Class	Retail Rate	Season	End-Use	Own-Price Elasticity (Peak)	Own-Price Elasticity (Off-Peak)	Substitution Elasticity	Comments/Source
Residential	TOU	Summer Non-Hot Day ⁵	HVAC	-0.248	0	NA	LBNL research funded by this GMLC project created the elasticity estimate.
Residential	TOU	Summer Hot Day	HVAC	-0.328	0	NA	Ibid
Residential	TOU	Non-Summer	HVAC	0	0	NA	Faruqui and Sergici [114] provide an own-price elasticity estimate of -0.47 for residential customer response in Australia to TOU during the winter time. Given the magnitude of the estimate in relation to LBNL research, coupled with lack of details surrounding its estimation, we are recommending it not be used.
Residential	TOU	Summer Non-Hot Day	Non-HVAC	-0.186	0	NA	LBNL research funded by this GMLC project created the elasticity estimate.
Residential	TOU	Summer Hot Day	Non-HVAC	-0.251	0	NA	Ibid

⁵ The segmentation by “Hot Days” and “Non-Hot Days” is intended to capture the fact that on hot days, residential customers’ use of HVAC is likely to be higher. So, the elasticity value on such days is likely to differ, for such customers, than those on non-hot days.

Residential	TOU	Non-Summer	Non-HVAC	0	0	NA	Faruqui and Sergici [114] provide an own-price elasticity estimate of -0.47 for residential customer response in Australia to TOU during the winter time. Given the magnitude of the estimate in relation to LBNL research, coupled with lack of details surrounding its estimation, we are recommending it not be used.
Commercial - Small (<50 kW)	TOU	Summer	HVAC	0	0	0	CRA International [105] and Faruqui et al. [104] didn't find any statistically significant elasticities and did not differentiate by HVAC or control of HVAC. Ham et al. [115] found no statistical significance of any elasticity with electric HVAC.
Commercial - Small (<50 kW)	TOU	Non-Summer	HVAC	0	0	0	Ibid
Commercial - Small (<50 kW)	TOU	Summer	Non-HVAC	0	0	0	CRA International [105] and Faruqui et al. [104] didn't find any statistically significant elasticities and did not differentiate by HVAC or control of HVAC. Ham et al. [115] found statistical significance of any elasticity without electric HVAC but that was 20 years ago.
Commercial - Small (<50 kW)	TOU	Non-Summer	Non-HVAC	0	0	0	Ibid

Commercial - Medium (50-200 kW)	TOU	Summer	HVAC	NA	NA	-0.0493	Jessoe and Rapson [116] found no statistically significant load impact for default, but our residential default effect analysis says this should not be surprising. CRA International [105] found statistically significant elasticity but did not differentiate by HVAC or not.
Commercial - Medium (50-200 kW)	TOU	Non-Summer	HVAC	NA	NA	-0.0493	Ibid
Commercial - Medium (50-200 kW)	TOU	Summer	Non-HVAC	NA	NA	-0.0493	Ibid
Commercial - Medium (50-200 kW)	TOU	Non-Summer	Non-HVAC	NA	NA	-0.0493	Ibid
Commercial - Large (>200 kW)	TOU	Summer	HVAC	NA	NA	0	Aigner et al. [106] found no statistically significant elasticity estimates.
Commercial - Large (>200 kW)	TOU	Non-Summer	HVAC	NA	NA	0	Ibid
Commercial - Large (>200 kW)	TOU	Summer	Non-HVAC	NA	NA	0	Ibid
Commercial - Large (>200 kW)	TOU	Non-Summer	Non-HVAC	NA	NA	0	Ibid
Industrial	TOU			NA	NA	NA	Literature too thin and not detailed enough (see [107]).

11.0 Load Model Calibration and Validation

Load model calibration is a complicated issue because of the accuracy of the load model itself and the power consumption uncertainties reflected in the measurement data [117] [118]. In addition, the WECC composite load model (CMPLDW model in PSLF) has more than 100 parameters and the model itself is non-linear, which presents additional difficulties to the model calibration. This chapter will present a load model validation framework and two approaches to calibrate WECC composite load model parameters to match the performances with real micro-PMU measurement data or detailed EMT-level simulation data given the measurement data is not available.

11.1 Trial and Error Approach

In this sub-chapter, the distribution-level PMUs information is used for composite load model validation (see Figure 11.1) [119]. Micro-PMUs were deployed by LBNL on several distribution feeders, and multiple system events were captured by these devices. Disturbance records “play-in” capabilities have been implemented by all major power system modeling packages, including GE PSLF, which is used in this study [5]. The play-in method has demonstrated very high efficiency for power plant model validation, and it has been used by many system planning and operating entities, as well as the research community [120] [121]. Similar approaches can be used to calibrate and validate composite load model by playing-in micro-PMU measurements into a GE PSLF composite load model [122]. Mitsubishi Electric also conducted an analysis of the parameter sensitivities for the CMPLDW model. The most sensitive parameters under different conditions were identified in the report [123].

A trial-and-error approach based on engineering judgement is proposed in this sub-chapter to benchmark the several sensitive load model parameters generated by LMDT program and is implemented in the prototype of load model validation tool, which would be a supplement to the LMDT application.

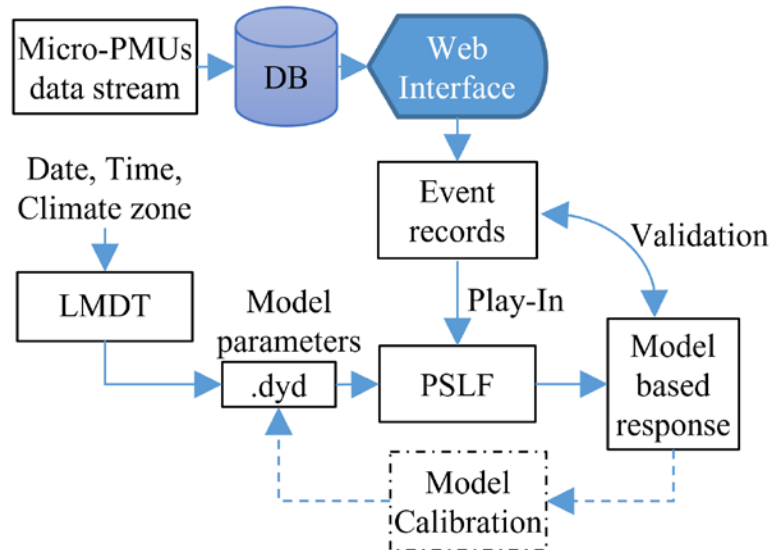


Figure 11.1 Composite Load Model Validation Concept

11.1.1 Description of Micro-PMUs

The micro-PMU data used for this work comes from a number of utility pilot deployment feeders with a customer composition of primarily residential and commercial loads. Three-phase voltage and current phasors are recorded at a rate of 120 Hz [124]. The structure of the micro-PMU system to collect

distribution network measurements is shown in Figure 11.2 [125]. Frequency events are identified via a threshold approach and data are post-processed to obtain their sequence representation for “*play-in*” in PSLF. Voltage events are detected via a threshold approach and grouped together using *k-means* clustering where the Euclidean distance between events, with their respective means subtracted, is used as a measure of similarity [126].

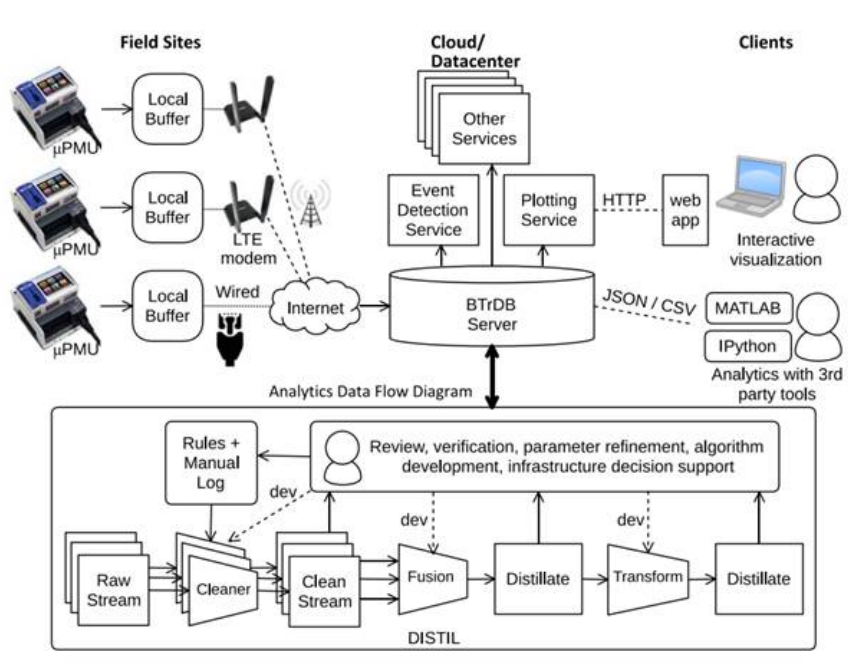


Figure 11.2 Distribution PMU System Configuration [125]

11.1.2 Load Model Validation Process

In this section, the load model data tool (LMDT) and a prototype of load model validation tool will be presented. The theories and implementations of load model calibration process, as a part of the load model validation tool (see Figure 11.1), will be discussed in detail.

Load Model Data Tool

The load model data tool was developed by PNNL in collaboration with Bonneville Power Administration (BPA) and WECC modeling and validation working group (MVWG) [3]. The LMDT is a standalone open source Windows application that generates composite load model parameters taking into account climate zone and seasonal information, operating hour and feeder type. The LMDT uses base case power flow conditions and supplemental load shape data to generate the dynamic records in GE PSLF and Siemens PTI PSS/E format. To create composite load dynamic records the user also needs to specify the percentage of different types of load (e.g., residential, commercial, industrial, etc.) connected to the feeder. The process of composite load model creation is illustrated in Figure 11.3.

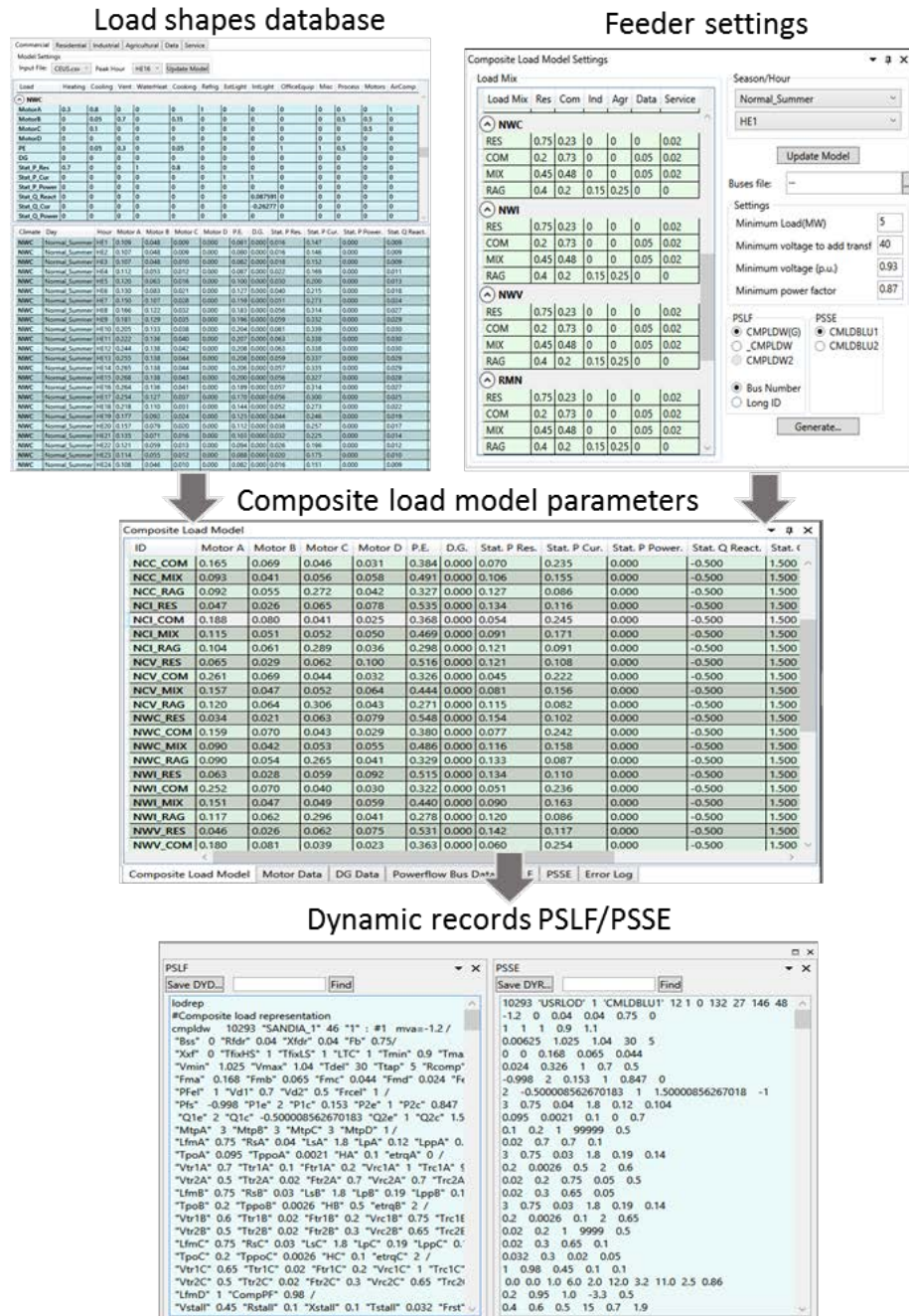


Figure 11.3 Composite Load Model Creation

Load Model Validation Tool

The load model validation tool, which could be interfaced with the LMDT tool, can automatically identify PMU data information, generate the PSLF dynamic simulation parameter records of CMPLDW model according to the seasons, hours and locations of PMU measurements, and run dynamic simulations to calibrate and validate the composite load model in a batch mode. The GE PSLF controllable voltage source model is utilized to play in voltage and frequency measurements from PMU. The simulated active

power waveforms at the load side are compared with the PMU measurement data to validate the calibrated CMPLDW model.

The micro-PMU event data can be outputted in comma separated values (CSV) format. A Python script is developed to read in the list of event data files, parse the file names to extract the information of the month, date and hour of the measurements, and retrieve the initial bus voltage, load active and reactive power to adjust the power flow case file. The LMDT tool generates dynamic simulation parameters of CMPLDW model for each event based on the extracted measurement timestamp and specified geographical locations [3]. Meanwhile, each of the event files is accessed through PSLF engineering process control language (EPCL) script. The EPCL script launches dynamic simulations to feed the measured voltage and frequency time series into the controllable voltage source and monitors the simulated active and reactive power at the composite load side. The entire process is depicted by Figure 11.4.

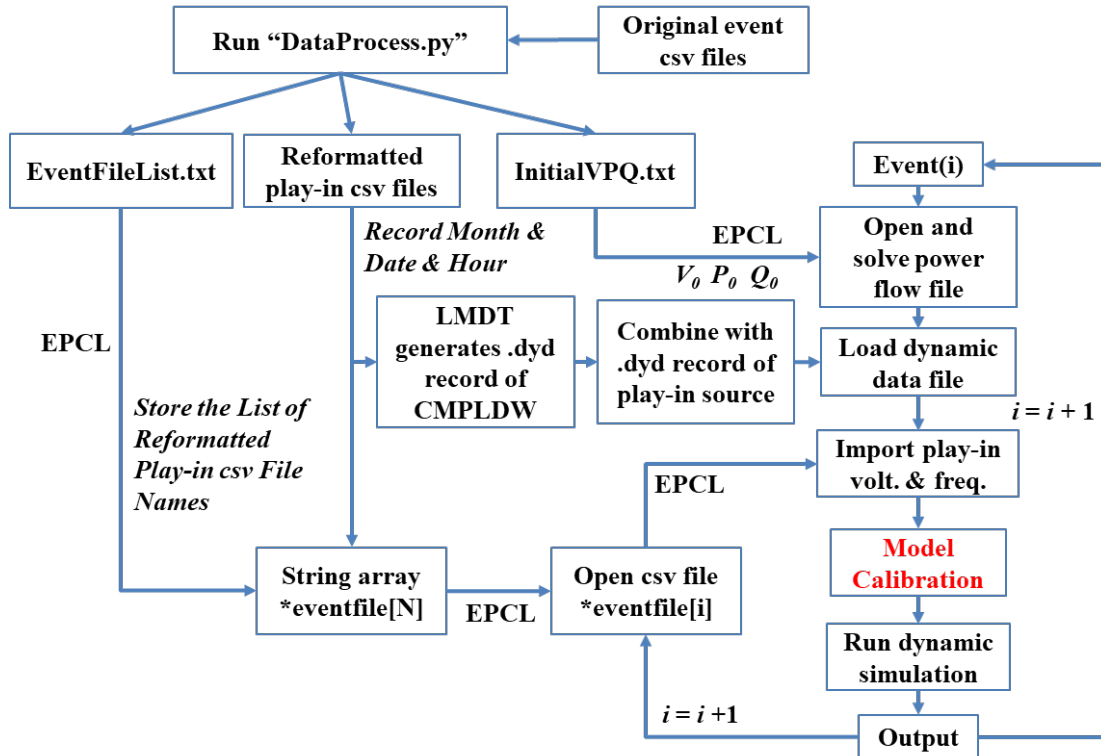


Figure 11.4 Implementation of Load Model Validation Tool

Load Model Calibration Process

The generated raw parameters of composite load model sometimes do not match the measurement data ideally. The calibration of the load model is essential in increasing the accuracy of the LMDT-generated CMPLDW model as shown in Figure 11.4. In this section, a trial-and-error approach is used to benchmark a CMPLDW model at an individual location in the WECC network, where measurement data are available.

Reactive power compensation is usually activated in the composite load model and affects the calibration accuracy. When it comes to the load model calibration, it is more meaningful to adjust the model parameters to match the active power of the load model with the measurement data. To properly calibrate the CMPLDW model, a priority list of parameters is selected based on sensitivity analysis [123]. The priority list used in this sub-chapter is presented in Table 11.1.

Table 11.1 Priority List of Parameters

Priority	Parameter Name	Description
1	FmA	Motor A fraction of load P
2	FmB	Motor B fraction of load P
3	FmC	Motor C fraction of load P
4	FmD	Motor D fraction of load P
5	fel	Electronic load fraction of load P
6	$Vstall$	Stall voltage of Motor D
7	$Tstall$	Stall time delay of Motor D
8	$Rstall$	Stall resistance of Motor D

To reduce the computational burden of the calibration process, the parameters in the priority list are tuned by pairs and in sequence, e.g. tuning (FmA , FmB) first and then (FmC , FmD). The calibration process starts with adding generated deviations to the original values of the first two parameters in the priority list, as shown in (11.1) and (11.2), run the simulation, and post-process the data by calculating the mean squared error (MSE) between the simulated and measured time series of power. The distribution of the deviations is illustrated in Figure 11.5, in which the coordinates of each small circle represent the deviations for parameters X and Y .

$$X = (1 + \Delta X) X_{orig} \quad (11.1)$$

$$Y = (1 + \Delta Y) Y_{orig} \quad (11.2)$$

where X_{orig} and Y_{orig} are the original values of parameters X and Y . ΔX and ΔY are unitless deviations. In this section, it is considered that $\Delta X, \Delta Y \in [-0.9, 5.0]$.

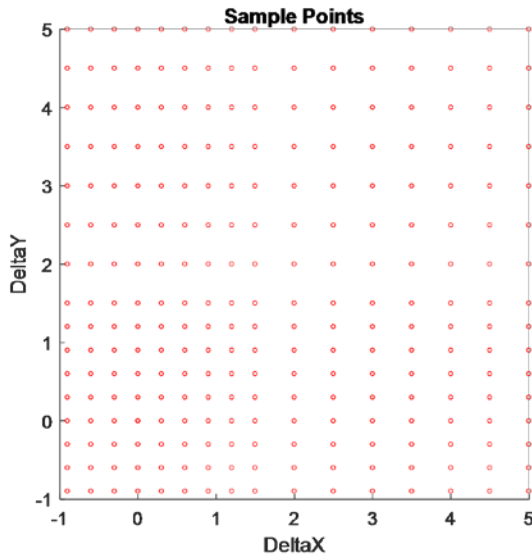


Figure 11.5 Distribution of Paired Deviations

The simulation is performed for each pair of deviations to generate the same number of output files as the number of deviation pairs. The output files recording the simulated and measured time series of power are accessed to compute the MSE. After all the deviation pairs are gone through, the minimum MSE is found along with the index of the output file (or the deviation pair), as expressed by (11.3) and (11.4).

$$\text{Objective} = \min_{k \in [1, M]} (MSE^{(k)}), \quad (11.3)$$

$$\text{subject to: } MSE^{(k)} = \frac{1}{N} \sum_{i=1}^N \left[P_{\text{measured}}^{(k)}(i) - P_{\text{simulated}}^{(k)}(i) \right]^2 \quad (11.4)$$

where, k represents the index of the output file (or deviation pair). M indicates the total number of output files, equal to the total number of deviation pairs. N is the total number of simulation or measurement data points in an event.

The entire flow chart implementation of load model calibration is depicted in Figure 11.6. The calibration process then proceeds to the adjustment of the next two parameters in the priority list. Before starting to play in deviations for the next two parameters, the previous two parameters need to be updated by adding the pair of deviations found to generate the minimum MSE in the previous tuning cycle. After the update on the values of the previous two parameters, the same process is followed to find the minimum MSE and the corresponding deviation pair by tuning the next two parameters. During this approach, the difference between the simulated and measured active power keeps decreasing after each tuning cycle. Finally, after all the parameters in the priority list are adjusted in sequence, the final MSE between the simulated and measured active power data is largely reduced.

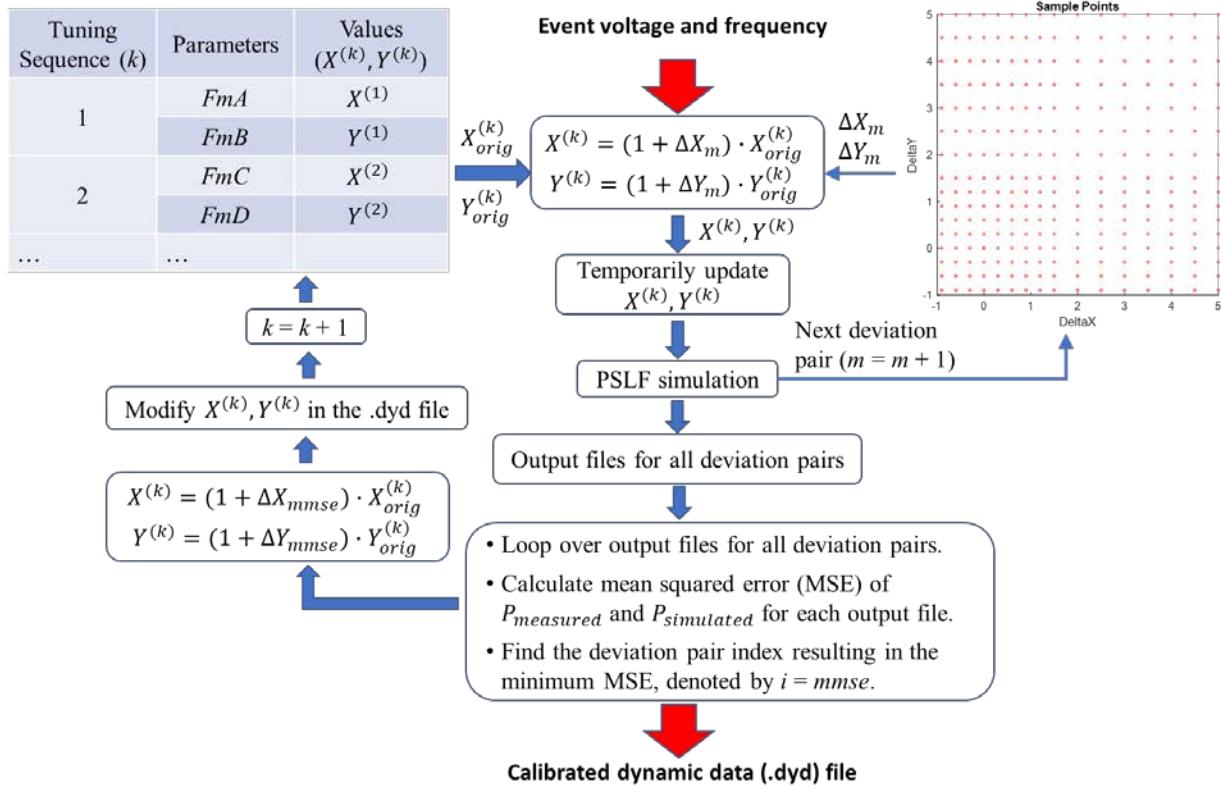


Figure 11.6 Flowchart Implementation of Load Model Calibration Process

11.1.3 Simulation Results

To generate the parameters of CMPLDW model from the LMDT tool, the measurement time, climate zone and feeder mix information needs to be entered. In this sub-chapter, the local times of the events are indicated in the file names of the data. The climate zone, as per LMDT tool, is Desert Southwest (DSW) [3]. The feeder is a residential feeder with a mix of 72% residential load and 28% commercial load.

The CMPLDW model to be calibrated is connected to a controllable voltage source, which the voltage magnitude and frequency can be played in. The connection is shown in Figure 11.7.

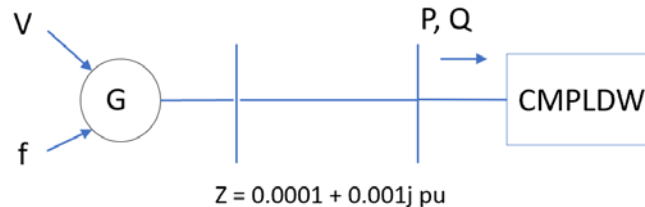


Figure 11.7 Schematic for Load Model Calibration

Three events of frequency droop were captured by micro-PMU along with corresponding voltage, active and reactive power measurements at substation level. The CMPLDW model at the same substation is benchmarked using the proposed method to match simulated active power with measurement data for each event, resulting in three sets of calibrated parameters listed in Table 11.1.

The simulation results of calibrated model are presented in Figure 11.8 - Figure 11.10, comparing the measured active power, originally simulated active power, and simulated active power after tuning

parameters. It can be concluded from these figures that the simulated power after model calibration is more approximate to the measured active power. The uncertainties of power consumption and the lack of high-quality measurement data still pose difficulties to load model validation. The load model validation tool builds up a platform to utilize real PMU measurements to validate the simulation model. The empirical model calibration methodology utilized in this sub-chapter is easier to implement and harness compared to advanced algorithms of parameter calibration [127].

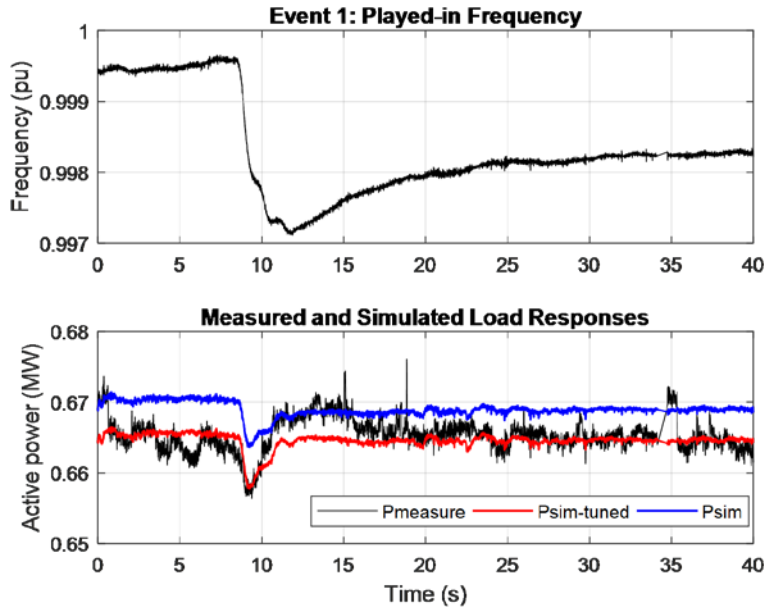


Figure 11.8 An Example of the Load Model Calibration (**Event 1**)

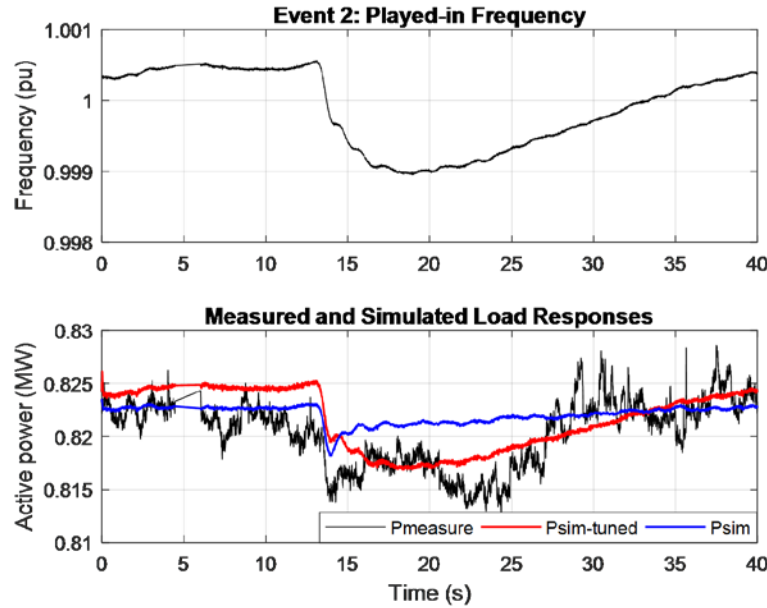


Figure 11.9 An Example of the Load Model Calibration (**Event 2**)

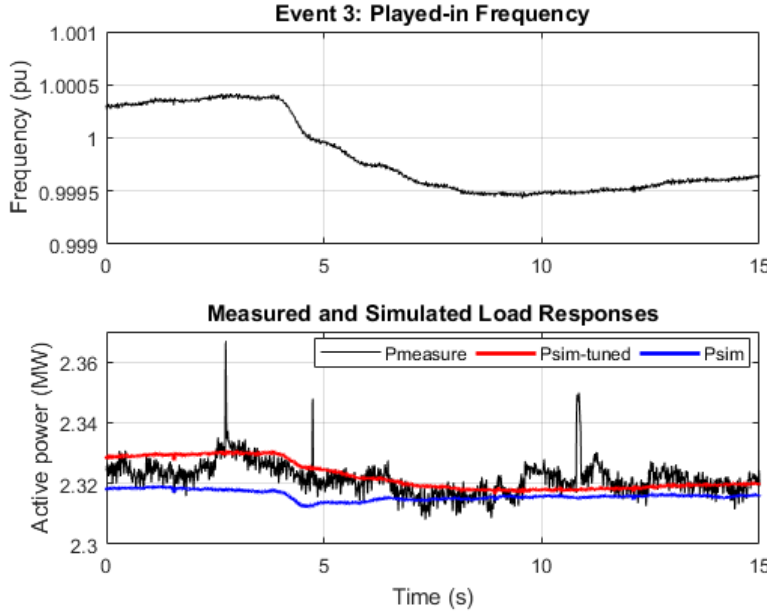


Figure 11.10 An Example of the Load Model Calibration (Event 3)

The model parameters before and after calibration are presented in Table 11.2. It is noted that the original CMPLDW parameters generated by LMDT tool are based on load aggregation of measured or surveyed data at feeder level [6]. Previously, the simulation results using the original parameters were not validated against measurement data. Founded on the original LMDT-generated parameters, the model now can be benchmarked against feeder-level measurement data (if available) following the calibration process described in this sub-chapter. The results of the model calibration would be used to update the LMDT-generated parameter records.

Table 11.2 Calibrated Parameters of the Composite Load Model

<i>FmA</i>	<i>FmB</i>	<i>FmC</i>	<i>FmD</i>	<i>Fel</i>	<i>Vstall</i>	<i>Tstall</i>	<i>Rstall</i>
Event 1: Original Parameters							
0.09	0.065	0.029	0.081	0.195	0.6	0.033	0.1
Event 1: Calibrated Parameters							
0.036	0.007	0.012	0.032	0.195	0.6	0.033	0.1
Event 2: Original Parameters							
0.057	0.048	0.043	0.041	0.237	0.6	0.033	0.1
Event 2: Calibrated Parameters							
0.091	0.288	0.069	0.246	0.024	0.6	0.033	0.1
Event 3: Original Parameters							
0.043	0.068	0.018	0.147	0.146	0.6	0.033	0.1
Event 3: Calibrated Parameters							
0.009	0.26	0.003	0.324	0.429	0.6	0.033	0.1

Table 11.3 shows the numerical performance of the model calibration in supplement to the graphs shown in Figure 11.8 - Figure 11.10. It can be seen from Table 11.3 that with model calibration, the calculated MSE of simulated active power time series against measurement data is smaller than that without model calibration. The model calibration process further reduces the difference between the simulation results and the measurement data.

Table 11.3 Numerical Comparison of Results

Event #	.dyd Record	MSE of $P_{simulated}$ vs. $P_{measured}$ ($\times 10^{-5}$)
Event 1	Original	1.814
	Calibrated	0.616
Event 2	Original	0.986
	Calibrated	0.666
Event 3	Original	5.533
	Calibrated	2.494

11.1.4 Summary

A methodology and a set of software applications have been developed for composite load model parameter estimation and validation. Simulation results based on actual distribution feeders synchrophasor measurements confirmed the efficiency of the proposed method and developed tools. The proposed load model calibration method in this sub-chapter results in some improvements in the accuracy of load modeling. In the future, advanced parameter estimation algorithms need to be developed to perform more precise model calibration based on the LMDT-generated dynamic simulation parameters of CMPLDW using micro-PMU data.

11.2 Machine Learning Approach

A simulation model is used to generate more data for training the machine learning model since insufficient measurement data are accessible.

11.2.1 PSCAD Model

Model Details

The model of the whole system is described in Figure 11.11. In the model, six commercial buildings are supplied by two distribution taxonomy feeders. The six commercial buildings include hotel, medium retail, large retail, school, warehouse and supermarket. In each commercial building, different functional motors are modeled to drive corresponding mechanical loads. The detailed description of the feeder and building models is explained in [63] and not repeated here. Since there are no publicly available time-series measurements from utilities, the intention that we model this distribution system in PSCAD simulation is to use it as a testbed to glean response data that could be used to train and validate the WECC composite load model representing a commercial distribution system.

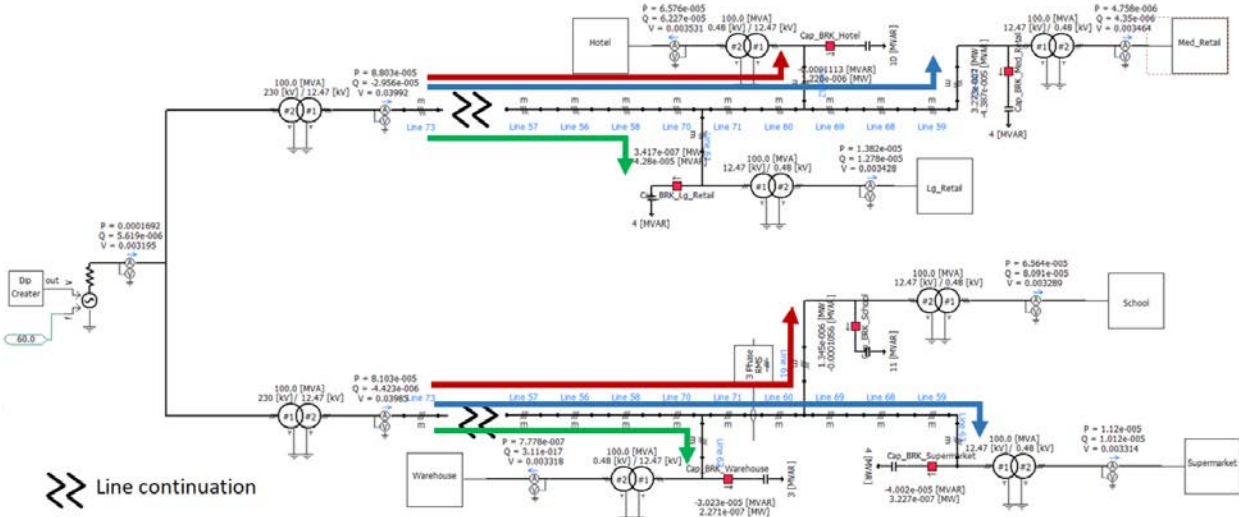


Figure 11.11 Overall System Model and Feeder Configuration

Creating Voltage Dip Scenarios

A controllable voltage source is modeled at the feeder head to represent external power grid as shown in Figure 11.11. Various voltage dip scenarios are created to emulate the impacts of external grid faults by configuring the 'Dip Creator' component at the feeder head. The 'dip' or fault can be characterized using the following parameters as shown in Figure 11.12. The range of the parameters are shown below:

- t_1 : dropping interval is chosen from values 0.01, 0.02, 0.03, 0.04 s.
- t_2 : depression interval is chosen from values corresponding to {3, 4, 5, 6, 7, 8, 10, 12, 16, 20} cycles
- t_3 : rising interval is chosen from values corresponding to {1, 2, 3, 4} cycles
- V_I : voltage magnitude before dip is fixed at 1 p.u.
- V_2 : voltage magnitude during depression is chosen from {0.9, 0.8, 0.7, 0.6, 0.5, 0.4, 0.3, 0.2, 0.1, 0} p.u.
- V_3 : voltage magnitude after depression is fixed at 0.9 p.u.

Discrete values are selected from each of the above parameter sets to create a voltage dip scenario. Considering all combinations of the parameters, a total of 1600 voltage dip scenarios are created. A piece of Python API code was developed to control the batch simulation of the 1600 scenarios in PSCAD. For each scenario, the voltage magnitude, active and reactive power responses at the feeder head are monitored and outputted as time series into a csv file. Since the existence of reactive power compensation in the grid which poses challenge to model validation, active power is used as the performance metrics to calibrate the WECC composite load model against the detailed PSCAD feeder model.

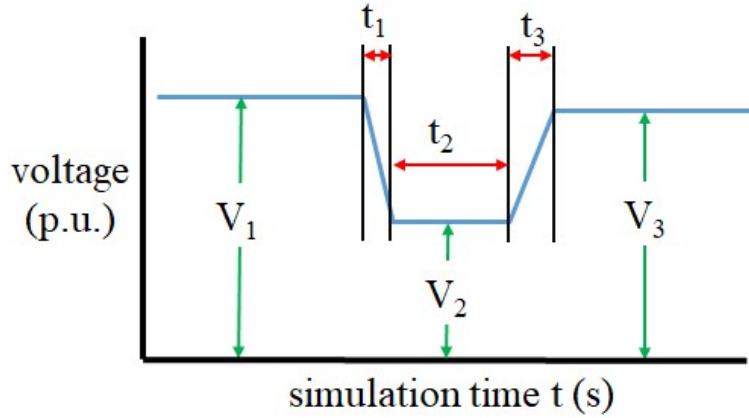


Figure 11.12 Parameters Defining a Fault Scenario

The results of several voltage dip scenarios are presented in Figure 11.13, which captures the real power (P_{feeder}), reactive power (Q_{feeder}) and voltage magnitude V_{feeder} at the feeder head.

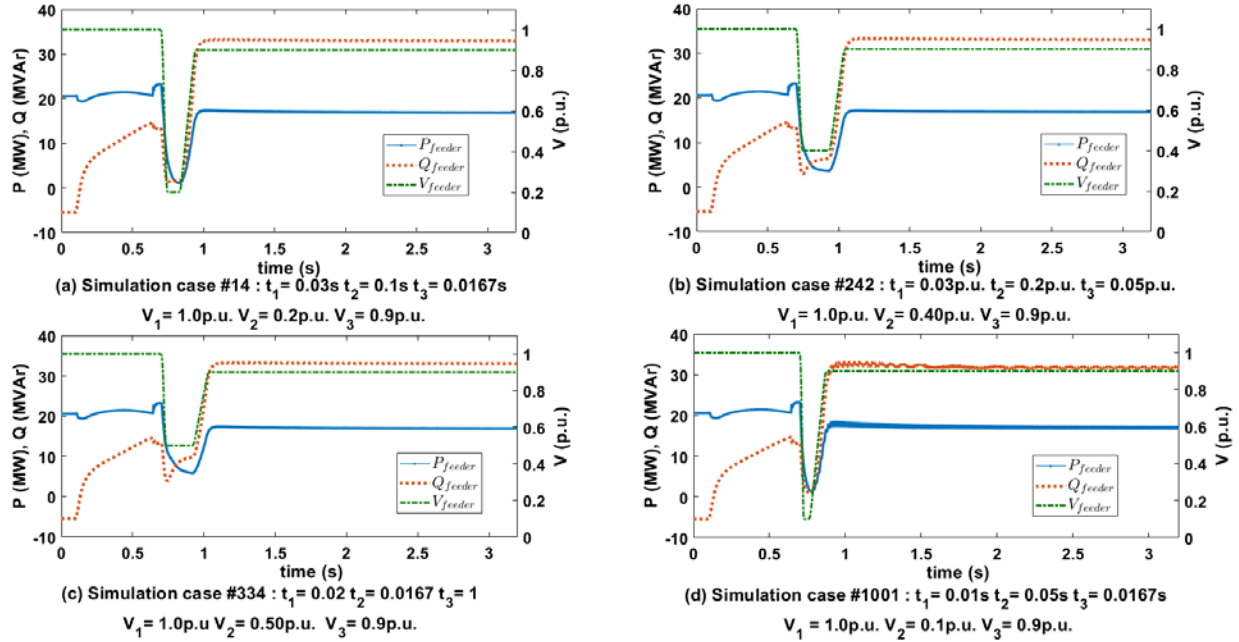


Figure 11.13 Feeder Response for Various Simulation Cases

11.2.2 Validation Framework

A. Autoencoder

An autoencoder takes an input $x \in \mathbb{R}^d$ and first maps it to the latent representation $h \in \mathbb{R}^{d'}$ using a deterministic function of the type $h = f_\theta = \sigma(Wx + b)$ with parameters $\theta = \{W, b\}$. This coded representation h is then used to reconstruct the input by reverse mapping of f : $y = f_{\theta'} = \sigma(W'h + b')$ with $\theta' = \{W', b'\}$. The parameters are optimized, minimizing an appropriate cost function over the training set $\mathcal{D}_n = \{(x_0, t_0), \dots, (x_n, t_n)\}$.

B. Convolutional Autoencoder

The Convolutional Autoencoder is intuitively similar to Autoencoder, except that the weights are shared. For a mono-channel input x the latent representation of k -th feature map is given by $h^k = \sigma(x \star W^k + b^k)$, where the bias is broadcasted to the whole map, σ is an activation function and \star denotes the 1D convolution. A single bias per latent map is used as we want each filter to specialize on features of the whole input (one bias per pixel would introduce too many degrees of freedom). The reconstruction is obtained using $y = \sigma(\sum_{k \in H} h^k \star \tilde{W}^k + c)$, where c is bias per input channel. H identifies the group of latent feature maps, \tilde{W} identifies the flip operation over both dimensions of weights. For example, the convolution of an $m \times m$ matrix with an $n \times n$ matrix may result in either a $(m+n-1) \times (m+n-1)$ matrix (full convolution) or a $(m-n+1) \times (m-n+1)$ (valid convolution). The associated loss function to be minimized is $E(\theta) = \frac{1}{2n} \sum_{i=1}^n (x_i - y_i)^2$. We have applied backpropagation algorithm to compute the gradient of the error function with respect to the parameters. This can be computed using the formula: $\frac{\partial E(\theta)}{\partial W^k} = x \star \delta h^k + \tilde{h}^k \star \delta y$, where δy and δh are the deltas of reconstruction and hidden states, respectively. The weights are then updated using stochastic gradient descent.

C. Max-Pooling

For convolutional network, we introduce a max-pooling layer to obtain translation-invariant representations. Max-pooling down-samples the latent representation by a constant factor, usually taking the maximum value over non overlapping sub-regions. This helps improving filter selectivity, as the activation of each neuron in the latent representation is determined by the “match” between the feature and the input field over the region of interest. Here we introduce a max-pooling layer that introduces sparsity over the hidden representation by erasing all non-maximal values in non-overlapping sub-regions. This forces the feature detectors to become more broadly applicable, avoiding trivial solutions such as having only one weight “on” (identity function). During the reconstruction phase, such a sparse latent code decreases the average number of filters contributing to the decoding of each pixel, forcing filters to be more general. Consequently, with a max-pooling layer there is no obvious need for L₁ and/or L₂ regularization over hidden units and/or weights.

D. Preliminaries of Tensor Train (TT) Decomposition

Tensor Train (TT) decomposition [128] is a generalization of singular value decomposition (SVD) from matrices to higher dimensional matrices or tensors. A d dimensional tensor (\mathcal{A}) is said to be in the TT-format if for each dimension $k = 1, 2, \dots, d$ and for each possible value of the k -th dimensional index $j_k = 1, \dots, n_k$ there exists a matrix $\mathcal{G}_k[j_k]$ such that all the elements of \mathcal{A} can be written as a matrix product, $\mathcal{A}(j_1, j_2, \dots, j_d) = \mathcal{G}_1[j_1]\mathcal{G}_2[j_2] \dots \mathcal{G}_d[j_d]$. All $\mathcal{G}_k[j_k]$ are of dimension $r_{k-1} \times r_k$. r_0 and r_d equal 1, in order to keep the matrix product scalar, for each element of \mathcal{A} . The sequences $\{r_k\}_{k=0}^d$ is referred as TT-ranks, and r denotes the maximal TT-rank, i.e., $r = \max\{r_0, r_1, \dots, r_d\}$.

Now, for a feedforward network of weight tensor A of dimension $M.N = \prod_{k=1}^d m_k n_k$, instead of storing $M.N$ elements during each training iteration, we will store TT-formatted $\{\mathcal{G}_k\}_{k=1}^d$ of cumulative dimension $\sum_{k=1}^d m_k n_k r_{k-1} r_k$. The dimensional reduction ratio (η), due to TT-decomposition, is defined as $\eta = \frac{\sum_{k=1}^d m_k n_k r_{k-1} r_k}{\prod_{k=1}^d \{m_k n_k\}}$. Given a 2 dimensional tensor ($d = 2$) \mathcal{A} , of dimension ($M = 70, N = 12$), and the maximal rank $r = 2$, $\eta = \frac{84+40}{840} = 0.148$, which indicates a reduction of computation complexity by a factor 0.148.

E. Gated Recurrent Unit (GRU) Parameters Factorization

In this section, we apply TT-format to represent a gated RNN. Among several RNN architectures with gating mechanism, we choose GRU to be reformulated in TT-format because it has less complex formulation and similar performance as LSTM. We call this model TT-GRU for the rest of this chapter.

The single TT-GRU architecture is illustrated in Figure 11.14. Most of RNN equations are composed by multiplication between the input vector and their corresponding weight matrix

$$\mathbf{y} = \mathbf{W}\mathbf{x} + \mathbf{b} \quad (11.5)$$

where $\mathbf{W} \in \mathbb{R}^{M \times N}$ is the weight matrix, $\mathbf{x} \in \mathbb{R}^N$ is the input vector, $\mathbf{y} \in \mathbb{R}^M$ is the output vector, and $\mathbf{b} \in \mathbb{R}^M$ is bias vector. To reduce the number of parameters significantly, we need to represent the weight matrices with the factorization of higher-order tensor. First, we apply tensorization on the weight matrices. Tensorization is the process to transform a lower-order dimensional array into a higher-order dimensional array. In our case, we tensorize GRU weight matrices into tensors, using TT decomposition. Given a weight matrix $\mathbf{W} \in \mathbb{R}^{M \times N}$, it can be represented as a tensor $\mathcal{W} \in \mathbb{R}^{m_1 \times m_2 \times \dots \times m_d \times n_1 \times n_2 \times \dots \times n_d}$, where $M = \sum_{k=1}^d m_k$ and $N = \sum_{k=1}^d n_k$. For mapping each element in matrix \mathbf{W} to tensor \mathcal{W} , we define one-to-one mapping between row-column and tensor index with bijective functions $f_i: \mathbb{Z}_+ \rightarrow \mathbb{Z}_+^d$ and $f_j: \mathbb{Z}_+ \rightarrow \mathbb{Z}_+^d$. Function f_i transforms each row $p \in 1, \dots, M$ into $f_i(p) = [i_1(p), \dots, i_d(p)]$ and f_j transforms each column $q \in 1, \dots, N$ into $f_j(q) = [j_1(q), \dots, j_d(q)]$. Following this, we can access the value from matrix $\mathbf{W}(p, q)$ in the tensor \mathcal{W} with the index vectors generated by $f_i(p)$ and $f_j(q)$ with these bijective functions.

Now we apply TT decomposition for designing TT-GRU cell. As shown in Figure 11.14 we focus on the following six dense weight matrices ($\mathbf{W}_r, \mathbf{W}_z, \mathbf{W}_d, \mathbf{U}_r, \mathbf{U}_z, \mathbf{U}_d$). Weight matrices $\mathbf{W}_r, \mathbf{W}_z, \mathbf{W}_d \in \mathbb{R}^{M \times N}$ are parameters for projecting the input layer to the reset gate, the update gate, the candidate hidden layer, and $\mathbf{U}_r, \mathbf{U}_z, \mathbf{U}_d \in \mathbb{R}^{M \times M}$ are respectively parameters for projecting previous hidden layer into the reset gate, the update gate and candidate hidden layer. We factorize $M = \prod_{k=1}^d m_k$ and $N = \prod_{k=1}^d n_k$ and set TT-rank as $\{r_k\}_{k=0}^d$. Subsequently all dense weight matrices ($\mathbf{W}_r, \mathbf{W}_z, \mathbf{W}_d, \mathbf{U}_r, \mathbf{U}_z, \mathbf{U}_d$) are replaced with $(\mathcal{W}_r, \mathcal{W}_z, \mathcal{W}_d, \mathcal{U}_r, \mathcal{U}_z, \mathcal{U}_d)$ in TT-format. Tensors $\mathcal{W}_r, \mathcal{W}_z, \mathcal{W}_d, \mathcal{U}_r, \mathcal{U}_z, \mathcal{U}_d$ are represented by a set of TT-formatted cores $\{\mathcal{G}_k^{(\cdot)}\}_{k=1}^d$, where $\mathcal{G}_k^{(\cdot)} \in \mathbb{R}^{m_k \times n_k \times r_{k-1} \times r_k}$. Using these cores, we can represent a TT-GRU cell (for more detailed explanation see [129]). Table 11.4 shows a comparison of a fully connected and a TT layer (for a forward pass training scenario), where r and d are introduced in Section D of this sub-chapter, and ‘O(.)’ represents complexity in the worst training scenario.

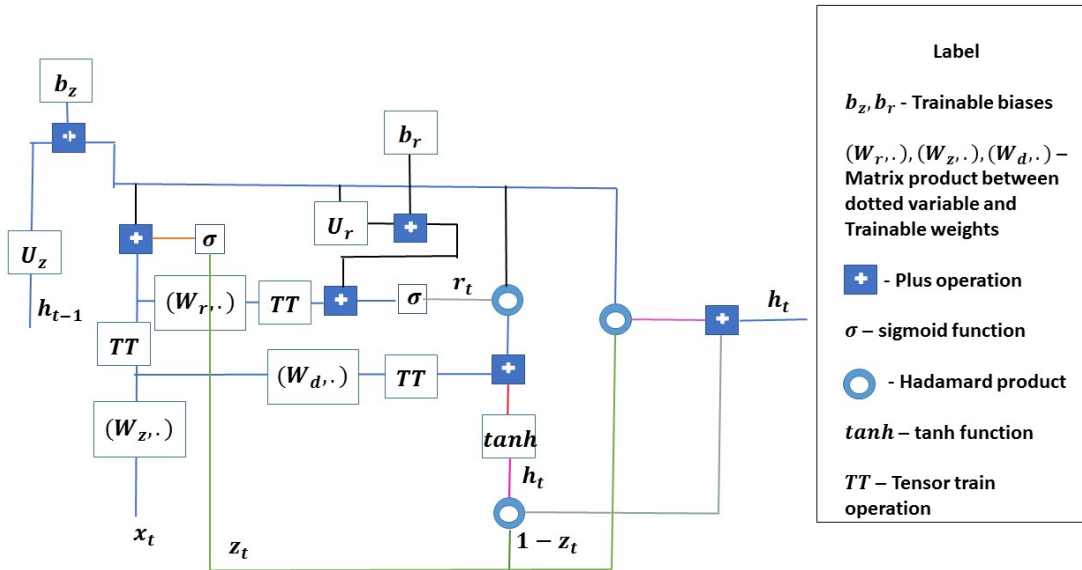


Figure 11.14 Single TT-GRU Architecture

Table 11.4 Time and Memory Comparison between Fully Connected and TT-Layer

Type	Time	Memory
Fully connected	$O(M.N)$	$O(M.N)$
TT-layer	$O(d^2 r^4 \max(M,N))$	$O(r^3 \max(M,N))$

F. Partial Least Square (PLS)

The PLS is a dimensionality reduction technique which projects the high dimensional space onto a latent space, where the covariance between the feature and its label is maximized. The PLS technique works as follows. Let $\mathbf{X} \in \mathbb{R}^m$ be a matrix of independent variables representing the samples (activities) in m -dimensional space, which is drawn from the convolution layers. Let \mathbf{y} be the matrix dependent variables denoting the class label in a k -dimensional space, where k represents the number of present fault scenarios as described in Section B of this sub-chapter. The PLS projects \mathbf{X} onto a new c -dimensional space, $\mathbf{X}' \in \mathbb{R}^c$, in terms of $\mathbf{X}' = \mathbf{XW}$, where \mathbf{W} is a weight matrix and can be computed, iteratively, using the nonlinear iterative partial least squares (NIPALS) algorithm [130], see Algorithm 1 in Table 11.5.

The NIPALS algorithm computes a column of \mathbf{W} at each iteration, which represents the maximum covariance between \mathbf{X} and \mathbf{y} . \mathbf{X} is normalized before passing through Algorithm 1 in Table 11.5.

Table 11.5 NIPALS Algorithm

Algorithm 1 NIPALS Algorithm

Input: $\mathbf{X}, \mathbf{y}, c$

Output: \mathbf{W}

- 1: **for** $a = 1$ to c **do**
 - 2: Initialize $\mathbf{u} \in \mathbb{R}^{m \times 1}$
 - 3: **while** until \mathbf{u} converges **do**
 - 4: $\mathbf{w}_a = \frac{\mathbf{X}^T \mathbf{u}}{\|\mathbf{X}^T \mathbf{u}\|}$, where $\mathbf{w}_a \in \mathbf{W}$
 - 5: $\mathbf{t}_a = \mathbf{X} \mathbf{w}_a$
 - 6: $q_a = \frac{\mathbf{y}^T \mathbf{t}_a}{\|\mathbf{y}^T \mathbf{t}_a\|}$
 - 7: $\mathbf{u} = \mathbf{y} q_a$
 - 8: **end while**
 - 9: $\mathbf{p}_a = \mathbf{X}^T \mathbf{t}_a$
 - 10: $\mathbf{X} = \mathbf{X} - \mathbf{t}_a \mathbf{p}_a^T$
 - 11: $\mathbf{y} = \mathbf{y} - \mathbf{t}_a q_a$
 - 12: **end for**
 - 13: **return** \mathbf{W}
-

G. Proposed Framework

Our proposed framework is schematically shown in Figure 11.15. The top part represents the proposed convolution based stacked autoencoder. Projection operation has been used to project output at various layers of the stacked autoencoder using the Algorithm 1 in Table 11.5 and define a basis for the temporal cells to identify parameters on. There are five temporal GRU cells which represent identified parameters, which use basis identified from the actual active power to estimate the modeling parameters.

Finally, all the modeling parameters are connected via a fully connected network for predicting the active power. This proposed framework is trained in two stage, initially the stacked autoencoder is trained to reconstruct the stack of active power and then the second stage of the training involves identifying the time-varying parameters and subsequent estimation of the active power.

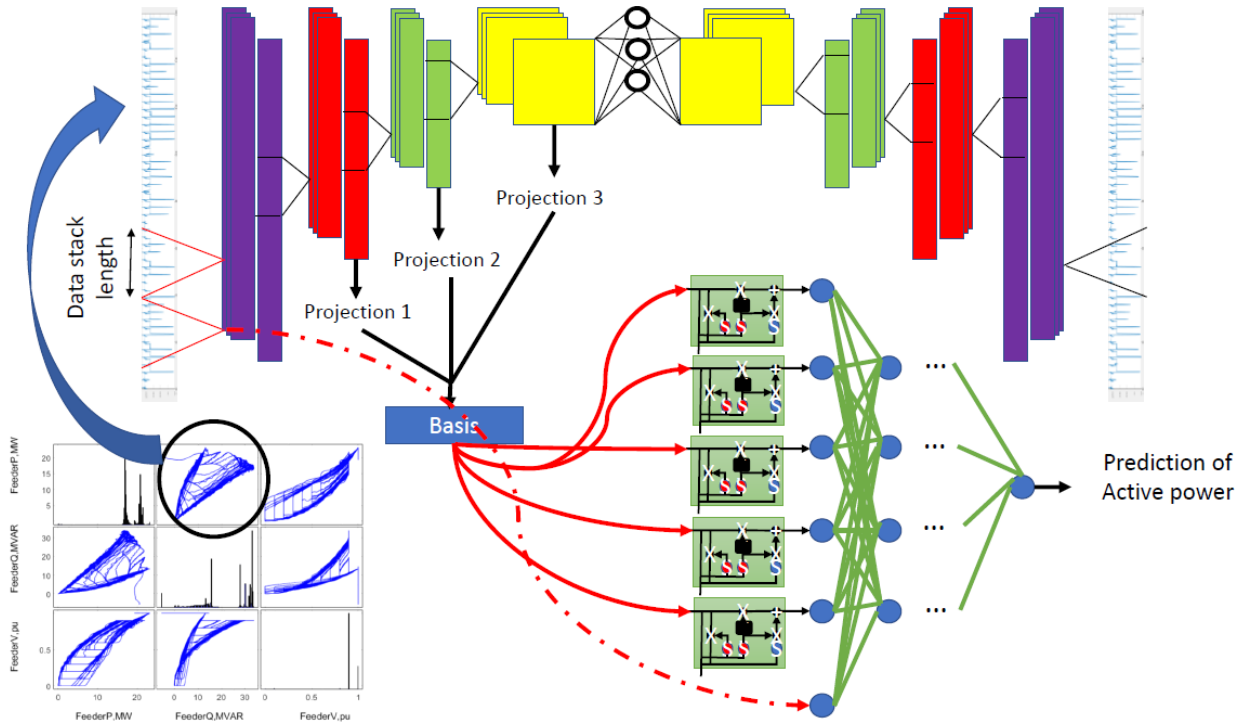


Figure 11.15 Schematic of the Whole Proposed Framework

11.2.3 Performance Results

In this sub-chapter, we will predict the following parameters: R_{fdr} , X_{fdr} , X_{xf} , FmA , FmB , FmC and Bss in the WECC composite load model [5], which are explained in Table 11.6. The WECC composite load model implemented in an open-source simulation tool is utilized to validate the developed load calibration framework [131] [132]. It is noted that the Motor D, static load and electronic load models are deactivated in the feeder provided in Figure 11.11 at the current stage of analysis to focus on predicting parameters for aggregate feeder and transformer models and fractions of three-phase induction motors.

Table 11.6 Names of Predicted Parameters

Parameter Name	Description
R_{fdr}	Feeder equivalent resistance
X_{fdr}	Feeder equivalent reactance
X_{xf}	Substation transformer reactance
FmA	Motor A fraction of load P
FmB	Motor B fraction of load P
FmC	Motor C fraction of load P
Bss	Substation shunt capacitor susceptance

Figure 11.16 shows the active power profile variation with feeder voltage value for six different voltage dip scenarios. In Figure 11.16, dashed line shows the V_{feeder} - P_{feeder} profile of predicted model and the solid line shows the profile of detailed model for several selected voltage dip cases. Figure 11.17 compares the variation of active power profile with time for both detailed and predicted models.

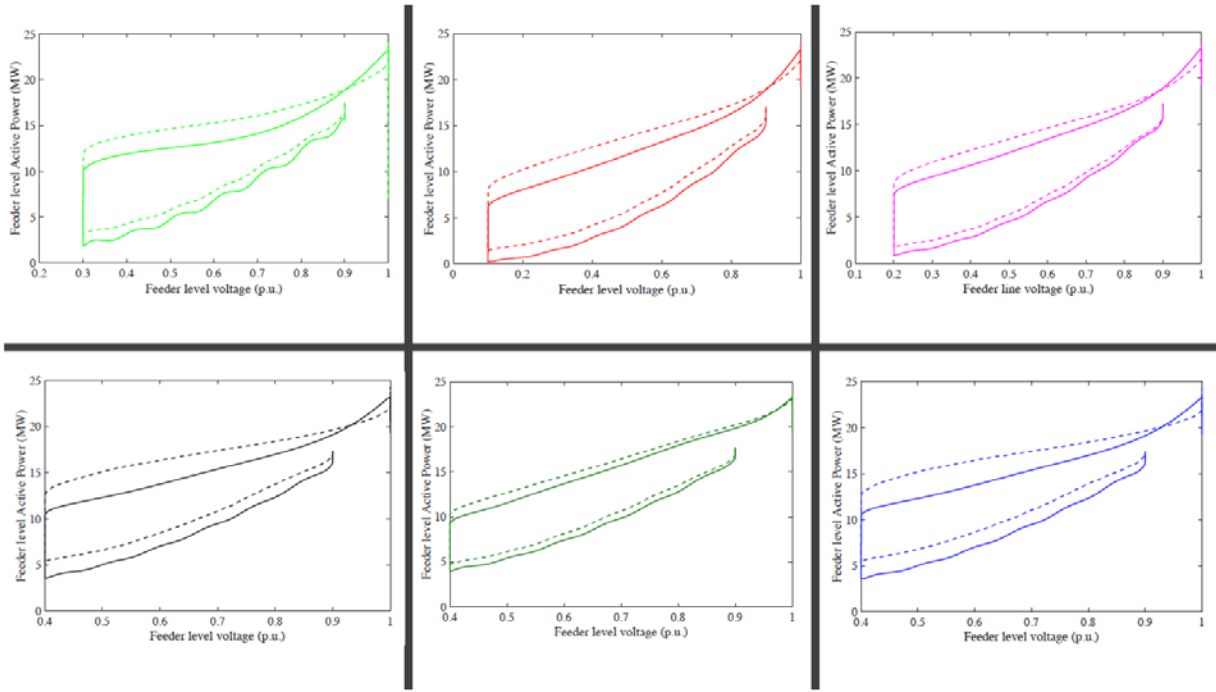


Figure 11.16 Performance Profile (V_{feeder} vs. P_{feeder}) of Predicted Composite Load Model (Dashed Line) and Detailed Feeder Model (Solid Line)

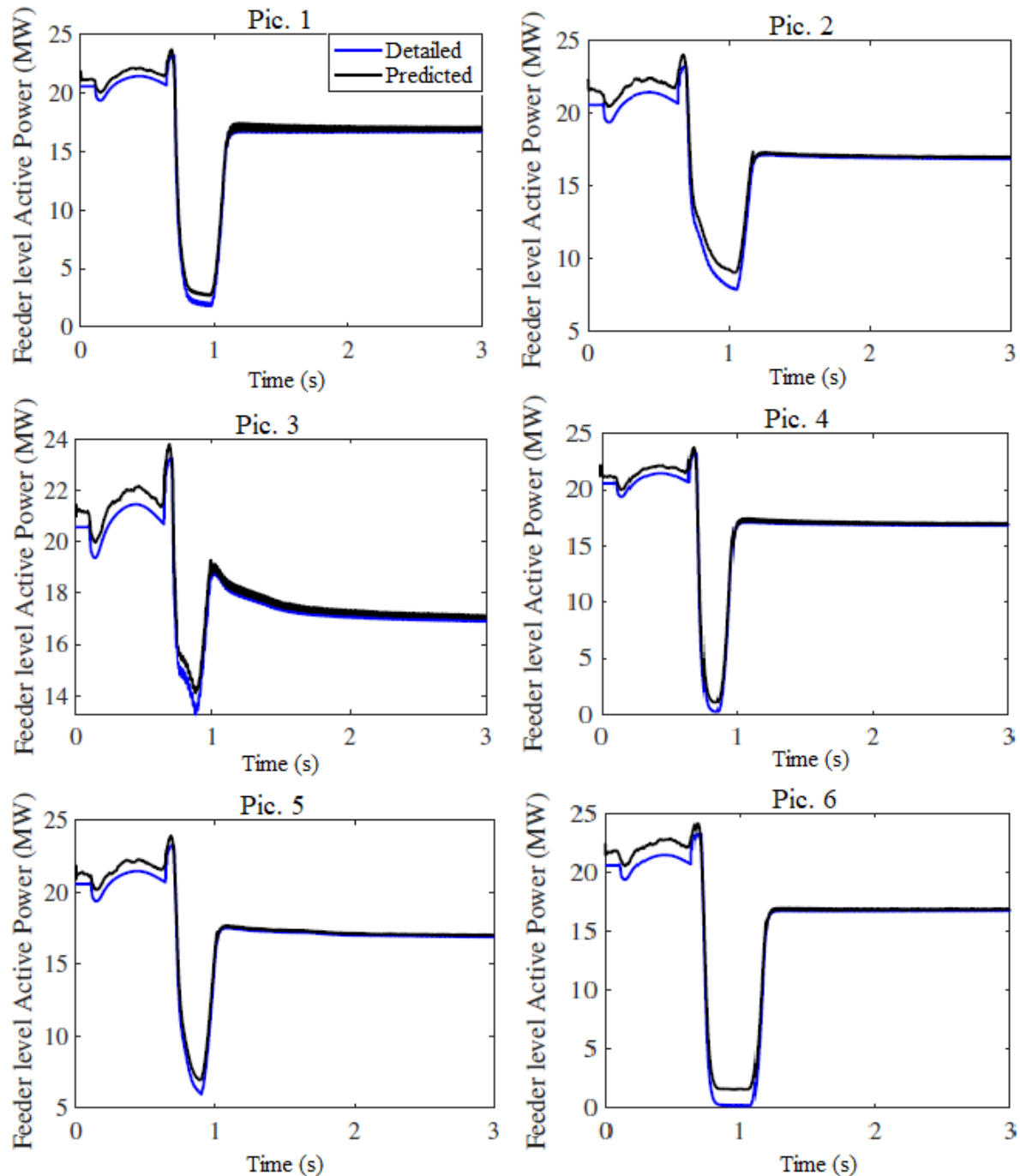


Figure 11.17 Time Series Comparison of Feeder Head Active Power Produced by Detailed Feeder Model and Predicted Composite Load Model

12.0 Conclusions and Future Works

This report summarizes the deliverables and research outcome of load modeling project led by PNNL. The following task-wise key achievements and findings are highlighted in the Conclusions chapter:

A prototype of the next-generation nation-wide load composition model with wider categories and diversity of loads is generated using three mathematical approaches, including weighted difference method, cross-correlation method and machine-learning techniques. This work first updates the WECC load composition model by using up-to-date NEEA residential-sector load shape data, and then leverages the correlations between load composition data and national weather information (NOAA data) to estimate the load shape dataset for the EI and ERCOT systems. The resultant load shapes portray a reasonable power consumption pattern for different climate zones in the EI and ERCOT grids. In the future, corporation needs to be established with utilities in WECC, EI and ERCOT to validate the generated load composition model.

The development of aggregate motor protection profile is accomplished through literature review and EnergyPlus simulation. The developed profiles of five protection categories for the four motor types in WECC composite load model are presented. Meanwhile, to make this outcome compatible for use by transmission simulators (e.g. PSLF and PSS/E), optimization-based and cross-categorical transfer learning methods are proposed and implemented to transform the representation of five protection diagrams into two-dimensional (fault duration and fault depth) space in a functional form. The generated two-dimensional protection parameters can be directly used by the four motor components in the WECC composite load model.

Three platforms based on different simulation tools are constructed for use in the validation and calibration of composite load models. Detailed commercial and residential feeders and building (or house) models that include different motors and motor protection schemes are implemented in PSCAD, GridLAB-D and InterPSS. In addition, the simulation results of the commercial and residential feeder models reveal that the system voltage profiles are improved with all the motors equipped with dedicated protection schemes. In this report, the PSCAD feeder model is used as a surrogate for realistic distribution system to generate active and reactive power response data to train and validate the machine-learning-based composite load model calibration tool. In the future, the other developed platforms are anticipated being used in the model calibration tasks to overcome the difficulty of data collection from the distribution system operators.

PNNL actively maintains and updates the Load Model Data Tool (LMDT) program, which has been used by multiple utilities including NERC, WECC, BPA, CAISO, SCE, PG&E, PacifiCorp. The most up-to-date version supports the latest GE PSLF and Siemens/PTI PSS/E composite load models. These models include PSLF CMPLDWG (composite load model with DG), PSS/E CMLDBLU2, and PSLF_CMPLDW. The penetration of distributed energy resource (DER) models is also accounted for in the current release of the LMDT program. The load model data tool has been improved to support data generation for modular composite load models and distributed energy resources. In the future, the LMDT tool is planned to be used in more DOE-funded projects to evaluate the bulk grid responses with varying load and DER profiles. PNNL has also been working closely with utilities to promote LMDT program and improve its features.

The latest PSLF motor model (MOTORLD) with progressive protection schemes is tested by PNNL to align with industrial partners' vision. A comparison between the trendy progressive protection scheme and the traditional two-level protection scheme reveals that different implementations of protection models could have significant impacts on the system's dynamic behavior and transient stability. In the

future, more research efforts should be devoted to the development, refinement and validation of aggregate protection models that are suited for bulk system simulation.

In this GMLC project, LBNL presents a concept development of price-responsive aggregate load model, which accounts for differences in the level and timing of electricity consumed by end-uses in response to the new demand response opportunities. In the future, efforts could be put in to implement this price-responsive model in transmission simulators.

A model without validation lacks credibility. PNNL proposes an empirical and a machine-learning technique to calibrate the WECC composite load model. Both PMU measurement data and simulation data are used to validate the model calibration algorithms. The accuracy of the composite load model is improved after the model calibration process. The development of this calibration tool invokes the attention that load models require benchmarking to more precisely simulate system performances in transient stability analysis.

13.0 References

- [1] Y. Liu, V. Vittal, J. Undrill and J. H. Eto, "Transient model of air-conditioner compressor single phase induction motor," *IEEE Transactions on Power Systems*, vol. 28, no. 4, pp. 4528-4536, Nov. 2013.
- [2] Y. Liu, "Modeling of air-conditioner compressor single phase induction motor for transient analysis," M.S. thesis, Department of Electrical Engineering, Arizona State University, Tempe, AZ, USA, 2012.
- [3] D. P. Chassin et al., "ARRA Interconnection Planning – Load Modeling Activities," 2015. [Online]. Available: http://www.pnnl.gov/main/publications/external/technical_reports/PNNL-24425.pdf.
- [4] L. Pereira, D. Kosterev, P. Mackin, D. Davies, J. Undrill and W. Zhu, "An interim dynamic induction motor model for stability studies in the WSCC," *IEEE Transactions on Power Systems*, vol. 17, no. 4, pp. 1108-1115, 2002.
- [5] General Electric, *PSLF User's Manual*, 2018.
- [6] Siemens PTI, *PSS/E 33.5 Program Operation Manual*, 2013.
- [7] Powerworld Corporation, "PowerWorld Simulator Online Help," 2019. [Online]. Available: <https://www.powerworld.com/WebHelp/>.
- [8] Powertech Labs Inc., "TSAT Transient Security Assessment Tool," [Online]. Available: <https://www.dsatools.com/wp-content/uploads/2017/07/TSAT.pdf>.
- [9] The Edison Foundation Institute for Electric Innovation, "Utility-Scale Smart Meter Deployments: Building Block of the Evolving Power Grid," Sept. 2014. [Online]. Available: https://www.edisonfoundation.net/iei/publications/Documents/IEI_SmartMeterUpdate_0914.pdf.
- [10] Electric Power Research Institute (EPRI), "Load Shape Library," [Online]. Available: <http://loadshape.epri.com/>.
- [11] Northwest Energy Efficiency Alliance, "Residential Building Stock Assessment," 2012. [Online]. Available: <http://neea.org/resource-center/regional-data-resources/residential-building-stock-assessment>.
- [12] Jackson Associates, "MAISY Utility Customer Energy Use and Hourly Loads Database," [Online]. Available: <http://www.maisy.com/>.
- [13] U.S. Energy Information Administration, "Consumption and Efficiency Data," [Online]. Available: <https://www.eia.gov/consumption/data.php>.
- [14] D. Kosterev, A. Meklin, J. Undrill, B. Lesieutre, W. Price, D. Chassin, R. Bravo and S. Yang, "Load modeling in power system studies: WECC progress update," in *IEEE PES General Meeting*, Pittsburgh, PA, USA, 2008.
- [15] A. Arif, Z. Wang, J. Wang, B. Mather, H. Bashualdo and D. Zhao, "Load modeling - a review," *IEEE Transactions on Smart Grid*, vol. 9, no. 6, pp. 5986-5999, 2018.
- [16] WECC, "WECC MVWG Load Model Report ver. 1.0," June 2012. [Online]. Available: <https://www.wecc.org/Reliability/WECC%20MVWG%20Load%20Model%20Report%20ver%201%200.pdf>.
- [17] Itron Inc., "California Commercial End-Use Survey," March 2006. [Online]. Available: <https://ww2.energy.ca.gov/2006publications/CEC-400-2006-005/CEC-400-2006-005.PDF>.
- [18] Bonneville Power Administration, "Description of Electric Energy Use in Single-Family

- Residences in the Pacific Northwest: 1986 - 1992," December 1992. [Online]. Available: https://elcap.nwcouncil.org/Documents/ELCAP%20Description%20of%20Electric%20Energy%20Use%20in%20Single%20Family%20Residences%20in%20the%20PNW%201986_1992.pdf.
- [19] F. J. Peterson, J. E. Patton, M. E. Miller, R. A. Gillman, W. M. Warwick and W. F. Sandusky, "End-use load and consumer assessment program: motivation and overview," *Energy and Buildings*, vol. 19, no. 3, pp. 159-166, 1993.
 - [20] Northwest Energy Efficiency Alliance, "Residential Building Stock Assessment: Metering Study," 28 April 2014. [Online]. Available: <https://neea.org/img/documents/residential-building-stock-assessment-metering-study.pdf>.
 - [21] Y. Liu, Z. Hou, P. Etingov and H. Zhou, "Update of residential load profile for WECC load composition model using cross-correlation method," in *IEEE PES General Meeting*, Atlanta, GA, USA, 2019.
 - [22] M. A. Hall, "Correlation-based feature selection for machine learning," Ph.D. thesis, Department of Computer Science, The University of Waikato, Hamilton, New Zealand, 1999.
 - [23] R. H. Shumway and D. S. Stoffer, Time series regression and exploratory data analysis, Cham: Springer, 2017.
 - [24] H. Zhou, Z. Hou, P. Etingov and Y. Liu, "Machine learning of commercial and residential load components in the Northwestern United States," in *e-Energy '19: Proceedings of the Tenth ACM International Conference on Future Energy Systems*, 2019.
 - [25] H. Zhou, Z. Hou, P. Etingov and Y. Liu, "Machine-learning-based investigation of the associations between residential power consumption and weather conditions," in *2019 3rd International Conference on Smart Grid and Smart Cities (ICSGSC)*, Berkeley, CA, USA, 2019.
 - [26] National Oceanic and Atmospheric Administration (NOAA), "Data Tools: Local Climatological Data (LCD)," [Online]. Available: <https://www.ncdc.noaa.gov/cdo-web/datatools/lcd>.
 - [27] Q. Cheng, J. Yao, H. Wu, S. Chen, C. Liu and P. Yao, "Short-term load forecasting with weather component based on improved extreme learning machine," in *Chinese Automation Congress*, 2013.
 - [28] T. Dokic, M. Pavlovski, D. Gligorijevic, M. Kezunovic and Z. Obradovic, "Spatially aware ensemble-based learning to predict weather-related outages in transmission," in *Hawaii International Conference on System Sciences - HICSS*, 2019.
 - [29] P. Dehghanian, B. Zhang, T. Dokic and M. Kezunovic, "Predictive risk analytics for weather-resilient operation of electric power systems," *IEEE Transactions on Sustainable Energy*, vol. 10, no. 1, pp. 3-15, 2019.
 - [30] K. M. Powell, A. Sriprasad, W. J. Cole and T. F. Edgar, "Heating, cooling, and electrical load forecasting for a large-scale district energy system," *Energy*, vol. 74, pp. 877-885, 2014.
 - [31] H. Gadd and S. Werner, "Daily heat load variations in Swedish district heating systems," *Applied Energy*, vol. 106, pp. 47-55, 2013.
 - [32] M. Braun, H. Altan and S. Beck, "Using regression analysis to predict the future energy consumption of a supermarket in the UK," *Applied Energy*, vol. 130, pp. 305-313, 2014.
 - [33] R. Kohavi and G. H. John, "Wrappers for feature subset selection," *Artificial Intelligence*, vol. 97, no. 1-2, pp. 273-324, 1997.
 - [34] H. Peng, F. Long and C. Ding, "Feature selection based on mutual information criteria of max-dependency, max-relevance, and min-redundancy," *IEEE Transactions on Pattern Analysis*, vol. 27, no. 8, pp. 1226-1238, 2005.
 - [35] A. Pardo, V. Meneu and E. Valor, "Temperature and seasonality influences on Spanish electricity

- load," *Energy Economics*, vol. 24, no. 1, pp. 55-70, 2002.
- [36] J. W. Taylor and P. E. McSharry, "Short-term load forecasting methods: an evaluation based on European data," *IEEE Transactions on Power Systems*, vol. 22, no. 4, pp. 2213-2219, 2007.
- [37] Y. M. Wi, S. K. Joo and K. B. Song, "Holiday load forecasting using fuzzy polynomial regression with weather feature selection and adjustment," *IEEE Transactions on Power Systems*, vol. 27, no. 2, pp. 596-603, 2012.
- [38] L. Chuan and A. Ukil, "Modeling and validation of electrical load profiling in residential buildings in Singapore," *IEEE Transactions on Power Systems*, vol. 30, no. 5, pp. 2800-2809, 2015.
- [39] B. Yildiz, J. I. Bilbao and A. B. Sproul, "A review and analysis of regression and machine learning models on commercial building electricity load forecasting," *Renewable and Sustainable Energy Reviews*, vol. 73, pp. 1104-1122, 2017.
- [40] Q. Li, Q. Meng, J. Cai, H. Yoshino and A. Mochida, "Applying support vector machine to predict hourly cooling load in the building," *Applied Energy*, vol. 86, no. 10, pp. 2249-2256, 2009.
- [41] C. L. Hor, S. J. Watson and S. Majithia, "Analyzing the impact of weather variables on monthly electricity demand," *IEEE Transactions on Power Systems*, vol. 20, no. 4, pp. 2078-2085, 2005.
- [42] A. P. Douglas, A. M. Breipohl, F. N. Lee and R. Adapa, "The impacts of temperature forecast uncertainty on Bayesian load forecasting," *IEEE Transactions on Power Systems*, vol. 13, no. 4, pp. 1507-1513, 1998.
- [43] X. Qiu, Y. Ren, P. N. Suganthan and G. A. Amaralunga, "Empirical mode decomposition based ensemble deep learning for load demand times series forecasting," *Applied Soft Computing*, vol. 54, pp. 246-255, 2017.
- [44] L. Breiman, *Classification and regression trees*, Routledge, 2017.
- [45] C. Fan, F. Xiao and S. Wang, "Development of prediction models for next-day building energy consumption and peak power demand using data mining techniques," *Applied Energy*, vol. 127, pp. 1-10, 2014.
- [46] L. Breiman, "Random forests," *Machine Learning*, vol. 45, no. 1, pp. 5-32, 2001.
- [47] J. Huo, T. Shi and J. Chang, "Comparison of random forest and SVM for electrical short-term load forecast with different data sources," in *7th IEEE International Conference on Software Engineering and Service Science (ICSESS)*, 2016.
- [48] G. Dudek, "Short-term load forecasting using random forests," in *Intelligent Systems' 2014: Springer*, 2015.
- [49] J. Friedman, T. Hastie and R. Tibshirani, *The element of statistical learning*, Springer, 2001.
- [50] D. Kosterev, M. Osman and O. Lutalo, "NERC LMTF Update," 3 April 2019. [Online]. Available: <https://www.wecc.org/Administrative/NERC%20LMTF%20Update-%20Kosterev.pdf>.
- [51] D. James and J. Kueck, "Commercial Building Motor Protection Response Report. No. PNNL-24468," June 2015. [Online]. Available: https://www.pnnl.gov/main/publications/external/technical_reports/PNNL-24468.pdf.
- [52] U.S. Department of Energy, "EnergyPlus," [Online]. Available: <https://energyplus.net/>.
- [53] ANSI/ASHRAE/IES 90.1-2013, "Energy Standard for Buildings Except Low-Rise Residential Buildings," American Society of Heating, Refrigerating and Air-Conditioning Engineers, Atlanta, GA, 2013.
- [54] ASHRAE 62.1-2013, "Ventilation for Acceptable Indoor Air Quality," American Society of Heating, Refrigerating and Air-Conditioning Engineers, Atlanta, GA (USA), 2013.
- [55] ASHRAE Handbook, "HVAC Systems and Equipment," American Society of Heating, Refrigerating and Air-Conditioning Engineers, Atlanta, GA (USA), 2016.

- [56] Energy Information Administration (EIA), "Commercial Buildings Energy Consumption Survey (CBECS)," U.S. Department of Energy, 2012.
- [57] U.S. Department of Energy Office of Energy Efficiency & Renewable Energy, "Commercial Prototype Building Models," [Online]. Available: https://www.energycodes.gov/development/commercial/prototype_models.
- [58] ASHRAE, "Standard 90.1-2004, Energy Standard for Buildings Except Low-Rise Residential Buildings (I-P and SI versions)," [Online]. Available: <https://www.ashrae.org/technical-resources/standards-and-guidelines/standards-addenda/addenda-to-standard-90-1-2004>.
- [59] S. Kundu, Z. Chu, Y. Liu, Y. Tang, Q. Huang, D. James, Y. Zhang, P. Etingov and D. P. Chassin, "A nonlinear regression method for composite protection modeling of induction motor loads," in *2020 IEEE Power & Energy Society Innovative Smart Grid Technologies Conference (ISGT)*, Washington, DC, USA, 2020.
- [60] Q. Huang, Y. Zhang, S. Kundu, Y. Tang, D. James, Y. Liu and P. Etingov, "Aggregate protection response of motor loads in commercial buildings," in *IEEE/PES Transmission & Distribution Conference and Exposition (T&D)*, Denver, CO, USA, 2018.
- [61] Y. Tang, S. Kundu, Y. Zhang, D. James, Y. Liu, Q. Huang, J. Zhang, Y. Xie, P. Etingov and D. P. Chassin, "Generation of composite load protection profiles for reliable system operation," in *2018 IEEE Power & Energy Society Innovative Smart Grid Technologies Conference (ISGT)*, Washington, DC, USA, 2018.
- [62] A. Wachter and L. T. Biegler, "On the implementation of an interior-point filter line-search algorithm for large-scale nonlinear programming," *Mathematical Programming*, vol. 106, no. 1, pp. 25-57, 2006.
- [63] Y. Liu, Y. Zhang, Q. Huang, S. Kundu, Y. Tang, D. James, P. Etingov, B. Mitra and D. P. Chassin, "Impact of building-level motor protection on power system transient behaviors," in *IEEE PES General Meeting*, Portland, OR, 2018.
- [64] I. Chakraborty, S. Kundu, Y. Liu and P. Etingov, "Cross-categorical transfer learning based composite load protection modeling," in *e-Energy '19: Proceedings of the Tenth ACM International Conference on Future Energy Systems*, 2019.
- [65] M. Abadi and et al., "Tensorflow: Large-scale machine learning on heterogeneous distributed systems," 16 Mar 2016. [Online]. Available: <https://arxiv.org/abs/1603.04467>.
- [66] J. Kueck, D. Kosterev, J. Undrill and J. Eto, "Voltage sag and recovery influence for modeling motor loads," in *IEEE PES Transmission and Distribution Conference and Exposition (T&D)*, Chicago, IL, 2014.
- [67] Q. Huang and V. Vittal, "Integrated transmission and distribution system power flow and dynamic simulation using mixed three-sequence / three-phase modeling," *IEEE Transactions on Power Systems*, vol. 32, no. 5, pp. 3704 - 3714, 2017.
- [68] M. A. Pai, *Energy function analysis for power system stability*, Springer Science & Business Media, 2012.
- [69] K. P. Schneider, Y. Chen, D. P. Chassin, R. G. Pratt, D. W. Engel and S. E. Thompson, "Modern Grid Initiative Distribution Taxonomy Final Report," 1 Nov. 2008. [Online]. Available: <https://www.osti.gov/biblio/1040684/>.
- [70] U.S. Department of Energy, "GridLAB-D A Unique Tool to Design the Smart Grid," [Online]. Available: <https://www.gridlabd.org/>.
- [71] MathWorks, "Explore COM Objects," [Online]. Available: https://www.mathworks.com/help/matlab/matlab_external/exploring-your-object.html.

- [72] Y. Fu, S. Huang, Y. Liu, T. E. McDermott, D. Vrabie and W. Zuo, "A multidisciplinary model to couple power system dynamics and building dynamics to enable building-to-grid integration," in *16th IBPSA International Conference & Exhibition Building Simulation 2019*, Rome, Italy, 2019.
- [73] Manitoba Hydro International Ltd., "Power Systems Computer Aided Design (PSCAD) User's Guide," 2018. [Online]. Available: https://hvdc.ca/uploads/knowledge_base/pscad_manual_v4_6.pdf?t=1528395602.
- [74] B. K. Bose, "Global energy scenario and impact of power electronics in 21st century," *IEEE Transactions on Industrial Electronics*, vol. 60, no. 7, pp. 2638-2651, 2013.
- [75] Schneider Electric, "Square D Overload Relays and Thermal Units Catalog," [Online]. Available: <https://www.se.com/us/en/download/document/9065CT9701/>.
- [76] Y. Liu, Z. Chu, P. Etingov, Y. Zhang, Y. Tang, Q. Huang, S. Kundu, D. James and D. P. Chassin, "Detailed modeling of residential end-use motor load and protection for distribution system transient study," in *2019 IEEE Power & Energy Society Innovative Smart Grid Technologies Conference (ISGT)*, Washington, DC, USA, 2019.
- [77] Schneider Electric, "Practical values of power factor," [Online]. Available: http://www.electrical-installation.org/enwiki/Practical_values_of_power_factor.
- [78] Draft Logic, "List of the Power Consumption of Typical Household Appliances," [Online]. Available: <https://www.daftlogic.com/information-appliance-power-consumption.htm>.
- [79] Wholesale Solar, "How Much Power Do Your Appliance Use?," [Online]. Available: <https://www.wholesalesolar.com/solar-information/power-table>.
- [80] Quora, "How many watts are required by a one-ton split AC?," [Online]. Available: <https://www.quora.com/How-many-watts-are-required-by-a-one-ton-split-AC>.
- [81] HVACDirect.com, "Sizing air conditioner and heater," [Online]. Available: <https://hvacdircet.com/sizing-air-conditioner-and-heater.html>.
- [82] Quora, "Which consumes less power, an air conditioner in fan mode or a ceiling fan?," [Online]. Available: <https://www.quora.com/Which-consumes-less-power-an-air-conditioner-in-fan-mode-or-a-ceiling-fan>.
- [83] U.S. Energy Information Administration, "Residential Energy Consumption Survey," [Online]. Available: <https://www.eia.gov/consumption/residential/data/2015/>.
- [84] B. Lesieurte, D. Kosterev and J. Undrill, "Phasor modeling approach for single phase A/C motors," in *IEEE PES General Meeting*, Pittsburgh, PA, USA, 2008.
- [85] F. K. Tuffner, K. P. Schneider, J. Hansen and M. A. Elizondo, "Modeling load dynamics to support resiliency-based operations in low-inertia microgrids," *IEEE Transactions on Smart Grid*, vol. 10, no. 3, pp. 2726-2737, 2019.
- [86] GridLAB-D Wiki, "Feeder Taxonomy," [Online]. Available: http://gridlab-d.shoutwiki.com/wiki/Feeder_Taxonomy.
- [87] Y. Liu, V. Vittal and J. Undrill, "Performance-based linearization approach for modeling induction motor drive loads in dynamic simulation," *IEEE Transactions on Power Systems*, vol. 32, no. 6, pp. 4636-4643, 2017.
- [88] Y. Liu and V. Vittal, "Modeling of rectifier-controlled induction motor drive load in transient stability simulation tools," *IEEE Transactions on Power Systems*, vol. 33, no. 5, pp. 4719-4729, 2018.
- [89] Y. Liu, "Representation of vector-controlled induction motor drive load in electro-magnetic transient and positive sequence transient stability simulators," Ph.D. thesis, Department of Electrical Engineering, Arizona State University, Tempe, AZ, USA, 2016.

- [90] Y. Liu and V. Vittal, "Distribution side mitigation strategy for fault induced delayed voltage recovery," in *IEEE PES General Meeting*, National Harbor, MD, USA, 2014.
- [91] Edgewall Software, "Load model data tool," [Online]. Available: <https://svn.pnl.gov/LoadTool>.
- [92] B. Price and J. Sanchez-Gasca, "BPA/GE Load Model Improvements Project," January 2018. [Online]. Available: https://www.nerc.com/comm/PC/LoadModelingTaskForceDL/BPA-GE_Load_Model_Improvements.pdf.
- [93] D. Trudnowski and J. Undrill, "Appendix 2: The MinniWECC System Model," 2008.
- [94] W. J. Hausman and J. L. Neufeld, "Time-of-day Pricing in the U.S. Electric Power Industry at the Turn of the Century," *The RAND Journal of Economics*, vol. 15, no. 1, pp. 116-126, 1984.
- [95] California Public Utilities Commission, "Decision Adopting Dynamic Pricing Timetable and Rate Design Guidance for Pacific Gas and Electric Company: Application of Pacific Gas and Electric Company to Revise Its Electric Marginal Costs, Revenue Allocation, and Rate Design," 2006.
- [96] Wedgemere Group, "Demand Response: The Road Ahead," 2016. [Online]. Available: <http://www.wedgemere.com/wp-content/uploads/2013/03/Evolution-of-DR-Dialogue-Project-Report.pdf>.
- [97] L. J. Hill, "Electricity Pricing as a Demand-Side Management Strategy: Western Lessons for Developing Countries," Oak Ridge National Laboratory, Oak Ridge, TN, 1990.
- [98] California Public Utilities Commission, "Order Instituting Rulemaking on the Commission's Own Motion to Conduct a Comprehensive Examination of Investor Owned Electric Utilities' Residential Rate Structures, the Transition to Time Varying and Dynamic Rates, and Other Statutory Obligations," 2015.
- [99] U.S. Department of Energy, Electricity Delivery & Energy Reliability, "Smart Grid Investment Grant Program: Interim Report on Customer Acceptance, Retention and Response to Time-based Rates from the Consumer Behavior Studies.,," June 2015. [Online]. Available: https://www.smartgrid.gov/files/CBS_interim_program_impact_report_FINAL.pdf.
- [100] Federal Energy Regulatory Commission, "2012 Assessment of Demand Response and Advanced Metering," December 2012. [Online]. Available: <https://www.ferc.gov/legal/staff-reports/12-20-12-demand-response.pdf>.
- [101] Navigant Consulting, Inc ., "Assessing Demand Response (DR) Program Potential for the Seventh Power Plan - Updated Final Report," 19 January 2015. [Online]. Available: https://www.nwcouncil.org/sites/default/files/npcc_assessing-dr-potential-for-seventh-power-plan_updated-report_1-19-15.pdf.
- [102] P. Alstone, et al., "Interim Report on Phase 1 Results - 2015 California Demand Response Potential Study: Charting California's Demand Response Future.,," April 2016. [Online]. Available: <https://www.osti.gov/biblio/1421793-california-demand-response-potential-study-charting-californias-demand-response-future-interim-report-phase-results>.
- [103] A. Faruqui, N. Lessem, S. Sergici, D. Mountain, F. Denton, B. Spencer and C. King, "Analysis of Ontario's Full Scale Roll-out of TOU Rates – Final Study," 3 February 2016. [Online]. Available: <http://www.ieso.ca/-/media/files/ieso/document-library/conservation-reports/final-analysis-of-ontarios-full-scale-roll-out-of-tou-rates.pdf>.
- [104] A. Faruqui, S. Sergici and L. Akaba, "The Impact of Dynamic Pricing on Residential and Small Commercial and Industrial Usage: New Experimental Evidence from Connecticut," *The Energy Journal, International Association for Energy Economics*, vol. 0, no. 1, 2014.
- [105] CRA International, "California Statewide Pricing Pilot: Commercial and Industrial Analysis Update," Oakland, CA, 2006.

- [106] D. J. Aigner and J. G. Hirschberg, "Commercial/industrial customer response to time-of-use electricity prices: some experimental results," *The Rand Journal of Economics*, vol. 16, no. 3, pp. 341-355, 1985.
- [107] ICF International, "Partnership for Growth, Ghana TOU Tariff Analysis and Program Development - Final Report," March 2015. [Online]. Available: https://pdf.usaid.gov/pdf_docs/PA00SX87.pdf.
- [108] A. Faruqui and J. R. Malko, "The residential demand for electricity by time-of-use: A survey of twelve experiments with peak load pricing," *Energy*, vol. 8, no. 10, pp. 781-795, 1983.
- [109] Charles River Associates, "Impact Evaluation of the California Statewide Pricing Pilot," 16 March 2005. [Online]. Available: https://www.smartgrid.gov/files/Impact_Evaluation_California_Statewide_Pricing_Pilot_200501.pdf.
- [110] Summit Blue Consulting, LLC, "Final Report for the myPower Pricing Segments Evaluation," 21 December 2007. [Online]. Available: http://www.madrionline.org/wp-content/uploads/2017/02/mypower_pricing_final_report_2007.pdf.
- [111] Connecticut Light and Power, "Results of CL&P Plan-It Wise Energy Pilot, Filing in Response to the Department of Public Utility Control's Compliance Order No. 4, Docket No. 05-10-03RE01," 2009.
- [112] L. R. Jimenez, J. M. Potter and S. S. George, "SmartPricing Options Interim Evaluation," 23 October 2013. [Online]. Available: https://www.smartgrid.gov/files/MASTER_SMUD_CBS_Interim_Evaluation_Final_SUBMITTED_TO_TAG_20131023.pdf.
- [113] S. Patel, S. Borgeson, R. Rajagopal, C. A. Spurlock and A. Todd, "Time Will Tell: Using Smart Meter Time Series Data to Derive Household Features and Explain Heterogeneity in Pricing Programs," in *2016 ACEEE Summer Study on Energy Efficiency in Buildings*, 2016.
- [114] A. Faruqui and S. Sergici, "Household Response to Dynamic Pricing of Electricity-A Survey of the Empirical Evidence," 12 February 2010. [Online]. Available: https://papers.ssrn.com/sol3/papers.cfm?abstract_id=1134132.
- [115] J. C. Ham, D. C. Mountain and M. L. Chan, "Time-of-Use Prices and Electricity Demand: Allowing for Selection Bias in Experimental Data," *The RAND Journal of Economics*, vol. 28, no. 0, pp. S113-S141, 1997.
- [116] K. Jessoe and D. Rapson, "Commercial and Industrial Demand Response under Mandatory Time-of-Use Electricity Pricing," *The Journal of Industrial Economics*, vol. 63, no. 3, pp. 397-421, 2015.
- [117] P. Etingov, F. Tuffner, J. Follum, X. Li, H. Wang, R. Diao, Y. Zhang, Z. Hou, Y. Liu, D. Kosterev, S. Yang and G. Matthews, "Open-source suite for advanced synchrophasor analysis," in *2018 IEEE/PES Transmission and Distribution Conference and Exposition (T&D)*, Denver, CO, USA, 2018.
- [118] H. Renmu, M. Jin and D. J. Hill, "Composite load modeling via measurement approach," *IEEE Transactions on Power Systems*, vol. 21, no. 2, pp. 663-672, 2006.
- [119] Y. Liu and P. Etingov, "Distribution-level phasor measurement units application to composite load model validation," in *51st North American Power Symposium*, Wichita, KS, USA, 2019.
- [120] Y. Li, R. Diao, R. Huang, P. Etingov and et al., "An innovative software tool suite for power plant model validation and parameter calibration using PMU measurements," in *IEEE PES General Meeting*, 2017.
- [121] P. Pourbeik, "Approaches to validation of power system models for system planning studies," in

IEEE PES General Meeting, 2010.

- [122] R. J. Bravo and D. P. Chassin, "Fault Induced Delayed Voltage Recovery (FIDVR) model validation," in *IEEE PES Transmission and Distribution Conference and Exposition (T&D)*, 2016.
- [123] N. W. Tenza and S. Ghiocei, "An Analysis of the Sensitivity of WECC Grid Planning Models to Assumptions Regarding the Composition of Loads," Produced by Mitsubishi Electric Power Products (MEPPI) for the Consortium for Electric Reliability Technology Solutions (CERTS), 2016.
- [124] E. M. Stewart, A. Liao and C. Roberts, "Open μ PMU: A real world reference distribution micro-phasor measurement unit data set for research and application development," Lawrence Berkeley National Laboratory, Berkeley, CA, 2016.
- [125] A. V. Meier, E. Stewart, A. McEachern, M. Andersen and L. Mehrmanesh, "Precision micro-synchrophasors for distribution systems: A summary of applications," *IEEE Transactions on Smart Grid*, vol. 8, no. 6, pp. 2926-2936, 2017.
- [126] D. B. Arnold, C. Roberts, O. Ardakanian and E. M. Stewart, "Synchrophasor data analytics in distribution grids," in *IEEE PES Innovative Smart Grid Technologies Conference (ISGT)*, 2017.
- [127] K. Zhang, H. Zhu and S. Guo, "Dependency Analysis and Improved Parameter Estimation for Dynamic Composite Load Modeling," *IEEE Transactions on Power Systems*, vol. 32, no. 4, pp. 3287-3297, 2017.
- [128] I. V. Oseledets, "Tensor-train decomposition," *SIAM Journal on Scientific Computing*, vol. 33, no. 5, p. 2295–2317, 2011.
- [129] A. Tjandra, S. Sakti and S. Nakamura, "Compressing recurrent neural network with tensor train," 23 May 2017. [Online]. Available: <https://arxiv.org/abs/1705.08052>.
- [130] H. Wold, "Partial Least Squares," in *Encyclopedia of Statistical Sciences*, John Wiley & Sons, Inc., 2006.
- [131] Q. Huang, R. Huang, B. J. Palmer, Y. Liu, S. Jin, R. Diao, Y. Chen and Y. Zhang, "A Reference Implementation of WECC Composite Load Model in Matlab and GridPACK," 2 Aug. 2017. [Online]. Available: <https://arxiv.org/abs/1708.00939>.
- [132] Q. Huang, R. Huang, B. J. Palmer, Y. Liu, S. Jin, R. Diao, Y. Chen and Y. Zhang, "A generic modeling and development approach for WECC composite load model," *Electric Power Systems Research*, vol. 172, pp. 1-10, 2019.
- [133] D. J. Aigner, J. Newman and A. Tishler, "The Response of Small and Medium-Size Business Customers to Time-of-Use (TOU)," *Journal of Applied Econometrics*, vol. 9, no. 3, pp. 283-304, 1994.
- [134] C. A. Goldman, et al., "Customer Response to Day-ahead Wholesale Market Electricity Prices: Case Study of RTP Program Experience in New York," June 2004. [Online]. Available: <https://drrc.lbl.gov/publications/customer-response-day-ahead-wholesale>.
- [135] R. Patrick, "Rate Structure Effects and Regression Parameter Instability Across Time-of-Use Electricity Pricing Experiments," *Resources and Energy*, pp. 179-195, 1990.



Pacific Northwest
NATIONAL LABORATORY

Proudly Operated by **Battelle** *Since 1965*

902 Battelle Boulevard
P.O. Box 999
Richland, WA 99352
1-888-375-PNNL (7665)
www.pnl.gov



U.S. DEPARTMENT OF
ENERGY